UNIVERSIDADE FEDERAL DO RIO GRANDE DO SUL

INSTITUTO DE QUÍMICA

PROGRAMA DE PÓS-GRADUAÇÃO EM QUÍMICA

Polyolefins as Polymeric Matrix for Magnetic and Conductive Nanocomposites

Doctorate candidate: ***Muhammad Nisar***

Porto Alegre, February 2018

UNIVERSIDADE FEDERAL DO RIO GRANDE DO SUL

INSTITUTO DE QUÍMICA

PROGRAMA DE PÓS-GRADUAÇÃO EM QUÍMICA

Muhammad Nisar

Polyolefins as Polymeric Matrix for Magnetic and Conductive Nanocomposites

This thesis is submitted in fulfillment of the
requirements of the degree of Doctor in Chemistry

Supervisors:
Prof. Griselda Barrera Galland

Porto Alegre, February 2018

Preface

This work was carried out in the Chemical Institute, Universidade Federal do Rio Grande do Sul, from February 2014 to February 2018 under the supervision of the Prof. Griselda Barrera Galland, and is submitted in fulfillment of the requirements of the degree of Doctor in Chemistry. This thesis is the result of my own work and includes nothing that is the outcome of work done in collaboration except where specifically indicated in the text. None of the work contained in this thesis, or any part thereof, has been submitted for any other degree at the Universidade Federal do Rio Grande do Sul or any other institution. The thesis was judged by the following examination commission.

Examination Jury

Prof. Dr. Sandro Campos Amico

Dr. Fernando Silveira

Prof. Dr. Sônia Marlí Bohrz Nachtigall

Prof. Dr. Rafeal Stieler

Supervisor: Prof. Dr. Griselda B. Galland

Candidate: Muhammad Nisar

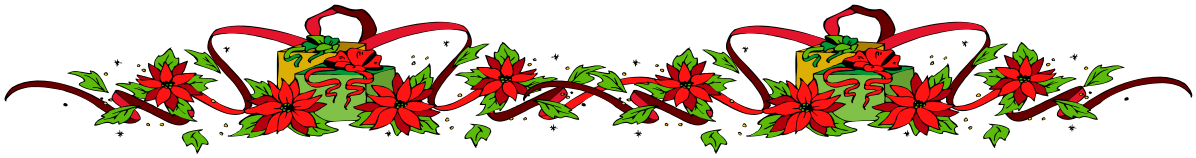

Dedicated to my

Beloved parents

Especially to my mother

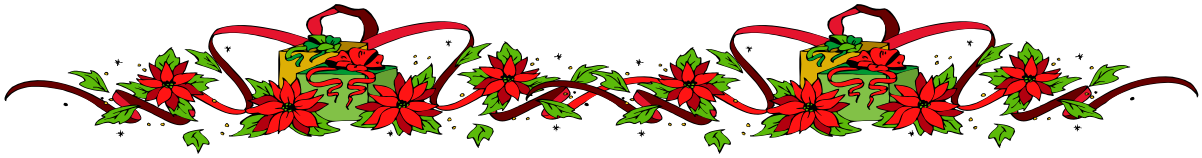

Acknowledgement

I have really no words to express the deepest sense of gratitude to Almighty Allah the most merciful and compassionate, the Creator of the universe, who gave me the strength and perseverance for completing my PhD research. I offer my humblest and sincerest words of thanks to the Holy Prophet (Peace be upon Him) who is always a torch of guidance and knowledge for humanity.

It is a matter of great pleasure and honor for me to express my deep sense of devotion and gratitude to my Supervisor Dr. Griselda Barrera Galland, Professor from the Chemical Institute of the Federal University of Rio Grande do Sul (UFRGS), and Prof. Dr. Raul Quijada from the University of Chile, for their consistent support, scientific guidance, kindness, giving to me the opportunity and freedom to carry out my research work at my own pace in their research laboratories. I would like to thank Prof. Carlos Bergmann from Department of Engineering (UFRGS) for providing his lab for the synthesis of carbon nanotubes and Prof. Nara Basso (PUCRS) for providing the reduce graphene oxide used in this work. I also thanks to Prof. Julian Geshev from Department of Physics (UFRGS) for magnetic characterization of the materials and for his valuable time and ideas during the discussions. I would like to thanks to the amazing personality Prof. Rashid Ahmad from the Department of Chemistry of the University of Malakand (Pakistan) for his constant guidance who has been always a source of inspiration for me.

I would also like to acknowledge the generous financial support that I have received from National Council for Scientific and Technological Development (CNPq, Brazil), and The Academy of Sciences for Developing World (TWAS, Italy).

I really like to thanks to all the amazing people I met in Brazil, who made my time really memorable during my stay, particularly to all the colleagues of K-106 and K-125 (with whom I spent most of my time) for their help, guidance, in learning Portuguese and especially for their friendship.

Finally I acknowledge the help, encouragement, endless love, support and prayers of my family, which have always been a source of inspiration and guidance for me all the way. My deepest gratitude goes to my parents who always encouraged and raised their hands for my

successful completion of research and make my aims a reality and taking care of my happiness all along my life. I would also like to thank my brother and sisters for their support.

List of publication composing the thesis

1. **M. Nisar,** C. Bergmann, J. Geshev, R. Quijada, G. B. Galland. An efficient approach to the preparation of polyethylene magnetic nanocomposites, *Polymer* 97 (**2016**) 131-137.

2. **M. Nisar,** C. Bergmann, J. Geshev, R. Quijada, G. B. Galland. Synthesis and characterization of polypropylene/iron encapsulated carbon nanotube composites with high magnetic response at room temperature, *Polymer* 118 (**2017**) 68-74.

3. **M. Nisar,** C. Bergmann, J. Geshev, R. Quijada, T. Maraschin, N.R.S. Basso, E.G. Barrera, G.B. Galland. Synthesis of high-density polyethylene/rGO-CNT-Fe nanocomposites with outstanding magnetic and electrical properties, *J. Appl. Polym. Sci.* 134 (40) (**2017**) 45382

4. **M. Nisar,** P.S. Thue, C. A. Heck, J. L. S. Cuaila, J. Geshev,E. C. Lima, G. B. Galland. Synthesis of polyethylene/nickel–carbon stimuli-responsive material under magnetic field at room temperature: effect of the filler on the properties, *European polymer journal* 99 (**2018**), 378-383.

Submitted Articles

1. **M. Nisar,** M.G.S. Bernd, L. C.P. Silva Filho, J. Geshev, G.B. Galland. Thermal, mechanical, gas barrier, and magnetic properties of polypropylene/carbon nanotube composites obtained using carbon nanotubes from waste furniture sawdust, *Macromolecular Materials and Engineering* (2018)
2. **M. Nisar,** J. Geshev, G. B. Galland. Electrically-conductive polypropylene/rGO-CNT-Fe magnetic nanocomposite with improved mechanical, thermal and barrier properties, *J.App.Polym. Sci.* (2018)

Additional publication

1. R. Mensez, B. Constant, C. Garzon, **M. Nisar,** S.M.B. Nachtigall, R.Quijada, Barrier, mechanical and conductive properties of polycaprolactam nanocomposites containing carbon-based particles: Effect of the kind of particle, Polymer 130 (2017) 10-16.

Patent

1. Nanocompósito e processo de obtenção de nanocomposite, BR10201603016

Works presented in events and conferences

1. **M. Nisar**, G. B. Galland, Study of polyolefins as polymeric matrix for conductive and magnetic nanocomposites, 14th International Symposium on Advance Materials, 2015 Islamabad Pakistan.

2. R.Quijada, R. Mensez, B. Constant, C. Garzon, **M. Nisar**, S.M.B. Nachtigall, Barrier, properties of polycaprolactam composites melt mixed with carbon-based particles: Effect of the kind of particle. XV Simposio Latino Americano de Polimeros (2016) Mexico.

3. **M. Nisar**, C. Bergmann, J. Geshev, R.Quijada, T. Maraschin, N.R.S. Basso, E.G. Barrera, G.B.Galland, Magnetic and semiconductor flexible nanocomposites, XV Simposio Latinoamericano de Polimeros (2016) Mexico.

4. **M. Nisar**, C. Bergmann, J. Geshev, R. Quijada, G. B. Galland. An easy approach to synthesis and characterization of polyethylene magnetic nanocomposites, 3rd Brazilian Conference on Composites Material (2016) RS Brazil.

5. **M. Nisar,** M.G.S. Bernd, L. C.P. S. Filho, J. Geshev, G.B. Galland. Nanocomposites of polypropylene with carbon nanotubes from sawdust of the furniture industry: study of properties. XVI Brazil MRS meeting (2017) RS Brazil.

6. S.M.B. Nachtigall, B. Constant R. Quijada, **M. Nisar**. Effect of carbon based filler on the barrier properties of polycaprolactam, XVI Brazil MRS meeting (2017) RS Brazil.

7. **M. Nisar**, C. Bergmann, J. Geshev, R. Quijada, G. B. Galland. Synthesis of polyolefin magnetic and conducting nanocomposites by in situ polymerization, 14° CONGRESSO BRASILEIRO DE POLÍMEROS (2017) SP Brazil.

Table of contents

Preface ..... **I**
Acknowledgement ..... **III**
List of publication composing the thesis V
Submitted Articles V
Additional publication V
Patent V
Works presented in events and conferences VI
Table of contents VII
List of Figures X
List of Tables XI
Abbreviations XII
Abstract XIV
Resumo XV
1. Introduction **1**
2. Objectives 3
2.1. General Objective 3
2.2. Specific Objectives 3
2.3. Structure of the thesis **4**
3. Literature Review **8**
3.1 Polymer nanocomposites: 8
3.2 Polyethylene (PE) 11
3.3 Polypropylene (PP): 12
3.4. Carbon nanotubes 13
3.4.1 Types of Carbon nanotubes: 14
3.4.1.1 Single-walled CNT: 15
3.4.1.2 Multiwalled carbon nanotubes: 15
3.4.2 Synthesis of carbon nanotubes: 16
3.4.2.1 Arc-discharge method: 16
3.4.2.2 Laser ablation: 17

3.4.2.3 Chemical vapor deposition (CVD): 17
3.4.3 Properties of carbon nanotubes: 17
3.5 Graphite and Graphene: 18
3.5.1 Methods used to obtain graphene: 20
3.5.1.1 Direct exfoliation of graphite : 20
3.5.1.2 Exfoliation of treated graphite: 20
3.5.1.3 Graphite oxide (GO) treatment: 21
3.5.1.4. Brodie's oxidation method: 22
3.5.1.5 Staudenmaier method: 22
3.5.1.6 Hofmann method: 22
3.5.1.7 Hummers method: 23
3.6 Activated carbon: 23
3.7 Polyolefins carbon based filler nanocomposites: 24
3.8 Electrical Conductivity: 28
3.9 Magnetism: 28
3.10 Magnetic polymer nanocomposites: 32
4. Experimental Part: 34
4.1 Materials: 34
4.2 Synthesis of carbon nanotubes containing iron: 35
4.3 Synthesis of carbon nanotube contain iron using sawdust from furniture industry: 36
4.4 synthesis of nickel activated carbon: 36
4.5 Reduced graphite oxide synthesis: 36
4.6 Synthesis of nanocomposites: 37
4.6.1 Polyethylene/CNT-Fe nanocomposites: 37
4.6.2 Polypropylene/CNT-Fe nanocomposites: 38
4.6.3 Polyethylene/rGO/CNT-Fe nanocomposites: 39
4.6.4 Synthesis of Polypropylene nanocomposites by melt compounding: 39
4.7 Characterization of the nanocomposites: 40
4.7.1 Differential scanning calorimetry (DSC): 40
4.7.2 Thermogravimetric Analysis (TGA): 40
4.7.3 Dynamic Mechanical Analysis (DMA) : 40

4.7.4 Mechanical properties: 41
4.7.5 Transmission electron microscopy (TEM):..... 41
4.7.6 Scanning electron microscopy (SEM): 41
4.7.7 Gel permeation chromatography (GPC): 41
4.7.8 Electrical conductivity measurement: 42
4.7.9 Atomic absorption spectroscopy: 42
4.7.11 Inductive coupled plasma emission spectroscopy (ICP):..... 43
4.7.12 Raman spectroscopy:..... 43
4.7.13 X-ray diffraction (XRD): 43
5. 1 Conclusion: 44
5.2 Future plan: 47
***References* 48**
***Annex 1*..... 58**

List of Figures

Figure 1. Types of composites microstructure:(a) Unintercalated (b) Intercalated (c) Exfoliated. Reproduced from [23]. 8
Figure 2.The melt intercalation process. Reproduced from [20]. 9
Figure 3. The exfoliation adsorption process. Reproduced from [20] 10
Figure 4. Schematic example of in situ polymerization process involving the synthesis of nylon-6/clay nanocomposites. Reproduce from [19] 10
Figure 5. Polypropylene structure. Reproduced from [40] 12
Figure 6. Structure model of C60 molecule. 13
Figure 7. Roll-up of a graphene sheet leading to three different types of SWCNTs. Reproduced from [55] 15
Figure 8. Multi-walled carbon nanotubes. Reproduced from [57] 16
Figure 9. Schematic view of graphite layered structure. reproduced from [88] 19
Figure 10. Schematic illustration of the preparation of expended graphite from natural graphite flakes: solid lines denoted graphite sheets. Reproduced from [101]. 21
Figure 11. Structure of graphite oxide. Reproduced from [125]. 23
Figure 12. Schematic representation of the polymerization techniques. Reproduced from [143]. 26
Figure 13. Schematic representation of the process flow of PP/Graphene nanocomposites and the test samples before and after applying force. Reproduced from [147]. 27
Figure 14. Typical hysteresis loop. Reproduced from {157]. 29
Figure 15. The magnetic domains and the magnetization of ferromagnetic material in the presence of external magnetic field. 31
Figure 16. Diagrammatic presentation of the tube. 35
Figure 17. Graphene oxide synthesis and thermal reduction. 37
Figure 18. Schematic representation of the synthetic rout of polymer nanocomposites. 38

List of Tables

Table 1:Comparison between SWCNT and MWCNT. Reproduced from [58] *14*
Table 2:Type of CNT and its Young's Modulus reported in the literature. *18*
Table 3:Solvent and reagents used. *34*
Table 4:Resume of magnetic and conductive properties of the synthesized nanocomposites. *46*

Abbreviations

ASTM:	American standard of testing materials
aPP:	Atactic polypropylene
CNTs:	Carbon nanotubes
CVD:	Chemical vapor deposition
CNF:	Carbon nanofiber
DSC:	Differential scanning calorimetry
DMA:	Dynamic Mechanical Analysis
DC:	Direct current
EP:	Ethane/Propene
GNP:	Graphene nanoplatelets
GIC:	Intercalated graphite
GPC:	Gel permeation chromatography
HDPE:	High density polyethylene
HOPG:	Highly oriented pyrolytic graphite
H_c:	Coercive
iPP:	Isotactic polypropylene
ICP:	Inductive coupled plasma emission spectroscopy
LDPE:	Low density polyethylene
LLDPE:	Liner low density polyethylene
MAO:	Methylaluminoxane
MWCNTs:	Multi walled carbon nanotubes
Ms:	Saturation magnetization
M_R:	Residual magnetization
NPs:	Nanoparticles

PE:	Polyethylene
PP:	Polypropylene
SEM:	Scanning electron microscopy
sPP:	Syndiotactic polypropylene
SWCNTs:	Single walled carbon nanotubes
SSBM:	Solid state ball milling
TEM:	Transmission electron microscopy
TGA:	Thermogravimetric Analysis
TRGO:	Thermally reduce graphene oxide
UHMWPE:	Ultrahigh molecular weight polyethylene
VSM:	Vibrating sample magnetometer
XRD:	X-ray diffraction

Abstract

In this present thesis polyethylene (PE) and polypropylene (PP) conductive and magnetic nanocomposites were synthesis by *in situ* polymerization using metallocene catalysts, bis(n-butyl cyclopentadienyl) zirconium dichloride [$(nBuCp)_2ZrCl_2$] for ethylene polymerization and *rac*-ethylene bis(indenyl) zirconium dichloride[*rac*-$Et(Ind)_2ZrCl_2$)] for propylene polymerization and methylaluminoxane (MAO) as a co-catalyst. The preparation of PP magnetic and conducting nanocomposites was also done by melt mixing method. The fillers used were carbon nanotubes with iron nanoparticles, reduced graphite oxide and activated carbon with nickel encapsulated. The carbon nanotubes (CNT), were obtained by two approaches, (i) chemical vapor deposition method (CVD) using ferrocene as the precursor and catalyst and high surface area silica (SiO_2) as support of synthesis, (ii) pyrolysis of sawdust from the furniture industry. Reduced graphite oxide (rGO) was obtained from oxidation of the flakes using a modified Staudenmaier method and thermal reduction. The nickel activated carbon (Ni-C) was obtained by microwave assisted pyrolysis. The catalytic activities of the *in situ* polymerization of ethylene or propylene were high hence no deactivation of the catalysts was observed. The fillers were well dispersed in the polyethylene and polypropylene matrices as evidenced by scanning electron microscopy (SEM) and transmission electron microscopy (TEM). Only small amounts of magnetic fillers, 0.8 - 0.9 wt.%, changed the diamagnetic polyethylene and polypropylene matrixes into ferromagnetic polymers at room temperature. The addition of the 2.4 wt.% of rGO or 3.8 wt.% of CNT changes the insulating polyolefin matrices to semi-conductors. The thermal stability of the nanocomposites investigated by thermogravimetric analysis and differential scanning calorimetry showed an enhancement in the maximum degradation, crystallization and melting temperatures as compared to the neat polymer. The elastic modulus was enhanced by the presence of the fillers. Some fillers decreased the permeability towards oxygen. The novelty of the work was the production of thermoplastics with all the same or higher outstanding properties of the original matrixes increased of magnetic and conducting properties with the use of a small amount of the filler. The outstanding properties of the nanocomposites are attributed to the use of the two techniques, namely the encapsulation of iron in the CNT which protect iron particles from easy oxidation, secondly the *in situ* polymerization which guarantee the uniform dispersion of the filler in the polymer matrix. There were also tested two fillers that can be considered eco-friendly because they come from waste.

Resumo

Na presente tese, nanocompósitos condutores e magnéticos de polietileno e polipropileno foram sintetizados pela polimerização *in situ* utilizando o catalisador de metalocênico dicloreto de bis(n-butil ciclopentadienil) zircônio [$(nBuCp)_2ZrCl_2$] na polimerização de etileno e [*rac*-etileno bis (indenil) zircônio (*rac*-Et $(Ind)_2ZrCl_2$)] na polimerização de propileno e metilaluminoxano (MAO) como co-catalisador. A preparação de nanocompositos magnéticos e condutores de PP também foi feita por meio do método de mistura em fusão. As cargas utilizadas foram nanotubos de carbono com nanopartículas de ferro, óxido de grafite reduzido e carvão ativado com níquel encapsulado. Os nanotubos de carbono (CNT) foram sintetizados por dois método: i) deposição química de vapor (CVD) utilizando ferroceno como precursor e catalisador e sílica de alta área superficial (SiO_2) como suporte de síntese, ii) pirólise da serragem da indústria moveleira. O óxido de grafite reduzido (rGO) foi obtido a partir da oxidação dos flocos usando o método de Staudenmaier modificado e redução térmica. O carbono ativado com níquel (Ni-C) foi obtido por pirólise assistida por microondas. As atividades catalíticas da polimerização *in situ* de etileno e propileno foram altas, portanto, nenhuma desativação dos catalisadores foi observada. As cargas foram bem dispersas nas matrizes de polietileno e polipropileno, como evidenciado por microscopia eletrônica de varredura (SEM) e microscopia eletrônica de transmissão (TEM). Apenas pequenas quantidades de nanopartículas magnéticas, 0,8 - 0,9% em peso, alteraram as matrizes diamagnéticas de polietileno e polipropileno em polímeros ferromagnéticos à temperatura ambiente. A adição de 2,8% em peso de rGO ou 3,8% em peso de CNT altera as matrizes isolantes de poliolefina para semi-condutores. A estabilidade térmica dos nanocompósitos investigados por análise termogravimétrica e calorimetria de exploratória de varredura mostrou um aprimoramento na temperaturas máxima de degradação, cristalização e fusão em comparação com o polímero puro. O módulo elástico aumentou pela presença da cargas. Alguma nanopartículas diminuíram a permeabilidade em relação ao oxigênio. A novidade do trabalho foi a produção de termoplásticos mantendo ou melhorando as propriedades das matrizes originais e incrementando propriedades magnéticas e condutoras com o uso de uma pequena quantidade de nanopartículas. As propriedades notáveis dos nanocompósitos são atribuídas ao uso principalmente de duas técnicas, isto é, o encapsulamento de ferro nos CNT que protege as partículas de ferro da oxidação, e também a utilização da polimerização *in situ* que garante a dispersão uniforme da carga na matriz polimérica. Também

foram testados dois enchimentos que podem ser considerados ecológicos porque provêm de resíduos.

1. Introduction

Polyethylene (PE) and polypropylene (PP) are the most important polyolefins due to their low cost, good processability, lightness and recyclability. Moreover, they are also non toxic, biocompatible, and resistant against chemicals. There is also possibility to improve or impart new properties to polyolefins for new applications.[1]An alternative is the use of uniform dispersion of nanofillers to enhance the gas barrier, mechanical and rheological properties.[2] The polymeric nanocomposites are considered, scientific and technological, interesting materials, obtained from polymer and organic or inorganic fillers with nanometric scale.[3]

The introduction of carbon nanotubes (CNT) in 1991 by Iijima, attracted much attention. Ajayan *et al* in 1994 reported the first polymer nanocomposites using carbon nanotubes as filler to improve thermal, electrical and mechanical properties of the polymer. Earlier work was concentrated in the use of carbon black, silica, clays, and carbon nanofiber (CNF) as fillers.[4] The tremendous properties of CNT such as, high flexibility, low mass density, and high aspect ratio (100-300) in addition to their excellent mechanical, thermal and electrical properties, have turned them into potential candidates to create multifunctional polymer nanocomposites.[5] One of the difficulties that the researchers face during the preparation of CNT polymer nanocomposites, is the homogenous dispersion of the nanotubes in the polymer matrix. To transfer the exceptional properties of the CNT to the polymer matrix, two key aspects must be taken in consideration. First, the CNT must be homogenously dispersed through the polymers; secondly a degree of interaction between the macromolecular chains and the CNT must be present.[6] Different methods have been used to overcome these difficulties. Solution blending, melt blending, and *in situ* polymerization are widely used techniques.[7] The *in situ* polymerization is even more attractive when metallocene catalysts are used for the polymerization of olefins, because of their unique catalytic properties, such as, high activity, molecular weight and polydispersity control, besides perfect control of the polymer microstructure, which is not observed in traditional catalytic systems. [8]

On the other hand, both the academic and industrial researchers are extensively involved in exploring the magnetic nanocomposites. The magnetic properties can be obtained by the incorporation of magnetic elements such as iron,[9] cobalt, [10] and nickel.[11] In spite of the fact that metallic Fe nanoparticles present the most convenient magnetic properties, it is very difficult to

protect them from easy oxidation. In the aim to prevent oxidation, different protective layers or encapsulation of iron nanoparticles into a non-magnetic carbon shell have been applied. [12]

Similarly, the importance of graphene in many technological fields such as electronics, energy storage and conversion, sensors, capacitors, and composites materials triggered enormous attention.[13] Graphene with only one atom thick is the strongest material known. The professors of the University of Manchester, Andre Geim and Konstantin Novoselov[14] received the Nobel Prize of Physics in 2010 for their innovative experiments on this material.[15] Graphene is 200 times stronger than steel and conducts electricity at room temperature faster than any other material known, it is almost completely transparent (97.3%) and extremely lightweight. A wide variety of applications of graphene seems possible, including the creation of new materials and manufacturing of innovative electronic products.

The present work aims to obtain nanocomposites of polyethylene and polypropylene with iron encapsulated in carbon nanotubes (PE-CNT-Fe and PP-CNT-Fe) and nickel activated carbon (PE-Ni-C), through *in situ* polymerization using metallocenes ($(nBuCp)_2ZrCl_2$ and (*rac*-$Et(Ind)_2ZrCl_2$)) as catalysts and methylaluminoxane (MAO) as a co-catalyst and by melt mixing technique. The main objective is to obtain a multifunctional material with magnetic and electrical properties.

2. Objectives

2.1. General Objective

The basic objective of the work is the production of conductive and magnetic materials with good processability using conducting and magnetic nanometric fillers immobilized in a polyolefinic matrix.

2.2. Specific Objectives

- Study of the synthesis of carbon nanotube/polyolefin nanocomposites by in situ polymerization using metallocene catalyst to obtain a magnetic material
- Study of the synthesis of carbon nanotube/graphene /polyolefin nanocomposites by *in situ* polymerization using metallocene catalysts to obtain a magnetic and electric material.
- Uses of other magnetic and conductive fillers.
- Comparison with the melt-mixing method for preparation of nanocomposites.
- Study of the thermal, mechanical, magnetic and electrical properties of all the materials produced.

2.3. Structure of the thesis

The thesis was structured according to the resolution N° 093/2007, of 12/06/2007 of the post-graduation assembly of the Federal University of Rio Grande do Sul (UFRGS) in the form of scientific articles. The assembly established the guidelinehs for the publication and writing of Ph. D thesis. In this regards the thesis was structured as follow.

1. **General introduction:** brief presentation of the background, the scope and the objective of the thesis.

2. **Literature review:** review the literature related to the polymer and their nano composites, the production techniques according to their usefulness. Nanofillers and the common methods used for their preparation. Hence, carbon nanotubes, graphite derivates and carbon activated which were used as fillers and polyethylene and polypropylene as polymer matrix were discussed in detail.

3. **Experimental part:** describes the methods used in this work for the preparation of the carbon nanotubes, reduced graphite oxides and nickel activated carbon as well as the method for the preparation of the polymer nanocomposites. The advanced techniques used to characterize the synthesized materials, the analytical techniques to determine the iron amount encapsulated in the carbon nanotubes and also the amount of zirconium in the supported catalyst method were also described.

4. **Conclusion and future plans:** Summarized the major results obtained in this work and future plans.

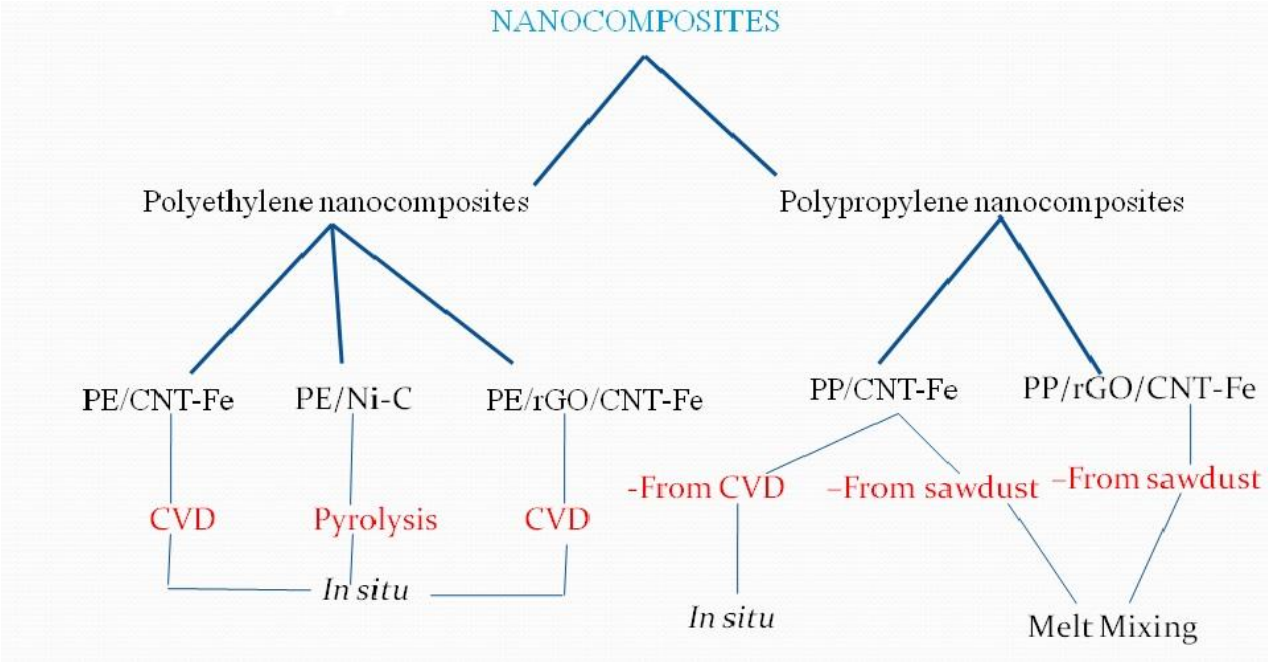

Schematic diagram of synthesized nanocomposites

5. **Annex 1:** describes the preparation and characterization of the polyethylene magnetic nanocomposites by *in situ* polymerization using commercial and synthetic carbon nanotubes (CNT-Fe). Ferrocene was used as precursor of synthesis and high surface area silica as substrate for the nucleation of CNT. Polymer nanocomposites were obtained using the metallocene, $(nBuCp)_2ZrCl_2$, as catalyst combine with methylaluminoxane (MAO) as co-catalyst. The presence of iron nanoparticles in the carbon nanotubes turned the polyethylene matrix from diamagnetic to ferromagnetic with only 0.9 wt% of the filler. Several characterization techniques were used to see the effect of the filler on the polymer matrix, including transmission electron microscopy, scanning electron microscopy, thermal analysis, gel permeation chromatography and magnetic characterization.

6. **Annex 2:** demonstrate the study related to the preparation of polypropylene (PP)/CNT-Fe nanocomposites using the metallocene, *rac*-$Et(Ind)_2ZrCl_2$,as catalyst and MAO as co-catalyst by *in situ* polymerization. Chemical vapor deposition (CVD) was used as synthetic route for the

production of carbon nanotubes using ferrocene and silica. Several characterizations were used to see the effect of the synthetic filler on the different properties. It was optimized that 0.8 wt% of the CNT-Fe were enough to change the PP to a ferromagnetic material, and the electrical percolation threshold lied between 3.0 wt% and 3.8 wt% of the filler. It was also evaluated that the synthesized material was ferromagnetic at room temperature. The dispersion of the filler in the polymer matrix was evaluated by scanning electron microscopy and transmission electron microscopy. The thermal properties were also investigated.

7. **Annex 3:** presented the synthesis of the semi conducting and magnetic polyethylene nanocomposites by using the combination of two carbon based fillers (rGO and CNT-Fe) by supported catalyst method. It was clear from the **annex 1** and **annex 2** that a very small amount (0.8 wt%) of the magnetic filler (CNT-Fe) was enough to produce the magnetic properties in the PE and PP matrixes but to obtain conducting properties the amount of CNT-Fe must be quite higher (3.8 wt.%). As the CVD technique to produce the CNT-Fe is time consuming, the combination of two fillers was used to produce both magnetic and conducting properties in the PE matrix with possible minimum filler loading. For this purpose to develop a new idea for the production of magnetic material with conductive properties a small amount of the CNT-Fe was used for magnetic properties and the conductive network was produced by the use of the reduced graphite oxide (rGO). The synthetic route of rGO is more convenient and cost effective as compared to the CNT-Fe one. The material was characterized by several techniques to see the effect of the combination of these two filler on the properties.

8. **Annex 4:** shows the effect of nickel activated carbon based magnetic fillers on different properties of polyethylene nanocomposites, using the filler range from 0 to 8.5 wt %. The nanocomposites were also prepared by *in situ* polymerization. The nickel-carbonized material was prepared from biomass by the pyrolysis of wood sawdust. The nanocomposites thermal stability was investigated by thermogravimetric analysis (TGA) and differential calorimetric analysis (DSC). The addition of the Ni filler resulted in a ferromagnetic behavior of the polyethylene nanocomposites. The mechanical properties showed an improvement, mainly with the higher amount of the filler.

9. **Annex 5 and 6:** presents the synthesis of Polypropylene (PP) magnetic and conducting nanocomposites by melt mixing method. The carbon nanotubes containing iron encapsulated

(CNT-Fe) were synthesis by the pyrolysis of sawdust from the furniture industry. The polymer matrix was changed to ferromagnetic with the addition of very small amount of the magnetic filler (0.5 wt%). The mechanical, thermal and gas barrier properties were improved as compared to the neat polymer. As a small amount of the CNT-Fe was sufficient to produce magnetic properties in the PP matrix, to introduce both magnetic and conducting properties, simultaneously, the reduced graphite oxide was introduce together with the CNT-Fe to form PP-rGO-CNT-Fe nanocomposites. Different characterizations techniques show the improvement in the properties of the polymer matrix, these are outstanding results to produce a low-cost thermoplastic with both magnetic and conducting properties.

3. Literature Review

3.1 Polymer nanocomposites:

Polymers can be defined as macromolecules composed of one (homopolymer) or various types (copolymer) of long chains formed by units named monomers. In the last decades, polymeric nanocomposite materials have been extensively reported in the scientific literature, due to the enhancement of certain properties even at very low loading of nanoparticles. Polymeric nanocomposites are materials consisting of two or more phases, where at least one phase is in nanoscale and the major phase is a polymer. Materials are considered nanoscales, when at least one of the external dimensions is in the range from 1 nm to 100 nm.[16,17] The synthetic routes to obtain polymeric nanocomposites are: melt intercalation, template synthesis, exfoliation adsorption, and *in situ* polymerization.[17-23] Three types of microstructure can be obtained, depending upon the method and materials used as can be seen in Figure 1..

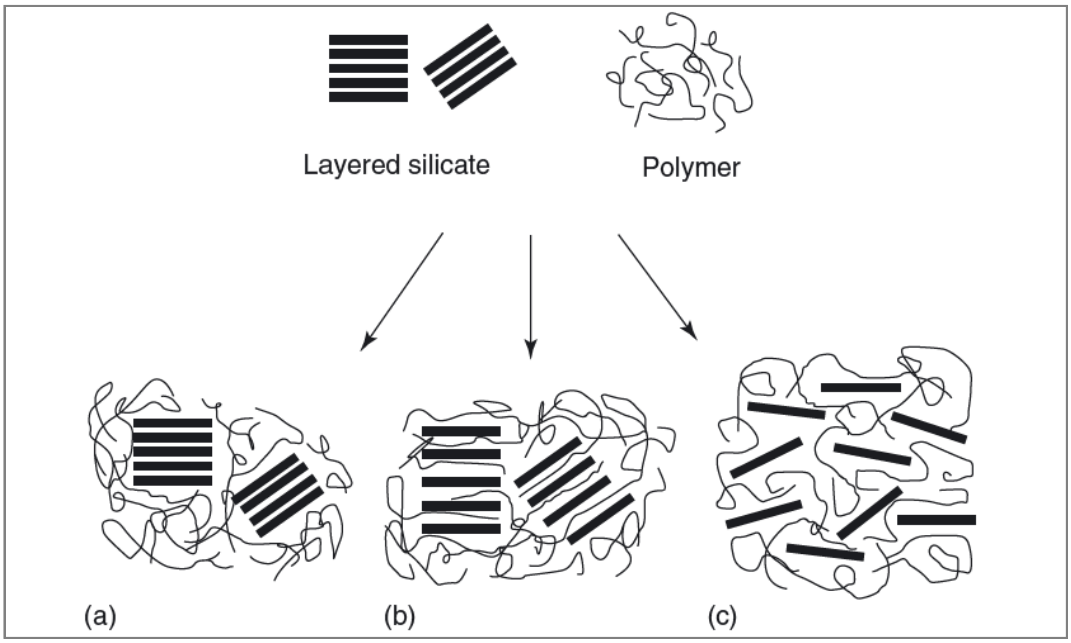

Figure 1. Types of composites microstructure:(a) Unintercalated (b) Intercalated (c) Exfoliated. Reproduced from [23].

Melt intercalation is the method most widely used because it is an environmental friendly process due to the lack of solvent. It involves the melting of the polymer at high temperatures,

the addition of the filler, and finally the manipulation of the composites to achieve uniform distribution of the filler. In addition it is consider more economical and compatible with industrial process such as injection molding and extrusion. However, the disadvantage of the technique is the damage of some fillers which decompose at temperatures higher than 140 ℃. Whereas, the processing temperature of the melt intercalation technique is in the range of 190-220 ℃.[20]

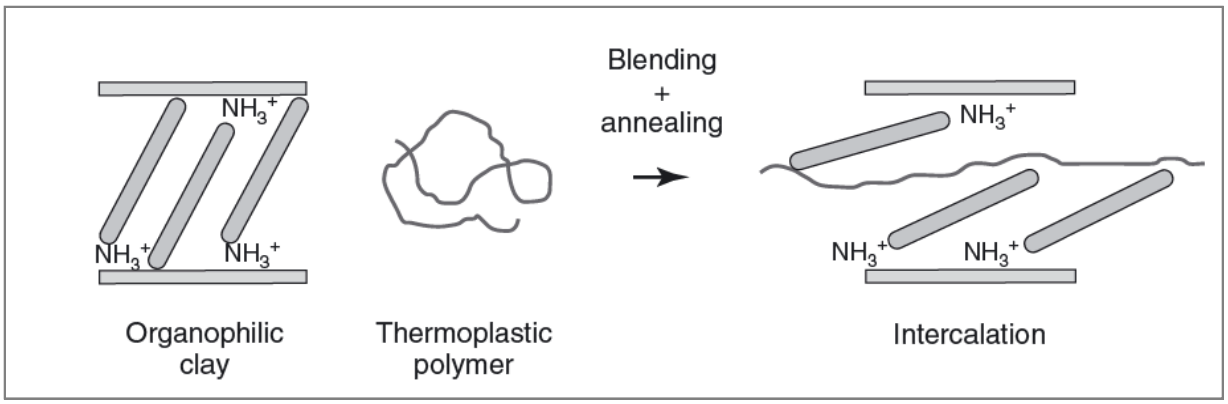

Figure 2.The melt intercalation process. Reproduced from [20].

Template synthesis, also known as sol-gel technology is mostly developed for double-layered hydroxide based nanocomposites. The handicap of the process includes the high temperature which degrades the polymer chain and the high tendency of filler aggregation, which make this process less common. [23]

Exfoliation adsorption, also known as polymer intercalation from solution is based on the solubility of the polymer in a solvent. The filler is first swollen and dispersed in the solvent and then it is mixed into the polymer solution. Ultimately, the solvent is removed and a multi layered structure trapped in the polymer chain is formed; this approach is widely used for water soluble polymers. [19,22,23]

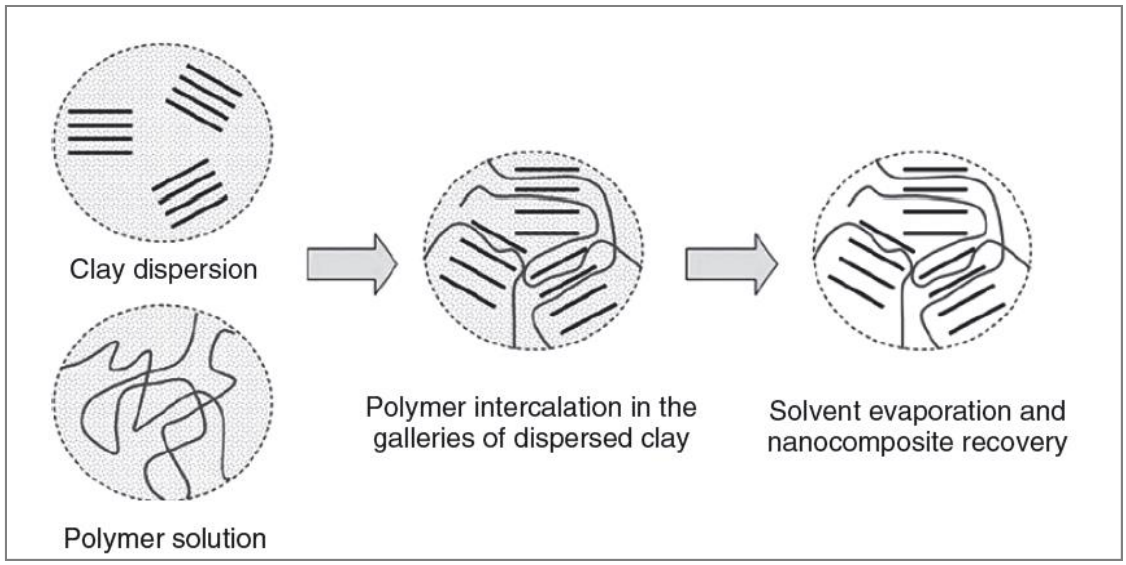

Figure 3. The exfoliation adsorption process. Reproduced from [20].

In situ polymerization involves the direct incorporation of the filler during the polymerization of the monomer. This process has the advantage of a single step polymerization, where the filler is introduced directly to the low molecular weight monomer. The monomer polymerizes in between the interlayer producing a more exfoliated structure. This approach provides an easy way to produce more uniform dispersion of the filler as compared to conventional melt mixing approach. In Figure 4 the synthesis of nylon-6/clay nanocomposites by *in situ* polymerization is illustrated. [21,22,23]

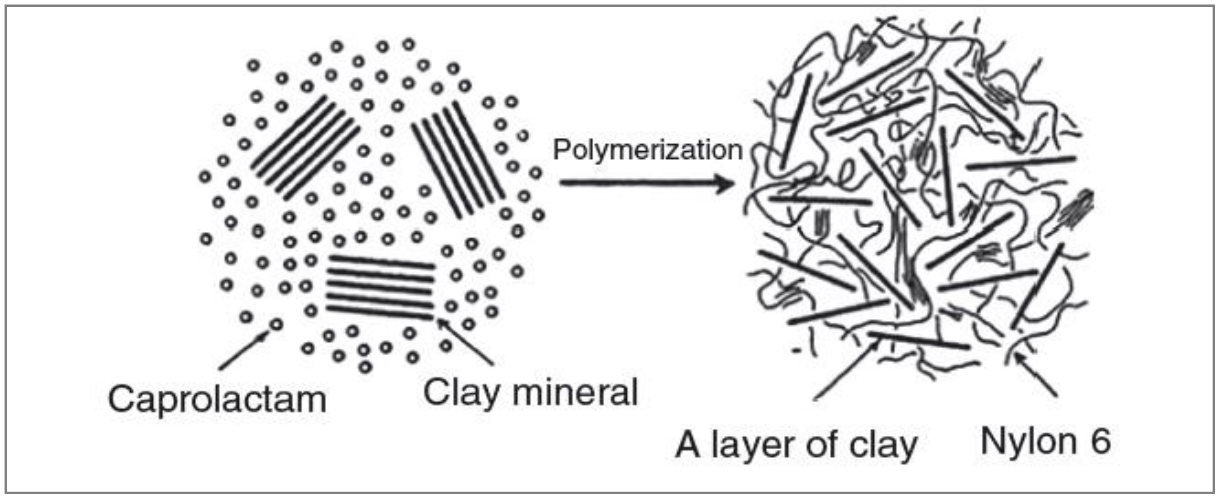

Figure 4. Schematic example of in situ polymerization process involving the synthesis of nylon-6/clay nanocomposites. Reproduce from [19].

3.2 Polyethylene (PE)

Polyethylene is semi-crystalline polymer and due to its low cost, easy processing, recyclability, and versatility it is one of the principal polymers produced worldwide. [24] The first high pressure high density polyethylene (HDPE) was synthesis in 1950, then, with the discovery of transition metal catalysis, the production of low pressure HDPE became possible.[25] The PE exist in different forms depending on the chain structure, density level and crystallinity. As mostly mention in the literature these are high density polyethylene (HDPE), low density polyethylene (LDPE), liner low density polyethylene (LLDPE), ultralow density polyethylene (ULDPE), and ultrahigh molecular weight polyethylene (UHMWPE). [26]Previously the classification of polyethylene was on the basis of manufacturing processes either produced by high pressure or low pressure.

Polyethylene (PE) is the most broadly used polymer and has a combination of many practical properties: light weight, low cost, high chemical resistance, low dielectric constant and good processability, etc. [28] Among PEs, high-density polyethylene (HDPE) has low affinity toward the chemical attacks, its permeability toward water and inorganic bases is lower and does not react with organic acids, salts and alkaline solutions. [29] The HDPE stand for high crystalline structure and high molecular weight, which results high tensile strength and low branching. The gases barrier properties, thermal stability, and electrical conductivity of the HDPE can be improved by various techniques to broaden its application. [30]

Due to the low cost and low energy consumption during the processing, HDPE resin are consider the ideal materials for many application, such as shopping bags, films, pipes and bottles.[31]Moreover, the HDPE has the ability to resist corrosion, as well as moisture, acids, alkalis and the majority of solvent at room temperature. [32] HDPE pipes have a wide range of application for the transportation of low pressure material (water, gas).[33] In injection molding HDPE is molded at temperature 200-260ºC and pressures of 70-140 MPa.[34] Blow mold articles are one of the largest uses of HDPE. It is widely used for food packaging application. HDPE is rigid, resistant and the softening temperature is high, which helps in the film formation.[35] Rolled hallow film of HDPE is used for shopping bags. It has a wide variety of application in wire, cable encapsulation, communication, and power control.[36]

3.3 Polypropylene (PP):

Polypropylene is a flexible thermoplastic, which is form by the successive combination of the propene monomers by the chemical reaction called polymerization. Due to its low cost, easy processability, recyclability, thermal stability, and intrinsic properties such as low density, high stiffness, good tensile strength, and inertness toward acids, alkalis and solvent make it one of the more commercially used polymers. [37-39]

Isotactic polypropylene was first discovered in 1954 and rapidly became very popular to have the lowest density of the commodity plastics.[40,41] Furthermore its exceptional resistance to chemicals, PP can be processed by different converting methods, for instant injection molding and extrusion. The resistance to relatively higher temperature broadens the application of PP in various public sector uses, such as the carboy, trays, funnels, pails, bottles, and the trays for instrument in the clinical environment which need to be sterilized frequently. Polypropylene is a vinyl polymer where each carbon is attach to a methyl group as shown in the Figure 5.[41]

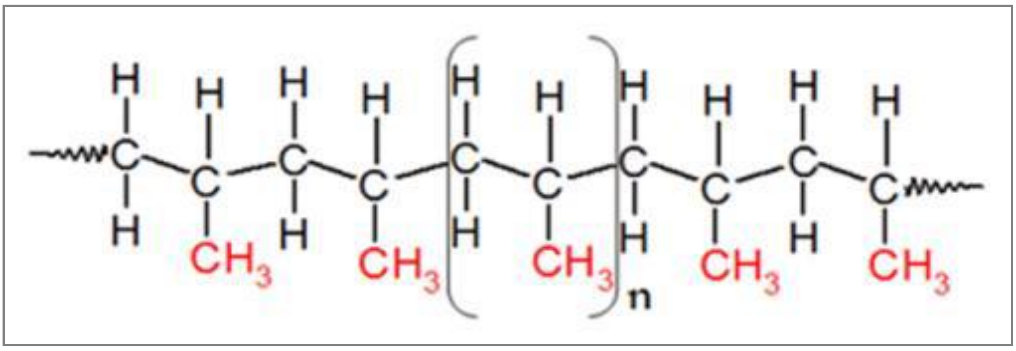

Figure 5. Polypropylene structure. Reproduced from [40].

Depending on the synthesis, PP can present three types of stereoisomers, which differ with relation to the methyl position.[42]

-Isotactic (iPP): All the methyl are on the same plan, this polymer has a high crystallinity. iPP has excellent mechanical properties, such as, tenacity, rigidity and impact resistance, and a high thermal stability.

-Syndiotactic (sPP): The methyl alternates the position on both sides of the principal chain. This turns this polymer less crystalline than iPP. On the other hand, sPP is less rigid and is less thermally stable, thus have more transparency and flexibility.

-Atactic (aPP): The position of the methyl is random, which turns this polymer more amorphous. Thus this polymer is soft and sticky and it can be used in adhesives and water proofing.

The structure of polypropylene is an important factor to determine the future application since the tacticity directly interferes in their final properties. iPP due to the good chemical resistance, low density (~0.9 g/cm^3) and high melting point (~165^{0}C) it is used principally for packaging, molded articles by blowing and injection (bottles, chairs, buckets) fibers and fabrics.[43]

3.4. Carbon nanotubes

In 1985 the discovery of a new material which opened a new area of research in carbon based materials was published by the journal Nature. [44] The structure of this material referred to carbon cage molecules known as fullerenes. The most stable fullerene molecule consists of 60 carbon atoms (C60) and is similar to a soccer ball, exhibiting hexagonal and pentagonal faces (sp^2 hybridization) as it is shown in the Figure 6.

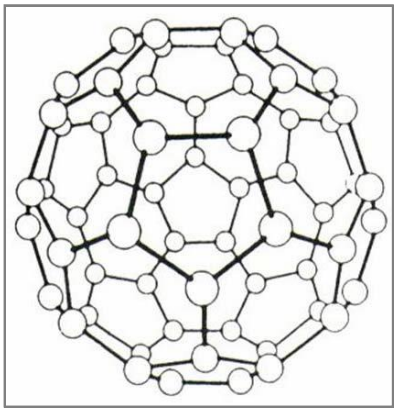

Figure 6. Structure model of C60 molecule.

In 1991, Sumio Iijima, found graphene cylinders deposited on the cathode, while he was working on producing C60 by arc discharge method and gave them the name of carbon nanotubes.[45]Carbon nanotubes (CNT) are, thus, composed of rolled-up co-axial graphene sheets closed by fullerene hemispheres. CNT belong to the fullerene family, fullerene are spherical buckyballs whereas CNTs are cylindrical. The main body of an ideal CNT is formed of carbon atoms exhibiting sp^2 hybridization, whereas the end caps have the buckyball structure. The

amazing fact connected to the properties of the nanotubes is their dependence on the shape. [46] CNT attracted the attention of the scientific community short after its discovery. In fact many physicists and chemists were surpassed by their physico-chemical properties. The diameter and the chirality are the most important factors for the electronic properties of CNT, and either can show the semiconductor or metallic behavior, in spite of, the CNT always exhibits conductive properties.[47, 48] Moreover, the excellent longitudinal Young's modulus combine with transversal flexibility and high aspect ratio made them the core of interest for the composite materials community. [49-51]

3.4.1 Types of Carbon nanotubes:

Carbon nanotubes can be divided into two categories on the bases of the tubes present in the CNT, as single walled CNT (SWCNT), and multi walled CNT (MWCNT).[52] The difference between these two structures are reported in Table 1.

Table 1:Comparison between SWCNT and MWCNT. Reproduced from [58]

SWNTS	MWCNTs
-Single layer of graphene.	-Multiple layers of graphene.
-Required proper control over atmospheric conditions and growth, bulk synthesis is difficult.	- Bulk synthesis is easy.
-The dispersion is difficult and form bundle structure.	-Homogenously dispersed with no apparent bundle formation.
-Catalyst is required for synthesis.	-Can be synthesized in absence of catalyst.
-Resistivity ranging from 10^{-4}-$10^{-3}\Omega$.m.	-Resistivity ranging from 1.8×10^{-5}-$6.1\times10^{-5}\Omega$.m.
-During functionalization the chance of defect is high.	-The chance of defect is less particularly when synthesizes by arc-discharge method.
-Easy characterization and evaluation.	-More complex structure.
-Low purity.	-High purity

3.4.1.1 Single-walled CNT:

A SWCNT is a tubular shell of graphene sheet roller up around itself, which is benzene type of hexagonal structure of carbon atoms with diameters ranging from 2 to 50 nm and the length can vary depending on the synthesis method.[52-54] As it is clear from the Figure 7, SWCNT shows three chiralities: armchair, zig-zag, and chiral, based on the orientation of the tube axis with respect to the hexagonal lattice.[55]

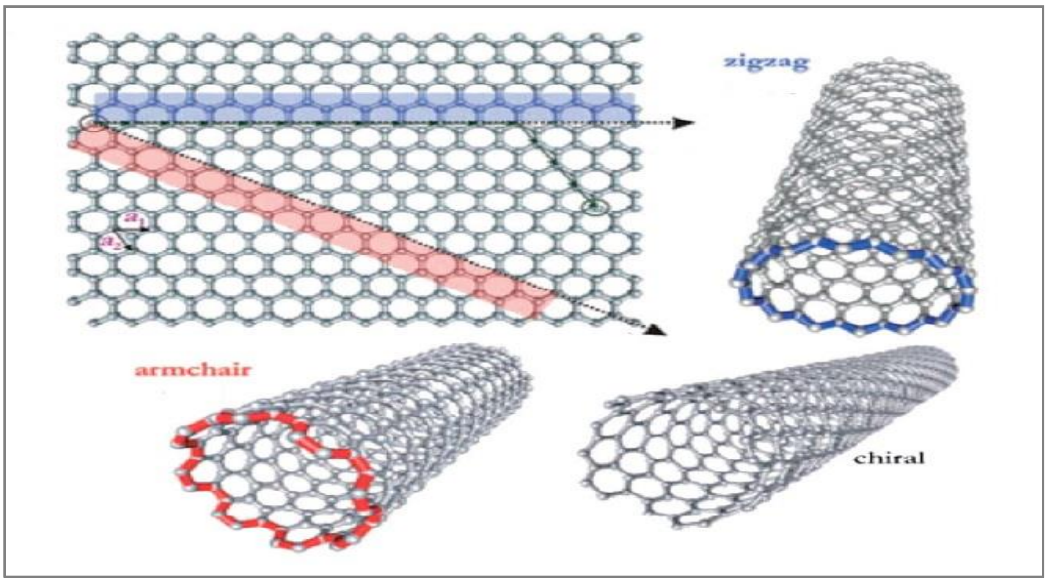

Figure 7. Roll-up of a graphene sheet leading to three different types of SWCNTs. Reproduced from [55].

3.4.1.2 Multiwalled carbon nanotubes:

MWCNT consist of multiple layers of graphene rolled upon itself with diameters ranging from 2 to 50 nm depending on the number of graphene tubes. These tubes have an approximate inter-layer distance of 0.34 nm. [56]

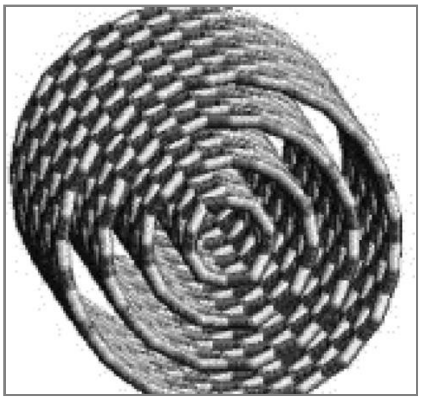

Figure 8. Multi-walled carbon nanotubes. Reproduced from [57].

3.4.2 Synthesis of carbon nanotubes:

As mention above the MWCNT were first discovered in the soot of the arc-discharge method by Iijima.[45] It took two more years, after the discovery, for the synthesis of SWCNT by the use of metal catalyst in the arc-discharge method be reported.[59, 60] Soon after, significant progress was made by laser ablation and chemical vapor deposition methods. [61, 62] The detail of the methods of synthesis of CNT is discussed below.

3.4.2.1 Arc-discharge method:

In 1991 Iijima reported the existence of new type of tubular shaped species using an arc-discharge evaporation method similar to the used for the production of fullerene synthesis.[45] The structure consisted in needle like tubes having a diameter of 4 to 30 nm and length of 1mm.These tubes were grown on the negative end of a carbon electrode using the direct current (DC) arc-discharge evaporation of carbon in an argon filled vessel (100 torr).[63] The arc-discharge chamber consisted of two electrodes installed vertically in the center of the chamber. Iijima used a mixture of 10 torr methane and 40 torr argon gas. The lower electrode which serves as cathode has a shallow dip to hold a small piece of iron during the evaporation. The application of the DC current of 200 A at 20 V between the two electrodes generates the arc-discharge. Methane, argon, and iron were the three critical component used for the synthesis of the SWCNTs. In the arc-discharge method other researchers used different electrodes, current, and pressure of helium atmosphere.[60,64]

3.4.2.2 Laser ablation:

In 1996, Thess *et al.* produced high yield (>70%) of SWCNTs by means of laser ablation methods, where the vaporization of the graphite rod take place at 1200 ^{0}C using small amount of Ni and Co.[61] The tube grows until too many catalyst aggregate on the end of the nanotubes. The large particles detach or become over-coated with sufficient amount of carbon to poison the catalyst. This allows to terminates the tube with a fullerene like tip or with a catalyst particle.[63]

3.4.2.3 Chemical vapor deposition (CVD):

In the above mentioned techniques there are two major problems, that is, the large scale production and the control on the growth direction. However, in 1996, a new method called CVD was introduced for the nanotubes synthesis, that has the advantage to control the directional growth and enables the large scale production.[65,66] During this process a mixture of hydrocarbon gases or other carbon source is introduced to the reaction chamber, in the presence of catalyst, at less than 1200 ^{0}C and at atmospheric pressure.[67] This technique have two main advantages, the lower temperature synthesis and the deposition of the catalyst on the substrate, which allows the CNT to adopt a well-organized structure.

3.4.3 Properties of carbon nanotubes:

The reports in the literature show the extremely high surface area, aspect ratio and remarkably high mechanical strength of the CNT. The electrical and thermal conductivities of CNT reaches that of copper, and the tensile strength is 100 times greater than that of steel.[68,69] These outstanding properties make CNT excellent candidates for polymer and ceramic composites to use as fillers.[70]

The unique conductive properties of CNT is greatly influenced by the geometrical differences such as defects, chirality, different diameters and the degree of crystallinity of the tubular structure.[71,72] SWCNTs are metals with resistivity that range from 0.34×10^{-4} to 1.0×10^{-4} ohm.cm.[73] CNT due to its electronic properties can be used in transistor and other switching application in advanced electronics. The most important recent application of the CNT is there use as lower voltage emitter.[52]

CNT are consider the strongest material existing in the nature, especially in the axial direction. [74] The Young's modulus and tensile strength range from 270-950 GPa, and 11-63 GPa

respectively. CNT show rather soft behavior in the radial direction as clear from several reports.[75] Treacy *et al.* reported an average Young's modulus of 1-1.8 TPa.[69] Table 3 reported some of the moduli measured in the literature. The differences in the measures of Young's modulus of the CNT depends on their diameter, crystallinity, helicity. [76-78]

Table 2:Type of CNT and its Young's Modulus reported in the literature.

Kind of CNTs	Young's Modulus	Reference
MWCNT	1.8±1.4 TPa	Treacy et al. [69]
MWCNT	0.91±0.18 TPa	Demezyk et al. [79]
MWCNT	1.72±0.64 TPa	Pan et al. [80]
MWCNT	1.28±0.59 TPa	Wong et al. [81]
MWCNT	1 TPa	Poncharal et al. [82]
MWCNT	0.91-1.24 TPa	Qi et al. [83]
SWCNT	1.24±0.45 TPa	Krishnan et al. [84]
SWCNT	45±7 GPa	Walter et al. [85]
SWCNT	1 TPa	Salvetal [86]

3.5 Graphite and Graphene:

Graphite is a metallic gray mineral found in nature in the form of flakes or powder with various particle sizes. Brazil is the third largest producer of graphite, preceded by China and India, possessing great natural reserves.[87] Graphite is a modification of carbon, like diamond and fullerene, which presents itself in the form of hexagonal crystals and layered structure. The structure consists of stacking planar layers within which each carbon atom has three nearest neighbors with sp^2 hybridization and C-C bond length of 1.42 Å. Each layer that composes graphite is formed by graphene sheets; the space between two graphene sheets is in the order of 3.35 Å, and between two graphite aggregates 7-16 Å, as may be seen in Figure 9.[88]

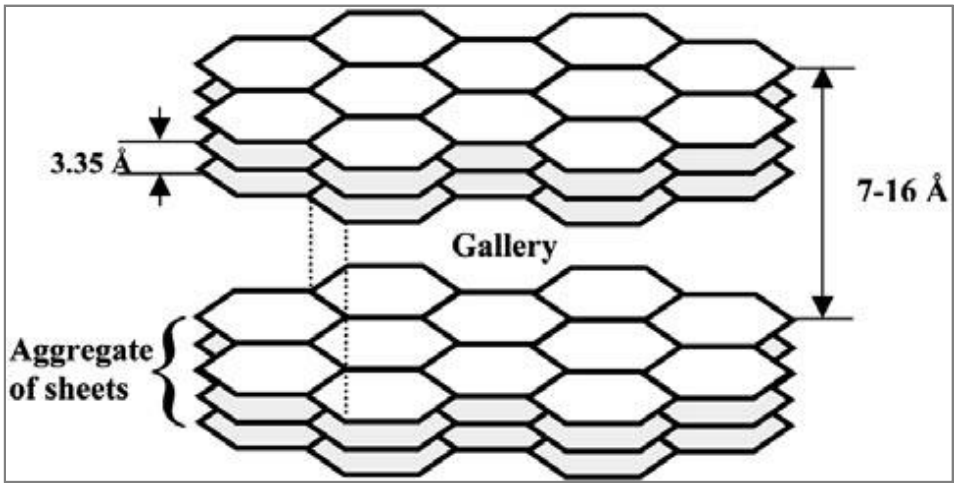

Figure 9. Schematic view of graphite layered structure. reproduced from [88].

The dominant role of the graphite in the electronic properties is due to the high mobility of the loosely bound л-electrons.[89]

The special structure of graphite makes it interesting for various applications such as electrical and thermal conductivity, excellent lubricating properties and resistance to high temperatures. The electrical and thermal conductivity of graphite is due to delocalized πbonds resulting from sp^2 hybridization; as well as the softness and the lubricating action are due to the weak connections between the graphene sheets, which facilitate the sliding of the sheets over each other.[88]

The industrial interest in graphite as a filler is increasing enormously in the recent decade. The intercalation and exfoliation of graphite produce the graphene. Graphene, a monolayer of sp^2–hybridized carbon atoms arranged in a two-dimensional lattice has attracted tremendous attention owning to its outstanding mechanical, thermal, and electrical properties. [90, 91] A single graphene layer has exceptional gas impermeability, specific surface area of ~2600 m^2/g, Young´s modulus of ~ 1.0 TPa and thermal conductivity of ~5000k/w k.[90]

The 2010 Nobel Prize in physics was received by Andre Geim and Konstantin Novoselov for their contribution to the study of the graphene properties and innovative experiments. They reported that graphene conducts electricity at room temperature higher than any other known materials and is 200 times stronger than steel. Further on, it is extremely light weight and highly transparent (97.3%), due to these tremendous properties a variety of application seems possible ranging from new materials and novel electronic products.[92]

3.5.1 Methods used to obtain graphene:

Currently graphene production routes include bottom-up and top-down processes. The bottom-up processes are related to the synthesis of the material, where as the top-down processes are related to fragmentation of the material until reaching the desired scale. In the bottom-up processes, graphene can be synthesized through several methods, for example, chemical vapor deposition (CVD) [93], epitaxial growth in insulating substrate [94], CO [95] reduction and arc discharge [96]method. These methods produce graphene free of defects, but have the disadvantage to obtain graphene on a very small scale, besides the complexity of synthesis and difficulty of purification. Thus the most feasible alternative to obtain graphene on a large scale is from the graphite commodity, either by its exfoliation or by treatment of its oxide.

3.5.1.1 Direct exfoliation of graphite :

This method also known as mechanical exfoliation, it was the procedure developed by Geim *et al.*[97] that led to the outstanding discovery of the graphene electronic and mechanical properties. In this method commercially available highly oriented pyrolytic graphite (HOPG) sheets were stuck onto a photo resist and peeled off layer by layer by scotch tape. The peeled off thin flakes were washed by acetone and transferred to a silicon wafer. It was reported that the thin flakes consisted of monolayer or few layer of graphene, such approach is limited for its low production.[98]

3.5.1.2 Exfoliation of treated graphite:

The chemical exfoliation method consists on the modification of the graphite structure by means of chemical and physical treatments. Usually the starting material used for the graphene or graphite synthesis with a small stacking of graphene layers is composed of intercalated graphite (GIC). The weak interaction of Van der Waals forces between layers, allows that chemical species occupy spaces between the graphene layer to form GIC. [99] One of the most used process for the formation of GIC is the mixing of graphite flakes with sulfuric and nitric acids.[100] as can be seen bellow.

$$n(\text{graphite}) + n(H_2SO_4 + 0.5n[O] \rightarrow n[\text{graphite}.\ H_2SO_4] + 0.5\ nH_2O$$

Where O is the oxidant and graphite.H_2SO_4 is the graphite intercalated compound (GIC).[101]
The resulting GIC contains carbon layers and the intercalating layers that stack one on top of the other in periodic fashion. The stacking can be on the form of C-C-I-C-C-I-C-C-I-C, where “C” is

the carbon layer and "I" is an interacting layer. The number of the carbon layers between each pair of intercalated layer is the stage number. For example the above structure is a stage 2, intercalated graphite. The stage structure of intercalated graphite depends to a great extend on the intercalation conditions. Stage 1 to 5 intercalated structures are produced if conventional intercalation conditions are apply.[101]

The rapid thermal treatment of GIC at high temperature (600-1000 °C) produces the volatilization of intercalates. As a result, the production of a light material takes place, which maintains the layer structure of natural graphite flakes and it is called expanded graphite (EG). [99.102] The exfoliated graphite flakes expand hundreds of times along their *c* axis. The original graphite flake of thickness 20 µm may expand to up to 20-20000µm. [101]

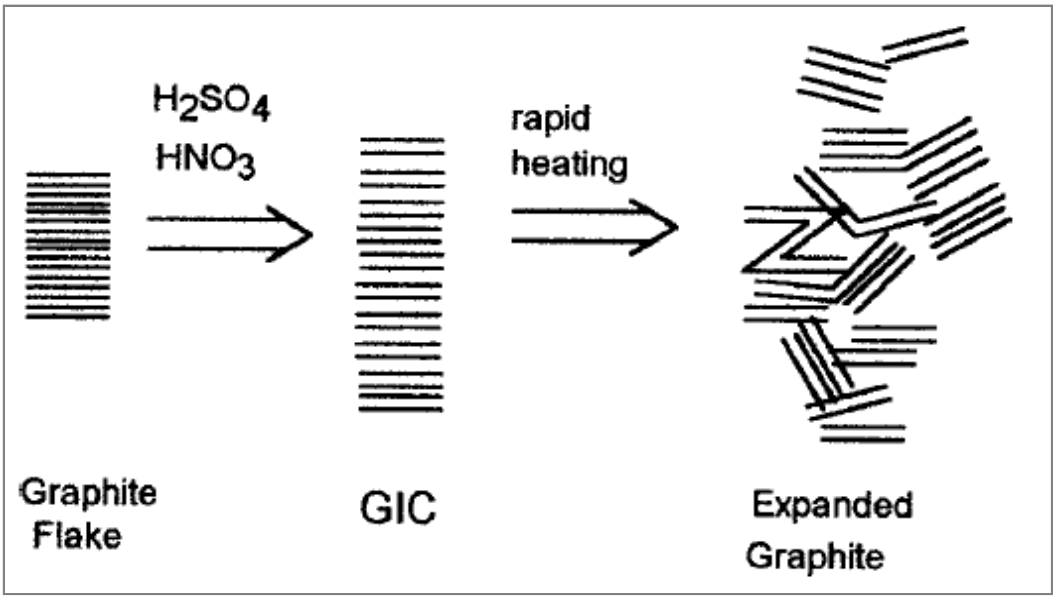

Figure 10. Schematic illustration of the preparation of expended graphite from natural graphite flakes: solid lines denoted graphite sheets. Reproduced from [101].

3.5.1.3 Graphite oxide (GO) treatment:

A large number of studies have been reported in the literature, dealing with the exfoliation of graphite via graphite oxide, due to high yield of monolayer sheets, with dimension up to hundreds of micron, that have the ability to dissolve in common solvents like water.[103-105] This method is based on the exfoliation and reduction of the graphene oxide for the large scale production of graphene. Graphene oxide can be considered as precursor for graphene synthesis by either chemical, thermal or microwave reduction process. Generally graphene oxide is produced by treating the graphite with strong acids and oxidizing reagents, such as H_2SO_4 and

HNO_3 as acids and $KMNO_4$, $NaClO_3$, $KClO_3$ and $NaNO_3$ as oxidizing agents, basically by the Brodie, [106] Staudenmaier, [107], Hofmann [108] and Hummers [109] methods as discussed below.

3.5.1.4. Brodie's oxidation method:

In 1859 B. C. Brodie developed the oxidation of graphite in the presence of fuming nitric acid and potassium chlorate ($KClO_3$),[106] and got a new compound containing carbon, oxygen and hydrogen which was confirm later on, as a result in an increase in the overall mass of the graphite flake.[110] Consecutive oxidative reactions resulted in an increase in the oxygen content reaching the maximum value after a number of reactions. After heat treatment at 220 °C the C:H:O composition of this material was 80.13:0.58:19.29 percent with the release of carbonic acid and carbonic oxide. These methods have several disadvantages as long reaction times as well as loss of toxic gases during reaction. However this method has been used by several research groups for the production of graphite oxide. [111-115]

3.5.1.5 Staudenmaier method:

The Brodies´ work was improved by Staudenmair in 1898 using excess amount of oxidizing agent and concentrated sulfuric acid as extra additive. [107] He added multiple aliquots of the potassium chlorate solution into the reaction mixture, and enhanced the acidity of the mixture by adding concentrated sulfuric acid (H_2SO_4). These changes led to the production of highly oxidized graphite oxide in a single reaction vessel, as a result it simplified the GO synthesis process. On the other hand, this method also has draw backs, such as time consuming and the release of hazardous gases such as chlorine dioxide. Although this method has been used by many researchers for the synthesis of graphite oxide.[116-118]

3.5.1.6 Hofmann method:

In 1937 Hofmann [108] used the combination of concentrated sulfuric acid and concentrated nitric acid with $KClO_3$ for the oxidation of graphite to form graphite oxide. The $KClO_3$ oxidizes the graphite powder in acid solution as it is a strong oxidizing agent and also is an *in situ* source of dioxygen, which is a reactive specie during the reaction. Different research groups are using Hofmann method for the synthesis of GO for different application purposes.[119-120]

3.5.1.7 Hummers method:

In 1958, Hummers proposed an alternative method for the oxidation of graphite by means of reacting a mixture of H_2SO_4, $NaNO_3$ and $KMnO_4$ with graphite powder.[109] The graphite powder was first stirred with $NaNO_3$ in sulfuric acid and cooled to 0 °C. The suspension became thick as the $KMnO_4$ was added during the stirring; hot water was used to dilute the suspension and treated with H_2O_2 to reduce the suspension to colorless soluble manganese sulfate. The dilute suspension was filtered and washed by hot water several times. The last step to obtain dry graphite oxide was centrifugation followed by dehydration at 40 °Cover phosphorus pentoxide in vacuum. The Hummers improved method have been used by researchers in the recent times to produce graphite oxide. [121-123]

The method most used to reduce GO is the thermal exfoliation and reduction of the graphite oxide (TRGO), where GO is submitted to a thermal shock by treating it at high temperature for a short time. The rapid heating provides the formation and volatilization of species like H_2O, CO and CO_2. The pressure formed exceeded the Van der Waals interactions causing the separation to isolated layers or small agglomerates. [124] The chemical structure of GO is given in Figure 11.

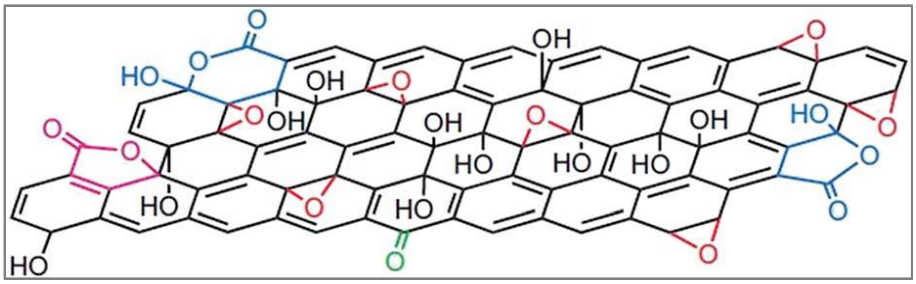

Figure 11. Structure of graphite oxide. Reproduced from [125].

3.6 Activated carbon:

Activated carbon is a carbon based material with a high surface area and relatively high porosity. Its structure contains of sp^2 graphite crystallites primarily composed of 3 to 4 parallel hexagonal carbon rings separated by 3.44-3.65 Å. However, the main structure in the activated carbon is composed of microcrystalline and amorphous graphite-like sheets called “based planes”.[126] This special structure makes the activated carbon more porous and important for various application such as catalysis, adsorption and as filler in the polymer matrix.

In the last decades, the development of low-cost activated carbon from the biomass derived from industrial and agricultural solid waste, such as sugar cane bagasse, wood chips, and wood sawdust, [127-129] etc, make those materials preferred compared to the expensive coal based activated carbon.

Two main processes are widely used to produce activated carbon: conventional process and, more recently, microwaves assisted pyrolysis. In the traditional process the heating system consist in an external heat source, such as oil bath or heating mantle, and the heat transfer from the surface to the center of the material is made by conduction, convection and radiation. Whereas, the second process used energy conversion rather than heating, where electromagnetic energy is transformed to heat energy, this process is more easy and cost effective. The common activated agents used during the carbonization process are $FeCl_3$, H_3PO_4, KOH, and K_2CO_3.[130-132]

3.7 Polyolefins carbon based filler nanocomposites:

Polyolefins has attracted research interest in the last 60 years, and led to the world wide large scale plastic industry, due to the fact that polyolefins have a variety of properties, for example low cost, easily available raw materials and are non-toxic. [133-134] Metallocene based polyolefins have reached a production of 4 million tons per year and they include, polyethylene, ethylene-1-octene copolymers, ethylene/propylene (EP) elastomers, and polypropylenes (PP). The zirconocenes, hafnocenes, half-sandwich titanocenes or other zirconium, nickel, and iron complexes are activated by co-catalysts such as methylaluminoxane (MAO). [135]

Polyethylene is one of the main polymers produced in the world due to its low cost, recyclability, easy processing and versatility. Between the polyethylenes, high density polyethylene (HDPE) stands out due to the high molar mass and low branching. The low level of branching makes HDPE to have high density, causing the alignment, orientation and packaging of the chains more efficiently. This results in the enhancement of the intermolecular forces, producing greater crystallinity and increase in the melting temperature of the polymer. [136,137]

The use of filler to enhance the properties of the polymer matrix is well accepted. At the beginning, the use of the filler was considered to make the polymer cost effective. However, with the passage of time, fillers attracted great attention to improve the properties of the polymer, especially for reinforcing the mechanical properties of the matrix. The reinforcement of the

polymer matrix with an inorganic filler, relatively stiff, can bring dramatic changes on the properties over the pure polymer.[138] Mostly used traditional fillers include talc, glass fiber, carbon black and calcium carbonate particles in micrometer range. However, higher degree of reinforcement is achieved using particles ranging from 100 nm and smaller.[139] Results showed that 3%-5% by weight of nanofillers give the same results of 20%-30% of microsized filler. Therefore the nanocomposites have the advantage of light weight over the conventional composites materials. Carbonaceous nanofillers such as nanotubes and graphene display excellent properties due to their high mechanical strength and high aspect ratio.[138]

The addition of filler can broaden the application range of polyolefins by improving their properties such as gases barrier and thermal stability or by adding new properties such as electrical conductivity. [140] Several researchers prepared PE/CNT and PP/CNT nanocomposites and reported the improvement in the properties compare to the neat polymer.[141]

For instant, different techniques have been reported for the synthesis of polymer nanocomposites. Bahuleny *et al*.[142] prepared the polyethylene/carbon nanotubes nanocomposites by *in situ* polymerization using metallocenes catalyst (Cp_2ZrCl_2 and Cp_2TiCl_2) in combination with methylaluminoxane and obtained the increase of crystallinity as compare to the neat polymer. Their TEM and SEM observations showed “sausage” like or “shish-kebab” like morphology.

However, the dispersion of CNT in the polymer matrix is a technical challenge since this kind of one dimensional nanofillers has very strong л-л interactions which cause aggregates. Consequently the polymer/filler nanocomposites greatly depend upon the homogenous dispersion of the filler in the polymer matrix. Bonduel *et al.*[143] reported PE/CNT nanocomposites using the supported metallocenes catalyst method to achieve the homogenous dispersion of CNT. The nanotubes were first treated with metallocenes based complex e.g Cp_2ZrCl_2/MAO and achieved homogenous surface coating of the CNT by *in situ* polymerization of ethylene. They reported the enhancement in the thermal properties of the nanocomposites and also the catalytic activity was increased with the increase of the polymerization temperature.

Similarly, Trajillo *et al*.[144] studied the morphology, nucleation and crystallization of polyethylene/CNT composites using *in situ* polymerization of ethylene, they treated the surface of CNT with the metallocene catalyst. They found an excellent nucleation effect of the CNT in the crystallization of the HDPE. The thermal properties were also enhanced.

McNally *et al.*[145] prepared PE/MWCNTs composites by melt blending with fillers ranging from 1 to 10 wt% using a mini-twin screw extruder. The morphological characterization showed both individual tubes and agglomeration of MWCNTs in the polymer matrix. The electrical percolation was obtained at 7.5 wt% and the electrical conductivity of PE was increased by 16 order from 10^{-20} to 10^{-4} S/cm as well as the thermal decomposition temperature was enhanced by 20 ºK with the addition of 10 wt% of the filler.

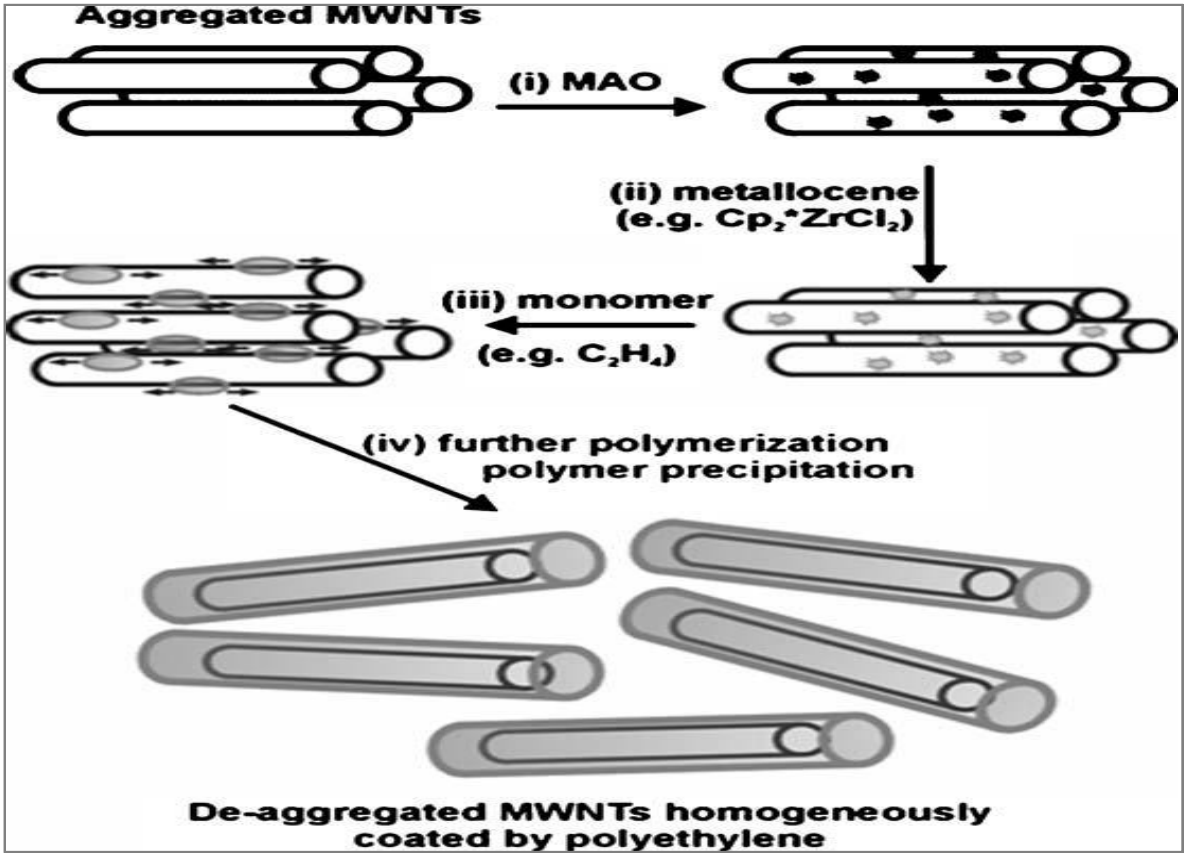

Figure 12. Schematic representation of the polymerization techniques. Reproduced from [143].

Jiang *et al.*[146] investigated the effect of the exfoliated graphene nanoplatelets (GNP) on the crystallization behavior, thermal conductivity, and electrical conductivity of the HDPE/GNP nanocomposites. The nanocomposites were fabricated by melt mixing followed by injection molding. At first the HDPE and GNP were mixed during 100 min by a novel polymer processing technology called solid state ball milling (SSBM). Then, the mixture was injection molded to produce the nanocomposites. The thermal stability and thermal conductivity of HDPE/GNP nanocomposites were found to be significantly enhanced as a function of GNP concentration.

The electrical percolation threshold which is normally around (~10-15 vol.%) for HDPE/GNP prepared by melt mixing and injection molding reduced to 5 vol.% of GNP loading by applying SSBM method.

To achieve the homogenous dispersion of the graphene as nanofiller in the polymer matrix is a challenging task. Song *et al.*[147] prepared PP/graphene nanocomposites and to achieve homogenous dispersion, the graphene was coated with polypropylene (PP) latex and then melt blending with PP matrix. Due to the uniform dispersion the mechanical properties were improve to a great extent with the incorporation of only 0.42 vol % of graphene. The thermal stability and the glass transition temperature also showed an enhancement. The procedure is described in Figure 13.

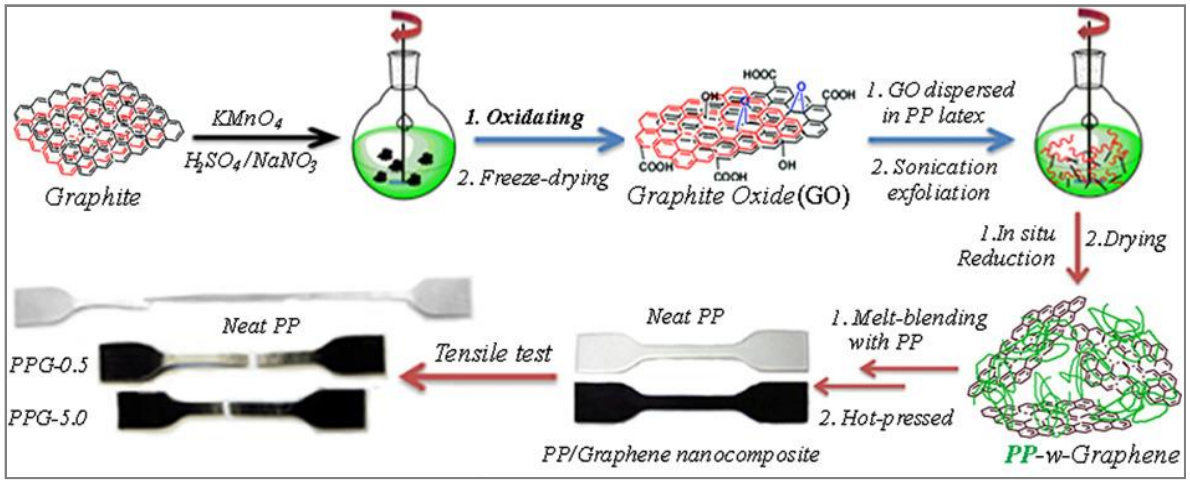

Figure 13. Schematic representation of the process flow of PP/Graphene nanocomposites and the test samples before and after applying force. Reproduced from [147].

More recently our group prepared the polyethylene/graphite nanosheets, polypropylene/ graphite nanosheets and polypropylene-1-octene/graphite nanosheets nanocomposites using *in situ* and supported catalyst methods. [3,24,92,148-150] They obtained the homogenous dispersion of the filler in the PE and PP matrix, the mechanical thermal and conductive properties were significantly improved. The presence of the graphite nanosheets acts as nucleating agents increasing the crystallization rate in the nanocomposites. Similarly the reinforcing effect of the filler was confirmed by the enhancement in modulus.

3.8 Electrical Conductivity:

Electrical conductivity can be defined as the measure of the amount of electrical current that a material can carry. Electrical conductivity is also known as specific conductance. Conductivity is an intrinsic property of a material. It is denoted by the symbol σ and has SI units of Siemens per meter (S/m). [151] Three type of material existes (i) Conductor (ii) Semi-conductor (iii) Insulator. In conductive materials, no band gaps exist so electrons move easily using a continuous, partly full conduction band. Whereas in semiconductor materials, the band gap between the conduction band and valence band is smaller and at normal temperature (room temperature), there is enough energy accessible to displace a few electrons from the valence band into the conduction band. As temperature increases, the conductivity of a semiconductor material increases. The insulators materials show totally different behavior, there is a large band gap between the conduction and valence band. The valence band remains full since no movement of electrons occurs and as a result, the conduction band remains empty as well.

Polyolefin is an insulating polymeric matrix. Various researchers introduced different type of conducting filler to promote the electrical conductivity in the polyolefin matrices. For instant carbon nanotubes, graphene and graphite oxide attracted the attention of researchers. [152-155]The minimum concentration of the conductive filler required to transfer the insulating material to a semi-conductor is known as the electrical percolation threshold, above which the insulating material behavior changes to the conducting material.[153]

3.9 Magnetism:

The story of magnetism started with the magnetite (Fe_3O_4) mineral, the first magnetic material known in the history of mankind. The word magnet is derived from the Greek word magnesia, that was the district where existed a large reserve of the magnetite, nowadays, this place is in Turkey. [156]

The most attracting demonstration of magnetism in solids is the spontaneous magnetization of ferromagnetic materials such as magnetite or iron, associated with the hysteresis. The essential characteristic of any ferromagnetic material is the irreversible magnetization M in response to an applied external magnetic field *H*. This response is represented by the hysteresis loops as shown in the Figure 14.[157]

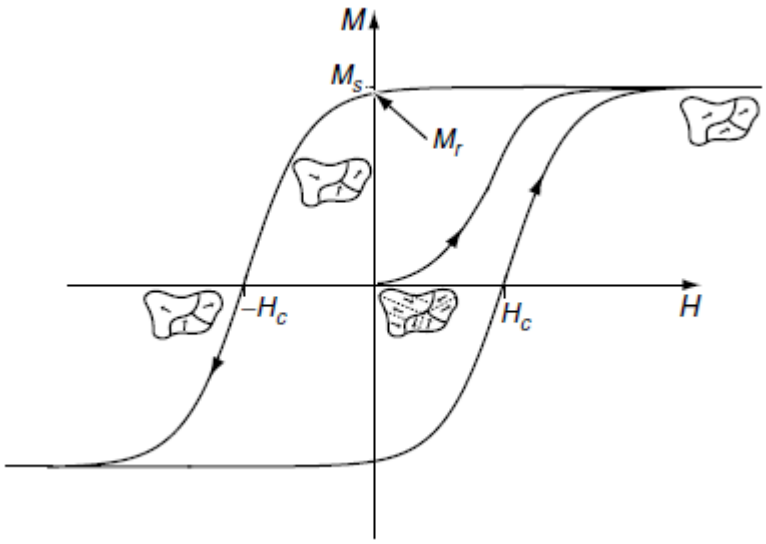

Figure 14. Typical hysteresis loop. Reproduced from {157].

To understand the hysteresis loops, some basic terms are necessary to understand such as the coercive force, (*Hc*), saturation magnetization, (*Ms*) and residual or remnant magnetization (M_R). *Hc* is defined as the applied external magnetic field which is required to bring the material to zero magnetization state. *Ms* is the state of a material at which the magnetization cannot be further increased with the increase of the external magnetic field. M_R is defined as the magnetization which remains in the material after removing the external magnetic field. [31] Usually two type of magnetic materials are found the hard and soft magnetic materials.

The hard magnetic materials have broad square *M (H)* loops. They are used as permanent magnets, as once magnetized by sufficient applied magnetic field $H \geq Ms$ to saturate, they remains in the magnetized state once the applied field is removed. Soft magnetic materials have very narrow loops. They are considered temporary magnets and lose the magnetization as the applied magnetic field is removed. In general, the loop gives the information of the intrinsic magnetic property. The spontaneous magnetization *Ms*, which corresponds to the domain of a ferromagnet, and two more extrinsic properties, M_R and *Hc* depend on various factors, such as, the shape of the sample, the surface roughness, the microscopic defects, the thermal history, as well as, the rate of the filed used to swept in order to trace the loop.[157] The magnetic materials are classifies into five classes: diamagnetic, paramagnetic, ferromagnetic, ferrimagnetic, and antiferromagnetic. The classification is based on the electronic structure and their response to the applied magnetic field (H).

Substances that are purely diamagnetic have no unpaired electrons in their outer shells, and therefore no net magnetic moments.[158] They have a negative magnetic susceptibility (χ), and exhibit a negative magnetization (M) in an applied field. Where M is the magnetic moment per unit volume and $\chi = M/H$.

Paramagnetism occurs when atoms have unpaired electrons in their outer electron shells, leaving them with net magnetic moments (μ). The susceptibility is small, positive, and temperature dependent. In the absence of applied magnetic field the moments are oriented in random directions, but with the introduction of the external applied magnetic field some of them line up in the direction of the field. The magnetic moments do not interact with each other, and return to random orientations when the field is removed.[158]

The magnetic moments of ferromagnetic materials align parallel to each other in an applied field. Unlike paramagnetic materials, however, nearly all of the electron spins align in the direction of the applied field. This parallel magnetic ordering, due to the very strong electronic interactions between the magnetic moments, is present even when there is no magnetic field. This net magnetization that is present in the absence of a field is referred to as the spontaneous magnetization. There is a maximum magnetization, the saturation magnetization, which can be reached when a ferromagnet is placed in a magnetic field. Increasing the applied field does not increase the magnetization once the saturation point has been reached. Hysteresis is another property of ferromagnets that differentiates them from paramagnets. Hysteresis loops (Figure 14), which are plots of magnetization vs. magnetic field, show how a ferromagnetic material "remembers" an applied field after this is removed. This remnant magnetization, along with the saturation magnetization and the coercive field (the field at which the magnetization goes to zero) can be seen in a hysteresis loop.

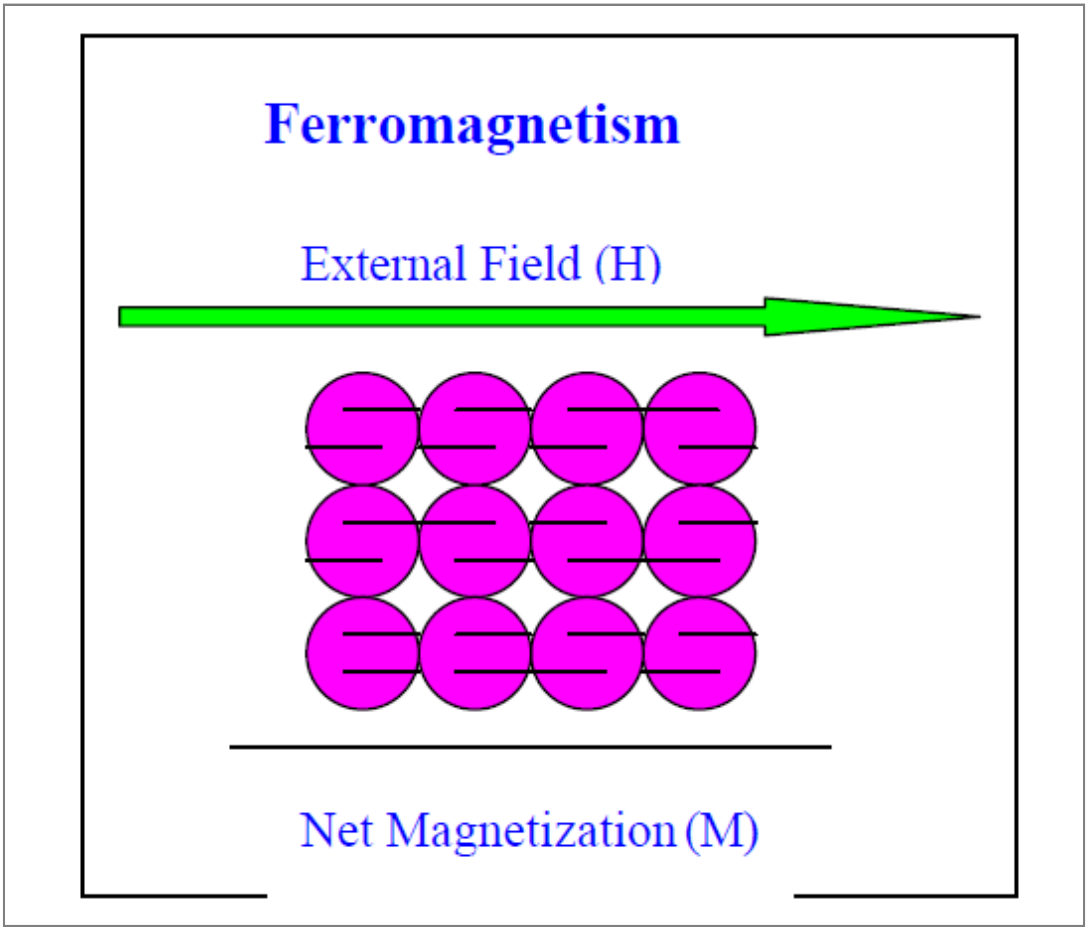

Figure 15. The magnetic domains and the magnetization of ferromagnetic material in the presence of external magnetic field.

In antiferromagnetic materials, the spins are coupled with anti-parallel orientation.[158,159] The material's net magnetic moment is zero, or nearly zero above a critical temperature.

Ferrimagnets behave very much like ferromagnets, but their magnetic ordering is like that of antiferromagnets.[158,159] Like ferromagnets, they exhibit spontaneous magnetization, hysteresis, and remanence. Like antiferromagnets, their spins are aligned parallel to each other and in opposite directions, but do not cancel each other out completely. This leads to a net moment as in the case of ferromagnetic ordering. The resulting magnetization and susceptibility are positive, but much weaker than those of ferromagnetic materials.

3.10 Magnetic polymer nanocomposites:

The magnetic materials have a wide range of applications in different fields of science and technology, such as data storage, nano adsorbent, biomedicine, drug delivery, biosensor, and

magnetic imaging devices. The incorporation of the magnetic materials in the polymeric matrix allows the obtainment of functional materials with improved mechanical properties and interesting magnetic properties.[160]

Magnetic polymer nanocomposites attract the attention of both academic and industrial researchers, and can be obtained by the incorporation of magnetic element such as iron, cobalt, and nickel to the non-magnetic polymer matrix. A variety of methods have been used to obtain magnetic polymeric nanocomposites, for instant, *in situ* polymerization, surface initiated polymerization, solution blending, ball milling and ion exchange technique. [161] However, the incorporation of the nanosized particles and their uniform dispersion in the polymer matrix is still an issue to be resolved. [162] To determine the nanocomposites behavior the dispersion of the filler is a key factor to be taken into consideration and when achieved the material often have properties superiors to the constituents.[163] Iron is the most conventionally used magnetic element. Iron nanoparticles (NPs) aroused extensive interest because of their magnetic and catalytic performances. The most significant disadvantage of iron NPs is their easy oxidation, whereas, due to large specific surface area, and Van der Waals forces iron NPs tend to agglomerate.[164] The protection strategies seem to be one of the solutions to resolve the above problems.[165]

Riquelme *et al.*[166] prepared isotactic polypropylene (iPP) nanocomposites with magnetic carbon based hybrid fillers. The magnetic filler were synthesis using CVD method, where the ferrocene was used as catalyst and precursor of synthesis and silica (SiO_2) or thermally reduced graphene oxide (TRGO) were used as support. The nanocomposites were prepared by melt mixing and reported the enhancement in the mechanical properties. Their results showed that the incorporation of the filler produce a conducting network in the insulating PP matrix. The introduction of 2 wt.% of the magnetic filler changed the diamagnetic nature of the polymer to ferromagnetic.

Nathani*et al.*[167] reported the preparation of nickel-ferrite-polyethylene nanocomposites synthesis by mechanical milling process. Their results showed the absence of hysteresis, remanence, and coerecivity at room temperature, suggesting the superperamagnetic nature of the composites.

Depending on the application different type of magnetic particles and polymer have been used to prepare magnetic polymer nanocomposites. Recently Santos *et al.*[160] used Fe_3O_4 synthetic talc as a filler in polyurethane/Fe_3O_4 nanocomposites. The magnetic behavior of the

nanocomposites was investigated by Mossbauer transmission and magnetic measurement. The nanocomposites showed improvement in the crystallization and thermal stability; however the nanocomposites presented better magnetic properties at very low temperature (2 ºK).

He *et al*. [161] prepared high density polyethylene magnetic nanocomposites, the decrease in the H_c from 193 to 9 Oe was observed, with the increase of the magnetic filler from 5 to 20 wt.%. The decrease in the H_c is attributed to the decrease in the inter particles distance which results demagnetization. Sim *et al* [168] prepared Fe_3O_4@PANI magnetic material using oxidation polymerization, and obtained a Coercivity of ~ 40 Oe.

4. Experimental Part:

4.1 Materials:

All the reagents were manipulated under argon atmosphere using standard schlenk techniques. Table 3 listed the solvent in the reagents and their characteristics.

Table 3:Solvent and reagents used.

Product	Producer	Purity	Method for purification
Hydrochloric acid	Merck	P.A	Used as received
Nitric Acid	Nuclear	P.A	Used as received
Sulfuric acid	Merck	P.A	Used as received
Benzophenone	Aldrich	--	Used as received
Potassium chlorate	Vetec	P.A	Used as received
$(n\text{-}BuCp)_2ZrCl_2$)	Sigma-Aldrich	--	Used as received
Ethanol	Nuclear	P.A	Used as received
Ethylene	White Martins	Polymer Grade Concentration	Used as received
Methylaluminoxane	Witco	10%wt/wt Al in toluene	Used as received
Metallic Sodium	Merck	--	Used as received
Toluene	Nuclear	P.A	Distilled with Na and Benzophenone
Graphite flakes	Nacional de grafite Ltda	--	Used as received
Propylene	Petrochim S.A	polymer grade	passed on the catalyst (BASF R3-11 and R3-12)
Ferrocene	Sigma-Aldrich	--	Used as received
Silica powder	Evonik (Aerosil 200)	--	Dried at 100 °C

The propylene gas was passed through two columns for purification. One for drying, containing molecular sieve (Merck, 4 A°), and other for removal of oxygen and sulfur (catalyst BASF R3-11 and R3-12).

4.2 Synthesis of carbon nanotubes containing iron:

The previously dried ferrocene and silica were used for the synthesis of the carbon nanotubes contains iron (CNT-Fe). The schematic diagram of the synthetic route is demonstrated in the Figure 16. The chemical vapor deposition (CVD) apparatus used in the experiment is composed of a 30 mm inner diameter quartz glass tube located into a moveable cylindrical furnace that can slide along the tube as shown in the figure 17. Highly pure helium gas at 300 standard cubic centimeter per min (sccm) (5×10^{-6} m^3/s) was pumped into the tube in order to guarantee that no oxidation take place during the growth of the CNT. A thermocouple was connected to the quartz tube where the reaction occurs and for controlling the temperature, a temperature controller was attached to the reactor.

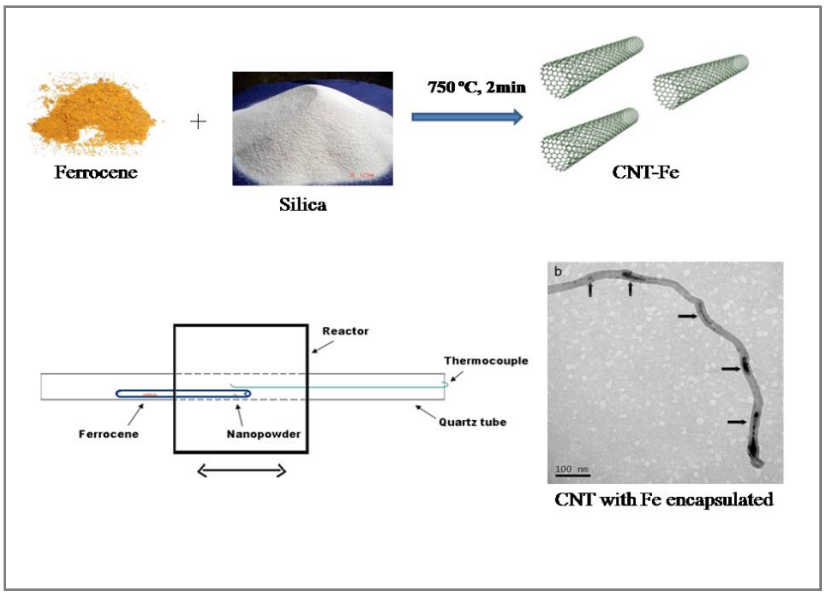

Figure 16. Diagrammatic presentation of the tube.

Before the synthesis 0.1 g of ferrocene was placed into the quartz tube next to the heat zone and 0.0025 g of silica used as substrate was placed in the heat zone. The temperature was increased upto750 °C and once this temperature was reached the furnace was sliced over the ferrocene

powder to undergo pyrolysis with nucleation and growth of CNT. The total time of the reaction was 2 min and it was obtained around 20-30 mg per reaction.

4.3 Synthesis of carbon nanotube contain iron using sawdust from furniture industry:

Synthesized CNTs were provided by the group of Prof. Luiz C. P. de Silva Filho. The synthesis method is reported in the reference 169. They used sawdust from the furniture industry as raw material. Commercially available zinc (Zn) was used as a reducing agent and calcite as bed materials. Ferrrocene ($Fe(C_2H_5)_2$) or Fe/Mo/MgO were used as a catalyst arrange in a column reactor and heated together until 750 °C for 3 h without blowing air . The conditions were optimized according to the thermodynamic simulation performed with the FactSage software. For each batch of the reaction 10 g of the sawdust, 2 g ferrocene, 2 g of zinc, 5 g of calcite and 0.6 g of clay were used.

4.4 Synthesis of nickel activated carbon:

The nickel activated carbon was synthesized by the group of Professor Eder C. Lima the detailed method is given in the reference 170. Sapelli sawdust was used as a precursor for the preparation of the composite activated carbons with nickel(II). It contains ca 98% of cellulose, hemicellulose, lignin and pectin. For the preparation, a known amount of nickel (II) chloride salt was dissolved in 50.0 mL of deionized water, after which 50.0 g of dried biomass (milled to diameter < 300 μm) was added to the solution and mixed continuously at approximately 80 °C for 120 min to overcome the natural recalcitrance of the lignocellulosic biomass structure, as well as to ensure a high interaction between the nickel ions and the lignocellulosic material. The impregnation mass ratios of metal salt/biomass were 1:1 (w/w).After mixing, the paste was oven-dried at 90 °C for 12 h. Pyrolysis of the dried sawdust impregnated with nickel was carried out in a quartz reactor, under a nitrogen atmosphere (150 mL min−1). The quartz reactor was placed in a conventional oven and heated for 2 h at 700 °C. The system was then cooled after carbonization for 1 h under 60 mL min-1 nitrogen flow. The final material was washed and dried at 105 °C for 24 h and stored for the fabrication of polymer nanocomposite.

4.5 Reduced graphite oxide synthesis:

Graphite oxide was synthesized from flakes (FK) using a modified Staudenmaier method as shown in the Figure 17. A round bottom flask, placed an in ice bath, was used to stir a mixture of acids H_2SO_4 (160 mL) and HNO_3(90 mL) for 1 h. Shortly 10 g of graphite (FK) were added and stirred for more 20 min. Subsequently, at controlled temperature (lower than 35°C) 110 g of $KClO_3$ were added over 15 min. To minimize the risk of explosion, due to the ClO_2 small amounts of KCl were added. The time for oxidation reaction was 24 h. After the reaction completed an aqueous solution of HCl (10 % v/v) was added to remove sulfate ions. The suspension was washed with deionized water and centrifuge (4500 rpm) several times until the suspension attains pH 3. Afterward, the produced suspension was placed in a dialysis membrane until the pH reached 5, and dried in an oven at 150 °C. In the last step the graphite oxide was placed in a close quartz ampoule and heated at 600 °C for 30s in an oven using normal atmosphere to obtain reduced graphite oxide (rGO).[92]

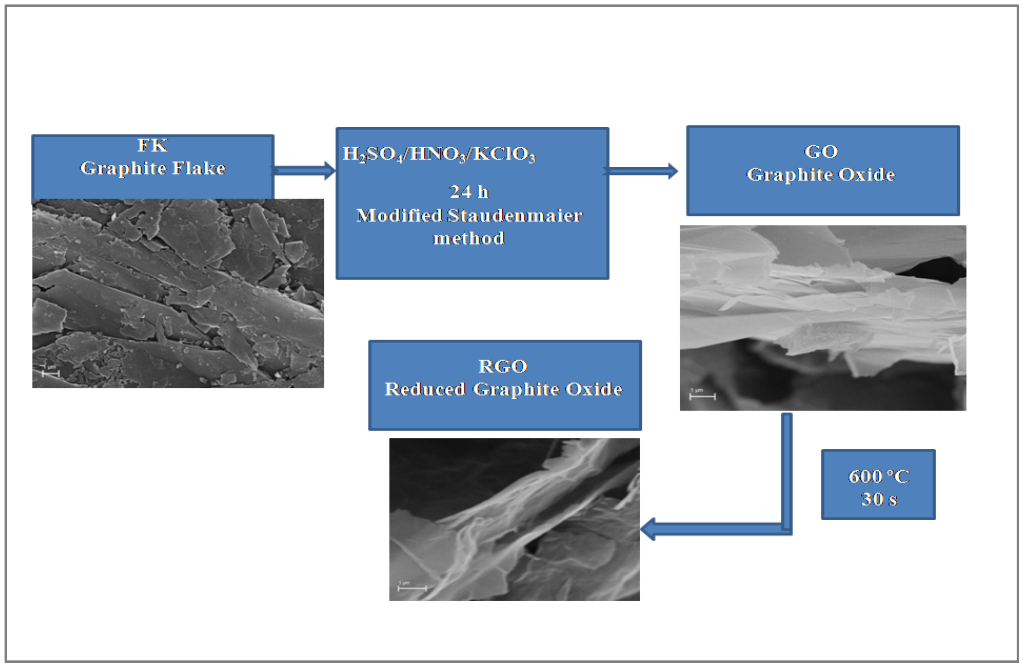

Figure 17. Graphene oxide synthesis and thermal reduction.

4.6 Synthesis of nanocomposites:

4.6.1 Polyethylene/CNT-Fe nanocomposites:

For the preparation of the polyethylene/CNT-Fe nanocomposites, the variable amount of synthesized CNT-Fe as discussed in (4.2) was treated with 15 wt.% MAO in toluene and stirred for 30 min. The polymerization reactions were carried out in a 300 mL PARR reactor having mechanical stirring and connected to a heating and cooling bath. Toluene was used as the solvent, MAO (methylaluminoxane) as cocatalyst (Al/Zr=1000) and bis(n-butyl) cyclopentadienyl zirconium dichloride$(n\text{-}BuCp)_2ZrCl_2$(5×10^{-6}mol) as catalyst. This catalyst was used because is the simplest and least expensive metallocene catalyst.In addition, this catalyst produces polyethylene in good yield.

All the reactions were carried out at 25 ° C using an ethylene pressure of 3bar during 30 min. The temperature (25 °C) was chosen to obtain high molecular weight PE and the Al/Zr (1000) ratio was chosen for high yield after best polymer yield under these conditions. First the reactor is filled with toluene and CNT-Fe previously treated with MAO, was added to the reactor as filler. The calculated amount of MAO (Al/Zr=1000) was added and stirred for 10 min. After the catalyst was added and the total volume of the reactor was raised to 150 mL using toluene, a 3 bar pressure of ethylene was kept constant for 30 min. The reaction was terminated by the addition of (10 vol.%) acidified ethanol. Finally, the obtained polymer was filtered and washed with ethanol and dried at constant weight. Figure 18 shows the schematic representation.

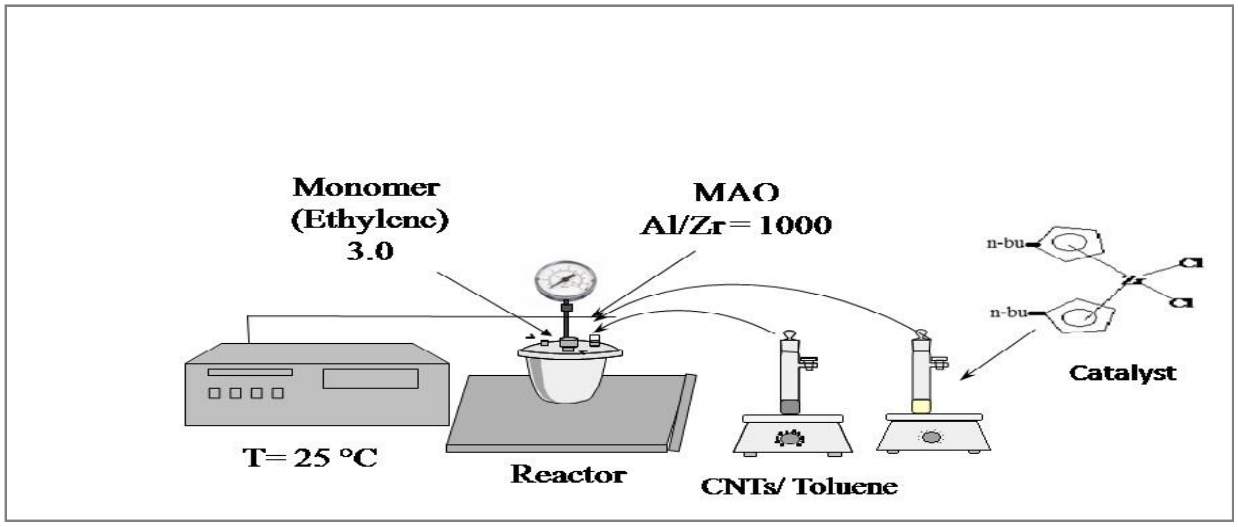

Figure 18. Schematic representation of the synthetic rout of polymer nanocomposites.

4.6.2 Polypropylene/CNT-Fe nanocomposites:

To perform all the necessary characterization higher amount of the polypropylene nanocomposites were synthesis using Buchi glass reactor having capacity of 1000 mL equipped with mechanical stirring and connected to the heating and cooling bath to control the temperature. The reactor was filled with toluene, MAO (Al/Zr 1000) and the CNT-Fe (various amounts) previously treated with 15 wt. %MAO. Subsequently, the system was saturated with propylene gas and, finally, a given aliquot of catalyst[(*rac*-Et(Ind)$_2$ZrCl$_2$) (5.0×10^{-6}mol)]solutionin toluene was introduced. The total volume of the reactor was kept in 500 mL. The rector was continuously fed with 2.0 bar pressure of propylene for 30 min at a constant temperature of 25°C with maximum variation of ± 3°C. The reaction was terminated with the addition of the acidified methanol solution. The resulted polymer was filtered, washed with methanol and dried until constant weight.

4.6.3 Polyethylene/rGO/CNT-Fe nanocomposites:

Before starting the polymerization variable amount of the filler (rGO/CNT-Fe) were placed in a schlenk vessel with toluene using argon atmosphere and sonicated with an ultrasound bath (Ultracleaner 1600 A, Unique, Brazil) operating at 40 kHz, for 8h at room temperature. After 15 wt% of MAO was added and sonicated for more 30 min. In the next step (n-BuCp)$_2$ZrCl$_2$ was added in an amount of 2 wt% Zr/rGO/CNT-Fe, followed by 2 h of stirring at 60 °C. The solid was then decanted and the supernatant eliminated, and washed twice with toluene.

The polymerization reaction was carried out in a 300 mL reactor (Parr instrument Company, IL). The reactor was filled with toluene and an extra amount of MAO (Al/Zr = 1000) was added as scavenger. Subsequently, the previously prepared (n-BuCp)$_2$ZrCl$_2$/rGO/CNT-Fe was used as catalyst for the ethylene polymerization. The ethylene pressure was kept constant at 3 bar for 30 min at 25 °C.

4.6.4 Synthesis of Polypropylene nanocomposites by melt compounding:

For the preparation of composites, a melt-mixer, Brabender Plasti-Corder (Diusburg, Germany), operating at 190^{o}C and at a speed of 110 rpm was used. Calculated amounts of iPP and CNT and a small amount (~0.005 g) of Irganox1010 as an antioxidant were used per mixing; the total amount used was approximately 30 g. The amount of the filler varied from 0 wt% to 20

wt%. The iPP was first mixed with the antioxidant, and subsequently half the amount of the polymer (~13 g) was added to the mixer operating at 110 rpm. After 2 min, the filler was added to the melted polymer for 3 min. In the last step, the rest of the polymer pellets were added and the speed of the mixer was kept constant at 110 rpm for 10 min. The total mixing time was approximately 15 min.

4.7 Characterization of the nanocomposites:

Most of the characterization of the fillers, and nanocomposites was performed in equipments available at UFRGS (IQ, IF, CME, LAMAT, CNANO).Those carried out in other institutions will be described in the text.

4.7.1 Differential scanning calorimetry (DSC):

The differential scanning calorimetry analysis was performed using a Perkin-Elmer differential calorimeter Model DSC Q20 (TA Instruments). The heating program used consist of heating the sample from 0 °C to 180°C, maintain at this temperature for 5 min and then cooled to -20 °C, and again heated up to 180 °C. The analysis was carried out with a constant nitrogen flow (50 mL/min) with a heating rate of 10 °C/min. The melting temperature, $T_m$was determined in the second scan, and the degree of crystallinity was calculated from the enthalpy of fusion data obtained from the DSC curves (293 J/g and 207 J/g were used as 100% crystallinepPolyethylene and polypropylene, respectively). The crystallinity of the synthesized polymer was calculated from the follow relation.

$$X_c = \frac{\Delta H_f}{\Delta H_f^\circ} \times 100$$

Where ***Xc*** represent the crystalline content, $\Delta H_f$is the heat of fusion of the materials (area of the endothermic curve) and ΔH_f° is the heat of fusion of 100 % crystalline material.

4.7.2 Thermogravimetric Analysis (TGA):

The thermal stability of the nanocomposites was studied using a thermal analyzer SDT Q600 (TA Instrument) at a scanning rate of 20 °C/min from 0 °C to 800 °C. The samples were analyzed in the form of powder and film using nitrogen atmosphere (100 mL/min). This

technique allows the determination of the initial and maximum degradation temperatures as well as the residue of the filler present in the nanocomposites.

4.7.3 Dynamic Mechanical Analysis (DMA) :

Dynamic mechanical analysis (DMA) was obtained using a DMA analyzer (TA Instruments model Q800). The samples were analyzed in single-cantilever mode at a frequency of 1 Hz and a strain level of 0.1% in the temperature ranging from -140°C to 120°C with heating rate of 1.5 °C/min. The test sample has the length of 15 mm and width 3.5 mm, obtained by cutting nanocomposites films in the rectangular mode.

4.7.4 Mechanical properties:

The mechanical properties were measured using HP model D-500 dynamometer according to ASTMD 638-10 at ~25°C. For each wt % of nanocomposites, five samples were tested and the results averaged over these five measurements (typical deviation *ca*.5%). Bone-shaped samples of overall length 120 mm with the distance between the two grips of 80 mm, width of 11.5 mm, and thickness of 1 mm were tested at a cross-head rate of 50 mm min^{-1}.

4.7.5 Transmission electron microscopy (TEM):

Transmission electron microscopy (TEM) was used to analyze the structure of the filler and its dispersion in the polymer matrix. A JEOL 1200 EXII microscope operating at 100 kV was used. Samples were produce by preparing suspension of the filler (CNT-Fe and rGO) in distilled acetone and dispersed in the ultrasonic bath for 10 min, after that a drop wasdepositedon agrid covered with carbon. The sample of the neat polymer and the nanocomposites were prepared by dissolving indecalin at 160 °C, after a drop of the solution was placed on the grid. The nanocomposites were also analyzed in the form of films cut under cryogenic conditions with a leicaUltracut UCT microtome at -70°C and placed on a grid of copper of 300 mesh covered with amorphous carbon.

4.7.6 Scanning electron microscopy (SEM):

Scanning electron microscopy (SEM) was performed using Phillips XL30 microscope operating at 20 kV. Each sample was fixed to a carbon double-side tape present at the base of the aluminum stub, as the materials analyzed were not conducting, they were covered by a thin layer

of gold by electro-vaporization (process of metallization). The images of the filler, pure polymer and the nanocomposites in the powder form were obtained.

4.7.7 Gel permeation chromatography (GPC):

The weight average molar mass (M_w) and its distribution (M_w/M_n) of the neat polymer was determined with a Water Alliance GPC chromatograph 2000 (University of Chile, Santiago), with coupled refractive index detector equipped with three styragel HT-type columns (HT3, HT5, and HT6E). The filtered and distilled 1,2,4-trichlorobenzene (TCB) was used as mobile phase, to which was added 2,6-di-t-butyl-4-methylphenol (0.025%) as an antioxidant. The analysis was carried out at a flow of 12 ml/min at 135 °C. The columns were calibrated with polystyrene standards.

4.7.8 Electrical conductivity measurement:

The electric resistivity was measured with the help of a megohmmeter (Megger BM11) operating at highest voltage of 1200 V. With this set-up, the standard two-point method was used. For each electrical value displayed in this contribution, at least four samples were prepared and four measurements for each one were carried out. In general, differences around one order of magnitude were detected in the non-percolated samples having low conductivity values (~10^{-9} S/cm). For percolated samples, the experimental error for conductivities was less than 50%. The samples prepared to use for the test were of 40mm ×15 mm and thickness 1 mm.

4.7.9 Atomic absorption spectroscopy:

The determination of Fe on the carbon nanotubes and polymers was carried out by HR-CS GF AAS by direct solid sampling (SS) using a contrAA 700 high-resolution continuum source atomic absorption spectrometer (Analytik Jena AG, Jena, Germany). The samples were directly weighed, without any prior preparation step, on pyrolytically coated graphite tubes. A pre-adjusted pair of tweezers, which is part of the SSA 6 manual solid sampling accessory (Analytik Jena), was used to transfer the platforms to the atomizer. The program temperatures and method used were followed and adapted from the literature.[34] A 10 µL volume of a mixture of 20 µg Pd + 12 µg Mg was used as the chemical modifier dosed onto the sample prior to platform introduction into the atomizer. Pyrolysis and atomization temperatures were 800 °C and 2500 °C, respectively, using the 283.245 nm line and only the central pixel for evaluation.

4.7.10 Magnetic measurement

The magnetic characterization of CNT-Fe and Ni-C and nanocomposites was performed using an EZ9 MicroSense vibrating sample magnetometer (VSM). All film samples were cut with a diameter of 5 mm and fixed, using a double sidedtape, on a clean sample holder made of quartz.A low quantity of powder sample (14 mg) was put into a small glass tube which was fixed to a quartz rod using teflon. All measurements were done at room temperature with a magnetic field (H) ranging from −20 kOe to +20 kOe, applied parallel to the surface in the case of the films. Aiming to avoid potential minor-loop effects, we ensured that the maximum H-value used was sufficiently high to effectively saturate each of the samples, by employing one of the criteria for magnetic saturation which consists in analyzing the second derivates of M with respect to H. This procedure also allow us to estimate the saturation field, H_S, representing the value of H above which $M(H)$ has effectively attained saturation.

4.7.11 Inductive coupled plasma emission spectroscopy (ICP):

The amount of zirconium on the surface of the filler was investigated by Inductive coupled plasma emission spectroscopy (ICP) in a Perkin-Elmer, optima 7320.

4.7.12 Raman spectroscopy:

The Raman analysis was performed at room temperature in a Olympusmicroscope coupled to a JobinYvon IH320 spectrometer and CCD (charged coupled device) type detectorcooled by liquid nitrogen. The source of excitation wasAr+ laser (514 nm) and the acquisition time of the measurements was 20s.

4.7.13 X-ray diffraction (XRD):

X-ray diffraction measurements were taken on a diffractometer Rigaku (DMAX 2220) equipped with a Cu tube and a secondary monochromater, the goniometer used was Siemens D500 and the detector was the scintillator (Nal and TI). The samples were analyzed in the powder form at room temperature.

5. 1 Conclusion:

The first part **(Annex 1)** showed the production of a new magnetic nanocomposite of polyethylene/CNT-Fe through the *in situ* polymerization of ethylene using $(nBuCp)_2ZrCl_2$/MAO as a catalyst system. Extremely high magnetizations (H_c ~1,000 Oe) with low amount of filler (0.9 wt.%) were obtained due to two techniques employed, as follows: 1) the encapsulation of Fe in CNT, which protected the iron NPs from oxidation and aggregation; and 2) the *in situ* polymerization method, that allows an uniform dispersion of CNT in the polymer matrix and avoids dipolar interactions, which tend to stabilize the demagnetized state. The thermal properties do not shows significant changes compared with the neat polyethylene.

The second part (**Annex 2**) showed the preparation of polypropylene magnetic and conducting nanocomposites obtained also by *in situ* polymerization. Magnetic and conducting properties are important for the design of new polymeric devices for different application. The SEM and TEM showed a good dispersion of the filler into the PP matrix, resulting in PP-CNT-Fe nanocomposites with improved thermal stability. The conductivity sharply raised to 7.8×10^{-5} S cm^{-1} with the addition of 3.8 wt.% of CNT-Fe and reached its highest value of 1.3×10^{-4} S cm^{-1} as the amount of filler increased to 7.5 wt.%. The magnetic properties of the nanocomposites were investigated by VSM, and the results showed the ferromagnetic nature of the PP with very low percentage of filler (0.8 wt.%) with Hc varying from 420 to 710 Oe.

In the third part of this work (**Annex 3**) polyethylene nanocomposites that present both electric and magnetic properties have been obtained. In this case, the CNT-Fe (0.8 wt%) were mixed with a variable amount of rGO to obtain the electrical properties turning the PE into a semiconductor. rGO was used instead of a higher amount of CNT-Fe because their synthesis is less cost effective than that of CNT. The thermal stability of the nanocomposites was characterized by T_{max} and T_{onset}, which increased by 14 and 29°C, respectively, with the incorporation of 6 wt.% of the filler. The electrical conductivities increased from 4.99×10^{-6} S cm^{-1} with the addition of only 2.8 wt.% of the filler and reached 7.29×10^{-4} S cm^{-1} with 6.0 wt.% of the filler. Atomic absorption revealed that the amount of Fe was 26.9 wt.% in the CNTs and 0.04–0.06 wt.% in the nanocomposites; however, the coercivity values were 280 and 890–980 Oe, respectively, confirming that good dispersion and high inter-particle distance can avoid notable dipolar interactions that would tend to stabilize the demagnetized state. The high

coercivity values are attributed to the encapsulation of Fe in the CNTs, which protect the magnetic nanoparticle from easy oxidation and aggregation in the polymer matrix. These results show that the synthetic CNT-Fe is an interesting material to produce magnetic polymer nanocomposites.TEM also confirmed that there was a good dispersion of CNT-Fe among the RGO and in the PE matrix, revealing isolated CNT-Fe particles.

These materials have the potential to be used in a variety of applications, where a flexible magnetic and electrical material with good processability be required, as for example, electromagnetic device application like electromagnetic interference suppression, micro electronics, and aircraft industries.

The forth part of the work (**Annex 4**) includes the synthesis of cost-effective polyethylene/nickel-activated carbon nanocomposites by *in situ* polymerization. The nickel carbonized material used as filler contains nickel nanoparticles which gives a ferromagnetic behavior to the polyethylene matrix. The coercity were in the order of 34-45 Oe inferior to the ones obtained with Fe. The introduction of the magnetic properties in the polymer matrices broadens its industrial application. The thermal stability was also enhanced; the melting and crystallization temperature showed a slight increase. The elastic modulus increased 33 %with the addition of 5.0 wt% of the filler.

In the fifth and sixth part of this work (**Annex 5 and 6**) we reported the synthesis of PP/CNT-Fe and PP/rGO-CNT-Fe nanocomposites by melt mixing method. The CNT-Fe used in this part were synthesized by eco-friendly pyrolysis of sawdust using ferrocene as catalyst. Even though the aspect ratio of those nanotubes is quite inferior to the ones obtained by the synthetic method already described, the results were very interesting considering the carbon source being waste. The SEM and TEM analysis showed the uniform dispersion of the filler in the polymer. The thermal stability was improved significantly as showed by the TGA and DSC analysis. The mechanical and gas barrier properties were also improved as compare to the neat polymer. The value of the room temperature coercivity (~150 Oe) shown by the nanocomposites is a rather remarkable result given that most research in this area has reported materials that are magnetic only at very low temperatures. The conductivity results from the presence of rGO that forms conducting network in the polymer matrix.

In general, the effect of the various filler such as the CNT-Fe from CVD method, CNT-Fe from the pyrolysis of the sawdust, and nickel activated carbon showed the same effect in the thermal, mechanical and morphological properties.

Table 4:Resume of magnetic and conductive properties of the synthesized nanocomposites.

Sample	Methods	*Hc* (Oe)	M_R/M_S	Conductivity (S Cm^{-1})
CNT-Fe	CVD	280	0.32	--
PE/CNT-Fe	*In situ*	1060	0.44	--
PP/CNT-Fe	*in situ*	710	0.40	1.3×10^{-4} (3.8 wt.%)
PP/CNT-Fe/rGO	CVD/FK/*in situ*	980	0.52	7.29×10^{-4} (2.8 wt.%)
Ni-C	Pyrolysis	39	0.10	--
PE/Ni-C	*in situ*	45	0.26	--
CNT-Fe	Sawdust	150	0.14	–
PP/CNT-Fe	Melt mixing	162	0.16	–
PP/CNT-Fe-rGO	Melt mixing	150	0.14	2.3×10^{-4} (3.1 wt.%)

On the other hand the CNT-Fe from the CVD method showed the best magnetic properties probably due to the high aspect ratio of the CNT, the proper encapsulation of iron and less defects in the CNT structure as compare to the CNT-Fe from the sawdust and nickel activated carbon. Similarly the 3.8 wt% CNT-Fe from CVD method introduced the conductive network in the polymer, whereas the CNT-Fe from the sawdust and nickel activated carbon alone do not showed the introduction of conductive network in the polymer matrix. This can be explain by the type of nanotubes obtained from sawdust that are very short and large, that means that the aspect ratio is low what does not favor conductivity. Beside this, it was clear from the results that a small amount of the CNT-Fe was enough to produce the magnetic property in the diamagnetic polymer matrix, which help to optimize the amount of the combination of the two filler (CNT-Fe + rGO) to produce conducting and magnetic network with the minimum possible amount of the filler.

5.2 Future plan:

In the future, the effect of these synthetic CNT will be investigated on bio-degradable polymers by melt mixing. Also the cost effective filler such as CNT obtained from the waste will be used for the PE and PP *in situ* polymerization as well as synthesizing the nanocomposites of these polymer in the melt mixing. The cobalt and nickel activated carbon produce by microwave assisted pyrolysis will be used as filler in different polymer and the different properties will be study.

References

1. Mittal, V.; Kim, S.; Nevhofer, S.; Paulik, C. *Colloid. Polym. Sci*. **2016**, 294, 291.

2. Jancar, J. Mineral fillers in thermoplastics I: raw materials and processing. **1999,** Springer, Berlin.

3. Milani, M. A.; Quijada, R.; Basso, N.R.S.; Graebin, A.P.; Galland, G,B. J. *Polym. Sci. Part A. Polym. Chem.***2012,** 50, 3598.

4. Moniruzzaman, M.; Winey, I. K. *Macromolecules* **2006,** 39, 5194.

5. Trujillo, M.; Arnal, M. L.; Muller, A. J. *Macromoléculas***2007**, 40, 6268.

6. Vega, J. F.; Martinez-Salazar, J.; Trujillo, M.; Arnal, M. L.; Muller, A. J.; Bredeau, S.; Dubois, P. *Macromolecules***2009,** 42, 4719.

7. Bredeau, S.; Peeterbroeck, S.; Bonduel, D.; Alexandre, M.; Dubios, Ph. *Polym. Int. 2008,***57,** 547.

8. Hlatky, G. G. In metallocene- based polyolefines; Scheirs, J.; Kaminsky, W., Willey: west Sussex, **2000**, p 201.

9. Khanna, S.; Linderoth, S. *Phys. Rev. Lett*. **1991,** 67(6), 742.

10. Petit, C.; Table, A.; Pileni, M. *J. Phys. Chem. B.* **1999,** 103(11), 1805.

11. Aspel, S.; Emmert, J.; Deng, J,;Bloomfild, L. *Phys. Rev. Lett*. **1996**, 76(9), 1441.

12. Schinteie, G.; Kuncser, V.; Palade, P.; Dumitrache, F.; Alexandrescu, R.; Morjan, I.; Filoti. G. *J. Alloy and Comp.* **2013,** 564, 27.

13. Shen, W.; Yu, Y.; Shu, J.; Cui, H. *Chem. Commun.***2012,** 48, 2894.

14. Novoselov, K. S.;Geim, A. K.; Morozov, S. V.; Jiang, D.; Zhang, Y.; Dubonos, S. V.; Grigorieva, I. V.;Firsov, A. A. *Science***2004,** 306, 666.

15. Disponível em: http://www.nobelprize.org/nobel_prizes/physics/laureates/2010/. Acessoem: 15 Sep. 2017.

16. Dang, Y.; Zhang, Y.; Fan, L.; Chen, H.; Roco, M. C. *J. Nanopart. Res*. **2010**, 12, 687–706.

17. Muller,K.;Bugnicourt, E.;Latorre,M.;Jorda,M.;Sanz, Y.E.; Lanaron, J. M.; Miesbauer, O.; Bianchin, A.; Hankin, S.; Bolz, G.; Jesdinszki, M.; Linder, M.; Schedueler, Z.; Castello, S.; Schmid, M. *Nanomaterials* 2017, 7(4), 31.

18. Mittal,V. In Optimization of Polymer Nanocomposite Properties (ed. V. Mittal), Wiley-VCH Verlag GmbH & Co. KGaA, Weinheim, **2010**, pp. 1–19.

19. Ray, S.S.; Okamoto,M. *Prog. Polym. Sci.* **2003**, 25, 1539.

20. Pavlidou, S.;Papaspyrides, C.D. *Prog. Polym. Sci.* **2008**, 33, 1119.

21. Abedi, S.; Abdouss, M. *Appl. Catal. Gen.***2014**, 475, 386.

22. Mittal, V. *Materials***2009**, 2, 992.

23. Alexandre, M.; Dubois, P. *Mater. Sci. Eng.***2000**, 28, 1.

24. Fim, F.C.; Basso, N.R.S.; Graebin, A.P.; Azambuja, D.S.; Galland. G.B. J. *Appl. Polym. Sci*.**2013,** 128(5), 2630.

25. Malpass.D.B. Introduction to industrial polyethylene: properties, catalysis, and process. Wiley online library, dio. 10.1002/9780470900468.

26. Nwabunma, D.; Kyu. T. Polyolefine composites. John Wiley & sons, Inc. **2008**, P. 6.

27. http://www.astm.org/standards/D_1248.html, access 26/09/2017. **Erro! A referência de hiperlink não é válida.**

28. Zhao, C.; Qin, H.; Gong, F.; Feng, M.; Zhang, S.; Yang. M. Polym. Degrad. Stabil. 2005, 87, 183.

29. Sae-oui, P.; Sirisinha, C.; Sa-nguanthammarong, P.; Thaptong, P. *Polym. Test*. **2010**, 29,346.

30. Chrissafis, K.; Paraskevopoulos, K.M.; Tsiaoussis, I.; Bikiaris, D. *J. Appl. Polym.Sci.***2009**, 1141606.

31. He, Q.; Yuan, T. .Zhu, J.; Luo Z.; Haldolaarachchige,N.; Sun, L.; Khasanov,A.; Li,Y.;Young,D.P.; Wei,S.; Guo,Z.*Polymer***2012**, 53, 3642.

32. Grigoridou,I.;Paraskevopoulos,K.; Chrissafis, K.; Pavlidou, E.; Stamkopoulos, T.G.; Bikiaris, D. *Polym. Degrad. Stab.* **2010**, 96, 151.

33. Ayoub, G.; Zairi, F.; Nait-Abdelaziz, M.; Gloguen, j. M**.** *Int. J. Plast*.**2010**, 26, 329.

34. Anderson, J. C. *Tribology International*. **1982**, 15, 43.

35. Bartczak, Z.; Argon, A.S,; Cohen, R. E.; Weinberg, M. *Polymer*. **1999**, 40, 2331.

36. Thongruang, W.; Spontak, R. j.; Balik, C. M. *Polymer*. **2002,** 43, 2279.

37. Kaminsky, W. ;Wiemann. K. *Compos. Interfaces*. **2006**, 13, 365.

38. Pavlidou, S.;Papaspyrides.C.D. *Prog. Polym. Sci.***2008**, 33, 1119.

39. An, J. ;Jeon,G.;Jeong,Y. *Fibers. Polym.***2012,** 13, 507.

40. Natta,G.;Pino,P. ;Corradini,P.; Danusso,F. ;Mantica, E.; Mazzaniti, G.;Moraglio.G.;*J. Am. Chem. Soc.***1955**, 77, 1708.

41. Maddah.H.A. *Am. J. Polym. Sci.***2016**, 6 (1), 1.

42. Fried. J.R. Polymer science and technology. 3rd edition. **2014**.

43. Allahvaisi.S. In polypropylene: Dogan. F. (Edt); In Tech: Rijeka, **2012**, p 3.

44. Kroto, H. W.; Health, J. R.; O'Brien, S.; Curl, R. F.; Smalley. E.*Nature* **1985**, 318 162.

45. Iijima.S. *Nature***1991**, 354, 56.

46. Zaporotskova, I.V.; Boroznina, N.P.; Parkhomenko,Y.N.; Kozhitov. L.V. Mod. Ele.Mater.**2016**, 2, 95.

47. Hamada, N.; Sawada, S.;Oshiyama.A.*Phys. Rev. Lett.* **1992,** 68, 1579.

48. Saito, R.;Fujita,M.; Dresselhaus,G.; Dresselhaus.M. S. *Appl. Phys. Lett.* **1992**, 60, 2204.

49. Treacy, M.; Ebbesen, T. W.; Gibson. J. M.*Nature* **1996**, 381, 678.

50. Wong,E. W.; Sheehan,P. E.; Lieber. C. M.*Science***1997**, 277, 1971.

51. Falvo, M. R.; Clary,G. J.; Taylor,R. M.; Chi,V.; Brooks,F. P.; Washburn, S.; Superfine, R. *Nature***1997,** 389, 582.

52. Saeed, K.; Ibrahim. *Carbon letters* **2013**, 14 (3), 131.

53. Meyyappan, M.; Delzeit, L.; Cassell, A.; Hash. D. *Plasma. Source. Sci. Tecnol.***2003**, 12, 2050216.

54. Saether, E.; Frankland, S.J.V.; Pipes. R.B. *Compos. Sci. Technol.***2003,** 63, 1543.

55. Gao, C.; Gao,Z.; Lio, J.H.; Huang. X, J.*Nanoscale***2012**, 4, 1948.

56. Ajayan, P. M. Bulk metal and ceramics nanocomposites, In: P.M. Ajayan, L.S. Schadler, P.V. Braun. eds. Nanocomposites science and technology, Wiley-VCH Verlag GmbH & Co., **2004,** 1.

57. Dresselhaus, M. S.; Lin, Y.M.; Rabin, O.;Jorio,A.; Souza,A. G.; Pimenta, M. A.; Saito, R.; Samsonidza, G.; Dresselhaus. G. *Mater. Sci. Engg:C.***2003,** 23, 129

58. Saifuddin, N.; Raziah, A. Z.; Junizah. A. R. *Journal of Chemistry*. **2013.** doi.org/10.1155/2013/676815

59. Iijima, S. ; Ichihashi, T. *Nature* (London) **1993**, 363, 603.

60. Bethune, D.S.; Kiang, C.H.; Vries, M.S.; Gorman, G.; Savoy, R.; Vazquez, J.: Beyers, R. *Nature* (London) **1993**, 363, 605.

61. Thess, A.; Lee,R.; Nikolaev,P.; Dai, H.; Petit,P.; Robert,J. ; Xu, C.; Lee,Y.H.; Kim,S.G.; Rinzler,A.G.; Colbert,D.T.; Scuseria, G.E.; Tomane´k,D.; Fischer,J.E.; Smalley. R.E.*Science* **1996**, 273,483.

62. Yacaman,M.J.; Yoshida,M.M.; Rendon,L.; Santiesteban,J.G. *Appl. Phys. Lett.* **1993**, 62,202.

63. Khare, R.; Bose. S. *J.Minerals& Materials Characterization & Engineering.* **2005,** 4(1). 31..

64. Journet, C.; Maser, W.K.; Bernier, P.; Loiseau, A.; Lamy de la Chapelle, M.; Lefrant, S.; Deniard, P.; Lee, R.; Fischer, J.E. *Nature* (London) 1997, 388, 756.

65. Dai. H. Surf. Sci. **2002,**500 (1–3), 218.

66. Muñoz, E.; Maser, W. K.; Benito, A. M. Appl. Phys. A.**2000**, 70(2), 145.

67. Xie, S.; Li, W.; Pan, Z.; Chang, B.; Sun. L. *Mater. Sci. Eng A.***2000**, 286, 11.

68. Ebbesen, T.W.; Lezec, H.J.; Hiura,H.; Bennett, J.W.; Ghaemi, H.f.;Thio. T.*Nature* **1996,**382, 54.

69. Treacy, M.M.J.; Ebbesen,T.w.; Gibson. J.M.*Nature* **1996,**381, 678.

70. Jin, F.L.; Park. S.J. *Carbon Lett.***2013**, 14, 1.

71. Chandra, B.; Bhattacharjee, J.; Purewal, M.; Son, Y.W.; Wu, Y.; Huang, M.; Yan,H.; Heinz, T.F.; Kim, P.; Neaton, J.B.; Hone. J.*Nano. Lett.***2000**, 9, 1544.

72. Dai, H.; Wong, E.W.; Lieber. C.N.*Science***1996,**272, 523.

73. Ebbesen, T.W.;Lezec,H.J.;Hiura,H.; Bennett, J.W.;Ghaemi,H.F.;Thio. T.*Nature***1996**, 382, 54.

74. Yu, M.F.; Lourie, O.; Dyer, M.J.; Moloni, K.; Kelly, T.F.; Ruoff. R.S. *Science* **2000,**287, 637.

75. Ruoff, R.S.; Tersoft, J.; Lorents, D.C. ; Subramoney, S. Chen. B. *Nature* **1993**, 364. 514.

76. Overney,G.; Zhong,W.; Tomanek. D.*Phys. D.***1993**, 27, 93.

77. Robertson, D. H.; Brenner, D. W.; Mintmire. J. W.*Phys. Rev. B.***1992**, 45, 12592.

78. Tersoff. J.*Phys. Rev. B.***1992**, 46,15546.

79. Demczyk, B. G.; Wang,Y. M.;Cumings,J.; Hetman,M.; Han, W.;Zettl, A.; Ritchie.R. O. *Mat. sci. Eng. A.* **2002**, 334, 173.

80. Pan, Z.; Xie, S.; Lu, L.; Chang, B.; Sun, L.; Zhou, W.; Wang, G.; Zhang, D. *Appl . Phys. Lett.***1999**, 74, 3152.

81. Wong,E. W.; Sheehan, P. E.;Lieber. C. M.; *Science***1997,**277, 1971.

82. Poncharal, P.; Wang, Z. L.; Ugarte, D.; Heer. W. d.*Science***1999,** 283, 1513.

83. Qi,H.;Teo,K.; Lau,K.; Boyce,M.; Milne, W.; Robertson, J.; Gleason. K.*J. Mech. Phys. Sol.***2003.**51, 2213.

84. Krishnan, A. ;Dujardin,E.; Ebbesen, T. W.; Yianilos, P. N.;Treacy. M. M. J.*Phys. Rev. B.* **1998**, 58, 14013.

85. Walter,D. A.; Ericson,L. M.; Casavant,M. J.; Liu, J.; Colbert, D. T.; Smith, K. A.; Smalley. R. E. *Appl . Phys. Lett.***2004,** 74,3803.

86. Salvetat,J. P.; Andrew,G.; Briggs,D.; Bonard,J. M.; Bacsa,R. R.; kulik,A. J.; Stockli,T. ; Burnham, N. A.; Forró. L. *Phys. Rev. Lett.***1999,**82, 944.

87. http://www.mme.gov.br/portalmme/opencms/sgm/galerias/arquivos/plano_duo_decenal/a_mineracao_brasileira/P28_RT41_Perfil_da_Grafita.pdf. Access: 30 Oct. 2017.

88. Gopakumar, T. G.; Pagé. D. J. Y. S. *Polym. Eng. Sci.* **2004,**44 (6), 1162.

89. Chung.D.D.L. *J. Mater. Sci.***2002,** 37, 1475.

90. Pokharel,P.; Bae, H.; Lim, J.G.; Lee,K.Y.; Choi.S. *J. Appl. Polym. Sci.***2015,** 42073.

91. Potts, J. P.; Dreyer, D. R.; Bielawski, C. W.; Ruoff, R. S. *Polymer***2011**,52, 5.

92. Pavoski, G.; Maraschin, T.; Fim, F.C.; Balzaretti, N.M.; Galland, G.B.; Moura, C. S.; Bosso. N. R. S. *Mater. Res.***2017,** 20 (1) , 53.

93. Di, C.; Wei, D.; Yu, G.; Liu,Y.;Guo, Y.; Zhu.D. *Adv. Mater.* **2008,** 20, 3289.

94. Sutter, P. W.; Flege, J.I.; Sutter.E. A. *Nature Mater.***2008,**7, 406.

95. Kim, C.-D.; Min,B.-K.; Jung.W.-S. *Carbon* **2009**, 47, 1610.

96. Li;N.; Wang,Z.; Zhao,K.; Shi,Z.; Gu, Z. ; Xu.S. *Carbon* **2010,**48, 255.

97. Novoselov, K. S.; Geim, A.k.; Morozov,S.V.; Jiang,D.; Zhang, Y.: Dubonos, S.V. Science **2004**, 306, 666.

98. Singh,V.;Joung, D.; Zhia, L.; Das,S.; Khondaker, S. I.; Seal. S.*Prog. Mater. Sci.***2011,** 56, 1178.

99. Chen, G.; Weng, W.; Wu, D.; Wu. C. *Eup. Polym. J* .**2003**, 39, 2329.

100. Chen, G.; Wu, C.;weng, W.; Wu, D.; Yun.W. *Polymer***2003,** 44.1781 .

101. Chen, G.H.; Wu. D.J.; Weng,W.G.; He, B.; Yan. W.*Polym. Int.***2001**, 50, 980.

102. Celzard, A. ; Mareche, J.F.; Furdin, G.; Puricelli. S. *J. Phys. D. Appl. Phys.* **2000**, 33, 3094.

103. Stankovich, S.;Dikin,D. A.; Piner,R. D.; Kohlhaas,K. A.; Kleinhammes, A.; Jia,Y.; Wu,Y.; Nguyen,S. T.; Ruoff.R. S. *Carbon* **2007,** 45, 1558.

104. Eda, G.; Chhowalla. M.*Adv. Mater.***2010,** 22 , 2392.

105. Loh, K. P.; Bao, Q. ; Eda, G.; Chhowalla. M. *Nat. Chem.* **2010,** 2 , 1015.

106. Brodie. B.C.*Philos.Trans. R.Soc. London***1859,** 149, 249.

107. Staudenmaier, L.; Dtsch. B. *Chem. Ges.***1898,**31, 1481.

108. Hofmann, U.;Konig,E. *Chem.***1937,** 234,311.

109. Hummers, W.S.; Offeman.R.E.*J.Am. Chem. Soc.***1958,**80, 1339.

110. Singh,R.K.; Kumar,R.; Sing.D.P. *Rsc. Adv.***2016,** 6, 64993.

111. Botas, C. ; Alvarez, P.; Blanco, P.; Granda, M.; Blanco, C.; Santamarıa, R.; Romasanta, L. J.; Verdejo, R.; Lopez- Manchado, M. A.; Menendez. R. *Carbon* **2013**, 65, 156.

112. Yan, Q. L;Gozin,M.; Zhao, F.Q.; Cohen,A.; Pang, S.P. *Nanoscale***2016**, 8, 4799.

113. Kuila, T.; Mishra, A. K.; Khanra, P.; Kim,N. H.; Lee, J. H.; *Nanoscale***2013,** 5, 52.

114. Mao, S.; Pu, H.; Chen, J. *RSC Adv*. **2012,** 2, 2643.

115. Jeong, H.K.; Lee, Y. P.; Lahaye, R. J. W. E.; Park, M.H.; An, K. H.; Kim, I. J.; Yang, C.W.; Park, C. Y.; Ruoff, R. S.; Lee, Y. H.; *J. Am. Chem. Soc.* **2008,** 130, 1362.

116. Poh, L.;Sanek, F.; Ambrosi, A.; Zhao, G.; Sofer, Z.; Pumera, M. *Nanoscale* **2012,** 4, 3515.

117. Hontoria-Lucas, C.;Lopez-Peinado, A. J.; Lopez- Gonzalez, J. d. D.; Rojas-Cervantes, M. L.; Martın-Aranda, R. M.*Carbon***1995**, 33, 1585.

118. Peng, Y.Y.; Liu, Y.M.; Chang, J.K.; Wu, C.H.; Ger, M.D.; Pu, N.W.; Chang, C.L. *Carbon***2015**, 81, 347.

119. Poh, H. L.; Simek, P.; Sofer, Z.; Pumera,M. *ACS Nano***2013,** 7, 5262.

120. Sacer, D.;Capeta,D.;SrutRakic,I.; Peter,R.; Petravic, M.; KraljicRokovic,M. *Electrochim. Acta***2016**, 193, 311.

121. Kang, J. H.; Kim,T.; Choi,J.; Park,J.; Kim,Y. S.; Chang,M. S.; Jung,H.; Park,K. T.;Yang, S. J.; Park,C. R.;*Chem. Mater*.**2016,** 28, 756.

122. Saha, U.; Jaiswal, R.; Goswami, T. H. *Electrochim. Acta* **2016,** 196, 386.

123. Pacile, D.; Meyer, J. C.; Fraile Rodrıguez, A.; Papagno, M.; Gomez-Navarro, C.; Sundaram, R. S.; Burghard, M.; Kern, K.;Carbone, C. Kaiser, U. *Carbon* **2011,** 49, 966.

124. He, H.; Klinowski, J.; Forster, M.; Lerf, A. *Chem. Phys. Lett.* **1998,** 287, 53.

125. Gao, W.; Alemany, L.B.; Ci, L.; Ajayan. P.M. *Nature* **2009,** 1, 403.

126. Do, D. D*. Chemical Engineering Science***1996**, 51, 4145.

127. Liou, T-H. *Chem. Eng. J.***2010**, 158, 129.

128. Sieliechi, J.M.; Thue,P.S. *Water Treat.***2015,** 55, 986.

129. Foo, K.Y.; Hameed,B.H.; *Bioresour. Technol*. **2012,** 111, 425..

130. Kaifang, F. ; Qinyan, Y.; Baoyu, G.; Yuanyuan, S.; Wang, Y.; Li, Q.; Pin, Z.; Chen, S. *J. Taiwan Inst. Chem. Eng.***2014**, 45, 3007.

131. Mohamad, A, N.; Williams, P.*Biomass Bioenerg***2012,** 37, 142.

132. Ahmed, M.J.; Theydan,S.K. *J. Anal. Appl. Pyrol.***2014,** 105, 199.

133. Freudenstein. M. *Kunststoffe* **2007,**97, 54.

134. Razavi, A.; Thewalt. U.; Coord. *Chem. Rev.***2006,** 250, 155.

135. Kaminsky, W.; Funk, A.; Hahnsen. H.; *Dalton. Trans.***2009,** 8803.

136. Villanueva, M. P.; Cabedo, L.; Lagarón, J. M.; Giménez, E. *J. Appl. Polym. Sci.***2010**, 115, 1325.

137. Coutinho, F. M. B.; Mello, I. L.; Maria, L. C. S.*Polímeros: Ciência e Tecnologia***2003**,13, 1.

138. Bhattachary. M. *Materials***2016,** 9, 262.

139. Edwards, D.C. *J. Mater. Sci.* **1990**, 25, 4175.

140. Chrissafis, K.; Paraskevopoulos, K.M.; Tsiaoussis, I.; Bikiaris. D.C. *J.Appl. Polym. Sci***2009,** 114,1606.

141. Yu, M.; Dyer, M.J.; Kelly, T.F.; Ruoff, R.S. *Science* **2000,** 287, 637.

142. Bahuleyan, B.K.; Atieh, M.A.; De, S.K.; Khan, M.J.; Al-Harthi. M.A. *J.Polym.Res.***2012,** 19, 9744.

143. Bonduel, D.; Bredeau, S.; Alexandre, M.; Monteverde, F.; Dubois. P. *J. Matter. Chem.* **2007,**17, 2359.

144. Trujillo, M.; Arnal, M.L.; Muller, A.J.; Laredo, E.;Bredeau, S.; Bonduel, D.; Dubois. P. *Macromolecules* **2007,**40, 6268.

145. McNally, T.; Potsschke, P.; Hally,P.; Murphy, M.; Martin, D.; Bell, S. E. J.; Brennan,G.P.; Bein, D.; Lemoine, P.; Quinn. J.P. *Polymer***2005,** 46, 8222.

146. Jiang, X. ; Drzal. L.T. *Polym. Compos* **2012,** 637.

147. Song, P. Cao, Z.; Cai, Y.; Zhao, L.; Fang, Z.; Fu. S. *Polymer***2011,**52, 4001.

148. Fim, F. C.; Guterres, J.; Basso, N. R. S.; Galland, G. B. *J. Polym. Sci. Part A. Chem.* **2010,** 48, 692.

149. Millani, M. A.; Gonzalez, D.; Quijada, R.; Basso, N.R. S.; Cerrada, M.L.; Azambuja, D. S.; Galland, G.B. *Compos. Sci. Technol*. **2013**, 84, 1.

150. Millani, M. A.; Gonzalez, D.; Quijada, Benavente, R.; Andres, J. A.; Galland, G.B. *Polymer* **2015**, 65, 134.

151. https://www.thoughtco.com/definition-of-electrical-conductivity-605064/ access date 08/01/2018.

152. http://electricalacademia.com/electrical-comparisons/difference-between-conductor-semiconductor-and-insulator/ access date 08/01/2018

153. Mendez, R.; Constant, B.; Garzon, C.; Nisar, M.; Nachtigall, S. M. B.; Quijada, R. *Polymer***2017**, 130, 10.

154. Compton, O. C.; Nguyen, S.B.T. *Small* **2010**, 6, 711.

155. Spitalsky, Z.; Tasis, D.; Papagelis, K.; Galiotis, C. *Prog. Polym. Sci.***2010**, 35, 357.

156. Cullity, B.D.; Graham, C.D. *Introduction to magnetic materials*, 2nd edition, John Wiley & sons, Inc.,

157. Coey, J.M.D. *Magnetism and magnetic materials*, Cambridge university press, New York.

158. Kittel, C. *Introduction to Solid State Physics*. John Wiley & Sons, Inc. New York,1996.

159. Moskowitz, B.M. Hitchhiker's Guide to Magnetism. http://www.geo.umn.edu/orgs/irm/hg2m/hg2m_index.html. access 09/01/2018.

160. Santos, L. M. D.; Ligabue, R.; Dumas, A.; Roux, C. L.; Micoud,P.; Meunier, J.F.; Martin, F.; Einloft, S.*Eup. Polym. J.***2015,** 69, 38.

161. He, Q.; Yuan, T.; Zhu, J.;Luo, Z.; haldolaarachchige, N.; Sun, L.; Khasanov, A.; Li, Y.; Young, D.P.; Wei, S.; Guo. Z. *Polymer***2012,** 53, 3641.

162. Kirchberg, S.; Rudolph, M.; Ziegmann, G.; Peuker, U.A. *J. Nanomater.***2012** 1.

163. Dalls, P.; Georgakijas, V.; Niarchos, D.; Komninou, P.; Kehagis, T.; Petridis,D.; *Nanotechnology***2006,** 2046.

164. Burke, N.A.D.; Stover, H.D.H.; Dawson, F.P.; *Chem. Mater.* **2002,**14 (11), 4752.

165. Morelos-Gomez, A.; Lopez-Urias, F.; Munoz-Sandvoal, E.; Dennis, C.L.; Shull, R.D.; Terrones, H.; Terrones, M. *J.Mater.Chem.* **2010**, 20, 5906.

166. Riquelme, J.; Garzon, C.; Bergmann, C.; Geshev, J.; Quijada, R.; *Eur. Polym. J.***2016,**75, 200.

167. Nathani, H.; Gubbala, S.; Misra, R.D.K. *Mater. Sci. Eng. B.* **2004,**111, 95.

168. Sim, B.; Chae, H. S.; Choi, H. J. *eXPRESS. Polym. Lett.* **2015**, 9, 736.

169. Bernd, M. G. S.; Braganca, S. R.; Heck, N. Filho, L. C. P. S. J. *Mater. Res. Tecnol.* **2017**, 6(2), 171.

170. Thue, P.S.; Reis, G.S.; Lima, E.C.; Sieliechi, J.M.; Dotto, G. L.; Wamba, A.G. N.; Dias, S.L. P.; Pavan, F.A. *Res. Chem. Intermed.* **2017**, 43 (2), 1063.

Annex 1

Polymer 97 (2016) 131–137

Contents lists available at ScienceDirect

Polymer

journal homepage: www.elsevier.com/locate/polymer

An efficient approach to the preparation of polyethylene magnetic nanocomposites

Muhammad Nisar [a], Carlos Bergmann [b], Julian Geshev [c], Raúl Quijada [d], Griselda Barrera Galland [a, *]

[a] Instituto de Química, Universidade Federal do Rio Grande do Sul, Av. Bento Gonçalves, 9500, 91501-970 Porto Alegre, Brazil
[b] Laboratório de Materiais Cerâmicos, Departamento de Materiais, Universidade Federal do Rio Grande do Sul, Porto Alegre, Brazil
[c] Instituto de Física, Universidade Federal do Rio Grande do Sul, Porto Alegre, Brazil
[d] Departamento de Ingeniería Química y Biotecnología, Facultad de Ciencias Físicas y Matemáticas, Universidad de Chile, Santiago, Chile

ARTICLE INFO

Article history:
Received 10 March 2016
Received in revised form
9 May 2016
Accepted 10 May 2016
Available online 11 May 2016

Keywords:
Polyethylene
Carbon nanotubes
Magnetic nanocomposites

ABSTRACT

In the present work, a new method is developed for the preparation of polyethylene magnetic nanocomposites by *in situ* polymerization. Carbon nanotubes (CNTs), synthesized by the chemical vapor deposition method using ferrocene as the precursor and catalyst and silica (SiO_2) as the support, were used as fillers and compared with a commercial CNT. The synthesized nanofillers had iron magnetic particles encapsulated in CNTs. The fillers were well dispersed into the polyethylene matrix, as evidenced by scanning electron microscopy (SEM) and transmission electron microscopy (TEM) micrographs. Even for a very low filler concentration of 0.9 wt%, the presence of magnetic nanoparticles changed the diamagnetic nature of the polymer matrix to a ferromagnetic one. The thermal properties showed that the polymeric matrix did not change their properties significantly.

1. Introduction

Polymer matrices filled with inorganic nanoparticles (NPs) with improved mechanical properties, thermal stability, flam retardancy, chemical resistance, and electrical conductivity represent an area of growing scientific interest [1,2]. Carbon nanotubes (CNTs) were first reported in 1991 by Iijima [3]. Apart from its status as a conventional filler, the attractive mechanical thermal and electrical properties, high flexibility [4], and low mass density [5] of CNTs have gained attention in various fields of research, such as chemistry, physics, material science, and electrical engineering [6–9]. Treacy et al. [10] found that the average Young's modulus of isolated CNT reaches 1.8 TPa. Theoretical and experimental results have confirmed that single-wall CNTs demonstrate a high tensile modulus and tensile strength [11,12]. Wong *et al.* [13] determined the mechanical properties of multi-walled carbon nanotubes (MWNTs) using atomic force microscopy; these researchers established that they can be characterized by a very high toughness. In 1994, Ajayan et al. [14] reported on polymer nanocomposites using CNTs as filler for the first time. Earlier works used carbon black, silica, clays, and carbon nanofibers (CNFs) as fillers. In electromagnetic induction shielding, nanotubes have significant advantage over the conventional nanofillers used in the manufacture of multifunctional polymer composites [7,15].

In recent years, the use of CNTs as a reinforcing material for polymer has received enormous attention [6,16–18]. However, the dispersion of CNTs in the polymer matrix has to be taken into consideration to transfer the exceptional properties of CNTs to a polymeric material. The homogenous dispersion of CNTs throughout a polymer matrix is difficult to achieve because there must be considerable interaction between the polymer chain and the CNTs. Their small size and large surface area, as well as the delocalization of π electron subject the CNTs to van der Waals forces, all enhance aggregation [19–21]. An important issue is the compatibility of non-polar polymer matrices and CNTs to induce strong interaction between a polymer phase and filler, and consequently, to produce the efficient reinforcement of composites. In contrast, in the case of polar matrices, the problem seems easier to overcome; Zhang et al. [22,23] presented good results using nylon-6. Applying the same route, however, Tang et al. [24] and Bhattacharyya et al. [25] were unable to achieve significant dispersion of CNTs in polyolefin matrices due to the low compatibility of their apolar nature, which results in CNT aggregation. A number of

* Corresponding author.

http://dx.doi.org/10.1016/j.polymer.2016.05.029
0032-3861/

methods in the literature have been reported for the dispersion of CNTs in polymer matrices, for example, solution blending, melt mixing, and *in situ* polymerization [13,26–28]. This last method, where the filler is introduced during the polymerization reaction, is one of the most attractive routes to produce nanocomposites. This technique is known to be more effective in obtaining homogeneous dispersions of filler as compared to other conventional mechanical melt mixings.

Both academic and industrial researchers are extremely interested in exploring multifunctional magnetic polymer nanocomposites. These materials can potentially be used in many fields, for example, as microwave absorber, magnetic recording materials, energy storage devices, magnetic sensors, and for drug delivery [29]. The physical or chemical dispersion of magnetic elements, such as iron [30,31], cobalt [32,33], and nickel [34,35], into a polymer matrix can be carried out through the following approaches: *in situ* polymerization [36,37], surface-initiated polymerization [38,39], solution blending [40,41], ball milling [42], surface wetting [43], ion exchange [44], and melt blending [45,29]. Iron is one of the most traditionally used magnetic elements [46], and the magnetic performance of iron NPs has recently attracted a great deal of attention. The synthesis routes of iron NPs from soluble precursors in solutions include chemical reduction [47,48] and thermal [49,50] or sonochemical decomposition [51]. Similar to the conventional CNTs, iron NPs also tend to aggregate due to van der Waals forces, high surface energy, and large specific area. To efficiently disperse and control the particle growth, dispersants or surfactants are added during the fabrication of NPs in solution [50,51]. For instance, Burke et al. [50] carried out several sophisticated steps to produce polymer-Fe nanocomposites in the presence of ammonia and polymer (polyisobutylene, polyethylene, and polystyrene) grated with tetraethylenepentamine from the decomposition of $Fe(CO)_5$. Similarly, Tannenbaum et al. [52] reported an iron oxide nanocluster (γ-Fe_2O_3) from the thermal decomposition of $Fe(CO)_5$, where the synthesis process also involves complicated steps.

One of the most significant disadvantages of iron NPs is their easy oxidation. A recent study showed that the encapsulation of magnetic nanoparticles in CNTs could solve this problem [53,54]. Ferrocene [$Fe(C_2H_5)_2$] is a feasible organometallic compound used as an alternative to produce CNTs that does not require high temperature and acts both as a precursor and a catalyst of synthesis [55,56]. More recently, Osorio et al. [57,58] optimized the synthesis of CNTs with ferrocene using silica nanopowders with different surface areas as a substrate. The results showed that it is possible to control the final magnetic properties, that is, the composition of iron-containing phases in CNTs, by varying the temperature and dwell time of synthesis.

Our research group have been extensively working on synthesizing polyolefin nanocomposites using *in situ* polymerization. Recently, we prepared polyethylene–graphite nanosheet (PE-GNS) and isotactic polypropylene–graphite nanosheet (iPP-GNS) nanocomposites and obtained homogenous dispersions of the filler in the polymer matrix [59–64]. The present work aims to obtain nanocomposites of polyethylene iron encapsulated in carbon nanotubes (PE-CNTFe) through *in situ* polymerization using metallocene [$(nBuCp)_2ZrCl_2$] as a catalyst and methylaluminoxane (MAO) as a *co*-catalyst. The characterization of the nanocomposites and their magnetic properties were also studied.

2. Experimental

2.1. Materials

All compounds sensitive to air and moisture (*i.e.*, the catalyst and co-catalyst) were manipulated under deoxygenated dry argon using the standard Schlenk and vacuum line techniques. CNTs were acquired from BAYER®. Toluene was distilled with metallic sodium and benzophenone. MAO (Witco, 10 wt% Al solution in toluene) and metallocene catalyst bis(*n*-butyl)cyclopentadienylzirconium dichloride (n-$BuCp)_2ZrCl_2$ (Sigma Aldrich) were used as received.

2.2. Carbon nanotube synthesis

Two types of CNTs were used in this work: Commercial CNTs were acquired from BAYER®, and synthetic CNTs containing iron were synthesized using the method reported in Refs. 57 and 58. The characterization of the CNT-Fe by TEM can be seen in reference 58 as well as in the Supplementary Data.

2.3. Fabrication of polymer nanocomposites

The CNTs were stirred with 15 wt% of MAO over 30 min in toluene. The polymerization reactions were performed in a 300 mL reactor equipped with mechanical stirring at a controlled temperature. Toluene was used as solvent, MAO as co-catalyst (Al/Zr = 1000) and (n-$BuCp)_2ZrCl_2$ as catalyst (5×10^{-6} mol). All the reactions were carried out at 25 °C with a constant ethylene pressure of 3 bar over 0.5 h. The CNTs that were previously treated with MAO were introduced to the reactor as filler using a changeable quantity under inert atmosphere. The obtained polymer was washed with 10 vol% of HCl in ethanol solution and dried until it reached a constant weight.

2.4. Characterization of polymer nanocomposites

Transmission electron microscopy (TEM) analyses were performed using a JEOL 1011 microscope operating at 120 kV. Samples were prepared *via* the deposition of a solution drop on a copper grid of 300 mesh covered with amorphous carbon. Scanning electron microscopy (SEM) was carried using a Phillips XL30 microscope operating at 20 kV. Samples were prepared by deposition on an aluminum stub and coating with gold.

The molecular weights were obtained with a Waters Alliance GPC 2000 instrument equipped with three Styragel HT-type columns (HT3, HT5, and HT6E). 1,2,4-Trichlorobenzene was used as solvent, with a flow rate of 1 ml/min and a temperature of 135 °C. The columns were calibrated with polystyrene standards.

The magnetic characterization of the CNTs was performed using an EZ9MicroSense vibrating sample magnetometer (VSM) at room temperature with a magnetic field (H) ranging from −20 kOe to +20 kOe. Dynamic mechanical analysis (DMA) were obtained using a DMA analyzer (TA Instruments model Q800). The samples were analyzed in single-cantilever mode at a frequency of 1 Hz and a strain level of 0.1% in the temperature range of −140 °C to 120 °C.

Differential scanning calorimetric (DSC) analyses were performed using a Perkin-Elmer differential calorimeter (model DSC Q20) operating at a heat rate of 10 °C/min and a temperature range from 0 to 180 °C. The melting temperature, T_m, was determined in the second scan, and the degree of crystallinity was calculated from the enthalpy of fusion data obtained from the DSC curves (293 J/g was used for 100% crystalline material). Thermogravimetric analysis (TGA) was performed on a SDT Q600 thermal analyzer Q20 (TA Instruments) at a scanning rate of 20 °C/min from 0 °C to 800 °C.

3. Results and discussion

Polymerizations of ethylene were performed in the presence of commercial CNT and of synthesized iron NPs encapsulated in CNTs (CNT-Fe). The catalytic activities of these reactions are listed in

Table 1
Results of nanocomposites of polyethylene with different amounts of CNTs and CNT-Fe.

Samples	Filler[b] (%)	Polymer (g)	Catalytic activity[a]	T_c (°C)	T_m (°C)	X_c (%)	T_g (°C)	T_{max}
PE	0	7.40	966	113	139	55	−114	487
PE_{CNT}	1.1	6.95	927	115	138	62	−111	490
PE_{CNT}	3.4	6.01	801	115	138	58	–	493
PE_{CNT-Fe}	0.9	8.20	1093	113	141	53	−113	484
PE_{CNT-Fe}	2.5	7.48	998	114	139	55	–	483

[a] KgPE/[Zr] h bar.
[b] CNT or CNT-Fe.

Table 1, along with the polymerization without filler (neat polyethylene). It can be seen that with the treatment using CNTs or CNT-Fe did not deactivate the catalyst, since the activities were almost the same in all the reactions.

Table 1 also shows the thermal properties of the neat polyethylene and its nanocomposites. Neither the crystallinity (X_c) nor the T_m showed significant variation compared with the original polymer. The crystallization temperature (T_c) of the nanocomposites, however, showed a slight increase of 1–2 °C with the addition of a small amount of CNTs (1.1%). In addition, the glass transition temperature, T_g, also increased up to 3 °C with the incorporation of CNTs, which provides evidence for the reinforcement effect of the CNTs. The molecular weight of the neat polymer was significantly high (4.4×10^5 g mol^{-1} with a polydispersity of 1.9), which was also confirmed by the high melting temperature (139 °C). Previous preparations of polyolefin nanocomposites using the same method showed that the nanocomposites maintain the same molecular weight as the neat polymer [61]; in this case, this was also confirmed by the similar T_m. The maximum temperature (T_{max}) of degradation obtained by TGA showed a slight increase with the incorporation of CNTs and a small decrease with the addition of CNT-Fe. The increase in degradation of the nanocomposites in the presence of synthetic filler is considered to be due to the presence of iron in the filler, which acts as a catalyst of degradation. The nanocomposites did not show conductivity, as the amount of the filler was below the electrical percolation threshold.

Fig. 1 gives SEM micrographs of polyethylene/CNT nanocomposites with different loadings of filler. The micrographs show a fibrous morphology, indicating that the CNTs were coated by polyethylene. This type of morphology is mainly attributed to the low-temperature polymerization; the fibrous morphology is more prominent as the loading of CNTs with iron increases. Bahuleyan et al. [65] reported the absence of fibrous morphology at high polymerization temperatures, such 60 °C. The nanotubes seem to have a uniform dispersion in the polymer matrix.

A TEM morphological assessment of the prepared nanocomposites was performed. Fig. 2 shows representative micrographs of nanocomposites with similar magnifications. The dispersion quality of the filler in the polymer matrix was very good, and all CNTs showed homogenous dispersion, as no aggregation was observed. The TEM images confirm that CNTs and the polymer matrix form close interfaces without gaps.

4. Magnetic properties

The room temperature magnetization hysteresis loops of the CNT-Fe powder, PE-CNT-Fe and PE-CNT samples are plotted in Fig. 3. The magnetization curve of the PE-CNT sample (not shown) presented only diamagnetic characteristics with no hysteresis, evidencing absence of magnetic material in the CNTs. The

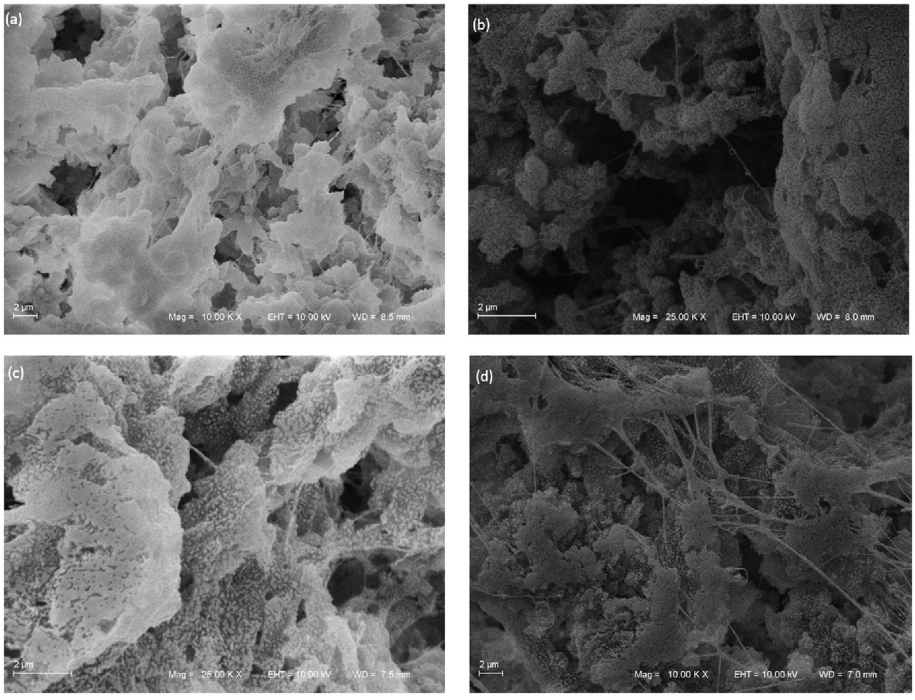

Fig. 1. SEM images of nanocomposites: (a) 1.1% and (b) 3.4% CNTs in PE; (c) 0.9% and (d) 2.5% CNT-Fe in PE.

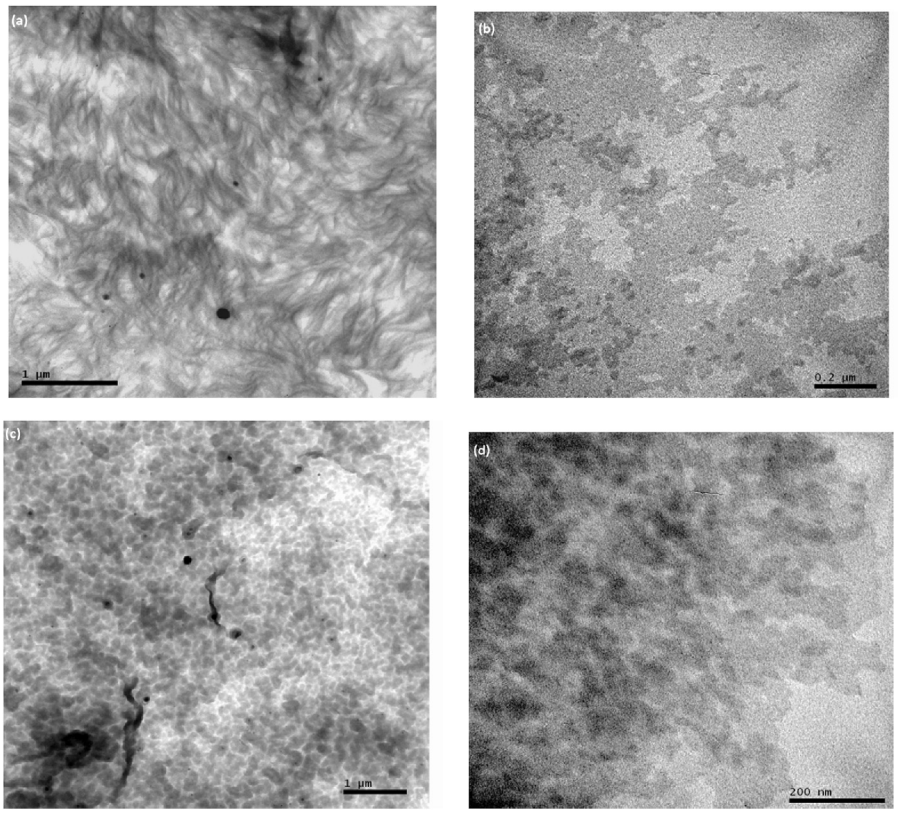

Fig. 2. TEM images of nanocomposites: (a) and (b) 2.5% CNTs-Fe in PE; (c) and (d) 0.9% CNTs-Fe in PE.

hysteresis loops for the PE-CNT-Fe 0.9 and 2.5 wt% samples turned out to be extremely similar, showing almost identical values of remnant magnetization/saturation magnetization (M_R/M_S) and coercivity (H_C), with the latter equal to ~1000 Oe. Table 2 gives the respective H_C and normalized (to the saturation magnetization value, M_S) remnant magnetization, M_R, of the nanocomposites. Recently, Riquelme et al. [29] reported on polypropylene magnetic nanocomposites by melt mixing, where they also used iron encapsulated in CNTs. They obtained a coercivity value of 500–550 Oe for 2–6% of nanotubes, which is half the value we obtained for 0.9–2.5% of filler. Similarly, Santos et al. [66] obtained coercivity of 275 and 250 Oe for polyurethanes, PU/3 and PU/10 wt % of Fe_3O_4 synthetic talc, that is, values approximately four times lower than ours. He *et al.* [67] reported a decrease from 193 to 9 Oe in H_C, with an increase from 5 to 20 wt% of magnetic particles in a high density polyethylene (HDPE) matrix. This can be ascribed to a decrease in inter-particle distance resulting in stronger (negative, demagnetizing) dipolar interactions, which tend to stabilize the demagnetized state with low remnant and coercivity values. In our case, H_C decreased slightly (from 1060 to ~1000 Oe) when the magnetic constituent was increased from 0.9 to 2.5%, which we attribute to the fact that the mean inter-particle distance is practically the same in both samples owing to the low amount of magnetic constituent (≤2.5%). This indicates a rather uniform dispersion of CNTs in the polymer matrix confirmed by the SEM and TEM analyses.

The above statement is strongly supported by additional

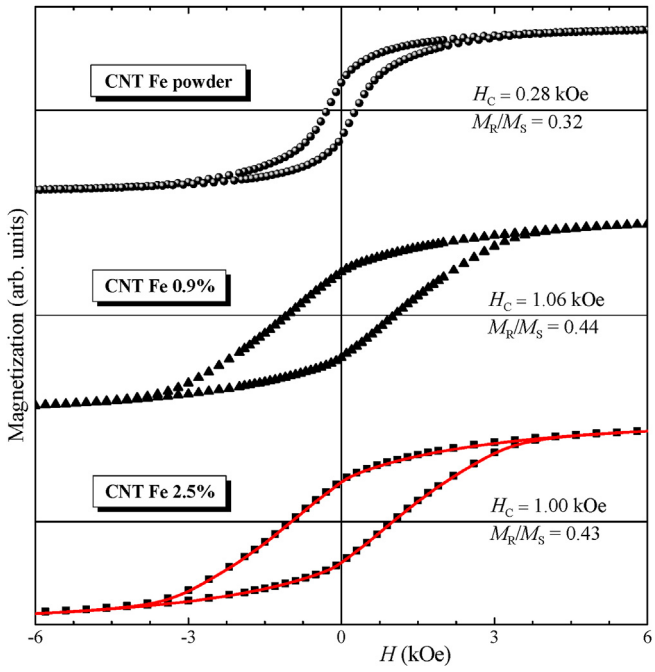

Fig. 3. Room-temperature hysteresis loops of (a) CNT-Fe powder, (b) CNT-Fe 0.9% in PE, and (c) CNT-Fe 2.5% in PE. The solid line in the bottom panel corresponds to a measurement on the same sample but performed approximately 6 months after the first loop trace (square symbols); during this period of time the sample was kept in air.

Table 2
H_C and M_R/M_S values of the nanocomposites extracted from the room-temperature VSM measurements.

Sample	H_C (Oe)	M_R/M_S
PE-CNT 3.4%	0	0
CNT-Fe	280(±10)	0.32
PE-CNT-Fe 0.9%	1060(±10)	0.44
PE-CNT-Fe 2.5%	1000(±10)	0.43

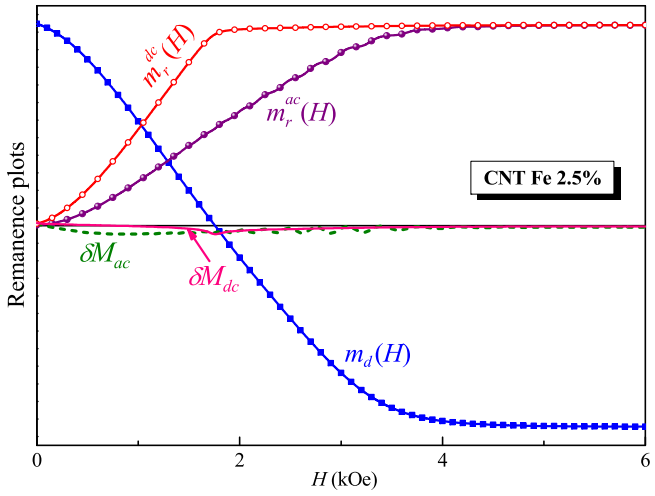

Fig. 4. Room-temperature remnant magnetization curves (both ac and dc types of demagnetization were used) and the corresponding δM plots for the CNT-Fe 2.5% PE nanocomposite.

interaction-effect measurements performed on the CNT-Fe 2.5% PE sample. We employed the so-called remanence-plots technique [68,69], which exploits relationships between the isothermal remanence magnetization [IRM or $m_r(H)$] and the dc demagnetization [DCD, or $m_d(H)$] curves, which are very sensitive to small changes in the remnant state produced by magnetic interactions; details of the method can be found elsewhere [70,71]. The value of the maximum field we used was sufficient for effective magnetic saturation, thereby avoiding minor-loop effects [72–76]. The $m_r(H)$ (measured on either an ac or dc demagnetized sample) and the $m_d(H)$ curves, together with the corresponding δM plots [77,78], are given in Fig. 4. Both δM plots confirm that the inter-particle interactions were demagnetizing and extremely weak.

Fig. 5 shows magnetic measurements on CNT-Fe in a powder form, being the interval between the first and the second loop traces of approximately 6 months, during which the sample was kept in air. One notes that the hysteresis loops are practically

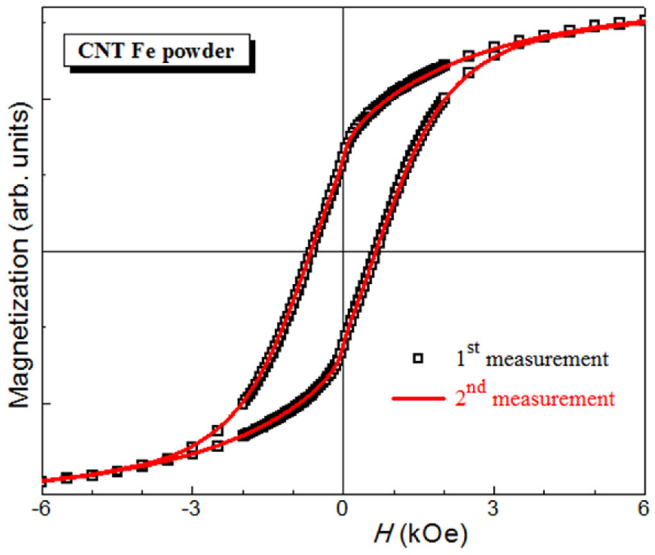

Fig. 5. Two room-temperature hysteresis loops traced on powdered CNT-Fe. The interval between the first and the second measurements is approximately 6 months, during which the powder was kept in air.

indistinguishable (the same holds for the sample CNT-Fe 2.5% in PE, see the bottom panel of Fig. 3), which strongly indicates that the encapsulation of the iron nanoparticles in CNT protects them from oxidation and aggregation.

5. Conclusions

A new magnetic nanocomposite of polyethylene/CNT-Fe was obtained through the *in situ* polymerization of ethylene using $(nBuCp)_2ZrCl_2$/MAO as a catalyst system. The rather high coercivity values (~1000 Oe) obtained here should be attributed to two techniques we employed, namely: 1) the encapsulation of Fe in CNT, which protected the iron NPs from oxidation and aggregation; and 2) the *in situ* polymerization method, that allows a uniform dispersion of CNTs in the polymer matrix and avoids dipolar interactions, which tend to stabilize the demagnetized state. This new material, which maintains all of the excellent properties of polyethylene and adds a magnetic characteristic, has the potential to be used in a variety of applications where a flexible magnetic material with good processability could be required.

Acknowledgments

The authors are grateful to the TWAS-CNPQ for the fellowship to Muhammad Nisar, the CNPq for the special visiting research fellowship to Professor Raúl Quijada, and CNPq grant 302902/2013-9. Professor Raúl Quijada acknowledges the Millennium Nucleus of Chemical Processes and Catalysis (CPC), grant number NC120082. We also thank CME and LRNANO from UFRGS for the microscopy analysis.

Appendix A. Supplementary data

Supplementary data related to this article can be found at http://dx.doi.org/10.1016/j.polymer.2016.05.029.

References

[1] J. Jancar, J.F. Douglas, F.W. Starr, S.K. Kumar, P. Cassagnau, A.J. Lesser, S.S. Sternstein, M. Buehler, Current issues in research on structural-property relationship in polymer nanocomposites, Polymer 51 (2010) 3321–3343.
[2] I.Y. Jeon, J.B. Baek, Nanocomposites derived from polymers and inorganic nanoparticles, Materials 3 (2010) 3654–3674.
[3] S. Iijima, Helical Microtubules of Graphitic Carbon, vol. 354, Nature, London, 1991, pp. 56–58.
[4] C.A. Cooper, R.J. Young, M. Halasll, Investigation into the deformation of carbon nanotubes and their composites through the use of Raman Spectroscopy, Compos. Part A 32 A (2001) 401–411.
[5] G. Gao, T. Cagin, W.A. Goddard III, Energetics, structure, mechanical and vibrational properties of single walled carbon nanotubes, Nanotechnology 9 (1998) 184–191.
[6] R.H. Baughman, A.A. Zakhivov, W.A. De Heer, Carbon nanotubes the route toward applications, Science 297 (2002) 787–792.
[7] P.M. Ajayan, Nanotubes from carbon, Chem. Rev. 99 (1999) 1787–1800.
[8] C.A. Grimes, C. Mungle, D. Kouzoudis, S. Fang, P.C. Eklund, The 500 MHz to 5.50 GHz complex permittivity spectra of single-wall carbon nanotube-loaded polymer composites, Chem. Phys. Lett. 319 (2000) 460–464.
[9] B.S. File, B.M. Mayeaux, Carbon nanotubes, Adv. Matter. Process 156 (1999) 47–49.
[10] M.M.J. Treacy, T.W. Ebbesen, J.M. Gibson, Exceptionally high Young's modulus observed for individual carbon nanotubes, Nature 381 (1996) 678–680.
[11] T. Uchida, S. Kumar, Single wall carbon nanotube dispersion and exfoliation in polymers, J. Appl. Polym. Sci. 98 (2005) 985–989.
[12] A. De Heer Walt, Nanotubes and the pursuit of applications, MRS. Bull. 29 (2004) 281–285.
[13] E.W. Wong, P.E. Sheehan, C.M. Lieber, Nanobeam mechanics: elasticity, strength and toughness of nanorods and nanotubes, Science 277 (1997) 1971–1975.
[14] P.M. Ajayan, O. Stephan, C. Colliex, D. Trauth, Aligned carbon nanotubes arrays formed by cutting a polymer resin-nanotube composites, Science 265 (1994) 1212–1214.
[15] M. Moniruzzaman, K.I. Winey, Polymer nanocomposites containing carbon nanotubes, Macromolecules 39 (2006) 5194–5205.

[16] E.T. Thostenton, Z. Ren, T.W. Chou, Advances in the *science* and *technology* of carbon nanotubes and their composites: a review, Compos. Sci. Technol. 61 (2001) 1899–1912.
[17] R. Andrews, M.C. Weisenberger, Carbon nanotube polymer composites, Curr. Opin. Solid State Mater. Sci. 8 (2004) 31–37.
[18] A.K.T. Lau, D. Hui, Strength and durability performance of concrete axially loaded members confined with AFRP composite sheets, Compos. Part B 33 (2002) 263–277.
[19] S. Bredeau, S. Peeterbroeck, D. Bonduel, M. Alexandre, P. Dubois, From carbon nanotube coatings to high-performance polymer nanocomposites, Polym. Int. 57 (2008) 547–553.
[20] P. Ajayan, in: H.S. Nalwa (Ed.), Handbook of Nanostructured Materials and Nanotechnology, 5, Academic Press, New York, 2000, pp. 501–575.
[21] C. Wang, Z. Guo, S. Fu, W. Wu, D. Zhu, Polymers containing fullerene or carbon nanotube structures, Prog. Polym. Sci. 29 (2004) 1079–1141.
[22] W.D. Zhang, L. Shen, I.Y. Phang, T. Liu, Carbon nanotubes reinforced nylon-6 composite prepared by simple melt-compounding, Macromolecules 37 (2004) 256–259.
[23] T. Liu, I.Y. Phang, L. Shen, S.Y. Chows, W.D. Zhang, Morphology and mechanical. properties of multiwalled carbon nanotubes. Reinforced Nylon-6 composites, Macromolecules 37 (2004) 7214–7222.
[24] W. Tang, M.H. Santare, S.G. Advani, Melt processing and mechanical property characterization of multi-walled carbon nanotube/high density polyethylene (MWNT/HDPE) composite films, Carbon 41 (2003) 2779–2785.
[25] A.R. Bhattacharyya, T.V. Sreekumer, T. Liu, S. Kumar, L.M. Ericson, R.H. Hauge, R.E. Smalley, Crystallization and orientation studies in polypropylene/single wall carbon nanotube composite, Polymer 44 (2003) 2373–2377.
[26] X.L. Xie, Y.W. Mai, X.P. Zhou, Dispersion and alignment of carbon nanotubes in polymer matrix: a review, Mater. Sci. Eng. 49 (2005) 89–112.
[27] L. Ashabi, S.H. Jafari, H.A. Khonakdar, B. Baghaei, Morphological, rheological and thermal studies in melt processed compatibilized PA6/ABS/clay nanocomposites, J. Polym. Res. 18 (2011) 197–205.
[28] K. Saeed, S.Y. Park, Preparation and characterization of multiwalled carbon nanotubes/polyacrylonitrile nanofibers, J. Polym. Res. 17 (2010) 535–540.
[29] J. Riquelme, C. Garzón, B. Bergmann, J. Geshev, R. Quijada, Development of multifunctional polymer nanocomposites with carbon-based hybrid nanostructures synthesized from ferrocene, Eur. Polym. J. 75 (2016) 200–209.
[30] S.N. Khanna, S. Linderoth, Magnetic behavior of clusters of ferromagnetic transition metals, Phys. Rev. Lett. 67 (6) (1991) 742–745.
[31] D. Farrell, S.A. Majetich, J.P. Wilcoxon, Preparation and characterization of monodisperse Fe nanoparticles, J. Phys. Chem. B 107 (2003) 11022–11103.
[32] X. Lin, C. Sorensen, K. Klabunde, G.C. Hadjipanayis, Temperature dependence of morphology and magnetic properties of cobalt nanoparticles prepared by an inverse micelle technique, Langmuir 14 (1998) 7140–7146.
[33] C. Petit, A. Taleb, M. Pileni, Cobalt nanosized particles organized in a 2D superlattice: synthesis, characterization, and magnetic properties, J. Phys. Chem. B 103 (1999) 1805–1810.
[34] S. Apsel, J. Emmert, J. Deng, L. Bloomfield, Surface-Enhanced magnetism in nickel clusters, Phys. Rev. Lett. 76 (1996) 1441–1444.
[35] T.O. Ely, C. Amiens, B. Chaudret, E. Snoeck, M. Verelst, M. Respaud, Synthesis of nickel nanoparticles. influence of aggregation induced by modification of poly(vinylpyrrolidone) chain length on their magnetic properties, Chem. Mater. 11 (1999) 526–529.
[36] T.H. Hsieh, K.S. Ho, X. Bi, Y.K. Han, Z.L. Chen, C.H. Hsu, Synthesis and electromagnetic properties of polyaniline-coated silica/maghemite nanoparticles, Eur. Polym. J. 45 (2009) 613–620.
[37] H. Nathani, R. Misra, Surface effects on the magnetic behavior of nanocrystalline nickel ferrites and nickel ferrite-polymer nanocomposites, Mater. Sci. Eng. B 113 (2004) 228–235.
[38] J. Zhu, S. Wei, L. Zhang, Y. Mao, J. Ryu, A.B. Karki, Polyaniline-tungsten oxide metacomposites with tunable electronic properties, J. Mater. Chem. 21 (2011) 342–348.
[39] J. Zhu, S. Wei, L. Zhang, Y. Mao, J. Ryu, N. Haldolaarachchige, Electrical and dielectric properties of polyaniline–Al_2O_3 nanocomposites derived from various Al_2O_3 nanostructures, J. Mater. Chem. 21 (2011) 3952–3959.
[40] J. Zhu, S. Wei, D. Rutman, N. Haldolaarachchige, D.P. Young, Z. Guo, Magnetic polyacrylonitrile-Fe@FeO nanocomposite fibers – electrospinning, stabilization and carbonization, Polymer 52 (2011) 2947–2955.
[41] X. Chen, S. Wei, C. Gunesoglu, J. Zhu, C.S. Southworth, L. Sun, Electrospun magnetic fibrillar polystyrene nanocomposites reinforced with nickel nanoparticles, Macromol. Chem. Phys. 211 (2010) 1775–1783.
[42] A. Ohlan, K. Singh, A. Chandra, S.K. Dhawan, Microwave absorption behavior of core-shell structured poly (3,4-ethylenedioxy thiophene)-barium ferrite nanocomposites, ACS Appl. Mater. Inter 2 (2010) 927–933.
[43] J. Zhu, S. Wei, J. Ryu, L. Sun, Z. Luo, Z. Guo, Magnetic epoxy resin nanocomposites reinforced with core-shell structured Fe@FeO nanoparticles: fabrication and property analysis, ACS Appl. Mater. Inter 2 (2010) 2100–2107.
[44] S. Mu, D. Wu, Y. Wang, Z. Wu, X. Yang, W. Yang, Fabrication of nickel oxide nanocomposite layer on a flexible polyimide substrate via ion exchange technique, ACS Appl. Mater. Inter 2 (2009) 111–118.
[45] J.L. Wilson, P. Poddar, N.A. Frey, H. Srikanth, K. Mohomed, J.P. Harmon, S. Kotha, J. Wachsmuth, Synthesis and magnetic properties of polymer nanocomposites with embedded iron nanoparticles, J. Appl. Phys. 95 (2004) 1439–1443.
[46] S. Wei, Q. Wang, J. Zhu, L. Sun, H. Lin, Z. Guo, Multifunctional composite core–shell nanoparticles, Nanoscale 3 (2011) 4474–4502.
[47] Z. Guo, L.L. Henry, V. Palshin, E.J. Podlaha, Synthesis of poly (methyl methacrylate) stabilized colloidal zero-valence metallic nanoparticles, J. Mater. Chem. 16 (2006) 1772–1777.
[48] Y. Hou, J. Yu, S. Gao, Solvothermal reduction synthesis and characterization of superparamagnetic magnetite nanoparticles, J. Mater. Chem. 13 (2003) 1983–1987.
[49] J. Zhu, S. Wei, Y. Li, L. Sun, N. Haldolaarachchige, D.P. Young, Surfactant-free synthesized magnetic polypropylene nanocomposites: rheological, electrical, magnetic and thermal properties, Macromolecules 44 (2011) 4382–4391.
[50] N.A.D. Burke, H.D.H. Stöver, F.P. Dawson, Magnetic nanocomposites: preparation and characterization of polymer coated iron nanoparticles, Chem. Mater. 14 (2002) 4752–4761.
[51] S. Wizel, S. Margel, A. Gedanken, The preparation of a polystyrene–iron composite by using ultrasound radiation, Polym. Int. 49 (2000) 445–448.
[52] R. Tannenbaum, M. Zubris, P.E. Goldberg, S. Reich, N. Dan, Polymer-directed nanocluster synthesis: control of particle size and morphology, Macromolecules 38 (2005) 4254–4259.
[53] A. Morelos-Gómez, F. Lopez-Urias, E. Munoz-Sandoval, C.L. Dennis, R.D. Shull, H. Terrones, M. Terrones, Controlling high coercivities of ferromagnetic nanowires encapsulated in carbon nanotubes, J. Mater. Chem. 20 (2010) 5906–5914.
[54] C. He, N. Zhao, C. Shi, J. Li, H. Li, Magnatic properties and transmission electron microscopy studies of Ni nanoparticles encapsulated in carbon nanocages and carbon nanotubes, Mater. Res. Bull. 43 (2008) 2260–2265.
[55] R. Bhatia, V. Prasad, Synthesis of multiwall carbon nanotubes by chemical vapor deposition of ferrocene alone, Solid State Commun. 150 (2010) 311–315.
[56] K.P.S.S. Hembram, G.M. Rao, Structural and surface features of multiwall carbon nanotubes, Appl. Surf. Sci. 257 (2011) 5503–5507.
[57] A.G. Osorio, C.P. Bergmann, Effect of surface area of substrates aiming the optimization of carbon nanotube production from ferrocene, Appl. Surf. Sci. 264 (2013) 794–800.
[58] A.G. Osorio, L.G. Pereira, J.B.M. Cunha da, C.P. Bergmann, Controlling the magnetic response of carbon nanotubes filled with iron-containing material, Mater. Res. Bull. 48 (2013) 4168–4173.
[59] F.C. Fim, J.M. Guterres, N.R.S. Basso, G.B. Galland, Polyethylene/Graphite nanocomposites obtained by *in situ* polymerization, J. Polym. Sci. Part A Polym. Chem. 48 (2010) 692–698.
[60] M.A. Milani, R. Quijada, N.R.S. Basso, A.P. Graebin, G.B. Galland, Influence of the graphite type on the synthesis of polypropylene graphene nanocomposites, J. Polym. Sci. Part A Polym. Chem. 50 (2012) 3598–3605.
[61] M.A. Milani, D. González, R. Quijada, N.R.S. Basso, M.L. Cerrada, D.S. Azambuja, G.B. Galland, Polypropylene/graphene nanosheet nanocomposites by *in situ* polymerization: synthesis, characterization and fundamental properties, Compos. Sci. Technol. 84 (2013) 1–7.
[62] F.C. Fim, N.R.S. Basso, A.P. Graebin, D.S. Azambuja, G.B. Galland, Thermal, electrical, and mechanical properties of polyethylene-graphene nanocomposites obtained by in situ polymerization, J. Appl. Polym. Sci. 128 (2013) 2630–2637.
[63] M.A. Milani, D. González, R. Quijada, R. Benavente, J. Arranz-Andrés, G.B. Galland, Synthesis, characterization and properties of poly(propylene-1-octene)/graphite nanosheet nanocomposites obtained by *in situ* polymerization, Polymer 65 (2015) 134–142.
[64] G. Pavoski, T. Maraschin, M.A. Milani, D.S. Azambuja, R. Quijada, C.M. Moura, N.R.S. Basso, G.B. Griselda, Polyethylene/reduced graphite oxide nanocomposites with improved morphology and conductivity, Polymer 81 (2015) 79–86.
[65] B.K. Bahuleyan, M.A. Atieh, S.K. De, M.J. Khan, M.A. Al-Hazrthi, Easy one-pot method to control the morphology of polyethylene/carbon nanotube nanocomposites using metallocene catalysts, J. Polym. Res. 19 (2012) 9744.
[66] L.M.D. Santos, R. Ligabue, A. Dumas, C.L. Roux, P. Micoud, J.F. Meunier, F. Martin, S. Einloft, New magnetic nanocomposites: Polyurethane/Fe_3O_4-synthetic talc, Eup. Polym. J. 69 (2015) 38–49.
[67] Q. He, T. Yuan, J. Zhu, Z. Luo, N. Haldolaarachchige, L. Sun, A. Khasanov, Y. Li, D.P. Young, S. Wei, Z. Guo, Magnetic high density polyethylene nanocomposites reinforced with in-situ synthesized Fe@FeO core-shell nanoparticles, Polymer 53 (2012) 3642–3652.
[68] P.R. Bissel, R.W. Chantrell, G. Tomka, J.E. Knowles, M.P. Sharrock, Remanent magnetisation and demagnetisation measurements on particulate recording media, IEEE Trans. Magn. 25 (1989) 3650–3653.
[69] P.I. Mayo, K. O'Grady, R.W. Chantrell, J.A. Cambridge, I.L. Sanders, T. Yogi, J.K. Howard, Magnetic measurement of interaction effects in CoNiCr and CoPtCr thin film media, J. Magn. Magn. Mater 95 (1991) 109–117.
[70] R. Cichelero, A. Harres, K.D. Sossmeier, J.E. Schmidt, J. Geshev, Magnetic interactions in exchange-coupled yet unbiased IrMn/NiCu bilayers, J. Phys. Condens. Matter 25 (2013) 426001.
[71] A. Harres, R. Cichelero, L.G. Pereira, J.E. Schmidt, J. Geshev, Remanence plots technique extended to exchange bias systems, J. Appl. Phys. 114 (2013) 043902.
[72] L. Klein, Comment on "exchange bias-like phenomenon in SrRuO3" [Appl. Phys. Lett. 88, 102502 (2006)], Appl. Phys. Lett. 89 (2006) 036101.
[73] J. Geshev, Exchange bias and vertical shift in CoFe2O4 nanoparticles, J. Magn. Magn. Mater 320 (2008) 600–602.
[74] J. Geshev, Comment on "Cluster glass induced exchange biaslike effect in the

perovskite cobaltites, Appl. Phys. Lett. 93 (2008) 176101.
[75] J. Geshev, L.G. Pereira, V. Skumryev, Comment on "exchange bias dependence on interface spin alignment in a Ni80Fe20/(Ni,Fe)O thin film, Phys. Rev. Lett. 100 (2008) 039701.
[76] A. Harres, M. Mikhov, V. Skumryev, A.M.H. de Andrade, J.E. Schmidt, J. Geshev, Criteria for saturated magnetization loop, J. Magn. Magn. Mater 402 (2016) 76–82.
[77] P.E. Kelly, K. O'Grady, P.I. Mayo, R.W. Chantrell, Switching mechanisms in cobalt-phosphorus thin film, IEEE Trans. Magn. 25 (1989) 3881–3883.
[78] A.D.C. Viegas, J. Geshev, L.S. Dorneles, J.E. Schmidt, M. Knobel, Correlation between magnetic interactions and giant magnetoresistance in melt-spun $CO_{10}Cu_{90}$ granular alloys, J. Appl. Phys. 82 (1997) 3047–3053.

Annex 2

Polymer 118 (2017) 68–74

Contents lists available at ScienceDirect

Polymer

journal homepage: www.elsevier.com/locate/polymer

Synthesis and characterization of polypropylene/iron encapsulated carbon nanotube composites with high magnetic response at room temperature

Muhammad Nisar [a], Carlos Pérez Bergmann [b], Julian Geshev [c], Raúl Quijada [d], Griselda Barrera Galland [a, *]

[a] Instituto de Química, Universidade Federal do Rio Grande do Sul, Av. Bento Gonçalves 9500, 91501-970 Porto Alegre, Brazil
[b] Laboratório de Materiais Cerâmicos, Departamento de Materiais, Universidade Federal do Rio Grande do Sul, Porto Alegre, Brazil
[c] Instituto de Física, Universidade Federal do Rio Grande do Sul, Porto Alegre, Brazil
[d] Departamento de Ingeniería Química y Biotecnología, Facultad de Ciencias Físicas y Matemáticas, Universidad de Chile, Santiago, Chile

ARTICLE INFO

Article history:
Received 15 February 2017
Received in revised form
18 April 2017
Accepted 19 April 2017
Available online 27 April 2017

Keywords:
Polypropylene
Carbon nanotube
Magnetic nanocomposites

ABSTRACT

Magnetic and conducting polypropylene (PP) polymer nanocomposites with different loadings of synthetic carbon nanotubes (CNT-Fe) were fabricated by *in-situ* polymerization. Chemical vapor deposition was used as the synthetic route for carbon nanotube (CNT) synthesis, in which high-surface-area silica (SiO_2) acts as the support and ferrocene as the precursor and catalyst. Scanning and transmission electron microscopy analyses evidence the homogenous dispersion of the filler in the polymer matrix. It was found that, with the addition of 3.8 wt.% of the filler, the insulating PP matrix changes to a semiconductor. The magnetic properties of the nanocomposites were investigated using a vibrating sample magnetometer. The addition of 0.8 wt.% CNTs results in ferromagnetic behavior in the diamagnetic polymer matrix and high coercivities at room temperature. The thermal properties were investigated by thermogravimetric analysis and differential scanning calorimetry. Results show an increase in the maximum degradation, crystallization, and melting temperatures of the nanocomposites as compared with neat PP.

1. Introduction

Inorganic–organic composite materials are becoming increasing important because of their remarkable properties, which can be attributed to the synergism between the properties of their components. There are several routes to prepare these materials, with the most important one perhaps being the incorporation of inorganic components in organic polymers. These materials have attracted the attention of the researchers owing to the significant changes in their mechanical, thermal, electrical, and magnetic properties, compared to pure organic polymers [1]. Polymer nanocomposites demonstrate remarkable enhancement in some properties with a very low amount of addition of fillers such as exfoliated nanosilicate layers, carbon nanotubes (CNTs), and graphite nanoplatelets. However, for the effective performance of these fillers, the strong interfacial adhesion between the nanofiller and polymer matrix and the homogenous dispersion of the filler in the polymer matrix are imperative [2].

The discovery of carbon nanotubes in 1991 by Iijima [3] has opened a new area of research on the structure, properties and applications of this unique material. In 1994, the first polymeric nanocomposite using CNTs as the filler was reported by Ajayan et al. [4] The exceptional combination of the mechanical, electrical, and thermal properties of the CNTs make them excellent candidates to alternate or balance the conventional nanofillers in the manufacture of multifunctional polymer nanocomposites [5]. The reinforcing behavior of CNTs in a polymer matrix has also generated a lot of research interest in the past two decades [6]. However, to confer the special properties of CNTs to the polymer matrix, the uniform dispersion of CNTs in the polymer matrix is required, which is difficult. The delocalization of π electrons, small size of CNTs, and large surface area result in van der Waals forces, which cause aggregation [7,8]. However, some researchers have demonstrated uniform distribution of the filler using *in situ*

* Corresponding author.
E-mail address: griselda.barrera@ufrgs.br (G.B. Galland).

http://dx.doi.org/10.1016/j.polymer.2017.04.067
0032-3861/

polymerization [9–12].

Polypropylene (PP) is one of principal polyolefin's with commercial importance because of its cost-effectiveness and intrinsic properties, such as low density, high stiffness, good tensile strength, and inertness toward acids, alkalis, and solvents. PP has been used in many industrial applications, such as packaging materials, textiles, and automotive parts. However, for advanced applications, the physicochemical properties of PP need to be further improved or new functionalities must be introduced [13]. In order to improve the dispersion of CNTs in a polymer matrix, various methods have been employed. Common methods for CNT-filled polymer nanocomposites include melt blending [14–16], solution mixing [17], and *in situ* polymerization [18]. The limitation of the melt blending method is that it does not always yield homogenous dispersion of the nanotubes because of the lack of compatibility [19]. In the case of PP and PE, the use of the solution mixing method becomes impossible since these polymers are soluble in solvents such as xylene and trichlorobenzene above 120 °C, which have considerable health risks [2]. The *in situ* polymerization is the most suitable technique used to achieve uniform dispersion of the filler, when compared to the conventional melt mixing [20].

Both academic and industrial researchers have been paying increased attention to magnetic polymer nanocomposites. Magnetic nanoparticles and nanocomposites have attracted significant scientific and technological interest because of their potential application in the fields of biomedicine, information technology, magnetic resonance imaging, catalysis, telecommunication, and environmental remediation [21–23]. In contrast, magnetic nanoparticles similar to conventional CNTs tend to aggregate in a polymer matrix and reduce the energy associated with high surface area of the nanosized particles [24]. Iron is the conventionally most-used magnetic material [25] and its excellent magnetic performance has recently attracted considerable interest. However, iron nanoparticles have significant disadvantages such as easy oxidation, which must be resolved when using iron NPs as the filler. Some researchers have reported that the encapsulation of magnetic NP in CNTs can resolve this difficulty [26,27]. Bhatia et al. [28] reported the synthesis of multiwall carbon nanotubes by chemical vapor deposition using ferrocene [$Fe(C_2H_5)_2$], an organometallic compound, which acts as both a catalyst and precursor of synthesis and does not require high temperature. Recently, Osorio et al. [29,30] used silica different surface areas as the substrate and ferrocene as the precursor, and optimized the conditions for the CNTs synthesis. They reported that variation in the temperature and dwell time of the synthesis can help tune the final magnetic properties, i.e., the composition of the iron-containing phases in the CNTs.

Our research group is extensively working on synthesizing polyolefin nanocomposites using *in situ* polymerization. Recently, we prepared polyethylene–graphite nanosheet (PE-GNS), isotactic polypropylene–graphite nanosheet (iPP-GNS) nanocomposites, and polyethylene-CNTs-Fe nanocomposites and obtained homogenous dispersions of the filler in the polymer matrix [31–37]. Park et al. [38] reported the synthesis of polypyrrole (PPy)-coated magnetite (Fe_3O_4) hybrid particles of dual stimuli-response under magnetic and electric fields. The aim of the present work is to prepare nanocomposites of polypropylene iron-encapsulated carbon nanotubes (PP-CNT-Fe) through *in situ* polymerization using metallocenes [rac-Ethylene bis (indenyl) Zirconium (*rac*-$Et(Ind)_2ZrCl_2$)] as a catalyst and methylaluminoxane (MAO) as a co-catalyst in order to obtain a dual stimuli responsive material under electric and magnetic fields. This multifunctional material has the potential to be applied as sensors in medicine and in electronic devices, low-temperature heaters, energy storage devices [39], solar cells, magnetic recording materials [40], magnetic sensors, [41] and microwave absorbers [42], in the aerospace and automotive industries.

2. Experimental

2.1. Materials

The metallocene catalyst *rac*-ethylenebis (indenyl) Zirconium (*rac*-$Et(Ind)_2ZrCl_2$) (Aldrich) was used as the propene polymerization catalyst and MAO (Chemtura, 10 wt% Al solution in toluene) as the cocatalyst. Metallic sodium and benzophenone were used for the distillation of toluene, which was used as solvent. The deoxygenating and drying process of propylene was carried out by passage through the columns of Cu catalyst (BASF) and activated molecular sieves (13X). All manipulates were carried out in inert nitrogen atmosphere using standard Schlenk techniques.

2.2. Carbon nanotube synthesis

The CNTs containing iron (CNT-Fe) were synthesized by chemical vapor deposition (CVD), using the method reported in Refs. [29,30]. Ferrocene was used as a precursor and high-surface-area silica as a support. The reaction time was approximately 2 min, and the temperature was increased up to 750 °C.

2.3. Polymerization reactions

The CNTs-Fe were stirred with 15 wt.% of MAO for 30 min in toluene. The polymerization reactions were carried out in a Buchi glass reactor of 1 L capacity equipped with a mechanical stirrer and thermocouple. First, toluene was introduced as a solvent, and previously treated CNTs-Fe with MAO were used as the filler, followed by addition of the co-catalyst (MAO, Al/Zr = 1000). Subsequently, the system was saturated with propylene gas and, finally, a given aliquot of catalyst [(*rac*-$Et(Ind)_2ZrCl_2$) (5.0×10^{-6} mol)] solution in toluene was introduced. The reaction was carried out at 25 °C under 2 bar pressure of propylene, with a stirring rate of 1000 rpm for 30 min. The reaction was terminated with the addition of 5% by volume HCl/methanol 10 vol% solution. Finally, the polymer was precipitated with methanol, filtered and washed before dry to constant weight.

2.4. Characterization of polymer nanocomposites

Transmission electron microscopy (TEM) analyses were performed using a JEOL 1011 microscope operating at 120 kV. Copper grid of 300 mesh covered with amorphous carbon was used for sample preparation. A drop of the solution was deposited on the copper grid or from ultrathin films (~50 nm) cut under cryogenic conditions with a Leica Ultracut UCT microtome at −70 °C and placed on a grid (polymeric nanocomposites).A Phillips XL30microscope operating at 20 kV was used for scanning electron microscopy (SEM). Samples were deposited on an aluminum stub and coated with gold.

The molecular weight analyses were carried out using a Waters Alliance GPC 2000 instrument operating with three Styragel HT-type columns (HT3, HT5, and HT6E). At a temperature of 135 °C and 1,2,4-trichlorobenzene with a flow rate of 1 ml/min was used as a solvent. Polystyrene was used as the column calibration standard.

The Fe on the carbon nanotubes was determined by HR-CS GF AAS through direct solid sampling (SS) using a contrAA 700 high-resolution continuum source atomic absorption spectrometer (Analytik Jena AG, Jena, Germany). The samples were directly weighed, without any prior preparation step, on pyrolytically coated graphite tubes. A pre-adjusted pair of tweezers, which is

part of the SSA 6 manual solid sampling accessory (Analytik Jena), was used to transfer the platforms to the atomizer. The program temperatures and methods used were followed and adapted from the literature. [43] A 10 μL volume of a mixture of 20 μg Pd + 12 μg Mg was used as the chemical modifier dosed onto the sample prior to platform introduction into the atomizer. Pyrolysis and atomization temperatures were 800 °C and 2500 °C, respectively, using the 283.245 nm line and only the central pixel for evaluation.

The electrical resistivity was measured with the help of a megohmmeter (Megger BM11) operating at the highest voltage of 1200 V. With this set-up, the standard two-point method was used. For each electrical value displayed in this contribution, at least four samples were prepared, and four measurements were taken for each sample. In general, differences of around one order of magnitude were detected in the non-percolated samples having low conductivity values (~10^{-9} S/cm). For percolated samples, the experimental error for conductivities was less than 50%. The samples prepared to use for the test were 40 mm × 15 mm in size and 1 mm in thickness.

The magnetic properties of the CNTs and nanocomposites were investigated by using an EZ9MicroSense vibrating sample magnetometer (VSM) at room temperature with a magnetic field (H) cycled between−20 kOe and +20 kOe.

The thermal properties were measured by differential scanning calorimetry (DSC) using a Perkin–Elmer differential calorimeter (model DSC Q20); the temperature was increase from 0 to 180 °C with a heat rate of 10 °C/min. The second scan was used to determine the melting temperature T_m, and the percent crystallinities were calculated from the enthalpy of fusion data obtained from the DSC curves (207 J/g was used for 100% crystalline material). Thermogravimetric analysis (TGA)/SDT Q600 thermal analyzer Q20 (TA Instruments) was used to determine the thermal stability of the nanocomposites with respect to the neat polymer. The samples were scanned in the range of 0–800 °C, at a scanning rate of 20 °C/min.

3. Results and discussion

3.1. Polymerization

Propylene polymerizations were carried out in the presence of iron encapsulated in carbon nanotubes (CNTs-Fe) using metallocene (*rac*-Et(Ind)$_2$ZrCl$_2$) as a catalyst and methylaluminoxane (MAO) as a cocatalyst. The CNT-Fe was first stirred with 15 wt% of MAO for 20 min to remove the impurities. Table 1 presents the results of a series of polymerization reactions performed with different percentages of CNT-Fe. The filler concentration in the PP/CNT-Fe nanocomposites ranged from 0.8 to 7.5 wt.%, as calculated from the polymer yield. It can be seen that the catalytic activity decrease up to 43% with the incorporation of 0.8% of the filler; in contrast, the amount of filler does not significantly affect the catalytic activities. In spite of this decrease, the catalytic activities still remain very high.

3.2. Thermal properties

Table 1 also shows the thermal properties of PP and its nanocomposites. The melting temperatures of the nanocomposites (141–144 °C) show an increase of 3 °C as compared with the neat PP. Similarly, the crystallization temperature (T_c) shows an increase of 9–11 °C for all the nanocomposites, indicating that the filler acts as a nucleating agent for PP. Interestingly, the nucleation effect gradually shifts to higher temperatures as the filler content increases; in other words, addition of higher amount of filler produces large heterogeneous nucleation effect. Similar effect has been found by other researchers for PP/MWNT and PP/SWNT [44,45]. The percentage crystallinity values gradually increased with increasing filler amount.

The thermal degradation behavior of neat PP and PP/CNT-Fe nanocomposites has been investigated by TGA analysis. It can be seen from Table 1 that, with the incorporation of the filler, the maximum (T_{max}) and the initial (T_{onset}) degradation temperatures increased by 9 and 26 °C, respectively. It can be noted that, at a low concentration of the filler (<1 wt.%), T_{max} decreases by approximately 3 °C, whereas T_{onset} remains almost constant. This is attributed to the presence of Fe, which acts as a catalyst for degradation; such a catalytic effect of Fe has been shown in a previous work with polyethylene/CNT-Fe nanocomposites [37]; for nanocomposites containing up to 3.8 wt.% of CNT-Fe, the catalytic activity of Fe is not significant. The explanation is that the thermal stabilizing effect is mostly attributed to the formation and stabilization of CNT-bonded macroradicals [46] and the nanotube barrier effect [47]. In contrast, the decrease in T_{max} and T_{onset} with the highest amount of filler (7.5 wt.%) is probably due to the presence of the higher percentage of Fe in the nanocomposites (see Table 2), which is twice the amount of Fe present in the nanocomposite with 3.8 wt.% CNT-Fe. This can compensate for the stabilization of CNTs and potentiate the catalytic effect of Fe towards degradation [45]. The TGA residue weight percentage (wt.%) at 500 °C is in close agreement with the amount of filler calculated from the polymer yield. These results confirm that a good distribution of the filler is achieved in the nanocomposites.

3.3. Effect of polymerization temperature on the molecular weight

The effect of the polymerization temperature on the molecular weight of the polymer was also studied. It was confirmed from the GPC results that the polymerization at 25 °C produces a polymer of comparatively higher molecular weight (4.4 × 10^4 g mol^{-1} with polydispersity of 1.9), whereas the polymerization that takes place at 60 °C produces a polymer of lower molecular weight (1.9 × 10^4 g mol^{-1} with polydispersity of 1.8). The previous results showed that the nanocomposites retain the same molecular weight

Table 1
Results of nanocomposites of polypropylene with different amounts of CNT-Fe.

Samples	Filler (%)	Polymer (g)	TGA residue (%)	Catalytic activity[a]	T_c(°C)	T_m (°C)	Xc(%)	T_{onset}(°C)	T_{max}(°C)
PP	0	40.8	0.95	8163	105	141	56	425	476
PP/CNT$_{Fe1}$	0.8	23.9	1.44	4709	114	143	57	426	473
PP/CNT$_{Fe2}$	2.3	17.18	2.38	3437	114	143	58	442	482
PP/CNT$_{Fe3}$	3.0	18.0	2.51	3602	114	143	62	451	483
PP/CNT$_{Fe4}$	3.8	18.5	2.44	3706	116	144	62	452	485
PP/CNT$_{Fe5}$	7.5	18.60	5.50	3713	116	144	57	415	483

[a] KgPE.[Zr]$^{-1}$.h^{-1}.bar^{-1}.

Table 2
Iron content, conductivity, saturation magnetization (M_S), normalized remnant magnetization (M_R/M_S), and coercivity (H_C) values of the nanocomposites of polypropylene with different amounts of CNT-Fe.

Sample	Filler (%)	Fe[a] (wt.%)	Conductivity (S cm^{-1})	M_S (emu/g)	M_R/M_S	H_C(Oe)
PP	–	0	6.5×10^{-11}	–	–	–
CNT-Fe	–	26.9	–	13.1(±1.0)	0.32(±0.1)	280(±5)
PP/CNT$_{Fe1}$	0.8	0.23	6.3×10^{-11}	17.9(±1.0)	0.33(±0.1)	420(±5)
PP/CNT$_{Fe2}$	2.3	0.63	6.9×10^{-11}	14.0(±1.0)	0.34(±0.1)	430(±5)
PP/CNT$_{Fe3}$	3.0	0.89	6.4×10^{-11}	11.3(±1.0)	0.37(±0.1)	530(±5)
PP/CNT$_{Fe4}$	3.8	1.02	7.8×10^{-5}	11.6(±1.0)	0.40(±0.1)	710(±5)
PP/CNT$_{Fe5}$	7.5	2.03	1.3×10^{-4}	16.0(±1.0)	0.34(±0.1)	450(±5)

[a] Fe,From Atomic Absorption.

as that of the neat polymer when using the same route for the study of the nanocomposites [33].

3.4. Morphology of the nanocomposites

SEM and TEM studies were carried out to observe the morphology and dispersion of the filler in the polymer matrix. Fig. 1 shows the SEM images of the neat PP and PP/CNT-Fe nanocomposites at the same magnification. It can be seen that the polymer is coated around the CNTs, clearly showing that the filler is uniformly distributed in the polymer matrix; no agglomerates were observed.

The CNT-Fe obtained by the method used in this work are a mixture of single and multiwall CNTs with various lengths [29,30]. Fig. 2 shows the TEM micrographs of PP nanocomposites with 0.8 wt.% (A), (B), and (C), and 7.5 wt.% (D), (E), and (F) of CNT-Fe, respectively, at different magnifications. The black spots observed in the figures are the Fe nanoparticles. It is clear from the images that CNTs are uniformly distributed in the PP matrix, and no aggregation was observed. At higher magnifications, for example 100 nm, the isolated CNTs can be clearly seen encapsulating Fe.

3.5. Conductive and magnetic behavior of the nanocomposites

One of the objectives of this work was to transform an insulating material to a semiconductor. A significant concentration of conductive filler, beyond the electrical percolation threshold, is mandatory to create a conductive network in the insulator polymer matrix. This decreases the electrical resistivity of the material immediately by several orders of magnitude. The aspect ratio and dispersion of the conductive nanofillers are the two major factors considered while taking into account the electrical percolation threshold [48]. The values of the electrical conductivity of PP and its nanocomposites are listed in Table 2 and plotted in Fig. 3. The conductivity of the neat PP is practically zero (6.5×10^{-11} S cm^{-1}) as expected, which matches the insulation nature of the material. It can be seen that, with the addition of only 3.8 wt.% CNT-Fe, the conductivity sharply raises to a value of 7.8×10^{-5} S cm^{-1}, and reaches a higher value of 1.3×10^{-4} S cm^{-1} with the addition of 7.5 wt.% of the filler. In our previous work, we obtained PE/CNT-Fe nanocomposites with good magnetic properties, and when the measurements were carried out after a 6-month interval, the same results were obtained confirming that the Fe is protected from oxidation since no losses in the magnetic properties were observed. However, the amount of the filler was not enough (2.5 wt.%) to transform the insulating PE to a semiconductor [37]. Fig. 3 clearly shows that the percolation threshold is between 3.0 and 3.8 wt.% of CNT-Fe in PP.

Magnetization hysteresis loops of the CNT-Fe powder and two representative PP/CNT-Fe nanocomposites, measured at room temperature, are plotted in Fig. 4(a) and (b), respectively; the PP alone (not shown) shows evidence of only a diamagnetic signal. The characteristics of the hysteresis loops change significantly as the magnetic filler content is varied; initially, both the remnant

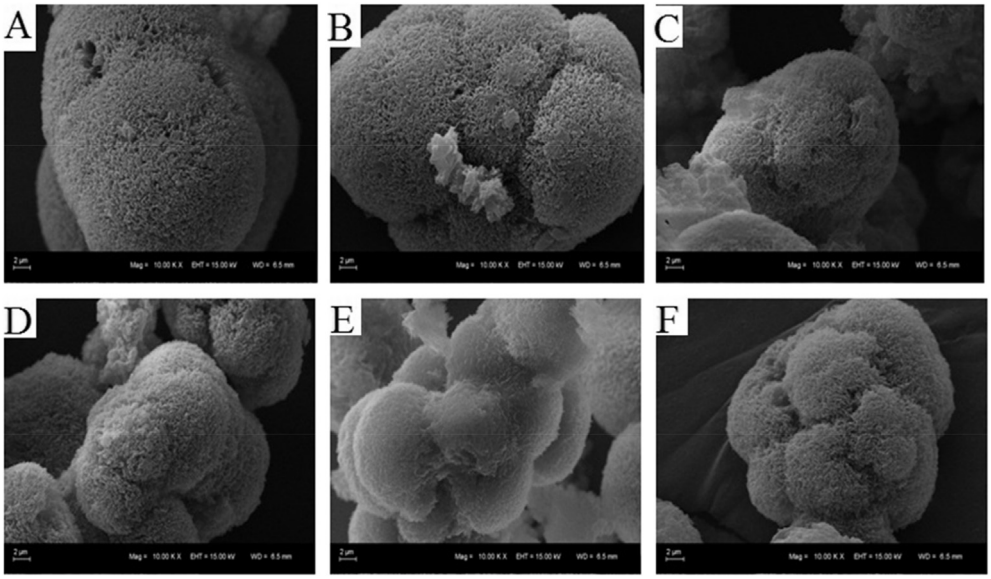

Fig. 1. SEM images of the (A) neat PP, (B) 0.8 wt. %, (C) 2.3 wt. %, (D) 3 wt.%, (E) 3.8 wt.%, and (F) 7.5 wt.% of CNT-Fe in PP.

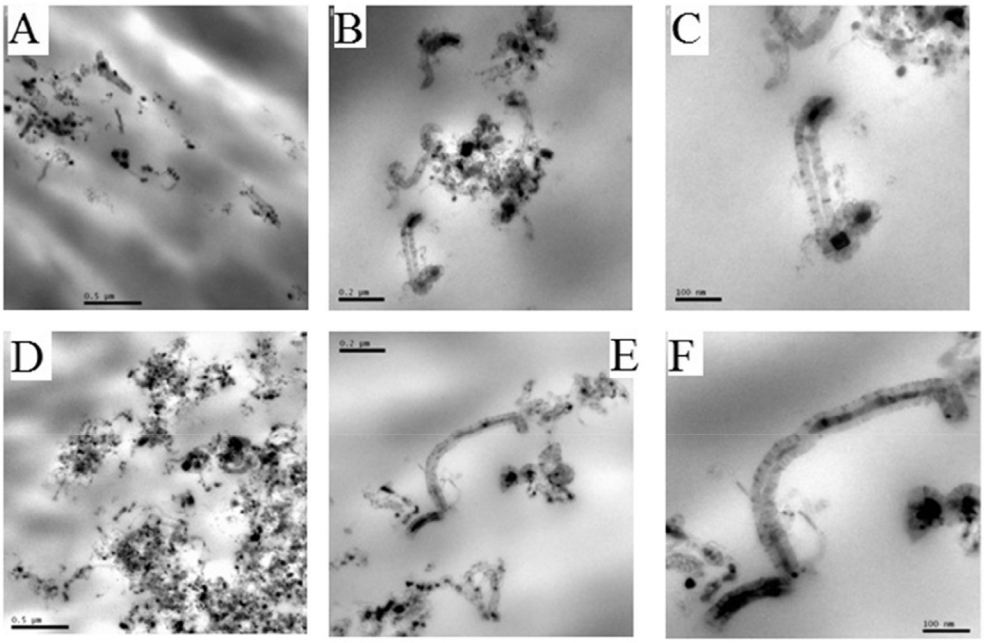

Fig. 2. TEM Images of 0.8 wt.% PP/CNT-Fe nanocomposites (A), (B), and (C) and 7.5 wt.% PP/CNT-Fe nanocomposites (D), (E), and (F).

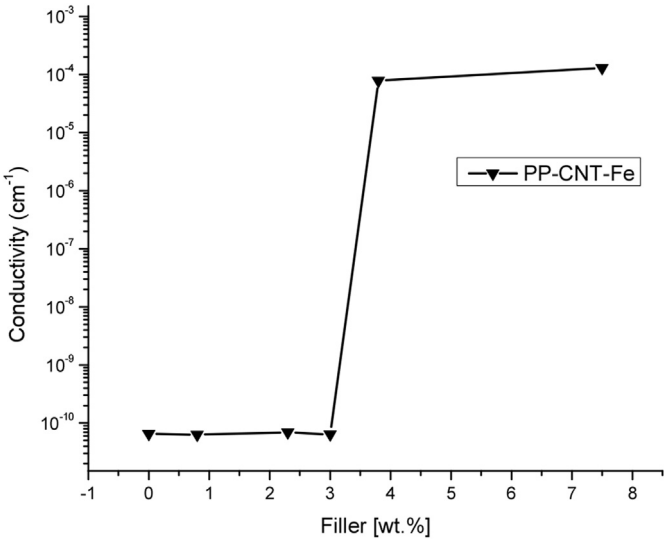

Fig. 3. Effect of the filler on the electrical conductivity of the polypropylene nanocomposites.

magnetization/saturation magnetization ratio (M_R/M_S) and the coercivity (H_C) increase sharply as the filler increases up to ~4 wt.%, as shown in Fig. 4(d) and (e), while M_S (plotted in Fig. 4(c)) shows a variation quite opposed to those of M_R/M_S and H_C. Fang et al. [49] reported a reduction of 12.8% in the saturation magnetization for the PANI coated carbonyl iron (CI) particles compared with pure CI. The magnitudes of the M_R/M_S and H_C of the samples with the highest filler content studied here, namely 7.5 wt.%, drop significantly, having values approximately equal to those of the PP/CNT-Fe nanocomposite with filler of 2.3 wt.%. The values of M_S, M_R/M_S, and H_C of all nanocomposites are given in Table 2. He *et al.* [50] showed a similar decreasing trend for high-density polyethylene (HDPE) matrix in H_C; as the percentage of the magnetic constituent increased from 5 to 20 wt.%, the value of H_C decreased quickly from 193 to 9 Oe. This much lower value of H_C for higher amount of loading is due to the stronger (demagnetizing) dipolar interactions caused by the decrease in the inter-particle distance. Burke et al. [51] also reported a similar decrease in H_C for polymer-coated Fe nanoparticles, where a decrease of 124 Oe was observed as the amount of Fe was increased from 21 to 51 wt.%.

Riquelme et al.[13]reported coercivity values ranging between 500 and 550 Oe for PP magnetic nanocomposites with 2–6 wt.% of CNT-Fe obtained by melt mixing. More recently, Sim et al. [52] have reported on Fe_3O_4@PANI magnetic materials prepared by oxidation polymerization of PANI on the surface of Fe_3O_4. They obtained a coercivity of ~40 Oe, which is a very low value as compared to our results. Santos et al. [53] used polyurethanes, PU/3 and PU/10 wt.% of Fe_3O_4 synthetic talc and obtained coercivities of 275 and 250 Oe at 2K, respectively, which represent values around three times lower than those reported here. Zhu et al. [54] also reported coercivities of 22 Oe for PP nanocomposites filled with 12 wt.% of Fe@Fe_2O_3core@shell nanoparticles at a higher applied field of 90 kOe at room temperature, producing soft ferromagnetic materials. Owing to the high coercivities at room temperature obtained in this work, we can say that they are ferromagnetic materials, in which magnetism can be modulated with the amount of filler.

4. Conclusions

Magnetic and conducting properties are important for the design of new polymeric devices for different applications. The SEM and TEM showed a good dispersion of the filler into the PP matrix, resulting in PP-CNT-Fe nanocomposites with improved thermal stability. The conductivity sharply rises to 7.8×10^{-5} S cm^{-1} with the addition of 3.8 wt.% of CNT-Fe and reaches its highest value of 1.3×10^{-4} S cm^{-1}as the amount of filler increases to 7.5 wt.%. The results show the ferromagnetic nature of the PP with very low percentage of filler at room temperature. This is one of the most remarkable results of this work; our nanocomposites show high coercivities at room temperature, when most works in this area have reported materials with high magnetization only at very low temperatures. This achievement is attributed to the protection of

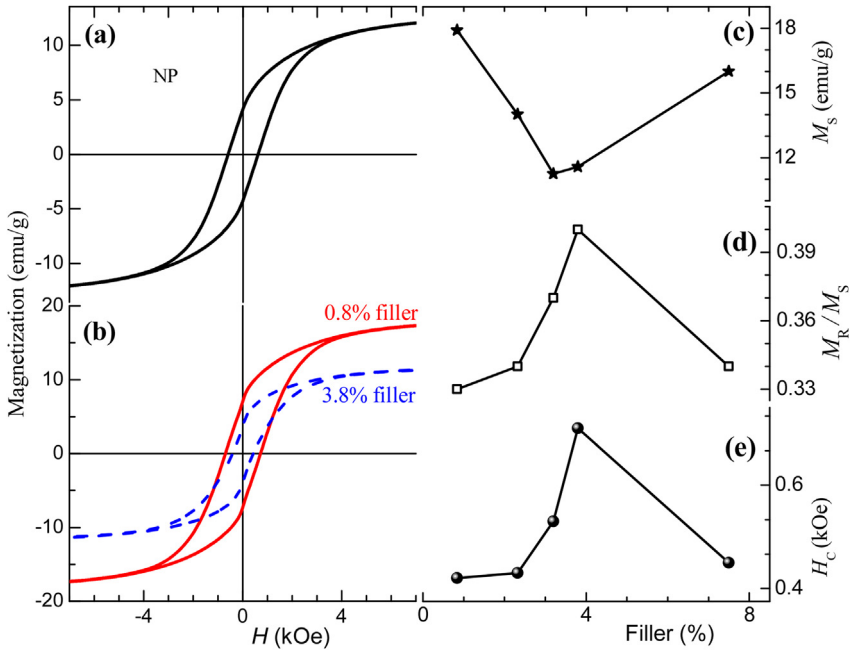

Fig. 4. (a) Room temperature magnetization hysteresis loop of the CNT-Fe powder and (b) representative loops for PP/CNT-Fe nanocomposites. The variations in M_S(c), M_R/M_S (d), and H_C (e) with the filler content are also plotted.

the Fe NPs by CNTs that avoid oxidation and to the good dispersion of the filler in the polymer matrix.

Acknowledgments

The authors are grateful to the TWAS-CNPq for the fellowship to Muhammad Nisar, the CNPq for the special visiting research fellowship to Professor Raúl Quijada, and CNPq grant 302902/2013-9. Professor Raúl Quijada acknowledges the Millennium Nucleus of Chemical Processes and Catalysis (CPC), grant number NC120082, and Dr. Victor Fuenzalida from Laboratorio de Superficies, Departamento de Fisica, Facultad de Cienciasfísicas y Matematicas, Universidad de Chile, for laboratory support. We also thank CME and LRNANO from UFRGS for the microscopy analysis and Dr. Eliana Galland Barrera for the Absorption Atomic analyses. The magnetic characterization was performed in collaboration with the Laboratory of Magnetism at IF-UFRGS.

References

[1] G. Kickbick, Concepts for the incorporation of inorganic building blocks into organic polymers on a nanoscale, Prog. Polym. Sci. 28 (2003) 83–114.
[2] P. Song, Z. Cao, Y. Cai, L. Zhao, Z. Fang, S. Fu, Fabrication of exfoliated graphene based-polypropylene nanocomposites with enhanced mechanical and thermal properties, Polymer 52 (2011) 4001–4020.
[3] S. Iijima, Helical microtubules of graphitic carbon, Nature 354 (1991) 56–58.
[4] P.M. Ajayan, O. Stephan, C. Colliex, D. Trauth, Aligned carbon nanotube arrays formed by cutting a polymer resin-nanotube composite, Science 265 (1994) 1212–1214.
[5] M. Moniruzzaman, K.I. Winey, Polymer nanocomposits containing carbon nanotubes, Macromolecules 39 (2006) 5194–5205.
[6] A.K.T. Lau, D. Hui, The revolutionary creation of new advanced materials—carbon nanotube composites, Compos. Part B 33 (2002) 263–277.
[7] S. Bredeau, S. Peeterbroeck, D. Bonduel, M. Alexandre, P. Dubois, From carbon nanotube coatings to high-performance polymer nanocomposites, Polym. Int. 57 (2008) 547–553.
[8] P. Ajayan, in: H.S. Nalwa (Ed.), Handbook of Nanostructured Materials and Nanotechnology, vol. 5, Academic Press, New York, 2000, pp. 501–575.
[9] A. Funk, W. Kaminsky, Polypropylene carbon nanotubes nanocomposites by *in situ* polymerization, Compos. Sci. Technol. 67 (2007) 906–915.
[10] P. Zapata, R. Quijada, Polypropylene nanocomposites obtained by in situ polymerization using metallocenes catalyst: influence of the nanoparticles on the final polymer morphology, J. Nano. Mater 194543 (2012) 6.
[11] R.S. Aranjo, R.J.B. Oliveira, M.F.V. Marques, Preparation of nanocomposites of polypropylene with carbon nanotubes via masterbatches produced by *in situ* polymerization and by melt extrusion, Macromol. React. Eng 8 (2014) 747–754.
[12] R.J.B. Oliveira, J.S. Santos, M.F.V. Marques, Preparation of Ziegler-Natta catalysts for the synthesis of polypropylene/carbon nanotubes nanocomposites by *in situ* polymerization, Polímeros 24 (2014) 13–19.
[13] J. An, G.Jeon, Y.Jeong, Preparation and properties of polypropylene nanocomposites reinforced with exfoliated graphene, Fibers Polym. 13 (2012) 507–514.
[14] J. Riquelme, C.A. Garzón, C.P. Bergmann, J. Geshev, R. Quijada, Development of multifunctional polymer nanocomposites with carbon-based hybrid nanostructures synthesized from ferrocene, Eur. Polym. J. 75 (2016) 200–209.
[15] P. Potschke, A.R. Bhattacharyy, A. Janke, Carbon nanotubes-filled polycarbonate composites produced by melt mixing and their use in blend with polyethylene, Carbon 42 (2004) 965–969.
[16] W.E. Dondero, R.E. Gorga, Morphological and mechanical properties of carbon nanotube/polymer composites via melt compounding, J. Polym. Sci. Polym. Phys. 44 (2006) 864–878.
[17] S. Curran, A.P. Davey, J. Coleman, A. Dalton, B. McCarthy, S. Maier, Evolution and evaluation of the polymer/nanotube composite, Synth. Met. 103 (1–3) (1999) 2559–2562.
[18] A. Funck, W. Kaminsky, Polypropylene carbon nanotube composites by *in situ* polymerization, Compos. Sci. Technol. 67 (5) (2007) 906–915.
[19] S.H. Lee, E. Cho, S.H. Jeon, J.R. Youn, Rheological and electrical properties of polypropylene composites containing functionalized multi-walled carbon nanotubes and compatibilizers, Carbon 45 (2007) 2810–2822.
[20] M.A. Milani, R. Quijada, N.R.S. Basso, A.P. Graebin, G.B. Galland, influence of the graphite type on the synthesis of polypropylene graphene nanocomposites, J. Polym. Sci. Part A Polym. Chem. 50 (2012) 3598–3605.
[21] J.M.D. Coey, Whither magnetic materials, J. Magn. Magn. Mater. 196–197 (1999) 1–7.
[22] R.D. Shull, L.H. Bennett, Nanocomposite magnetic materials, Nanostruct. Mater. 1 (1992) 83–88.
[23] J. Zhu, S. Wei, M. Chen, H. Gu, S.B. Rapole, S. Pallavkar, T.C. Ho, J. Hopper, Z. Guo, Magnetic nanocomposites for environmental remediation, Adv. Powder. Technol. 24 (2013) 459–467.
[24] S. Kalia, S. Kango, A. Kumar, Y. Haldorai, B. Kumari, S. Kumar, Magnetic polymer nanocomposites for environmental and biomedical applications, Colloid Polym. Sci. 292 (2014) 2025–2052.
[25] S. Wei, Q. Wang, J. Zhu, L. Sun, H. Lin, Z. Guo, Multifunctional composite core–shell nanoparticles, Nanoscale 3 (2011) 4474–4502.
[26] A. Morelos-Gómez, F. Lopez-Urias, E. Munoz-Sandoval, C.L. Dennis, R.D. Shull, H. Terrones, M. Terrones, Controlling high coercivities of ferromagnetic nanowires encapsulated in carbon nanotubes, J. Mater. Chem. 20 (2010) 5906–5914.
[27] C. He, N. Zhao, C. Shi, J. Li, H. Li, Magnetic properties and transmission electron

microscopy studies of Ni nanoparticles encapsulated in carbon nanocages and carbon nanotubes, Mater. Res. Bull. 43 (2008) 2260–2265.
[28] R. Bhatia, V. Prasad, Synthesis of multiwall carbon nanotubes by chemical vapor deposition of ferrocene alone, Solid State Commun. 150 (2010) 311–315.
[29] A.G. Osorio, C.P. Bergmann, Effect of surface area of substrates aiming the optimization of carbon nanotube production from ferrocene, Appl. Surf. Sci. 264 (2013) 794–800.
[30] A.G. Osorio, L.G. Pereira, J.B.M. da Cunha, C.P. Bergmann, Controlling the magnetic response of carbon nanotubes filled with iron-containing material, Mater. Res. Bull. 48 (2013) 4168–4173.
[31] F.C. Fim, J.M. Guterres, N.R.S. Basso, G.B. Galland, Polyethylene/graphite nanocomposites obtained by in situ polymerization, J. Polym. Sci. Part A Polym. Chem. 48 (2010) 692–698.
[32] M.A. Milani, R. Quijada, N.R.S. Basso, A.P. Graebin, G.B. Galland, Influence of the graphite type on the synthesis of polypropylene graphene nanocomposites, Polym. Sci. Part A Polym. Chem. 50 (2012) 3598–3605.
[33] M.A. Milani, D. González, R. Quijada, N.R.S. Basso, M.L. Cerrada, D.S. Azambuja, G.B. Galland, Polypropylene/grapheme nanosheet nanocomposites by in situ polymerization: synthesis, characterization and fundamental properties, Compos. Sci. Technol. 84 (2013) 1–7.
[34] F.C. Fim, N.R.S. Basso, A.P. Graebin, D.S. Azambuja, G.B. Galland, Thermal, electrical, and mechanical properties of polyethylene-graphene nanocomposites obtained by in situ polymerization, J. Appl. Polym. Sci. 128 (2013) 2630–2637.
[35] M.A. Milani, D. González, R. Quijada, R. Benavente, J. Arranz-Andrés, G.B. Galland, Synthesis, characterization and properties of poly(propylene-1-octene)/graphite nanosheet nanocomposites obtained by in situ polymerization, Polymer 65 (2015) 134–142.
[36] G. Pavoski, T. Maraschin, M.A. Milani, D.S. Azambuja, R. Quijada, C.M. Moura, N.R.S. Basso, G.B. Griselda, Polyethylene/reduced graphite oxide nanocomposites with improved morphology and conductivity, Polymer 81 (2015) 79–86.
[37] M. Nisar, C.P. Bergmman, J. Geshev, R. Quijada, G.B. Galland, An efficient approach to the polyethylene magnetic nanocomposites, Polymer 97 (2016) 131–137.
[38] D.E. Park, H.S. Chae, H.J. Choi, A. Maity, Magnetite-polypyrrole core-shell structured microspheres and their dual stimuli-response under electric and magnetic field, J. Mater. Chem. C 3 (2015) 3150–3158.
[39] P. Kim, N.M. Doss, J.P. Tillotson, P.J. Hotchkiss, M.J. Pan, S.R. Marder, J. Li, J.P. Calame, J.W. Perry, High energy density nanocomposites based on surface-modified BaTiO(3) and a ferroelectric polymer, ACS.Nano. 3 (9) (2009) 2581–2592.
[40] Q. Dai, D. Berman, K. Virwani, J. Frommer, P.O. Jubert, M. Lam, T. Topuria, W. Imaino, A. Nelso, Self-assembled ferrimagnet-polymer composites for magnetic recording media, Nano. Lett. 10 (2010) 3216–3221.
[41] T. Shimad, K. Ookubo, N. Komuro, T. Shimizu, N. Uehara, Blue-to-Red chromatic sensor composed of gold nanoparticles conjugated with thermoresponsive copolymer for thiol SensingLangmui 23 (22) (2007) 11225–11232.
[42] Z. Guo, S.E. lee, H. kim, S. Par, H.T. Hahn, A.B. Karki, D.P. Young, Fabrication characterization and microwave properties of polyurethane nanocomposites reinforced with iron oxide and barium titanate nanoparticles, Acta. Mater 57 (1) (2009) 267–277.
[43] M. Resano, E. Bolea-Fernández, E. Mozas, M.R. Flórez, P. Gringberg, R.E. Sturgeon, Simultaneous determination of Co, Fe, Ni and Pb in carbon nanotubes by means of solid sampling high-resolution continuum source graphite furnace atomic absorption spectrometry, J. Anal. At. Spectrom. 28 (2013) 657–665.
[44] S.P. Bao, S.C. Tjong, Mechanical behavior of polypropylene/carbon nanotube nanocomposites: the effect of loading rate and temperature, Mater. Sci. Eng. A 485 (2008) 508–516.
[45] W. Leelapornpisit, M.T. Ton-That, F. Perrin-Sarazin, K.C. Cole, J. Denault, B. Simard, Effect of carbon nanotubes on the crystallization and properties of polypropylene, J. Polym. Sci. Polym. Phys. 43 (2005) 2445–2453.
[46] N.R. Raravikar, L.S. Schadler, A. Vijayaraghavan, Y. Zhao, B. Wei, P.M. Ajayan, Synthesis and characterization of thickness-aligned carbon Nanotube–Polymer composite films, Chem. Mater 17 (2005) 974–983.
[47] B.B. Marosfio, A. Szabo, Gy Marosi, D. Tabuani, G. Camino, S. Pagliari, Thermal and spectroscopic characterization of polypropylene-carbon nanotube composites, J.Therm. Anal.Calorim. 86 (3) (2006) 669–673.
[48] M.H. Al-saleh, Electrical conductivity carbon naotubes/polypropylene nanocomposites with improve mechanical properties, Material Des. 85 (2015) 76–81.
[49] F.F. Fang, Y.D. Liu, H.J. Chio, Y. Seo, Core-shell structure carbonyl iron microspheres prepared via dual-step functionality coatings and their magneto rheological response, ACS. Appl. Mater. Interf. 3 (2011) 3487–3495.
[50] Q. He, T. Yuan, J. Zhu, Z. Luo, N. Haldolaarachchige, L. Sun, A. Khasanov, Y. Li, D.P. Young, S. Wei, Z. Guo, Magnetic high density polyethylene nanocomposites reinforced with in-situ synthesized Fe@FeO core-shell nanoparticles, Polymer 53 (2012) 3642–3652.
[51] N.A.D. Burke, H.D.H. Stover, F.P. Dawson, Preparation and characterization of polymer-coated iron nanoparticles, Chem. Matter 14 (2002) 4752–4761.
[52] B. Sim, H.S. Chea, H.J. Choi, Fabrication of polyaniline coated iron oxide hybrid particles and their dual stimuli-response under electric and magnetic fields, Exp. Polym. Lett. 9 (8) (2015) 736–743.
[53] L.M.D. Santos, R. Ligabue, A. Dumas, C.L. Roux, P. Micoud, J.F. Meunier, F. Martin, S. Einloft, New magnetic nanocomposites: polyurethane/Fe_3O_4 synthetic talc, Eur. Polym. J. 69 (2015) 38–49.
[54] J. Zhu, S. Wei, Y. Li, L. Sun, N. Haldolaarachchige, D.P. Young, C. Southworth, A. Kasanov, Z. Luo, Z. Guo, Surfactant-free synthesized magneticpolypropylene nanocomposites: rheological, electrical, magnetic, and thermal properties, Macromolecules 44 (2011) 4382–4391.

Annex 3

Journal of Applied Polymer Science

Synthesis of high-density polyethylene/rGO-CNT-Fe nanocomposites with outstanding magnetic and electrical properties

Muhammad Nisar,[1] Carlos Pérez Bergmann,[2] Julian Geshev,[3] Raúl Quijada,[4] Thuany Maraschin,[5] Nara R. de Souza Basso,[5] Eliana G. Barrera,[1] Griselda Barrera Galland[1]

[1]Instituto de Química, Universidade Federal do Rio Grande do Sul, Porto Alegre 91501-970, Brazil
[2]Laboratório de Materiais Cerâmicos, Departamento de Materiais, Universidade Federal do Rio Grande do Sul, Porto Alegre, Brazil
[3]Instituto de Física, Universidade Federal do Rio Grande do Sul, Porto Alegre 91501-970, Brazil
[4]Departamento de Ingeniería Química y Biotecnología, Facultad de Ciencias Físicas y Matemáticas, Universidad de Chile, Santiago, Chile
[5]Faculdade de Química, Pontifícia Universidade Católica do Rio Grande do Sul, Porto Alegre 90619-900, Brazil
Correspondence to: G. B. Galland (E-mail: griselda.barrera@ufrgs.br)

ABSTRACT: Semi-conducting polyethylene (PE) nanocomposites with outstanding magnetic properties at room temperature were synthesized. These exceptional properties, for a diamagnetic and insulating matrix as PE, were obtained by polymerizing ethylene in the presence of a catalytic system formed by a metallocene catalyst supported on a mixture of reduced graphene oxide (rGO) and carbon nanotubes with encapsulated iron (CNT-Fe). It was used a constant and very low amount of CNT-Fe, obtained by vapor chemical deposition using ferrocene. The percolation threshold, to achieve conductivity, was obtained using a variable amount of rGO. The nanocomposites were semiconductors with the addition of 2.8 wt % and 6.0 wt % of the filler, with electrical conductivities of 4.99 $\times$ 10^{-6} S cm^{-1} and 7.29 $\times$ 10^{-4} S cm^{-1}, respectively. Very high coercivity values of 890–980 Oe at room temperature were achieved by the presence of only 0.04–0.06 wt % of iron in the nanocomposites. The novelty of this work is the production of a thermoplastic with both, magnetic and electric properties at room temperature, by the use of two fillers, that is rGO and CNT-Fe. The use of a small amount of CNT-Fe to produce the magnetic properties and variable amount of rGO to introduce the electrical conductivity in PE matrix let to balance both properties. The encapsulation strategy used to obtain Fe in CNT, protect Fe from easy oxidation and aggregation. © 2017 Wiley Periodicals, Inc. J. Appl. Polym. Sci. **2017**, *134*, 45382.

KEYWORDS: fullerenes; graphene; magnetism and magnetic properties; nanotubes; polyolefins; thermogravimetric analysis (TGA)

Received 27 January 2017; accepted 5 May 2017
DOI: 10.1002/app.45382

INTRODUCTION

Polymer nanocomposites are hybrid materials formed by the dispersion of inorganic fillers, in the nanometric scale, in polymeric matrixes.[1] The combination of organic polymer and inorganic fillers can improve the properties of the nanocomposite such as magnetic, thermal, dielectric, mechanical, or optical depending on the filler used.[2] Among the polymeric matrixes, polyethylene (PE) has attracted considerable attention because of its low cost, recyclability, easy processing, and versatility. The addition of fillers can broaden the application range of PE by improving its properties such as its gas barrier and thermal stability or by adding new properties such as electrical conductivity.[3] Likewise, extensive research work has been carried out using carbon nanotubes (CNTs) as reinforcements in polymers because of their outstanding tensile properties.[4] The CNTs closed in a tubular shaped having a single graphite sheet are termed as single-walled carbon nanotubes (SWCNTs), where as those consisting of multiple graphite sheets are called multiwalled carbon nanotubes (MWCNTs).[5] Nevertheless, the expected transmission of the properties from the filler to the polymer matrix is still an issue of discussion owing to several drawbacks, such as the difficult dispersion of CNTs in viscous solutions, the high production cost,[6] and the caged structure of the CNTs.[7] Although functionalization of CNTs is considered to be a possible solution, it leads to the destruction of the caged structure of the CNTs, which in turn reduces the tensile strength.[8] The CNTs/polymer nanocomposites with PE, polymethylmethcrylate, polyamide, and polyurethane have been prepared using different methods such as melt mixing, electro spinning, graft, and *in situ* polymerization to enhance various properties.[9]

The discovery of graphene has opened a new area of research in polymer nanocomposites owing to its tremendous physical properties.[10] Graphene has triggered enormous interest in many technological fields such as electronics, energy storage and conversion, sensors, capacitors, and composites materials.[11,12]

Therefore, graphene is a nanofiller with the potential to improve the properties of neat polymers,[13] but obtaining adequate-quality graphene or few graphene nanosheets at a reasonable cost is a major issue to deal with. Some current production routes include chemical vapor deposition, CO reduction, and the exfoliation of graphite. The latter method is the only one that can provide large quantities of graphene at low cost and is the one used to obtain nanocomposites.[14] Hassan *et al.*[15] reported the production of high-yield graphene nanosheets from expanded graphite using aqueous phase exfoliation method. Han *et al.*[16] modified thermally reduced graphene with stearic acid to enhance its lipophilicity. Similarly, some researchers investigated the compatibility of thermally reduced graphene with multiblock copolyesters and graphene/polyaniline.[17,18] The addition of graphite oxide (GO) as an effective fire retardant of epoxy resin has been also reported, by controlling the degree of oxidation the chemical structure of GO can be varied.[19]

Furthermore, magnetic polymer nanocomposites have also attracted the interest of both academic and industrial researchers. Magnetic polymer nanocomposites can be obtained by the incorporation of magnetic elements such as nickel, cobalt, and iron into a non-magnetic polymer matrix by using different polymerization methods, including *in situ* polymerization, surface-initiated polymerization, solution blending, ball milling, surface wetting methods, and ion exchange techniques.[20] Although iron-based magnetic nanoparticles (NPs) are most-abundantly used, there are problems in their use owing to easy oxidation and aggregation. Encapsulation of iron NPs into a non-magnetic carbon shell is an alternative to address this issue.[2] Recently, Osorio and Bergmann[21] and Osorio *et al.*[22] optimized the synthesis of CNTs with ferrocene, using silica nanopowders with different surface areas as a substrate, obtaining CNTs with iron encapsulated (CNT-Fe). In a recent work, we used those CNT-Fe to obtain PE nanocomposites with magnetic properties. It was shown that 0.9 wt % of CNT-Fe in PE was enough to obtain rather high coercivity values (~1000 Oe), but it was insufficient to generate electrical conductivity.[23]

Our research group is extensively involved in graphene-based polyolefin nanocomposites using *in situ* polymerization with metallocene catalysts.[24–27] In the present work, we focus on a dual stimuli-responsive material under electric and magnetic fields using reduced graphene oxide (rGO) and iron encapsulated carbon nanotubes (CNT-Fe) as fillers. A metallocene catalyst was immobilized on a mixture of variable amounts of rGO and a small amount of CNT-Fe to polymerize ethylene aiming to simultaneously obtain a thermoplastic with conductive and magnetic properties. This multifunctional material has potential to be applied as sensors in medicine and in electronic devices, low-temperature heaters, energy storage devices,[28] solar cells, magnetic recording materials,[29] magnetic sensors,[30] and microwave absorbers,[31] in the aerospace and automotive industries.

EXPERIMENTAL

Materials

All materials were handled under deoxygenated dry argon using standard schlenk tube techniques. Flakes of graphite (Grafine 99200, FN) (average diameter $\leq$150 microns) were provided by Nacional de Grafite Ltd. (Brazil). Sulfuric acid, nitric acid, hydrochloric acid, and potassium chlorate were purchased from Merck, Sao Paulo, Brazil. Metallic sodium and benzophenone were used for the distillation of toluene. Methylaluminoxane (MAO) (Sigma Aldrich, Brazil, 4.6 wt % Al solution in toluene) and bis(*n*-butyl)cyclopentadienylzirconium dichloride ($(n\text{-BuCp})_2ZrCl_2$) (Sigma Aldrich, Brazil) were used as received.

Graphene Oxide Synthesis and Thermal Reduction

Graphene oxide was synthesized from flakes (FK) using a modified Staudenmaier method,[32,33] where the time of oxidation was changed from 96 to 24 h. To obtain rGO, the GO was heated at 600 °C for 3 s in an oven, using a closed quartz ampoule under normal atmosphere. Complete characterization of rGO can be found in the work by Pavoski *et al.*,[33] but for sake of clarity, we added X-ray diffraction (XRD) and Raman of this material in the Supporting Information Figures S1 and S2, respectively. In accordance with the previous work,[33] this rGO has 27% of oxygen calculated by elementary analysis.

Carbon Nanotube Synthesis

The CNTs containing iron (CNT-Fe) were synthesized by Chemical Vapor Deposition (CVD), where ferrocene was used as a precursor and silica as a support. The reaction time was approximately 2 min and the temperature was increased up to 750 °C. The detailed method of synthesis of these CNTs and complete characterization were published in the work by Osorio and Bergmann[21] and Osorio *et al.*[22]

Support of the Catalyst

Variable amount of rGO, between 71 and 333 mg, and around 25 mg of CNT-Fe were placed in a schlenk vessel with toluene using argon atmosphere and sonicated with an ultrasound bath (Ultracleaner 1600A, Unique, Brazil) operating at 40 kHz for 8 h at room temperature. The rGO-CNT-Fe was sonicated for 30 min more with the addition of 15 wt % MAO. In the next step, $(n\text{-BuCp})_2ZrCl_2$ was added in an amount of 2 wt % Zr/rGO-CNT-Fe, followed by 2 h of stirring at 60 °C. The solid was then decanted and the supernatant eliminated, and washed twice with toluene. Subsequently, $(n\text{-BuCp})_2ZrCl_2$/rGO-CNT-Fe was used as the catalyst system for the polymerization of ethylene.

Polymerization Reaction

Polymerization was carried out in a 300 mL reactor (Parr Instrument Company, IL). Toluene was used as the solvent, and an extra amount of MAO (Al/Zr = 100) was added as the scavenger. The reactions were carried out at 25 °C, using ethylene pressure of 3 bar for 30 min. The rGO-CNT-Fe previously treated with $(n\text{-BuCp})_2ZrCl_2$ was added as the filler and catalyst of the reaction.

CHARACTERIZATION

Transmission electronic microscopy (TEM) analysis was performed using a transmission electron microscope (JEOL 1200 ExII) operated at 120 kV. Samples were prepared by deposition of a solution drop on a grid (CNTs and rGO) or from ultrathin films (~50 nm) cut under cryogenic conditions with a Leica Ultracut UCT microtome at −70 °C and placed on a grid (polymeric nanocomposites). Scanning electron microscopy (SEM) was performed using a Phillips XL30 microscope operating at 20 kV. Samples were prepared by deposition on an aluminum stub and gold metallization.

The amount of zirconium deposited on the surface of the filler was investigated by inductive coupled plasma emission spectroscopy (ICP) in a Perkin–Elmer, Optima 7320.

Differential scanning calorimetric (DSC) analysis was performed using a Perkin–Elmer differential calorimeter (model DSC Q20) operating at a heating rate of 20 °C/min and a temperature range of 0–180 °C. The crystallization temperature, T_c, and the melting temperature, T_m, were determined in the second and third scans, respectively, and the degree of crystallinity was calculated from the enthalpy of fusion data obtained from the DSC curves (293 J/g was used for 100% crystalline material).

The thermal stability of the samples was investigated using SDT Q600 thermal analyzer Q20 (TA Instruments, USA). This analysis was performed under nitrogen (50 mL/min) at a scanning rate of 20 °C/min from 0 to 800 °C.

The molecular weights were obtained with a Waters Alliance GPC 2000 instrument equipped with three Styragel HT-type columns (HT3, HT5, and HT6E). 1,2,4-Trichlorobenzene was used as the solvent with a flow rate of 1 mL/min at a temperature of 135 °C. The columns were calibrated with polystyrene standards.

The determination of Fe on the CNTs and polymers was carried out by High Resolution-Continuum Source Graphite Fournace Atomic Absorption Spectroscopy (HR-CS GF AAS) by direct solid sampling (SS) using a contrAA 700 high-resolution continuum source atomic absorption spectrometer (Analytik Jena AG, Jena, Germany). The samples were directly weighed, without any prior preparation step, on pyrolytically coated graphite tubes. A preadjusted pair of tweezers, which is part of the SSA 6 manual solid sampling accessory (Analytik Jena), was used to transfer the platforms to the atomizer. The program temperatures and method used were followed and adapted from the literature.[34] A 10 µL volume of a mixture of 20 µg Pd + 12 µg Mg was used as the chemical modifier dosed onto the sample prior to platform introduction into the atomizer. Pyrolysis and atomization temperatures were 800 and 2500 °C, respectively, using the 283.245 nm line and only the central pixel for evaluation.

For the electric resistivity, a megohmmeter (Megger BM11) with a highest voltage of 1200 V was used. With this set-up, the standard two-point method was used. For each electrical value displayed in this contribution, at least four samples were prepared and four measurements for each one were carried out. In general, differences around one order of magnitude were detected in the non-percolated samples having low conductivity values ($\sim 10^{-9}$ S/cm). For percolated samples, the experimental error for conductivities was less than 50%. For these tests, samples of size 40 mm × 16 mm and thickness 1 mm were used.

The magnetic characterization of the nanocomposites was performed using an EZ9 MicroSense vibrating sample magnetometer (VSM) at room temperature with a magnetic field (H) ranging from −20 kOe to +20 kOe.

RESULTS AND DISCUSSION

PE nanocomposites, with variable amounts of rGO and fixed amount of CNT-Fe, were prepared by *in situ* polymerization using $(n\text{-BuCp})_2ZrCl_2$ as the catalyst supported in the filler (rGO and CNT-Fe) impregnated by MAO. The combination of the both rGO and CNT-Fe were used to prepare a dual stimuli-responsive material under electric and magnetic fields. The synthetic route of the magnetic material (CNT-Fe) is apparently harder and time consuming as compared with the preparation of rGO by the exfoliation technique. In fact, rGO comes from graphite, which is a cheap source, and does not require complicated steps for its synthesis. On the other hand, the synthesis of CNT-Fe requires more expensive reagents and is time consuming because each synthesis gives only few amounts of material. A small amount of CNT-Fe (<1%) is enough to produce good magnetic properties but it is not enough to attain percolation to have electrical conductivity.[23] Consequently, the idea of using the combination of these two carbon materials aims to use the rGO to generate a conductive network in the PE matrix and a small amount of CNT-Fe to convert the diamagnetic PE matrix to a ferromagnetic one. The small amount of CNT-Fe used was previously mixed with rGO, thus the support is constituted mainly of rGO. The interaction between CNT-Fe and rGO may consists π-interactions between graphenes. The main filler, rGO, has also the function to support the catalyst. The method used was the same published by Mülhaupt and coworkers[35] and consist in bonding and coating the surface of rGO with the cocatalyst, MAO. The ionic interaction between the catalyst and MAO[36] produces the catalytic site from which the PE grows. The characterization of rGO used was published in a previous work[33] and consist of 27% of oxygen, mainly hydroxyl groups that are essential to bond the MAO. PE/rGO-CNT-Fe nanocomposites with filler contents, calculated from the polymer yield, were in the range of 1.3–6.0 wt % (Table I) (Digital images, XRD and Raman of the materials can be seen in Supporting Information Figures S3–S5). The catalytic activities, obtained after taking into account the supported amount of Zr obtained by ICP, showed that there is a deactivation of the catalytic system with the increase in the filler content. This behavior has already been seen in polymerizations with rGO owing to the presence of some oxygen functional groups that remain in the rGO and deactivate part of the catalyst even with the protection of MAO.[14] Even though there is some deactivation of the catalyst all the catalytic activities can be considered very high.

Table I also shows the thermal properties of the PE and its nanocomposites. The melting temperatures of the nanocomposites (136–137 °C) were the same as that of the matrix and are typical of high-density polyethylene (HDPE). However, the crystallization temperatures (T_c) of all nanocomposites were 2–4 °C higher than those of the neat PE, indicating that the filler acts as a nucleating agent.

The thermal stability of neat PE and PE/rGO-CNT-Fe nanocomposites was investigated by thermogravimetric analysis (TGA) (the TGA curves are shown in Supporting Information Figure S6). Table I presents the TGA results of the nanocomposites. It can be seen that with increasing percentage of the filler, the maximum degradation temperatures (T_{max}) of the PE nanocomposites shifts to higher values as compared with the neat PE. It can be seen that in the nanocomposite with 6 wt % of filler, the T_{max} and the onset degradation temperature (T_{onset}) increase by 14 and

Table I. Catalytic Activities and Thermal Properties of PE/rGO-CNT-Fe Nanocomposites

Samples	Filler[a] (%)	Polymer (g)	TGA residue %	Catalytic activity[b]	T_c (°C)	T_m (°C)	X_c (%)	T_{onset} (°C)	T_{max} (°C)
PE	0	5.2	0	693	113	137	59	453	495
PE/GCFe$_1$	1.3	5.6	1.1	514	117	136	58	466	502
PE/GCFe$_2$	2.8	6.6	3.5	232	115	137	58	473	506
PE/GCFe$_3$	6.0	5.6	7.5	108	116	136	55	482	509

[a] Filler = GCFe= RGO + CNT-Fe.
[b] kgPE [Zr]$^{-1}$ h^{-1} bar^{-1}; the amount of Zr calculated by ICP was 0.9411 ± 0.0039 wt % Zr/rGO-CNT-Fe.

29 °C compared with the temperatures of neat PE, showing a significant increase in the thermal stability. This same behavior was already reported for nanocomposites PE/rGO.[25] However, we noticed that in PE/CNT-Fe nanocomposites, there was a decrease in T_{max} down to 4 °C with 2.5 wt % of CNT-Fe in PE, showing that iron acts as a catalyst of degradation.[23] It can be concluded that the thermal stability of PE/rGO-CNT-Fe nanocomposites is mainly transferred by rGO and that the amount of Fe is not enough to influence the degradation of PE. Table I also shows that the percentage of filler calculated from the TGA residue is in close agreement with the percentage of filler calculated from the polymer yield.

The molecular weight of the neat polymer is significantly high (4.4×10^5 g mol^{-1} with a polydispersity of 1.9), which was also confirmed by the high melting temperature of 137 °C. Previous preparations of polyolefin nanocomposites using the same

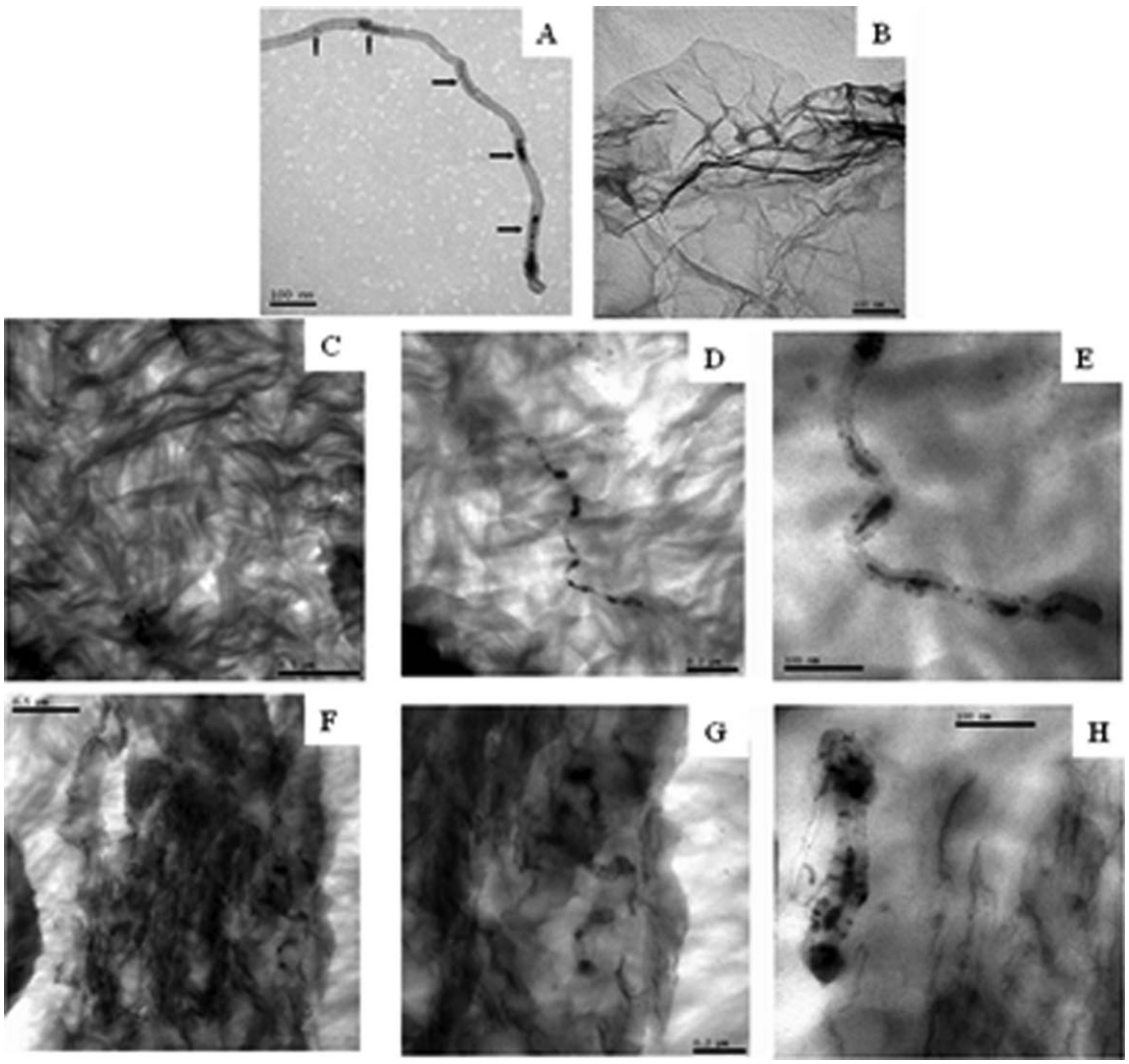

Figure 1. TEM micrographics of CNT-Fe[21] (A), rGO (B), PE/rGO-CNT-Fe nanocomposites 1.3 wt % (C–E), and PE/rGO-CNT-Fe nanocomposites 6.0 wt % (F–H).

Table II. Amount of Iron, CNT-Fe, and rGO in the Nanocomposites

Sample	Filler[a] (%)	CNT-Fe (wt %)	rGO (wt %)	Fe[b] (wt %)	Conductivity (S cm^{-1})	M_R/M_S	H_C (Oe)
PE	0	0	0	0	1.40×10^{-13}	0	0
CNT-Fe	0	100	—	26.9	—	0.32	280
PE/GCFe$_1$	1.3	0.46	0.8	0.04	7.70×10^{-11}	0.51	890
PE/GCFe$_2$	2.8	0.43	2.4	0.04	4.99×10^{-6}	0.52	910
PE/GCFe$_3$	6.0	0.45	5.5	0.06	7.29×10^{-4}	0.52	980

[a] Filler = GCFe = rGO + CNT-Fe.
[b] Fe, from atomic absorption.
Conductivity, normalized remnant magnetization, and coercivity values of nanocomposites of polyethylene with different amounts of reduced graphene oxide and CNT-Fe.

supported method showed that the nanocomposites have higher molecular weight than the neat polymer and maintain the polydispersity close to 2.[14]

The nanocomposites have been studied by TEM to see the morphologies and the dispersion of the fillers. Figure 1 presents the TEM micrographs of CNT-Fe [Figure 1(A)], rGO [Figure 1(B)] and PE/rGO-CNT-Fe nanocomposites with 1.3 wt % [Figure 1(C–E)] and 6.0 wt % [Figure 1(F–H)] of filler at different magnifications. As it can be seen in Figure 1(A), the iron NPs are encapsulated in the CNTs. Figure 1(B) shows the graphene sheets of rGO. All nanocomposites show uniform dispersion of the rGO in the polymer matrix where no aggregation is observed. In Figure 1(D–F,H), isolated CNTs encapsulating iron can be clearly observed. This homogenous dispersion is due to the catalyst supported method where the polymer is formed around the filler during the polymerization reaction. This reveals the advantages of this method over the non-supported catalyst method of polymerization.

The PE/rGO-CNT-Fe nanocomposites were studied by atomic absorption to verify the amount of Fe. Table II reveals that the CNT-Fe contain 26.9 wt % of Fe, and since a fixed amount of CNTs (0.43–0.46 wt %) were added in rGO, the amount of Fe in the nanocomposites remained almost the same, in the range 0.04–0.06 wt %. This is a very low content compared with the total filler (rGO-CNT-Fe) that varied from 1.3 to 6.0 wt %. TEM micrographs also confirm that the amount of Fe is low and that the CNT-Fe is isolated.

One of the most promising aspects of graphene-based materials is their potential for use in various devices and electronics applications, owning to their high electrical conductivity.[37] To obtain conductivity in an insulating matrix, the concentration of the conductive filler must be above the electrical percolation threshold, where a conductive network of filler particles is formed.[38] The percolation threshold is defined as the concentration where a connected assembly of conductive particles is formed in a polymer matrix and lead to a sudden rise in electrical conductivity.[39] One of the objectives of this work is to shift the insulating PE to a semiconductor material to enhance its applications. Table II presents the results of conductivity of the nanocomposites. It can be seen that the electrical conductivity quickly increases from 1.40×10^{-13} to 4.99×10^{-6} S cm^{-1} with the addition of only 2.8 wt % of filler, and reaches the highest value of 7.29×10^{-4} S cm^{-1} with 6.0 wt % of the filler. In previous works using *in situ* polymerization, we obtained semi-conductive nanocomposites with conductivities of 1.6×10^{-7} and 1.3×10^{-4} S cm^{-1} at higher amount of graphite nanosheets, 15.3 and 20.9 wt %, respectively.[25] These results are supported by An *et al.*[40] that they reported 10^{-6}–10^{-7} Ω cm for the incorporation of 3.0 wt % of exfoliated graphene (EG) in EG/polypropylene nanocomposites. Recently, Huang *et al.*[41] reported a value of electrical conductivity of 2.3×10^{-5} with the incorporation of 5 wt % of graphene in polypropylene matrix, where we obtained almost this value only with the addition of 2.8 wt % of the filler. The decrease in the percolation threshold can be attributed to two factors, i.e., the excellent exfoliation of rGO used in this work and, most probably, the presence of single graphene sheets that provides better dispersion in the polymer matrix. The second factor is the supporting methodology used for the catalyst that improves the dispersion of the filler and leads to the morphology of graphene sheets.

The room temperature magnetization hysteresis loops of the CNT-Fe powder and PE/rGO-CNT-Fe nanocomposites are plotted in Figure 2 The magnetization data of the PE (not shown) evidence only diamagnetic characteristics. It can be notice that the magnetization of CNT-Fe is almost three times lower than the one of the nanocomposites. The explanation for this behavior is that in the filler the iron NPs are closer than in the nanocomposites where they are well dispersed. Low inter-particle distances enhance demagnetization. The hysteresis loops for the PE/rGO-CNT-Fe samples turned out to be very similar, showing almost an identical value of their remnant magnetization/saturation magnetization ratio (M_R/M_S) of ~0.52, while the coercivity (H_C) varies between 890 and 980 Oe. All H_C and M_R/M_S values of the nanocomposites are given in Table II. The coercivity (H_C) values obtained for the nanocomposites are very high compared with another ferromagnetic nanocomposites in the literature. Composites of poly(aniline-*co*-aminonaphtalenesulfonic acid) with Fe_3O_4 NPs showed coercivity of 15–17 Oe at room temperature.[42] Recently, Sim *et al.*[43] have reported on Fe_3O_4@PANI magnetic materials prepared by oxidation polymerization of PANI on the surface of Fe_3O_4. They have obtained a coercivity of ~40 Oe, which is around 4% of the value in our results. Similarly, Riquelme *et al.*[44] reported coercivity values between 500 and 550 Oe for polypropylene magnetic nanocomposites with 2%–6% of CNT-Fe obtained by melt mixing. Santos *et al.*[45] obtained coercivities of 275 and 250 Oe

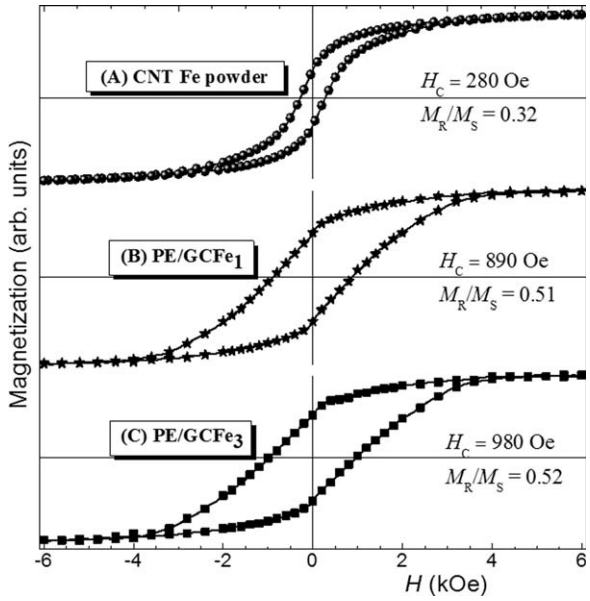

Figure 2. Room temperature hysteresis loops of (A) CNT-Fe powder, (B) PE/GCFe$_1$, and (C) PE/GCFe$_3$ nanocomposites. The lines are only a guide to the eyes.

at 2 K for polyurethanes with 3 and 10 wt % of Fe_3O_4 synthetic talc but any magnetization at room temperature. Reddy *et al.*[46] showed an increase in M_R and M_S from 0.5 to 13.2 and 0.08 to 2.42, respectively, by increasing the amount of Fe_3O_4 from 1 to 30 wt % in poly(3,4 ethylenedioxythiophene), but they reported the absence of hysteresis loop which indicates the superparamagnetic nature of the nanocomposites. He *et al.*[2] reported a decrease in H_C from 193 to 9 Oe with the increase in the amount of magnetic particles from 5 to 20 wt % in a HDPE matrix. This can be attributed to a decrease in the inter-particle distance resulting in stronger, demagnetizing, dipolar interactions; the latter tends to stabilize demagnetized state with low remnant and coercivity values. In our case, the M_R/M_S value of ~0.52 is very close to that (0.5) of systems consisting of non-interacting single-domain particles with uniaxial anisotropy.[47] For such configurations, the H_C value should be approximately twice lower than the anisotropy (or closure) field (H_A), i.e., the magnetic field above which the magnetization processes are only reversible.[48] The fact that in the present case, the values of H_C are rather lower than the respective magnetic anisotropy fields indicates that our samples present a distribution of the strength of their H_A, most probably due to the distribution in the particle sizes. One notes that H_C remains nearly the same, in agreement with the amount of the magnetic constituent (Fe) whose concentration is almost constant (0.04–0.06 wt %). The fact that the mean inter-particle distance remains practically the same in these samples owing to the low amount of magnetic constituent (≤0.06 wt %) indicates an uniform dispersion in the polymer matrix, which is in agreement with TEM data.

CONCLUSIONS

PEs that present both electric and magnetic properties have been obtained. The electric properties have been attained as a result of the rGO turning the PE into a semiconductor. The thermal stability of the nanocomposites was characterized by T_{max} and T_{onset}, which increased by 14 and 29 °C, respectively, with the incorporation of 6 wt % of the filler. The electrical conductivities increased from 4.99×10^{-6} S cm^{-1} with the addition of only 2.8 wt % of the filler and reached 7.29×10^{-4} S cm^{-1} with 6.0 wt % of the filler. Atomic absorption revealed that the amount of Fe was 26.9 wt % in the CNTs and 0.04–0.06 wt % in the nanocomposites; however, the coercivity values were 280 and 890–980 Oe, respectively, confirming that good dispersion and high inter-particle distance can avoid notable dipolar interactions that would tend to stabilize the demagnetized state. The high coercivity values are attributed to the encapsulation of Fe in the CNTs, which protect the magnetic NP from easy oxidation and aggregation in the polymer matrix. These results show that the synthetic CNT-Fe is an interesting material to produce magnetic polymer nanocomposites. TEM also confirmed that there was a good dispersion of CNT-Fe among the rGO and in the PE matrix, revealing isolated CNT-Fe particles.

This material has the potential to be used in a variety of applications, where a flexible magnetic and electrical material with good processability is required, as for example, electromagnetic device application like electromagnetic interference suppression, micro electronics, and aircraft industries.

ACKNOWLEDGMENTS

The authors are grateful to the TWAS-CNPQ for the fellowship to Muhammad Nisar, the CNPq for the special visiting research fellowship to Professor Raúl Quijada, and CNPq grant 302902/2013–9. Professor Raúl Quijada acknowledges the Millennium Nucleus of Chemical Processes and Catalysis (CPC), grant number NC120082. They also thank CME and LRNANO from UFRGS for the microscopy analysis.

REFERENCES

1. Schaefer, D. W.; Justice, R. S. *Macromolecules* **2007**, *40*, 8501.
2. He, Q.; Yuan, T.; Zhu, J.; Luo, Z.; Haldolaarachchige, V.; Sun, L.; Khasanov, A.; Li, Y.; Young, D. P.; Wei, S.; Guo, Z. *Polymer* **2012**, *53*, 3642.
3. Chrissafis, K.; Paraskevopoulos, K. M.; Tsiaoussis, I.; Bikiaris, D. C. *J. Appl. Polym. Sci.* **2009**, *114*, 1606.
4. Coleman, J. N.; Khan, U.; Blau, W. J.; Gun'ko, Y. K. *Carbon* **2006**, *44*, 1624.
5. Reddy, K. R.; Sin, B. C.; Yoo, C. H.; Sohn, D.; Lee, Y. *J. Colloid Interface Sci.* **2009**, *340*, 160.
6. Kuila, T.; Bose, S.; Mishra, A. K.; Khanra, P.; Kim, N. H.; Lee, J. H. *Polym. Test.* **2012**, *31*, 31.
7. Andrews, R.; Weisenberger, M. C. *Curr. Opin. Solid State Mater.* **2004**, *8*, 31.
8. Ma, P. C.; Siddiqui, N. A.; Marom, G.; Kim, J. K. *Compos. Part A: Appl. Sci. Manuf.* **2010**, *41*, 1345.
9. Raghu, A. V.; Jeong, H. M.; Lee, Y.; Raghu, A. V. *J. Polym. Sci. Part A: Polym. Chem.* **2010**, *48*, 1477.

10. Kim, H.; Abdala, A. A.; Macosko, C. W. *Macromolecules* **2010**, *43*, 6515.
11. Geim, A. K.; Novoselov, K. S. *Nat. Mater.* **2007**, *6*, 183.
12. Dikin, D. A.; Stankovich, S.; Zimney, E. J.; Piner, R. D.; Dommett, G. H. B.; Evmenenko, G.; Nguyen, S. T.; Ruoff, R. S. *Nature* **2007**, *488*, 457.
13. Wakabayashi, K.; Pierre, C.; Dikin, D. A.; Rouff, R. S.; Ramanathan, T.; Brinson, L. C.; Torkelson, J. M. *Macromolecules* **2008**, *41*, 1905.
14. Pavoski, G.; Maraschin, T.; Milani, M. A.; Azambuja, D. S.; Quijada, R.; Moura, C. M.; Basso, N. R. S.; Galland, G. B. *Polymer* **2015**, *81*, 79.
15. Hassan, M.; Reddy, R. K.; Hague, E.; Minett, A. I.; Gomes, V. G. *J. Colloid Interface Sci.* **2013**, *410*, 43.
16. Han, S. J.; Lee, H.; Jeong, H. M.; Kim, B. K.; Raghu, A. V.; Reddy, K. R. *J. Macromol. Sci. Part B: Phys.* **2014**, *53*, 1193.
17. Son, D. R.; Raghu, A. V.; Reddy, K. R.; Jeong, H. M. *J. Macromol. Sci. Part B: Phys.* **2016**, *55*, 1099.
18. Hassan, M.; Reddy, K. R.; Hague, E.; Faisal, S. N.; Ghasemi, S. *Compos. Sci. Technol.* **2014**, *98*, 1.
19. Lee, Y. R.; Kim, S. C.; Lee, H.; Jeong, H. M.; Raghu, A. V.; Reddy, R. K.; Kim, B. K. *Macromol. Res.* **2011**, *19*, 66.
20. Schinteie, G.; Kuncser, V.; Palade, P.; Alexandrescu, R.; Morjan, I.; Filoti, G. *J. Alloy Compd.* **2013**, *564*, 27.
21. Osorio, A. G.; Bergmann, C. P. *Appl. Surf. Sci.* **2013**, *264*, 794.
22. Osorio, A. G.; Pereira, L. G.; Cunha da, J. B. M.; Bergmann, C. P. *Mater. Res. Bull.* **2013**, *48*, 4168.
23. Nisar, M.; Bergmann, C.; Geshev, J.; Quijada, R.; Galland, G. B. *Polymer* **2016**, *97*, 131.
24. Milani, M. A.; González, D.; Quijada, R.; Basso, N. R. S.; Cerrada, M. L.; Azambuja, D. S.; Galland, G. B. *Compos. Sci. Technol.* **2013**, *84*, 1.
25. Fim, F. C.; Basso, N. R. S.; Graebin, D. S.; Azambuja, D. S.; Galland, G. B. *J. Appl. Polym. Sci.* **2013**, *128*, 2630.
26. Milani, M. A.; González, D.; Quijada, R.; Benavente, R.; Arranz-Andrés, J.; Galland, G. B. *Polymer* **2015**, *65*, 134.
27. Fim, F. C.; Guterres, J. M.; Basso, N. R. S.; Galland, G. B. *J. Polym. Sci. Part A: Polym. Chem.* **2010**, *48*, 692.
28. Kim, P.; Doss, N. M.; Tillotson, J. P.; Hotchkiss, P. J.; Pan, M. J.; Marder, S. R.; Li, J.; Calame, J. P.; Perry, J. W. *ACS Nano* **2009**, *3*, 2581.
29. Dai, Q.; Berman, D.; Virwani, K.; Frommer, J.; Jubert, P. O.; Lam, M.; Topuria, T.; Imaino, W.; Nelso, A. *Nano Lett.* **2010**, *10*, 3216.
30. Shimad, T.; Ookubo, K.; Komuro, N.; Shimizu, T.; Uehara, N. *Langmuir* **2007**, *23*, 11225.
31. Guo, Z.; Lee, S. E.; Kim, H.; Park, S.; Hahn, H. T.; Karki, A. B.; Young, D. P. *Acta Mater.* **2009**, *57*, 267.
32. Staudenmaier, L. *Chem. Ges.* **1898**, *31*, 1481.
33. Pavoski, G.; Maraschin, T.; Fim, F. C.; Balzaretti, N. M.; Galland, G. B.; Moura, C. S.; Basso, N. R. S. *Mater. Res.* **2017**, *20*, 53.
34. Resano, M.; Bolea-Fernández, E.; Mozas, E.; Flórez, M. R.; Gringberg, P.; Sturgeon, R. E. *J. Anal. At. Spectrom.* **2013**, *28*, 657.
35. Stürzel, M.; Kempe, F.; Thomann, Y.; Mark, S.; Enders, M.; Mülhaupt, R. *Macromolecules* **2012**, *45*, 6878.
36. Tait, P. J.; Ediati, R. In Metalorganic Catalysts for Synthesis and Polymerization; Kaminsky, W., Ed.; Springer. Heidelberg, **1999**; p 307.
37. Potts, J. R.; Dreyer, D. R.; Bielawski, C. W.; Ruoff, R. S. *Polymer* **2011**, *52*, 5.
38. Balogum, Y. A.; Buchanan, R. C. *Compos. Sci. Technol.* **2010**, 885.
39. Kuilla, T.; Bhadrab, S.; Yao, D.; Kim, N. H.; Bose, S.; Lee, J. H. *Prog. Polym. Sci.* **2010**, *35*, 1350.
40. An, J. E.; Jeon, G. W.; jeong, Y. G. *Fiber Polym.* **2012**, *13*, 507.
41. Huang, C. L.; Lou, C. W.; Liu, C. F.; Huang, C. H.; Song, X. M. *Appl. Sci.* **2015**, *5*, 1196.
42. Reddy, K. R.; Lee, K. P.; Gopalan, A. I. *J. Appl. Polym. Sci.* **2007**, *106*, 1181.
43. Sim, B.; Chae, H. S.; Choi, H. J. *eXPRESS Polym. Lett.* **2015**, *9*, 736.
44. Riquelme, J.; Garzón, C. A.; Bergmann, C. P.; Geshev, J.; Quijada, R. *Eur. Polym. J.* **2016**, *75*, 200.
45. Santos, L. M. D.; Ligabue, R.; Dumas, A.; Roux, C. L.; Micoud, P.; Meunier, J. F.; Martin, F.; Einloft, S. *Eur. Polym. J.* **2015**, *69*, 38.
46. Reddy, K. R.; Park, W.; Sin, B. C.; Noh, J.; Lee, Y. *J. Colloid Interface Sci.* **2009**, *335*, 34.
47. Stoner, E. C.; Wohlfarth, E. P. *Philos. Trans. R. Soc. Lond. Ser. A* **1948**, *240*, 559.
48. Harres, A.; Mikhov, M.; Skumryev, V.; de Andrade, A. M. H.; Schmidt, J. E.; Geshev, J. *J. Magn. Magn. Mater.* **2016**, *402*, 76.

Annex 4

European Polymer Journal 99 (2018) 378–383

Contents lists available at ScienceDirect

European Polymer Journal

journal homepage: www.elsevier.com/locate/europolj

Synthesis of polyethylene/nickel–carbon stimuli-responsive material under magnetic field at room temperature: Effect of the filler on the properties

Muhammad Nisar[a], Pascal S. Thue[a], Cesar A. Heck[a], J.L. Salazar Cuaila[b], J. Geshev[b], Eder C. Lima[a], Marly M. Jacobi[a], Griselda Barrera Galland[a,*]

[a] Instituto de Química, Universidade Federal do Rio Grande do Sul, 91501-970 Porto Alegre, RS, Brazil
[b] Instituto de Física, Universidade Federal do Rio Grande do Sul, 91501-970 Porto Alegre, RS, Brazil

ARTICLE INFO

Keywords:
Polyethylene
Nanocomposites
Magnetic properties
Nickel-activated carbon

ABSTRACT

In this study we investigated the effect of carbon-based magnetic fillers on the thermal, mechanical, morphological and magnetic properties of polyethylene nanocomposites, with the filler range from 0 to 8.5 wt%, prepared by *in situ* polymerization. The nickel-carbonized material was prepared from biomass by the pyrolysis of wood sawdust. The thermal stability was investigated by thermogravimetric analysis (TGA) and differential calorimetric analysis (DSC); the results show that, with incorporation of the filler, the onset and maximum degradation temperatures increased by 24 and 7 °C, respectively. The DSC results indicate an enhancement of 4 °C in the melting and crystallization temperatures, as compared to neat polyethylene. The addition of the Ni filler resulted in a ferromagnetic behavior of the polyethylene nanocomposites. While the variation on the coercivity with the Ni filler content was very little (a rise of ~30%), the effect on the normalized remnant magnetization was rather significant, presenting a threefold increase. The mechanical properties showed an improvement, mainly with the higher amount of the filler.

1. Introduction

Stimuli-responsive materials are attracting increasing attention because of their exceptional characteristics, where their properties are altered by external stimuli, such as pH, light, temperature and electric or magnetic fields [1]. Petrochemical-based plastics are used in a broad variety of sectors owing to their outstanding physical properties, easy processability, flexibility, and cost effectiveness [2]. In recent decades, nanometric-sized particles have been introduced to polymer matrixes to obtain multifunctional polymer nanocomposites with improved electrical, barrier, thermal and/or mechanical properties. These new materials have vast industrial applications ranging from electronics to aerospace [3,4]. The improvement in nanocomposite properties is strongly dependent on the choice of the filler, which plays a key role in the final application [5].

Nanometric fillers normally used to enhance the properties of the polymer matrix include clay, alumina, carbon nanotubes, silver, gold, and graphite [6]. To obtain improved properties of the polymer matrix, homogenous distribution of the filler in the polymer and the compatibility between the polymer and filler are the two important issues to be resolved since the components have, in general, low interaction energy [7]. The efficient load transfer from matrix to filler and, subsequently, efficient reinforcement of the composites, require a strong interface between the polymer phase and the filler [8].

Magnetic nanoparticles incorporated in various polymer matrices are very interesting owing to their numerous applications, such as magneto-optics, magneto-sensing, electronics, and magneto-optical devices [9]. Polymer composites with iron, cobalt and nickel with ferromagnetic properties have been reported [10]. Iron-based nanoparticles are broadly considered because of their potential applications in microelectronics, biomedicine and catalysis [11]. Although metallic iron nanoparticles present outstanding magnetic properties, the difficulty in protecting iron from easy oxidation means that their applications must involve stable iron oxides or metallic iron embedded in a protective layer, which can be oxide [12], carbide [13] or a noble metal/corrosion resistant shell [14]. Marayniak et al. [9] reported three types of nanocrystalline materials: Fe/C, Fe_3C/C and Fe/Fe_3C, obtained by carburization of nanocrystalline iron, and applied them as fillers in a poly(ether–ester) matrix. The protection strategies have been considered effective tools to chemically stabilize the magnetic constituent by coating, and including silica or carbon to avoid aggregation [15]. A ferromagnetic material containing iron protected by carbon nanotubes is produced when ferrocene [$Fe(C_2H_5)_2$] is used for the synthesis of multiwall carbon nanotubes by a chemical vapor-deposition method,

* Corresponding author.
E-mail address: griselda.barrera@ufrgs.br (G.B. Galland).

https://doi.org/10.1016/j.eurpolymj.2017.12.044
Received 16 November 2017; Received in revised form 26 December 2017; Accepted 30 December 2017
Available online 02 January 2018
0014-3057/

where ferrocene acts as a catalyst and as a synthesis precursor [16]. Recently, Osorio et al. [17,18] optimized the conditions for the synthesis of CNTs from ferrocene using silica with different surfaces as substrate.

A variety of methods have been reported for the preparation of polymer nanocomposites, such as surface-initiated polymerization [19], solution blending [20], ball milling [21], surface wetting method [22], ion exchange technique [23] and *in situ* polymerization [24]. The latter method is the most reported technique used to attain homogeneous distribution of the filler, as compared to the traditional melt-mixing [25]. The physicochemical properties of these polymer nanocomposites can notably be enhanced through a combination of the qualities of the organic polymer matrix and of the inorganic components with different nanostructure and size [26].

Our research group is working extensively on synthesizing polyolefin nanocomposites using *in situ* polymerization. Recently, we prepared polyethylene–graphite nanosheets (PE-GNS), isotactic polypropylene–graphite nanosheets (iPP-GNS), polyethylene-carbon nanotubes containing iron (PE-CNT-Fe) and polypropylene-carbon nanotube-iron (PP-CNT-Fe) nanocomposites, and obtained homogenous dispersions of the filler in the polymer matrix [25,27–33]. In the present work we focus on the production of a nickel-carbonized material from wood biomass (effective low-cost source) via microwave-assisted pyrolysis [34,35]. Lignocellulosic waste material was used to produce a highly porous and magnetic material. The aim of the work was to use nickel-activated carbon as filler in the production of high-density polyethylene nanocomposites by *in situ* polymerization using metallocenes[$(nBuCp)_2ZrCl_2$] as catalyst, and methylaluminoxane (MAO) as a co-catalyst to study the effect of this filler on the magnetic, mechanical, and thermal properties of the nanocomposites.

2. Experimental

2.1. Materials

All compounds sensitive to air and moisture (i.e., the catalyst and co-catalyst) were manipulated under deoxygenated dry argon using the standard Schlenk and vacuum line techniques. The carbonized material containing nickel (Ni-C) was synthesized by the method described elsewhere [35]. Toluene was distilled with metallic sodium and benzophenone. Methylaluminoxane (MAO) (Sigma-Aldrich, 4.6 wt% Al solution in toluene) and metallocene catalyst bis(n-butyl)cyclopentadienylzirconium dichloride $(n\text{-}BuCp)_2ZrCl_2$ (Sigma Aldrich) were used as received.

2.2. Synthesis of carbonized material containing-nickel (Ni-C)

Sapelli sawdust was used as a precursor for the preparation of the composite activated carbons with nickel(II). It contains *ca* 98% of cellulose, hemicellulose, lignin and pectin [34].

For the preparation, a known amount of nickel (II) chloride salt was dissolved in 50.0 mL of deionized water, after which 50.0 g of dried biomass (milled to diameter < 300 μm) was added to the solution and mixed continuously at approximately 80 °C for 120 min to overcome the natural recalcitrance of the lignocellulosic biomass structure, as well as to ensure a high interaction between the nickel ions and the lignocellulosic material. The impregnation mass ratios of metal salt/biomass were 1:1 (w/w).

After mixing, the paste was oven-dried at 90 °C for 12 h. Pyrolysis of the dried sawdust impregnated with nickel was carried out in a quartz reactor [35,36], under a nitrogen atmosphere (150 mL min^{-1}). The quartz reactor was placed in a conventional oven and heated for 2 h at 700 °C. The system was then cooled after carbonization for 1 h under 60 mL min^{-1} nitrogen flow. The final material was washed and dried at 105 °C for 24 h and stored for the fabrication of polymer nanocomposite.

2.3. Fabrication of polymer nanocomposites

The carbonized material containing nickel was stirred with 15 wt% of MAO for 30 min in toluene. The polymerization reactions were performed in a 300 mL reactor equipped with mechanical stirring at a controlled temperature. Toluene was used as solvent, MAO as co-catalyst (Al/Zr = 1000) and $(n\text{-}BuCp)_2\ ZrCl_2$ as catalyst (5×10^{-6} mol). All the reactions were carried out at 25 °C with a constant ethylene pressure of 2.5 bar for 0.5 h. The carbon material containing nickel previously treated with MAO was introduced to the reactor as filler in various amounts under inert atmosphere. The obtained polymer was washed with 10 vol% of HCl in ethanol solution and dried to constant weight.

3. Characterization

Transmission electron microscopy (TEM) analyses were performed using a JEOL 1011 microscope operating at 120 kV. Samples were prepared from ultrathin films (~50 nm thick) cut under cryogenic conditions with a Leica Ultracut UCT microtome at −70 °C and placed on a grid. Scanning electron microscopy (SEM) was carried using a Phillips XL30 microscope operating at 20 kV. Samples were prepared by deposition on an aluminum stub and coated with gold.

The molecular weights were obtained with a Waters Alliance GPC 2000 instrument equipped with three Styragel HT-type columns (HT3, HT5, and HT6E). 1,2,4-Trichlorobenzene was used as solvent, with a flow rate of 1 mL min^{-1} and a temperature of 135 °C. The columns were calibrated with polystyrene standards.

The magnetic characterization of the materials was performed using an EZ9MicroSense vibrating sample magnetometer (VSM) at room temperature with a magnetic field (*H*) ranging from −20 kOeto + 20 kOe.

Differential scanning calorimetry (DSC) analyses were performed using a Perkin-Elmer differential calorimeter (model DSC Q20) operating at a heat rate of 10 °C min^{-1} and a temperature range of 0–180 °C. The melting temperature, T_m, was determined in the second heating, and the degree of crystallinity was calculated from the enthalpy of fusion data obtained from the DSC curves (293 J g^{-1} was used for 100% crystalline material). Thermogravimetric analysis (TGA) was performed on a SDT Q600 thermal analyzer Q20 (TA Instruments) at a scanning rate of 20 °C min^{-1} from 0 to 800 °C under nitrogen atmosphere for the nanocomposites and under synthetic air atmosphere for the determination of nickel in Ni-C.

The mechanical properties were measured using HP model D-500 dynamometer according to ASTMD 638-10 at ~25 °C. For each wt% of nanocomposites, five samples were tested and the results averaged over these five measurements (typical deviation *ca*.5%). Bone-shaped samples of overall length 120 mm with the distance between the two grips of 80 mm, width of 11.5 mm, and thickness of 1 mm were tested at a cross-head rate of 50 mm min^{-1}.

4. Results and discussion

4.1. Elemental composition and nickel content in nickel-containing activated carbon

Table 1 shows the elemental composition of *nickel-containing activated carbon*. Compared to the precursor material, the sample after

Table 1
Elemental analysis of activated carbon containing nickel.

Sample	% C	%H	%N	%O[a]	%Ash
Ni-C	58.515	1.295	0.03	0.67	39.49

[a] Obtained by difference (%O = 100% - % C - %H - %N - %Ash).

Table 2
Catalytic activities and thermal properties of PE-Ni-C nanocomposites.

Samples	Filler[a] (%)	Ni (%)	Polymer (g)	TGA residue (%)	Catalytic activity[b]	T_c (°C)	T_m (°C)	X_c (%)	T_{onset} (°C)	T_{max} (°C)
PE	0	0	8.9	0	1428	119	132	47	433	474
PE-Ni-C_1	0.3	0.1	10.1	0.7	1616	119	133	48	440	479
PE-Ni-C_2	1.0	0.4	8.5	0.8	1344	119	134	42	425	468
PE-Ni-C_3	1.4	0.5	10.5	0.8	1680	118	134	40	418	452
PE-Ni-C_4	2.5	0.9	9.40	5.9	1504	119	135	42	458	479
PE-Ni-C_5	5.0	1.8	8.0	12.8	1294	123	136	43	456	481
PE-Ni-C_6	8.5	3.1	8.27	7.8	1323	122	137	42	454	481

[a] Filler = Ni-C.
[b] KgPE.$[Zr]^{-1}\,h^{-1}\,bar^{-1}$.

nickel treatment exhibited a higher carbon content and a small amount of oxygen content. Initially, the biomass exhibited 46.16% carbon, 6.17% hydrogen and 37.03% oxygen, but after pyrolysis and washing, the carbon content increased to 58.515%. Higher carbon content indicates that the aromatic structure becomes dominant after pyrolysis in the presence of metal chlorides [36].

It was also possible with TGA analysis to determine the nickel content in the Ni–C. In fact, the ash content is attributed to the inorganic material left after the carbonization process in the synthetic air atmosphere. Knowing that the ash content in biomass was 1.29% and in Ni–C it is 39.49%, it is possible to find the nickel content in the activated carbon (Ni-C) by the difference. The nickel content was found to be 38.20%.

4.2. Polymerization reaction

Polyethylene was polymerized in the presence of nickel-activated carbon using metallocene catalyst [(n-BuCp)$_2$ZrCl$_2$] and methylaluminoxane (MAO) as a co-catalyst. The nickel–carbon material was first stirred with 15 wt% of MAO for 20 min to eliminate impurities. Table 2 presents the results of a sequence of polymerization reactions carried with different amounts of nickel–carbon material. The nickel–carbon material proportion in PE-Ni-C nanocomposites ranged from 0.3 to 8.5 wt% as calculated from the polymer yield. The results show that the amount of the filler does not affect the catalytic activity, so no deactivation of the catalyst takes place during the polymerization reaction. All the catalytic activities were very high.

4.3. Thermal properties

The thermal properties of PE and its nanocomposites are summarized in Table 2. It can be seen from the results that the melting temperatures (132–137 °C) indicate an increase of 5 °C compared to the neat PE. Likewise, the crystallization temperatures (T_c) shows an increase of 3 °C, indicating that the filler acts as a nucleating agent for PE-Ni-C nanocomposites. The nucleation effect was more prominent as the filler content increased. These results demonstrate that the higher amount of the filler produces a large heterogeneous nucleation effect, which is supported by the results of other researchers [37,38,39]. However, this effect is not related directly with the degree of crystallinity. The percentage crystallinity value increased first with the addition of 0.3 wt% of the filler, but decreased up to approximately 10% with addition of 8.5 wt% of the filler as compare to the neat polymer. Crystallization starts relatively at higher temperature but the crystals formed may have a lower degree of perfection than those in pure polymer, this is the reason why the percentage of crystallinity is relatively lower [40]. McNally et al. [41] showed a similar decreasing trend in the crystalline content of the polyethylene multiwalled carbon nanotube composites.

The thermal degradation behavior of PE and its nanocomposites was examined by TGA analysis. Table 2 also shows the TGA results of the neat PE and its nanocomposites. In the samples with higher amount of filler from 2.5 to 8.5% there was an increase in the onset degradation temperature (T_{onset}) of around 25 °C and in the maximum degradation temperature (T_{max}) of 7 °C compared to the neat PE, representing a considerable enhancement in the thermal stability of the nanocomposites. However there was a decrease in T_{onset} and T_{max} in two samples with low amount of filler (1.0 and 1.4 wt%). This behavior is not easy to understand. Many authors [42–45] studied the effect of metals such as Fe, Al, Cu, Co and Ni in the thermal degradation of plastics such as PP [42], chitosan [43], LDPE [44] and HDPE [45]. They concluded that the surface interaction between a metal and a polymer can promote the thermal degradation of the organic phase at different rates. In the case of the nanoparticles studied in this work (Ni-C), nickel is mostly encapsulated by the amorphous carbon, avoiding the direct contact of the polymer with the metal and thus protecting the polymer from degradation. However, it is also possible that a small amount of nickel could be available to compete with the thermal stability given by the carbon part of the filler.

The obtained polymer achieved a high molecular weight (Mw = 4.4×10^5 g mol^{-1} with polydispersity of 1.9). Previous results showed that using the same technique for the polyolefin preparation, the nanocomposites retain identical molecular weight to that of neat polymer [46]. Table 2 also demonstrates that the wt% of the filler calculated from the polymer yield is, in general, in agreement with the wt% calculated from the TGA residue, except for the samples PE-Ni-C_4 and PE-Ni-C_5, showing some heterogeneity on the distribution of the filler in those samples. The wt% of the nickel calculated from TGA is also demonstrated in Table 2.

4.4. Morphology of the nanocomposites

Fig. 1 shows SEM images of the nickel–carbon material and its nanocomposites with polyethylene at the same magnification. The micrograph shows a uniform distribution of the filler in the polymer matrix. It can be seen that the polymer is wrapped around the filler, clearly demonstrating the homogenous distribution of Ni–C in the PE matrix.

Fig. 2 demonstrates the TEM micrographs of the nickel-activated carbon and PE/Ni-C nanocomposites. The micrographs indicate a uniform distribution of the filler in the polyethylene matrix. The black spots in the micrographs are most probably due to the presence of nickel particles in the carbon material. It can be seen very clearly that the PE matrix shows core–shell morphology around the filler and nickel particles; similar morphology was reported by He et al. [26] for high-density polyethylene/iron nanocomposites, where the authors reported the presence of black spots as iron. No aggregates were observed.

4.5. Mechanical properties

In general, the mechanical properties of the polymers were changed by the incorporation of filler, depending upon various factors; for instance, the dispersion of the filler, filler matrix adhesion, and the aspect ratio of the filler. Fig. 3 shows the results of the stress–strain curve and

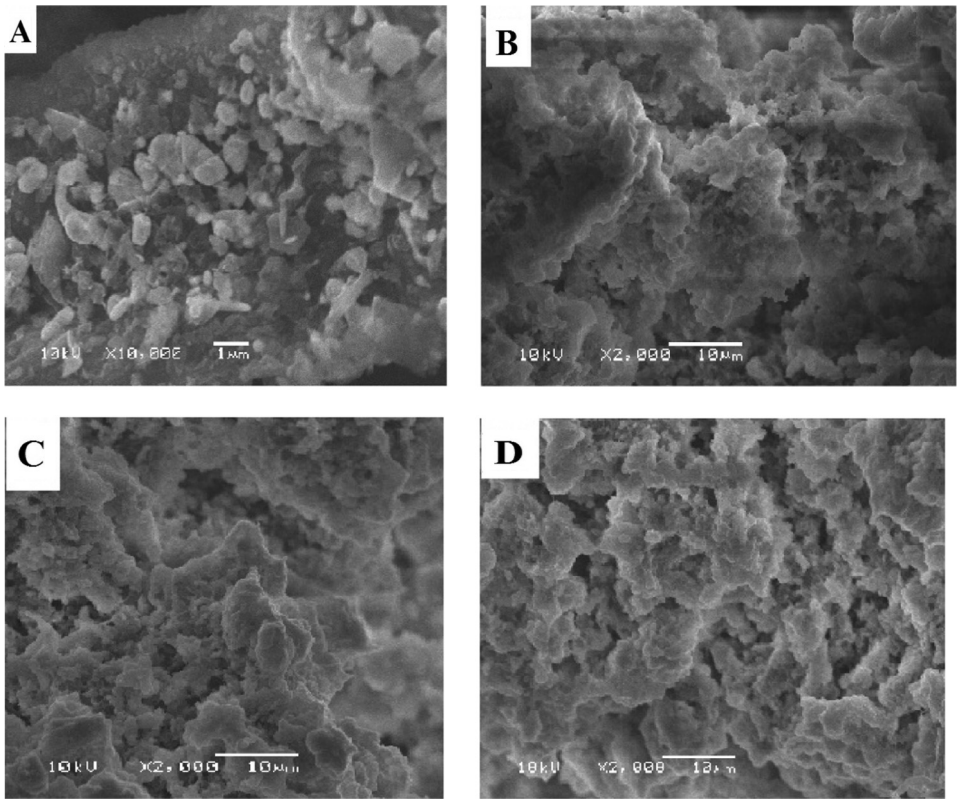

Fig. 1. SEM images of Ni-C (A) and (B), (C), (D) PE/Ni-C nanocomposites 1%, 2.5% and 5%.

the effect of the filler in the elongation at break point. An increase in elastic module is observed as compared to neat PE, from 386 MPa to 456 MPa and 498 MPa with incorporation of 5 wt% and 8.5 wt% of the filler, respectively. These results specify the improvement in material stiffness as a result of the filler loading [47]. This enhancement can be due to the excellent interface between polymer matrix and filler; the filler tends to have greater surface area per unit volume ratio, which enables good load transfer to the polymer [48]. Similar enhancements

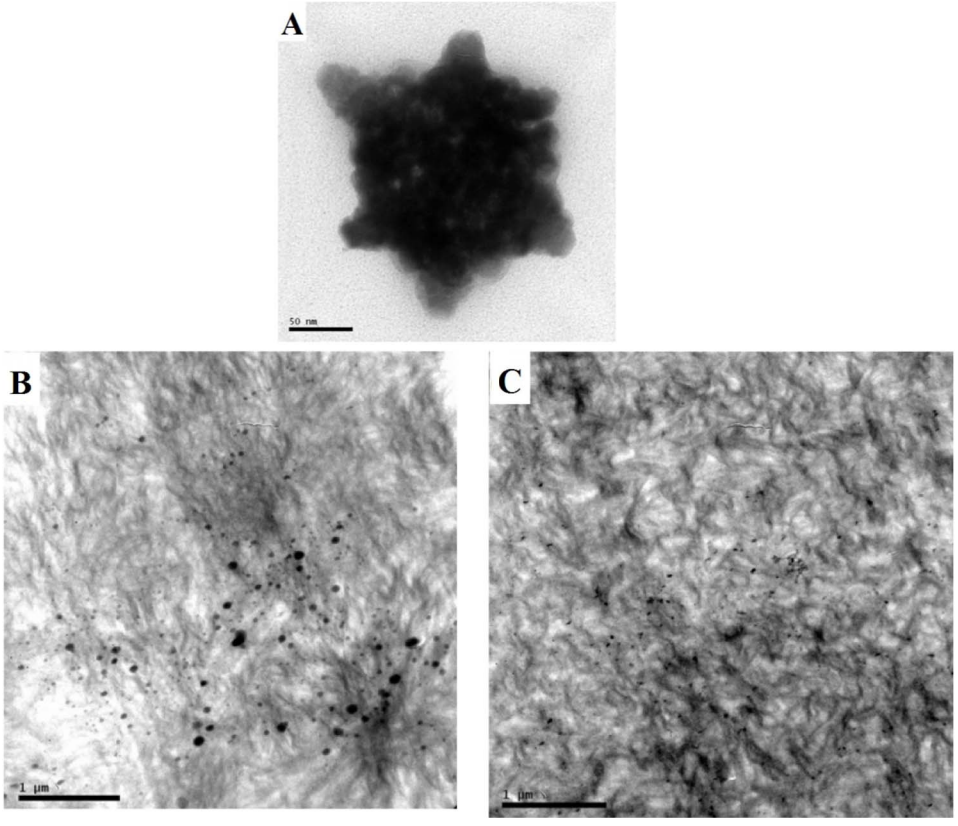

Fig. 2. TEM images of Ni-C (A), and PE/Ni-C nanocomposite 1% (B), and 5% (C).

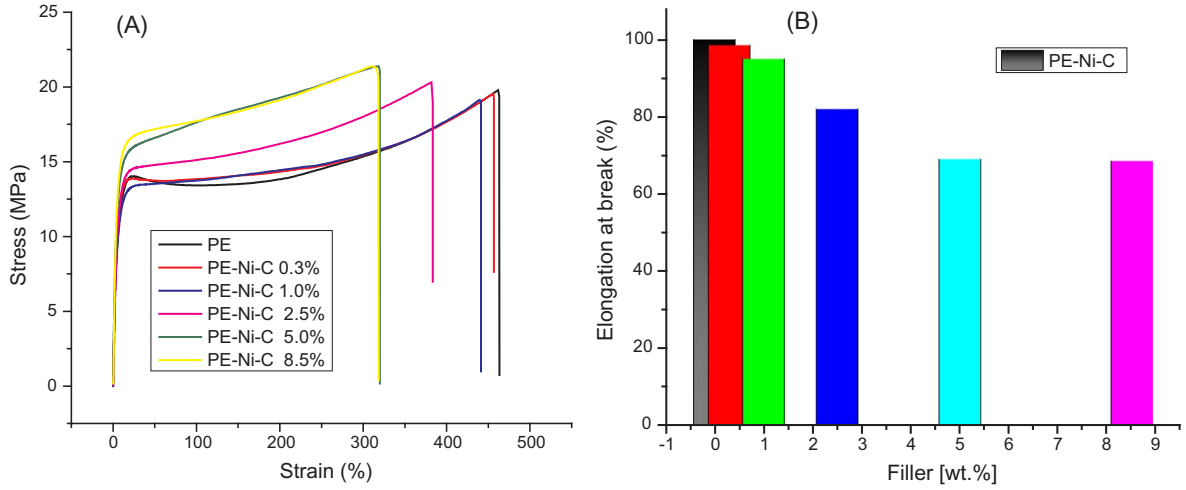

Fig. 3. (A) Stress-strain curve of neat PE and its nanocomposites (B) elongation at the break with the increase in the concentration of filler.

in the mechanical properties were also reported by other researchers using other fillers, such as graphene and carbon fibers [49,50].

As expected, the elongation at break decreases for the polymer nanocomposites as the filler wt% increases. Fig. 3(B) shows a gradual decrease in the elongation at break point as compared to neat PE. The nanoparticles strongly restrict the movement of the polymer chain when it is under stress [51]. The enhancement in the mechanical properties can be attributed to the higher intrinsic mechanical properties of the filler, as well as to a reasonable interfacial interaction between filler and PE matrix [52].

4.6. Magnetic properties

Fig. 4 presents the magnetization hysteresis loops (i.e., magnetization, M, normalized to its saturation value, M_S, versus magnetic field, H) traced for all samples at room temperature. Aiming to avoid potential minor-loop effects [53–56], we ensured that the maximum H-value used was sufficiently high to effectively saturate each of the samples, by employing one of the criteria for magnetic saturation proposed recently [53]. Namely, we analyzed the second derivatives of M with respect to H, which also allowed us to estimate the saturation field, H_S, representing the value of H above which $M(H)$ has effectively attained saturation.

The values of the coercivity, H_C (shown in the bottom-right inset) vary very little, i.e., between 34 and 45 Oe. The variation of the normalized saturation remanence, M_R/M_S, with the Ni filler content (given in the top-left inset) is more significant, presenting an increase from 0.08 to 0.26. The values of H_C and M_R/M_S for the powder sample are 39 Oe and 0.10, respectively. In regards to the shape of the loops, only the curves measured for the powder sample and that with 0.3% Ni filler content differ from the rest, presenting higher slopes at the field interval, as shown in Fig. 4. In the case of the powder sample, this should be attributed to a tendency to saturate at high magnetic fields, confirmed by the rather high value of H_S of ~1550 Oe as compared to those of all other samples (which varied very little, between 690 and 720 Oe). However, the relatively high value of the $M(H)$ slope in the case of the lowest Ni filler content of 0.3% corresponds, most probably, to a magnetic contribution of a portion of insolated, superparamagnetic entities, which are also responsible for the lowest H_C and M_R/M_S values for this sample. The low values of H_C and M_R/M_S for the powder sample, on the other hand, should be attributed to demagnetizing magnetic interactions, resulting in close-flux magnetic configurations.

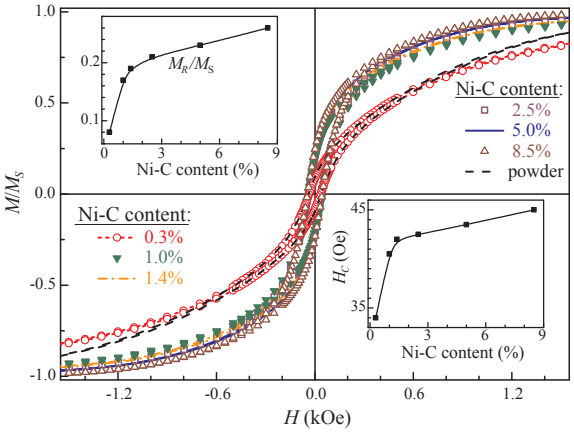

Fig. 4. Room temperature magnetization hysteresis loops traced on the PE-Ni-C nanocomposites with different Ni filler content. The insets present the normalized saturation remanence, M_R/M_S (top, left) and coercivity H_C (bottom, right).

5. Conclusion

Cost-effective polyethylene nanocomposites were synthesized by *in situ* polymerization, using a nickel–carbon material as filler. The results showed that the onset degradation temperature and the maximum degradation one increase by 21 °C and 7 °C, respectively. The melting temperature and crystallization temperature also showed slight enhancement. The elastic module was increased, up to ~33% with the addition of 5 wt% of the filler. The incorporation of nickel in the carbonized material makes it magnetic. The introduction of the magnetic properties in the polymer matrix broadens its application for the manufacture of different devices. The results show that the nanocomposites had both ferromagnetic and super-paramagnetic parts, with a very low percentage of filler at room temperature. Those results are remarkable because most of the works in this area report magnetic properties at low temperatures only. These results can be explained on the basis of good dispersion of the filler, where very little demagnetization takes place.

Conflicts of interest

There are no conflicts of interest to declare.

Acknowledgments

The authors are grateful to TWAS-CNPq (Brazil) for the fellowship to Muhammad Nisar (award number: 3240274293) and for the partial support from CNPq (Conselho Nacional de Desenvolvimento Científico

e Tecnológico) grants 305796/2016-0 and 302902/2013-9). We also thank CME and LRNANO from UFRGS for the microscopy analysis. The magnetic characterization was performed in collaboration with the Laboratory of Magnetism at IF-UFRGS.

References

[1] D.E. Park, H.S. Chae, H.J. Choi, A. Maity, Magnetite–polypyrrole core–shell structured microspheres and their dual stimuli-response under electric and magnetic fields, J. Mater. Chem. C 3 (2015) 3150–3158.
[2] T. Yasin, M. Nisar, M. Shafiq, Y. Nho, R. Ahmad, Influence of sepiolite and electron beam irradiation on the structural and physicochemical properties of polyethylene/Strachnanocomposites, Polym. Compos. 34 (3) (2013) 408–416.
[3] Y. Jia, K. Peng, X. Gong, Z. Zhang, Creep and recovery of polypropylene/carbon nanotube composites, Int. J. Plast. 27 (2011) 1239–1251.
[4] K. Chrissafis, D. Bikiaris, Can nanoparticles really enhance thermal stability of polymers? Part I: an overview on thermal decomposition of addition polymers, Thermochim. Acta 523 (2011) 1–24.
[5] J. Riquelme, C.A. Garz_on, C.P. Bergmann, J. Geshev, R. Quijada, Development of multifunctional polymer nanocomposites with carbon-based hybrid nanostructures synthesized from ferrocene, Eur. Polym. J. 75 (2016) 200–209.
[6] T.G. Gopakumar, D.J.Y.S. Pagé, Polypropylene/graphite nanocomposites by thermo-kinetic mixing, Polym. Eng. Sci. 44 (2004) 1162–1169.
[7] Q. Zheng, Q. Xue, K. Yan, L. Hao, Q. Li, X. Gao, Investigation of molecular interactions between SWNT and polyethylene/polypropylene/polystyrene/polyaniline molecules, J. Phy. Chem. C 111 (2007) 4628–4635.
[8] A.A. Koval'chuk, A.N. Shchegolikhin, V.G. Shevehenko, P.M. Nedorezova, A.N. Klyamkina, A.M. Aladyshev, Synthesis and properties of polypropylene/Multiwall carbon nanotube composites, Macromolecules 41 (2008) 3149–3156.
[9] M. Maryniak, N. Guskos, J. Typek, I. Kucharewicz, U. Narkiewicz, Z. Roshaniec, M. Kwiatkowska, W. Arabczyk, FMR study of polymer composites with nanocrystalline iron-carbon fillers, Rev. Adv. Mater. Sci. 12 (2006) 200–205.
[10] N.A.D. Burke, H.D.H. Stover, F.P. Dawson, Magnetic nanocomposites: preparation and characterization of polymer-coated iron nanopartricles, Chem. Matter. 14 (2002) 4752–4761.
[11] G. Schinteie, V. Kuncser, P. Palade, F. Dumitrache, R. Alexandrescu, I. Morjan, G. Filoti, Magnetic properties of iron-carbon nanocomposites obtained by laser pyrolysis in specific configuration, J. Alloys. Compounds 564 (564) (2013) 27–34.
[12] D. Predoi, O. Crisan, M. Jitianu, M.C. Valsangiacom, M. Raileanu, M. Crisan, M. Zaharescu, Iron oxide in a silica matrix prepared by the sol–gel method, Thin Solid Film 515 (16) (2007) 6319–6323.
[13] I. Morjan, F. Dumitrache, R. Alexandrescu, C. Fleaca, R. Birjega, C.R. Luculesscu, I. Soare, E. Dutu, G. Filoti, V. Kuncser, G. Prodan, N.C. Popa, L. Vekas, Laser synthesis of magnetic iron–carbon nanocomposites with size dependent properties, Adv. Power Technol. 23 (1) (2012) 88–96.
[14] O. Crisan, M. Angelakeris, Th. Kehagias, K. Simeonidis, M. Giersig, N.K. Flevaris, Structure effects on the magnetism of AgCo nanoparticles, Act. Mater. 54 (19) (2006) 5251–5260.
[15] K. Susheel, K. Sarita, K. Amit, H. Yuvaraj, K. Bandan, K. Rajesh, Magnetic polymer nanocomposites for environmental and biomedical application, Colloid. Polym. Sci. 292 (2014) 2025–2052.
[16] R. Bhatia, V. Prasad, Synthesis of multiwall carbon nanotubes by chemical vapor deposition of ferrocene alone, Solid State Commun. 150 (2010) 311–315.
[17] A.G. Osorio, C.P. Bergmann, Effect of surface area of substrates aiming the optimization of carbon nanotube production from ferrocene, Appl. Surf. Sci. 264 (2013) 794–800.
[18] A.G. Osorio, L.G. Pereira, J.B.M. da Cunha, C.P. Bergmann, Controlling the magnetic response of carbon nanotubes filled with iron-containing material, Mater. Res. Bull. 48 (2013) 4168–4173.
[19] Z. Guo, S.E. Lee, H. Kim, S. Park, H. Hahn, A. Karkietai, Fabrication, characterization and microwave properties of polyurethane nanocomposites reinforced with iron oxide and barium titanate nanoparticles, Act. Mater. 57 (1) (2009) 267–277.
[20] J. Zhu, S. Wei, D. Rutman, N. Haldolaarachchige, D.P. Young, Z. Guo, Magnetic polyacrylonitrile-Fe@FeOnanocomposite fibers - electrospinning, stabilization and carbonization, Polymer 52 (13) (2011) 2947–2955.
[21] A. Olhan, K. Singh, A. Chandra, S.K. Dhawan, Microwave absorption behavior of core − shell structured poly(3,4-ethylenedioxy thiophene) − barium ferrite nanocomposites, ACS. Appl. Mater. Interfaces 2 (3) (2010) 927–933.
[22] J. Zhu, S. Wei, J. Ryu, L. Sun, Z. Luo, Z. Guo, Magnetic epoxy resin nanocomposites reinforced with core − shell structured Fe@FeO nanoparticles: fabrication and property analysis, ACS. Appl. Mater. Interface 2 (2010) 2100–2107.
[23] S. Mu, D. Wu, Y. Wang, Z. Wu, X. Yang, W. Yang, Fabrication of nickel oxide nanocomposite layer on a flexible polyimide substrate via ion exchange technique, ACS. Appl. Mater. Interface 2 (1) (2009) 111–118.
[24] T.H. Hsieh, K.S. Ho, X. Bi, Y.K. Han, Z.L. Chen, C.H. Hsu, Y.C. Chang, Synthesis and electromagnetic properties of polyaniline-coated silica/maghemite nanoparticles, Eur. Polym. J. 45 (3) (2009) 613–620.
[25] M. Nisar, C.P. Bergmman, J. Geshev, R. Quijada, G.B. Galland, synthesis and characterization of polypropylene/iron encapsulated carbon nanotubes composites with high magnetic response at room temperature, Polymer 118 (2017) 68–74.
[26] Q. He, T. Yuan, J. Zhu, Z. Luo, N. Haldolaarachchige, L. Sun, A. Khasanov, Y. Li, D.P. Young, S. Wei, Z. Guo, Magnetic high density polyethylene nanocomposites reinforced with in-situ synthesized Fe@FeO core-shell nanoparticles, Polymer 53 (2012) 3642–3652.
[27] F.C. Fim, J.M. Guterres, N.R.S. Basso, G.B. Galland, Polyethylene/graphite nanocomposites obtained by in situ polymerization, J. Polym. Sci. Part A: Polym. Chem. 48 (2010) 692–698.
[28] M.A. Milani, R. Quijada, N.R.S. Basso, A.P. Graebin, G.B. Galland, Influence of the graphite type on the synthesis of polypropylene graphenenanocomposites, Polym. Sci. Part A: Polym. Chem. 50 (2012) 3598–3605.
[29] M.A. Milani, D. González, R. Quijada, N.R.S. Basso, M.L. Cerrada, D.S. Azambuja, G.B. Galland, Polypropylene/grapheme nanosheet nanocomposites by in situ polymerization: synthesis, characterization and fundamental properties, Compos. Sci. Technol. 84 (2013) 1–7.
[30] F.C. Fim, N.R.S. Basso, A.P. Graebin, D.S. Azambuja, G.B. Galland, Thermal, electrical, and mechanical properties of polyethylene-graphene nanocomposites obtained by in situ polymerization, J. Appl. Polym. Sci. 128 (2013) 2630–2637.
[31] M.A. Milani, D. González, R. Quijada, R. Benavente, J. Arranz-Andrés, G.B. Galland, Synthesis, characterization and properties of poly(propylene-1-octene)/graphite nanosheetnanocomposites obtained by in situ polymerization, Polymer 65 (2015) 134–142.
[32] G. Pavoski, T. Maraschin, M.A. Milani, D.S. Azambuja, R. Quijada, C.M. Moura, N.R.S. Basso, G.B. Griselda, Polyethylene/reduced graphite oxide nanocomposites with improved morphology and conductivity, Polymer 81 (2015) 79–86.
[33] M. Nisar, C.P. Bergmman, J. Geshev, R. Quijada, G.B. Galland, An efficient approach to the polyethylene magnetic nanocomposites, Polymer 97 (2016) 131–137.
[34] P.S. Thue, G.S. dos Reis, E.C. Lima, J.M. Sieliechi, G.L. Dotto, A.G.N. Wamba, S.L.P. Dias, F.A. Pavan, Activated carbon obtained from Sapelli wood sawdust by microwave heating for *O-cresol* adsorption, Res. Chem. Intermed. 43 (2) (2017) 1063–1087.
[35] P.S. Thue, E.C. Lima, J.M. Sieliechi, C. Saucier, S.L.P. Dias, J.C.P. Vaghetti, F.S. Rodembusch, F.A. Pavan, Effect of first row transition metal impregnation ratio on physicochemical properties of the micro-wave assisted activated carbon from wood biomass, J. Colloid. Inter. Sci. 486 (2017) 163–175.
[36] C. Saucier, M.A. Adebayo, E.C. Lima, R. Cataluna, P.S. Thue, L.D.T. Prola, M.J. Puchana-Rosero, F.M. Machado, F.A. Pavan, G.L. Dotto, Microwave-assisted activated carbon from cocoa shell as adsorbent for removal of sodium diclofenac and nimesulide from aqueous effluents, J. Hazard. Mater. 289 (2015) 18–27.
[37] S.P. Bao, S.C. Tjong, Mechanical behavior of polypropylene/carbon nanotubes nanocomposites: the effect of loading rate and temperature, Mater. Sci. Eng. A 485 (2008) 506–516.
[38] W. Leelapornpisit, M.T. Ton-That, F. Perrin-Sarazin, K.C. Coel, J. Denault, B. Simard, Effect of carbon nanotubes on the crystallization and properties of polypropylene, J. Polym. Sci. polym. Phys. 43 (2005) 2445–2453.
[39] B. Wunderlich, G. Czornyj, A study of equilibrium melting of polyethylene, Macromolecules 10 (5) (1977) 906–913.
[40] M.A. López Manchado, L. Valentini, J. Biagiotti, J.M. Kenny, Thermal and mechanical properties of single-walled carbon nanotubes–polypropylene composites prepared by melt processing, Carbon 43 (2005) 1499–1505.
[41] T. McNally, P. Potschke, P. Halley, M. Nurphy, D. Martin, S.E.J. Bell, G.P. Brennan, D. Bein, P. Lemoine, J.P. Quinn, Polyethylene multiwalled carbon composites, Polymer 46 (2005) 8222–8232.
[42] M. day, J.D. Cooney, M. Mackinnon, Degradation of contaminated plastic. A kinetic study, Polym. Degrad. Stab. 48 (1995) 341–349.
[43] C. Ou, S. Li, J. Shao, T. Fu, Y. Liu, W. Fan, X. Yang, X. Bi, Effect of transition metal ions on the thermal degradation of chitosan, Cogent Chem. 2 (2016) 1216247.
[44] P.K. Roy, P. Surekha, R. Raman, C. Rajagopal, Investigating the role of metal oxidation state on the degradation behavior of LDPE, Polym. Degrad. Stab. 94 (2009) 1033–1039.
[45] L.M. Gorghiu, S. Jipa, T. Zaharescu, R. Sentnescu, I. Mihalcea, The effect of metal on thermal degradation of polyethylenes, Polym. Degrad. Stab. 84 (2004) 7–11.
[46] M.A. Milani, D. Gonzale, R. Quijada, N.R.S. Basso, M.L. Cerrada, D.S. Azambuja, G.B. Galland, Polypropylene/graphenenanosheetnanocomposites by *in situ* polymerization: synthesis, characterization, and fundamental properties, compos, Sci. Technol. 84 (2013) 1–7.
[47] H. Zou, S. Wu, J. Shen, Polymer/silica nanocomposites: preparation, characterization, properties, and applications, Chem. Rev. 108 (2008) 3893–3957.
[48] S. Kanagaraj, F.R. Varanda, T.V. Zhil' tsova, M.S.A. Oliveira, J.A.O. Simoes, Mechanical properties of high density polyethylene/carbon nanotube composites, Compos. Sci. Technol. 67 (2007) 3071–3077.
[49] C.L. Huang, C.W. Lou, C.F. Lio, C.H. Huang, X.M. Song, J.H. Lin, Polypropylene/graphene and polypropylene/carbon fiber conductive composites: mechanical, crystallization and electromagnetic properties, Appl. Sci. 5 (2015) 1196–1210.
[50] P. Steurer, R. Wissert, R. Thomann, R. Mülhaupt, Functionalized graphenes and thermoplastic nanocomposites based upon expanded graphite oxide, Macromol. Rapid. Commun. 30 (2009) 316–327.
[51] S. Mohanty, S.K. Nayak, Effect of clay exfoliation and organic modification on morphological, dynamic mechanical, and thermal behavior of melt-compounded polyamide-6 nanocomposites, Polym. Compos. 28 (2007) 153–162.
[52] M.E. Achaby, F.E. Arrakhiz, S.b. Vaudreuil, A.K. Qaiss, M. Bousmina, O.F. Fehr, Mechanical, thermal, and rheological properties of graphene-based polypropylene nanocomposites prepared by melt mixing, Polym. Compos. 33 (5) (2012) 733–744.
[53] A. Harres, M. Mikhov, V. Skumryev, A.M.H. de Andrade, J.E. Schmidt, J. Geshev, Criteria for saturated magnetization loop, J. Magn. Magn. Mater. 402 (2016) 76–82.
[54] J. Geshev, Comment on: Exchange bias and vertical shift in $CoFe_2O_4$ nanoparticles, J. Magn. Magn. Mater. 320 (2008) 600–602.
[55] J. Geshev, Comment on "Cluster glass induced exchange biaslike effect in the perovskitecobaltites", Appl. Phys. Lett. 93 (2008) 176101.
[56] J. Geshev, L.G. Pereira, V. Skumryev, Comment on "Exchange Bias Dependence on Interface Spin Alignment in a $Ni_{80}Fe_{20}$/(Ni, Fe)O Thin Film", Phys. Rev. Lett. 100 (2008) 039701.

Annex 5

You are being carbon copied ("cc:'d") on an e-mail "To" "Griselda Barrera Galland" griselda.barrera@ufrgs.br
CC: nisarchem1984@gmail.com, mariasebag@yahoo.com.br, lcarlos66@gmail.com, julian@if.ufrgs.br

Dear Prof. Galland,

You are receiving this e-mail because you have been listed as an author on the following paper:

Your submission entitled "Thermal, mechanical, gas barrier, and magnetic properties of polypropylene/carbon nanotube composites obtained using carbon nanotubes from waste furniture sawdust" has been successfully submitted online and is presently being given full consideration in the Journal of Applied Polymer Science. The manuscript number for your submission is app.20180522.

If you are the corresponding author, you may view your submission by logging in to https://app.editorialmanager.com/ by entering your username (********) and password and selecting the "Author Login" option.

This message has also been sent to all named co-authors listed in the submission process to serve as notification of submission.

Thank you for submitting your work to the journal.

Kind regards,

Journal of Applied Polymer Science Editorial Office

E-mail: appmc@wiley.com
Web: http://www.onlinelibrary.wiley.com/app

Thermal, mechanical, gas barrier, and magnetic properties of polypropylene/carbon nanotube composites obtained using carbon nanotubes from waste furniture sawdust

Muhammad Nisar[1], *Maria da Graça Sebag Bernd*[2], *Luiz C.P. da Silva Filho*[2], *Julian Geshev*[3], *Griselda Barrera Galland*[1*]

[1] Instituto de Química, Universidade Federal do Rio Grande do Sul, Av. Bento Gonçalves 9500, 91501-970 Porto Alegre, RS, Brazil

[2] Laboratório de Ensaios e Modelos Estruturais, Escola de Engenharia Civil, Universidade Federal do Rio Grande do Sul, Av. Bento Gonçalves 9500, 91501-970 Porto Alegre, RS, Brazil

[3]Instituto de Física, Universidade Federal do Rio Grande do Sul, Av. Bento Gonçalves 9500, 91501-970 Porto Alegre, RS, Brazil

Abstract

Magnetic polypropylene (PP) nanocomposites with different loadings of carbon nanotubes with iron encapsulated (CNT-Fe) were fabricated using the melt-mixing method. Carbon nanotubes were synthesized by the pyrolysis of sawdust from the furniture industry. The morphological characterization shows the homogenous dispersion of the filler in the polymer matrix. The addition of 0.5 wt% CNT-Fe results in ferromagnetic behavior in the diamagnetic polymer matrix. The thermal properties were investigated using thermogravimetric analysis and differential scanning calorimetry. The results show an increase in the maximum degradation, crystallization, and melting temperatures of the nanocomposites compared with neat PP. The nanocomposites showed improvement in terms of mechanical and permeability properties. A very significant result of the work is the high remnant magnetization and coercivity values of the nanocomposites at room temperature whereas most of the works in this area show magnetic properties only at very low temperatures.

Key words: Polypropylene, Carbon nanotubes, Magnetic nanocomposites

*Corresponding author. E-mail: griselda.barrera@ufrgs.br (Griselda Barrera Galland)

1. Introduction

Nanofillers, such as exfoliated nanosilicate layers, carbon nanotubes (CNT), and graphite nanoplatelets, can improve or give new properties to a polymer, even at very low loadings. However, the transfer of the exceptional properties of the nanofiller to the polymeric matrix can only be achieved by a homogenous distribution of the nanofiller and a strong interfacial adhesion between the nanofiller and the polymer matrix.[1]

Carbon nanotubes were discovered by Iijima in 1991.[2] Due to their outstanding properties, such as high flexibility, large aspect ratio, and low mass density, CNT have been extensively studied by researchers in various fields, such as chemistry, physics, engineering, and material science. CNT display properties such as lightness, electrical and thermal conductivity, and mechanical strength that make them feasible for use in advanced technological applications, such as tips for atomic force microscopy (AFM),[3]cells for hydrogen storage,[4] nanotransistors,[5] electrodes for electrochemical applications,[6]sensors of biological molecules,[7] and catalysis.[8]Ajayan et al. reported the first polymer nanocomposite using CNT as fillers.[9] The unique combination of mechanical, thermal, and electrical properties makes them excellent candidates to substitute or balance conventional nanofillers in the fabrication of multifunctional polymeric nanocomposites.[10] The techniques for CNT production include electric arc discharge, laser ablation, and chemical vapor deposition (CVD).[11]Among these techniques, CVD methods are the most suitable for large-scale CNT production.[12] Silva Filho et al.[13,14] developed a low-cost CVD method using the pyrolysis of waste wood sawdust as a carbon source. This process has an environmental appeal because it also produces hydrogen. Wood sawdust was mixed with a reducing agent (commercial zinc), calcite (bed material), and a catalyst (ferrocene or Fe/Mo/MgO) arranged in a column reactor and then heated to 750 ºC for 3 h without blowing air. The presence of iron in the CNT makes them suitable for magnetic applications.

Magnetic nanoparticles and nanocomposites have applications in the areas of biomedicine, magnetic resonance imagining, information technology, telecommunication, environmental remediation, and catalysis and are attracting enormous attention in both the scientific and technological fields.[15-18] However, the incorporation of magnetic nanoparticles, such as iron, in the polymer matrix to achieve a uniform distribution of particles is a challenging task. The nanoparticles tend to agglomerate to reduce the energy associated with their high surface area.

Protection strategies have been considered effective tools to chemically stabilize the magnetic constituent by coating with silica or carbon to avoid aggregation.[19]A very interesting strategy is the use of iron nanoparticles contained in CNT synthetized using the CVD method in which ferrocene is used as a catalyst and precursor of synthesis.[20-22] In recent works, we obtained polyethylene-CNT-Fe and polypropylene(PP)-CNT-Fe nanocomposites by *in situ* polymerization with good magnetic properties at room temperature.[23,24] Various techniques have been reported for the preparation of polyolefin nanocomposites, such as solution blending, *in situ* polymerization, and melt mixing.[25-35] The latter is one of the most used techniques due to its simplicity, high yield and fast production, easy operation, and the fact that it does not need a hazardous solvent that could cause health problems.[36]

In the present work, we focus on the production of low-cost PP/CNT nanocomposites using an eco-friendly process developed by Silva Filho et al.[13,14] that produces CNT from a low-cost source, such as wood sawdust from furniture industry waste. PP/CNT nanocomposites were obtained using the melt-mixing technique and commercial PP. The effect of this nanofiller on the thermal, mechanical, gas barrier, and magnetic properties of the isotactic PP (iPP) matrix was studied.

2. Experimental

Commercially available iPP (PP2621) with a melt flow rate of 26 g/10 min (2.16 kg/230 ^{0}C) (Norm ASTM D-1238/95), Mw= 195 kg/mol, Mn = 71 kg/mol, PDI= 2.72, and a melting point of 160^{o}C and provided by Petroquim S.A. (Hualpén, Chile) was used as a polymer matrix. Irganox 1010 was used as an antioxidant agent during the composite preparation.

2.1 Carbon nanotubes synthesis

CNT were synthesized using a reported method [13] that used sawdust from the furniture industry as raw material. Commercially available zinc (Zn) was used as a reducing agent. Ferrocene ($Fe(C_2H_5)_2$) was used as a catalyst of synthesis. The detailed method of synthesis and characterization of the carbon nanotubes is given in Refs. 13 and 14.

2.2 Melt compounding

For the preparation of composites, a melt-mixer, Brabender Plasti-Corder (Diusburg, Germany), operating at 190^{o}C and at a speed of 110 rpm was used. Calculated amounts of iPP and CNT and a small amount (~0.005 g) of Irganox1010 as an antioxidant were used per mixing; the total amount used was approximately 30 g. The amount of the filler varied from 0 wt% to 20 wt%. The iPP was first mixed with the antioxidant, and subsequently half the amount of the polymer (~13 g) was added to the mixer operating at 110 rpm. After 2 min, the filler was added to the melted polymer for 3 min. In the last step, the rest of the polymer pellets were added and the speed of the mixer was kept constant at 110 rpm for 10 min. The total mixing time was approximately 15 min.

3. Characterization

The CNT nanoparticle morphology was investigated using transmission electron microscopy (TEM) (JEOL (JEM-2010)) operating at 200 kV and scanning electron microscopy (SEM) (JEOL JSM 6500F). The nanocomposites (iPP/CNT) were also analyzed using TEM (JEOL 1011) operating at 120 kV. Samples were prepared from ultrathin films (~50 nm thick) cut under cryogenic conditions with a Leica Ultracut UCT microtome at -70 °C and placed on a grid. SEM (Phillips XL30) operating at 20 kV was used to examine the nanocomposites. Samples were deposited on an aluminum stub and coated with gold.

The CNT magnetic properties and nanocomposites were investigated using an EZ9MicroSense vibrating sample magnetometer (VSM) at room temperature with a magnetic field (H) cycled between–20 kOe and +20 kOe. Oxygen permeability was measured using L100-5000 permeability equipment manufactured in the United Kingdom connected to a vacuum pump and a cooling and heating bath to control the temperature. The tolerance in percentage to equilibrium was 2, and the oxygen pressure was maintained at 5 bar. Three measurements were obtained for each sample, and the results were the average of these three measurements.

Thermal properties were measured, using differential scanning calorimetry (DSC), with a Perkin–Elmer differential calorimeter (model DSC Q20). The temperature was increased from 0 ^{o}C to 180 ^{o}C with a heat rate of 10 ^{o}C/min. The second scan was used to determine the melting temperature T_m, and the percent crystallinities were calculated from the enthalpy of fusion data obtained from the DSC curves (207 J/g was used for PP 100% crystalline). A thermogravimetric

analysis (TGA) performed with a SDT Q600 thermal analyzer Q20 (TA Instruments, New Castle, USA) was used to study the thermal stability of the nanocomposites with respect to the neat polymer. The samples were scanned in the range of 0 ^{o}C to 800 ^{o}C at a scanning rate of 20^{o}C/min.

The mechanical properties were measured using an HP model D-500 dynamometer according to ASTMD638-10 at ~25^{o}C. Five samples were tested for each wt% of nanocomposites, and the results were the average value of these five measurements (typical deviation ca.5%). The bone-shaped samples have an overall length of 120 mm with a distance between the two grips of 80 mm, a width of 11.5 mm, and a thickness of 1mm at a cross head. A rate of 50 mm/min was tested.

4. Results and Discussion

4.1 Thermal Analysis:

The thermal behavior of the polymers with the CNT incorporation was investigated using DSC and TGA. Table 1 gives the results of a number of the nanocomposites with the filler ranging from 0 wt% to 20 wt%. The amount of filler in wt% was determined from the amount added to the mixture and the yield of polymer obtained and also by using the TGA residue. Table 1 shows that most of the percentages are quite close, showing good homogeneity of the samples except two samples, 5 wt% and 20 wt%, where some agglomeration may take place. The melting temperature (*Tm*) of the nanocomposites with more than 3 wt% of filler increased from 163 ^{o}C to 165 ^{o}C, showing a slight increase of 1 ^{o}C to 2 ^{o}C. The CNTs are well known to convey intense changes to the crystallization behaviour of semi-crystalline polymers. They do not only influence the crystalline morphology, but they usual promote a fibrillar rather than a spherulitic structure.[37] Table 1 also shows that the crystallization temperature (T_c) changed from 115 ^{o}C to 123 ^{o}C, having a maximum increase of 8 ^{o}C compared to neat PP. Generally, the T_c of PP/CNT nanocomposites shifts relative to higher temperatures compared to the neat PP, which indicates that CNT act as nucleating agents for PP.[36] Leelapornpisit et al.[38]and Valentini et al.[39] reported a similar nucleating effect for PP/SWNT composites. Park et al.[40, 41] also reported the enhancement of the nucleation with the addition of a greater amount of multi-walled CNT during the crystallization process. High crystallization temperatures allow a reduction of the processing

cycle, thus increasing the production rate.[42] The degree of crystallinity of PP first decreases with the incorporation of a small amount of filler, ~ 0.5 wt%; however, an increase of almost 4.3% was observed when the filler was increased to ~3.0 wt%.

Table 1: Results of the thermal properties of polypropylene nanocomposites with different amounts of filler

Samples	Filler[1] (wt%)	Filler[2] (wt%)	T_c (ºC)	T_m (ºC)	Xc (%)	T_{onset} (ºC)	T_{max} (ºC)
PP	0	0	115	163	69	427	470
PP/CNT_1	0.5	0.6	116	162	64	429	474
PP/CNT_2	1.0	0.8	117	162	70	430	474
PP/CNT_3	2.0	2.4	118	162	70	435	476
PP/CNT_4	3.0	3.1	120	164	72	438	469
PP/CNT_5	5.0	2.9	120	164	72	436	464
PP/CNT_6	10	9.2	121	165	68	440	481
PP/CNT_7	20	12.1	123	165	72	443	471

[1] Calculated from yield; [2] Calculated from TGA residue.

The increase in the thermal stability of PP is also very important for industrial applications. TGA was used to investigate the thermal degradation behavior of neat PP and PP/CNT nanocomposites. Table 1 shows that with the presence of the filler the maximum (T_{max}) and the initial (T_{onset}) degradation temperatures increase 11 °C and 16 °C, respectively. Other researchers have also reported a similar increase in the PP-MWCNT thermal stability, PP-alkylated graphene oxide, and alkylated one-dimensional CNT nanocomposites.[43,44] The decomposition of PP involves free radical chain reactions; a number of free radicals may easily be trapped by CNT, thus increasing the thermal stability.[45] Similarly, other researcher reported the radical trapping by the iron present within the clay, enhance the thermal stability of the polystyrene (PS) in PS/clay

nanocomposites.[46] The CNTs used in this work contain iron that may have the same radical trapping behavior, however since the iron particles are inside the CNTs, their contact with the PP chain will be minimum and will not affect the stability of the polymer matrix until the wall of the nanotubes degrade. If this is the case, the role of the iron inside the CNTs might not be important for the thermal stability of the PP/CNTs nanocomposites so the thermal stability can be attributed only to the carbon part of the filler. Anyway, the role of the iron particles within the CNTs on the thermal degradation of PP/CNTs nanocomposites will need further investigation.[47] The higher the CNT amount, the higher the decomposition temperature, as shown in Table 1. The enhancement of the nanocomposites thermal properties produced by the CNT generated from sawdust is similar to that obtained using CNT from other carbon sources but with the advantage of a lower-cost procedure and environmental appeal.

4.2 Morphology of the nanocomposites:

Figure 1 shows scanning electron micrographs of the fractured surface of pristine PP and its nanocomposites with different CNT wt%. The sample was first cooled in liquid nitrogen and then broken without deformation. The CNT seem to be well distributed in the PP matrix, and no agglomerates were observed. When the CNT concentration increased, a more layered structure of the polymer matrix appeared which shows a strong interaction between the filler and the polymer matrix.

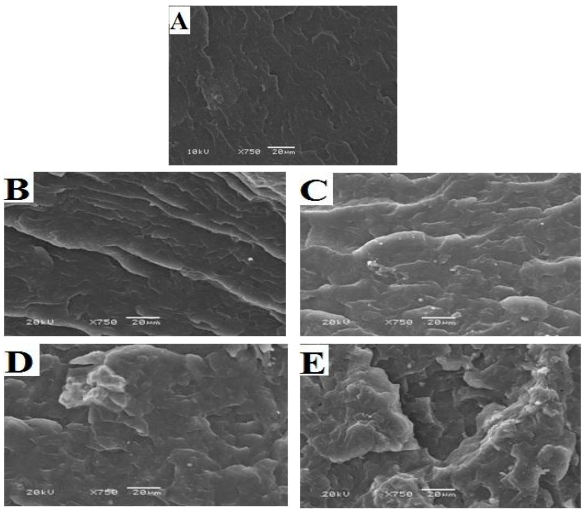

Figure 1. SEM images (a) neat PP, (b), (c), (d), and (e) 1, 5, 10, and 20 wt% of PP/CNT nanocomposites

Figure 2 shows the TEM images of the pristine CNT and PP/CNT nanocomposites at different magnifications. The nanotubes are quite large at ~100–200 nm and short at ~0.5–2 μm. The black spots inside the tube are metallic particles from the catalyst, mainly iron. The micrographs reveal homogenous distribution of the filler particles within the polymer matrix, and no aggregation was observed even at filler loadings as high as 10 wt%. However, a higher CNT amount was observed in the PP matrix as the filler concentration was increased.

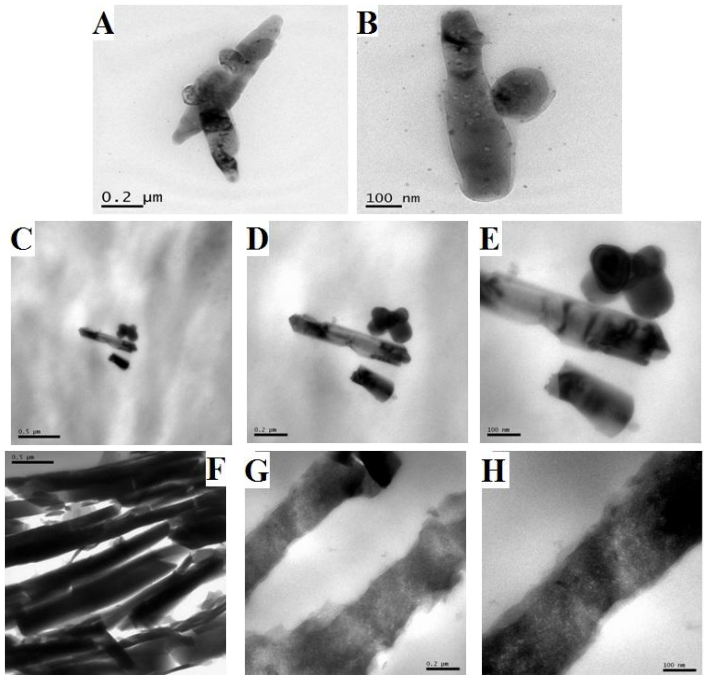

Figure 2. TEM CNT micrographs (A), (B); PP nanocomposites with 0.5 wt% (C), (D), (E); and 10 wt% (F), (G), (H) of CNT at different magnifications

4.3 Mechanical properties:

Generally the mechanical properties of the polymer matrix are affected by various factors, for instance, the dispersion of the filler, filler matrix adhesion and the aspect ratio of the filler. Figure 3 shows the results of the effect of the carbon-based filler on the Young's modulus and elongation at the break. With the increase in the amount of filler, an increase in the Young's modulus up to 25% (~376 MPa) was observed using 10 wt% of the filler, and an increase of 33 % (~491 MPa) was observed using 20 wt% of the filler (Fig. 3a). These results reflect the

enhancement of the materials' stiffness as a result of the filler loading.[48] This improvement is attributed to the excellent interface between filler and polymer matrix and the uniform dispersion of the filler; the great surface volume ratio of the filler enable good load transfer to the polymer.[49] Similar increasing tendencies were shown by Huang et al.[50] and Steurer et al.[51] for carbon-based filler nanocomposites. Parashantha et al.[52] reported an increase of up to 40% in the modulus using masterbatch-based multi-walled CNT-filled PP nanocomposites.

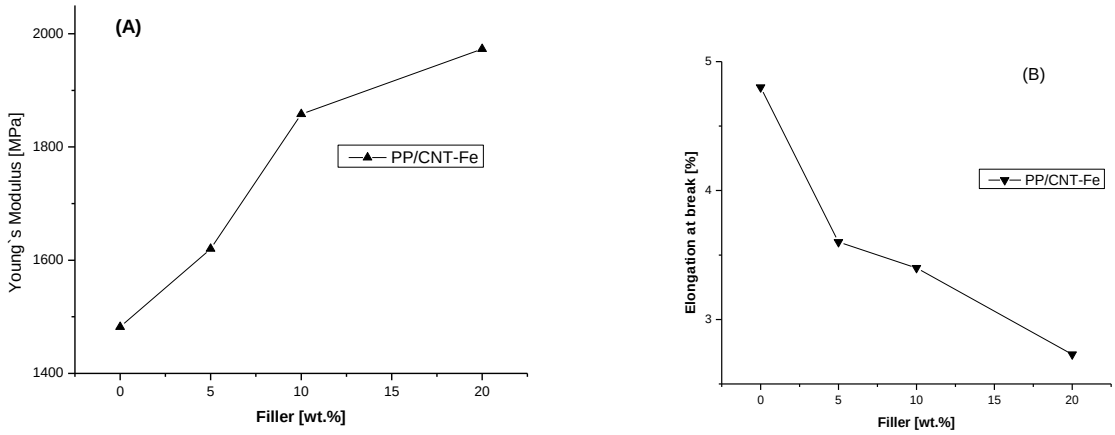

Figure 3(a) Variation in the Young's modulus and (b) elongation at the break with the increase in the concentration of filler.

It is clear from Fig.3 (b) that with the increase in the CNT concentration a decrease in elongation of ~29% and ~42% occurs at the break for 10 wt% and 20 wt% of the filler, respectively. The decrease in the elongation of the composites is because the nanoparticles strongly restrict the movement of the polymer chains, thus preventing them from stretching when they are under stress.[48,53]

4.4 Oxygen barrier property:

PP is one of the most commonly used packaging materials. Enhancing the barrier properties of plastic can be accomplished in two ways, either by adding a layer of barrier material or by mixing the barrier material into the polymer matrix, as in a nanocomposite.[54] Figure 4 and Table 2 show the effect of the filler percentage on the oxygen permeability at 23 °C for neat PP films

and their nanocomposites having a thickness of approximately 0.25 mm. It is clear from these results that with the addition of the filler the permeability of oxygen gradually decreases up to 50% with ~3.0 wt% CNT-Fe addition compared to neat PP. The drop in the oxygen permeability of these nanocomposites compared to the neat PP shows that the CNT make the permeation of gas through the PP matrix difficult.[55] PP contains both amorphous and crystalline regions, the permeation of the gas takes place only in the amorphous region, the gas permeability in the crystalline region is considered negligible. Our DSC results showed that the percentage of crystallinity increases with the incorporation of the filler which can help in the decrease of permeability. On the other hand, nanocomposites are multiphase systems in which the existence of different phases such as crystalline, inorganic and amorphous cause complex phenomena on the procedure of gas permeation. The presence of the filler CNT-Fe, which is considered impermeable, introduces a more tortuous path for the gas molecules to pass though the polymer. [56] The reduction in the penetrability is clear from the experimental results and it can be considered very significant compared with other works. Pannirselvamet al.[57] reported a 30% reduction in oxygen permeability using 5 Phr clay for PP–polyether treated clay composites. Similarly, Sadasivuni et al.[58] showed a decrease of 26% in oxygen permeability for poly(isobutylene-co-isoprene)/graphene nanocomposites using 5.0 Phr of the filler. In contrast, for a higher amount of the filler, 5.0 wt%, the permeability of the nanocomposites increases approximately 80%, which could be a consequence of some agglomeration of the filler.

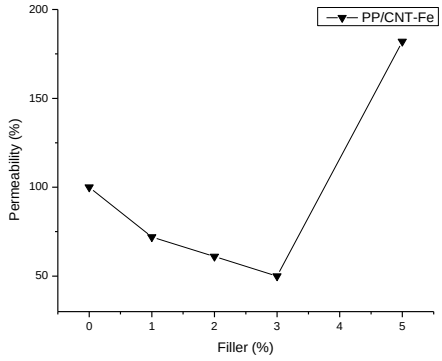

Figure 4. Effect of filler (%) on the permeability of oxygen

4.5 Magnetic properties:

The room temperature magnetization (M) versus H hysteresis loops of the nanocomposites with different amounts of CNT-Fe are plotted in Fig. 5 [neat PP (not shown) evidences only a diamagnetic signal]. Remarkably, the characteristics of all $M(H)$ curves normalized to the respective saturation magnetization values, M_S, are practically the same no matter the amount of filler content; the loops are typical for systems that consist of both ferromagnetic and super paramagnetic magnetic parts. The differences in the loops' shapes are almost negligible and are only detectable with a very thorough inspection of the intermediate field region; see the bottom panels of Fig. 5.

Table 2 gives the values of the remnant magnetization/saturation magnetization ratio (M_R/M_S), the coercivity (H_C), and the saturation field (H_S). The latter refers to the value of H above which an $M(H)$ has effectively attained saturation, that is, M becomes a single-valued function of H, and the magnetization processes take place by reversible rotations only.[59] To avoid possible minor-loop effects,[59-62] we assure that the value of the maximum magnetic field used is sufficient for effective saturation; see the inset in the top panel of Fig. 5. To determine whether saturation is achieved, we employed one of the criteria recently proposed by Harres et al.[59] by analyzing the first and, when possible, the second derivatives of M with respect to H, from which procedure we were able to determine the H_S values given in Table 2.

Table 2: Values of the normalized remnant magnetization (M_R/M_S), coercivity (H_C), saturation field (H_S), and oxygen permeability of the polypropylene nanocomposites with different amounts of CNT-Fe at 23 ^oC

Samples	Filler (%)	M_R/M_S	H_C (Oe)	H_S (kOe)	Oxygen permeability 0% [a]RH (mL/m^2 ×24h)
PP	0	0	0	0	52.0
PP/CNT$_1$	0.5	0.16±0.01	162±2	3.0±0.3	--
PP/CNT$_2$	1	0.15±0.01	152±2	3.2±0.3	40.0
PP/CNT$_3$	2	0.15±0.01	155±2	3.4±0.3	32.0
PP/CNT$_4$	3	0.15±0.01	154±2	3.5±0.3	26.0
PP/CNT$_5$	5	0.16±0.01	157±2	3.8±0.3	95.0
PP/CNT$_6$	10	0.15±0.01	154±2	5.6±0.3	--
PP/CNT$_7$	20	0.14±0.01	155±2	6.2±0.3	--
CNT-Fe	100	0.14±0.01	150±2	3.6±0.3	--

[a]Relative humidity

Notably, whereas all samples present almost identical M_R/M_S and H_C values, those of H_S show up to a twofold difference, varying from approximately 3.0 kOe for low concentrations of the filler to 6.2 kOe for the samples with the highest filler content. Such a difference cannot be attributed to inter-particle interactions because these would result in significant variations of M_R/M_S and H_C (not observed here). A plausible mechanism that could lead to the only effect observed, the H_S change, is an increase in the standard deviation (σ) value of the anisotropy field distribution. We performed numerical simulations[63, 64] of $M(H)$ (not presented here) using anisotropy fields with Gaussian distributions with different values of σ, which confirmed the above hypothesis, being the only effect that resulted in an increase of H_S with the increase of σ. In our real system, the increased σ for the samples with 10 wt% and 20 wt% filler could be related to the previously

discussed increase of the elastic modulus caused by the increase of the filler content. This would result in an enhancement in the material's stiffness that in turn could increase the anisotropy field or at least widen its distribution. The importance of the PP matrix for the enhancement of σ is further corroborated by the low σ-value of the pure CNT-Fe sample, practically equal to those of the samples with low filler content.

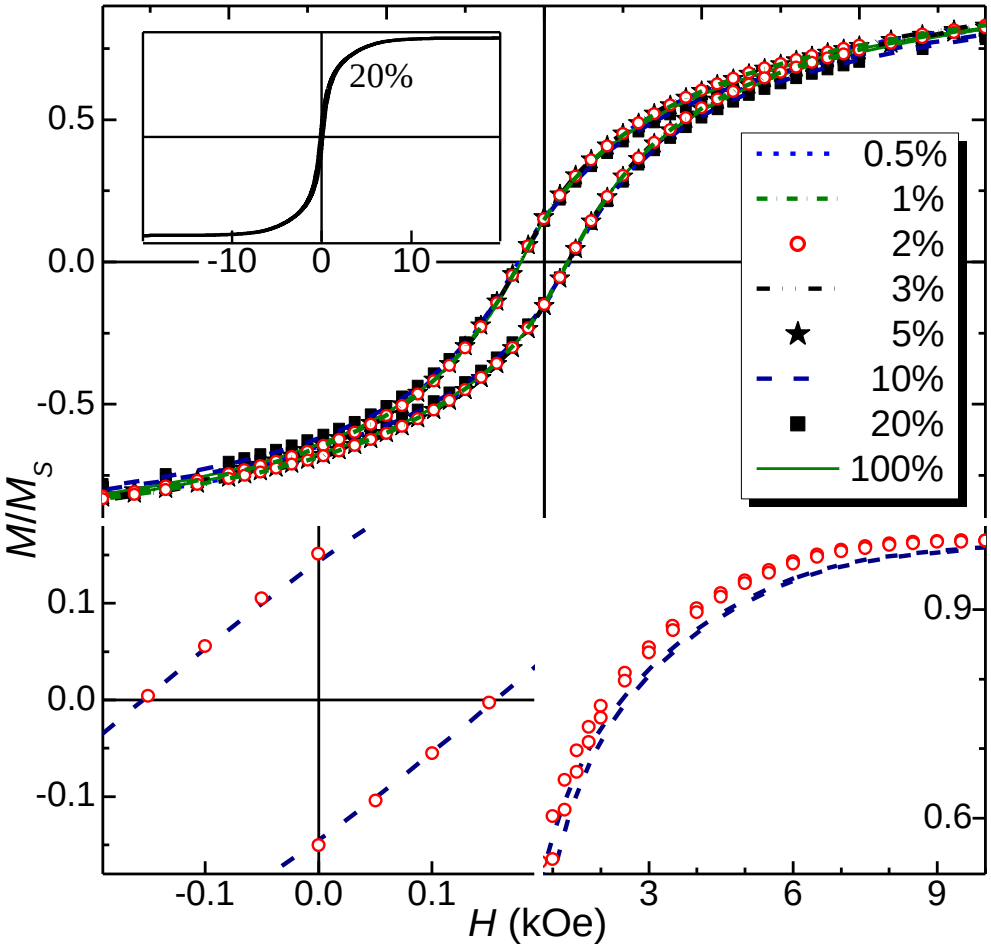

Figure 5. Top: room temperature magnetization hysteresis loops of the polypropylene nanocomposites with different amounts of CNT-Fe; the inset exemplifies the whole-field-range curve of the sample with (20 wt% filler). The low and the intermediate field regions of the samples with 2 wt% and 10wt% filler (two of those that show the most-significant difference) are given in the left and the right bottom panels, respectively.

5. Conclusion

Low-cost nanocomposites made from PP and CNT produced from wood sawdust from the furniture industry were obtained. These materials have improved thermal stability and higher crystallization temperatures than PP. The Young's modulus increased up to 33% with the addition of 20% filler, and oxygen permeability was reduced up to 50% with the use of 3 wt% of CNT. The CNT obtained were shown to have magnetic properties due to the use of a catalyst containing iron. The introduction of magnetic properties is of interest in designing new polymeric devices for different applications. The results show that the nanocomposites have both ferromagnetic and super paramagnetic parts with a very low percentage of filler at room temperature. This is a very remarkable result given that these nanocomposites show high coercivities at room temperature, whereas most research in this area has reported materials with high magnetization only at very low temperatures. The protection of the iron nanoparticles by CNT and consequently good dispersion in the polymer matrix may explain this result.

Conflicts of interest

There are no conflicts of interest to declare.

Acknowledgments

The authors are grateful to the TWAS-CNPq for the fellowship to Muhammad Nisar and to CNPq for grant 302902/2013-9. We thank Professor Raúl Quijada from the University of Chile for the support. We also thank CME and LRNANO from UFRGS for the microscopy analysis. The magnetic characterization was performed in collaboration with the Laboratory of Magnetism at IF-UFRGS.

Reference

1. Song, P.; Cao, Z.; Cai, Y.; Zhao, L.; Fang, Z.; Fu, S. *Polymer* **2011**, 52, 4001.
2. Iijima, S. *Nature* **1991**, 354, 56.
3. Hafner, J. H.; Cheung, C.-L.: Woolley A. T.; Lieber, C. M. *Progr. Biophys. Mol. Biol*. **2001,** 77, 73.
4. Darkrim, F. L. ; Malbrunot, P.; Tartaglia, G. P. *Int. J. Hydrogen Energy*. **2002,** 27, 193.
5. Baughman, R. H.; Zhakidov, A. A.; Heer, W. A. *Science* **2002,** 297,787.

6. Pedano, M. L.; Rivas, G. A. *Electrochem. Commun*. **2004,** 6, 10.
7. Lin, Y.; Lu, F.; Tu, Y.; Ren, Z. *Nanoletters* **2004,** 4, 191.
8. Serp, P.; Corrias, M.; Kalck, P. *Appl. Cat. A.* ***2003,*** 253, 337.
9. Ajayan, P. M.; Stephan, O.; Colliex, C.; Trauth, D. *Science* **1994,** 265, 1212.
10. Moniruzzaman, M. ; Karen, I. W. *Macromolecules* **2006**, *39*, 5194.
11. Ramesh, P.; Okazaki, T.; Sugai, T.; Kimura, J.; Kishi, N.; Sato, K.; Ozeki, Y.; Shinohara, H. *Chemical physics letteres* **2006,** 418, 408.
12. Mubarak, N.M.; Abdullah, E.C.; Jayakumar, N.S.; Sahu, J.N. *J. Ind. Eng. Chem.* **2014,** 20, 1186.
13. Bernd, G. S.; Braganca, S. R.; Heck, N.; Filho L.C.P.S. *J. Mater. Res. Technol*. **2017,** https://doi.org/10.1016/j.jmrt.2016.11.003
14. Filho L.C.P.S.; Heck, N.C.; Bernd, M.G.S Patente No. BR 10, 2012,022053-9 A2 [http://hdl.handle.net/10183/107424].
15. Coey, J.M.D. *J. Magn. Magn. Mater.* **1999,** 196–197, 1.
16. Shull, R.D.; Bennett, L.H. *Nanostruct Mater.* **1992,** 1, 83.
17. Lu, A-H.; Schmidt, W.; Matoussevitch, N.; Bonnemann, H.B.; Spliethoff, B.; Tesche, B.; Bill, E.; Kiefer, W. ; Schuth, F. *Angew. Chem. Int. Ed*. **2004,** 43, 4303.
18. Zhu, J.; Wei, S.; Chen, M.; Gu, H.; Rapole, S. B.; Pallavkar, S.; Ho, T.C.; Hopper, J. Guo, Z. *Adv. Powder. Technol*. **2013,** 24,459.
19. Susheel, K.: Sarita, K.; Amit, K.; Yuvaraj, H.; Bandan, K.; Rajesh, K. Colloid. *Polym. Sci.* **2014,** 292, 2025.
20. Bhatia, R.; Prasad, V. *Solid State Commun.* **2010,** 150, 311.
21. Osorio, A.G.; Bergmann, C.P. *Appl. Surf. Sci,* **2013,** 264,794.
22. Osorio, A.G.; Pereira, L.G.; Cunha, J.B.M.; Bergmann, C.P. *Mater. Res. Bull.* **2013,** 48, 4168.
23. Nisar, M.; Bergmman, C.P.; Geshev, J.; Quijada, R.; Galland, G.B. *Polymer* **2016,** 97, 31.
24. Nisar, M.; Bergmman, C.P.; Geshev, J.; Quijada, R.; Galland, G.B. *Polymer* **2017,** 118, 68.
25. Andrews, R.; Weisenberger, M.C. *Curr. Opin. Solid State Mater. Sci.* **2004,** 8, 31 .
26. Xie, X.L.; Mai, Y.W. ; Zhou, X.P. *Mater. Sci. Eng.* **2005,** 49, 89.

27. Habi, L. A. ; Jafari, S.H.; Khonakdar, H.A. ; Baghaei, B. *J. Polym. Res.* **2011,** 18, 197.
28. Saeed, K. ; Park, S.Y. *J. Polym. Res.* **2010,** 17, 535.
29. Yasin, T. ; Nisar, M. ; Shafiq, M. ; Nho, Y. ; Ahmad, R. *Polym. Compos*. **2013,** 34(3), 408.
30. Fim, F.C. ; Guterres, J.M. ; Basso, N.R.S. ; Galland, G.B. *J. Polym. Sci. Part A: Polym. Chem.* **2010,** 48, 692.
31. Milani, M.A. ; Quijada, R. ; Basso, N.R.S. ; Graebin, A.P. ; Galland, G.B. *Polym. Sci. Part A: Polym. Chem.*, **2012**, 50**,** 3598.
32. Milani, M.A.; González, D.; Quijada, R. ; Basso, N.R.S. ; Cerrada, M.L. ; Azambuja, D.S. ; Galland, G.B. ; *Compos. Sci. Technol*. **2013,** 84, 1.
33. Fim, F.C. ; Basso, N.R.S.; Graebin, A.P.; Azambuja, D.S.; Galland, G.B. *J. Appl. Polym. Sci.* **2013,** 128, 2630.
34. Milani, M.A.; González, D.; Quijada, R.: Benavente, R.; Arranz-Andrés, J. ; Galland, G.B.; *Polymer* **2015,** 65, 134.
35. Pavoski, G.; Maraschin, T.; Milani, M.A.; Azambuja, D.S.; Quijada, R. ; Moura, C.M. ; Basso, N.R.S. ; Galland, G.B. *Polymer* **2015,** 81, 79.
36. Bao, S. P.; Tjong, S.C. *Mater. Sci. Eng. A.* **2008,** 485, 506.
37. Jeon, K.; Lumata, L.; Tokumoto, T.; Steven, E.; Brooks, J.; Alamo, R. G. *Polymer* **2007**, 48, 4751.
38. Leelapornpisit, W.; Ton-That, M.T.; Perrin-Sarazin, F.; Cole, K.C.; Denault, J.; Simard, B. *J. Polym. Sci. Polym. Phys*. **2005,** 43, 2445.
39. Valentini, L.; Biagiotti, J.; Kenny, J.M.; Manchado, M.A.L. *J. Appl. Polym. Sci*. **2003,** 89, 2657.
40. Seo, M.K.; Lee, J.R.; Park, S.J. *Mater. Sci. Eng. A.***2005,** 404, 79.
41. Seo, M.K.; Park, S.J. *Mater. Sci. Eng. A.* **2004,** 289, 368.
42. Gopakumar, T.G.; Pagé, D.J.Y.S. *Polym. Eng. Sci.* **2004,** 44, 1162.
43. Ganβ, M.; Satapathy, B.K.; Thungs, M.; Weidisch, R.; Potschke, P.; Jehnichen, D. *Acta Materialia*. **2008,** 56, 2247.
44. Yun, Y.S.; Bae, Y.H.; kim, D.H.; Lee, J.Y.; Chin, I.; jin, H. *Carbon* **2011,** 49, 3553.
45. . Zhang, J.; Hereid, M.; Hagen, D.; Bakirtzis, M. A.; Delichatsios, A.; Fina, A.; Castrovinci, G.; Camino, F.; Samyn, Bourbigot, S. *Fire Safety J.* **2009,** 44(4), 504.

46. Zhu, J.; Uhl, F. M.; Morgan, A. B.; Wilkie, C. A.; *Chem. Mater*. **2001,** 13, 4649.
47. Kashinagi, T.; Grulke, E.; Hilding, J.; Harris, R.; Awad, W.; Dougas, *J. Macromol. Rapid. Commun.* **2002,** 23, 761.
48. Zou, H.; Wu, S.; Shen, J. *Chem. Rev.* **2008,** 108, 3893.
49. Kanagaraj, S.; Varanda, F. R.; Zhiltsova, T. V.; Oliveira, M. S.A.; Simoes, J. A.O. *Compos. Sci. Technol.* **2007,** 67, 3071.
50. Huang, C. L.; Lou, C. W.; Lio, C. F.; Huang, C. H.; Song, X, M.; Lin, J H. *Appl. Sci.* **2015,** 5, 1196.
51. Steurer, P.; Wissert, R.; R. Thomann, and R. Mülhaupt, *Macromol. Rapid Commun.* **2009**, 30, 316.
52. Parshantha, K.; Soulestin, J.; Lacrampe, M.F.; Krawcrak, P.; Dupin, G.; Claes, M. *Compos. Sci. Technol.* **2009,** 69, 1756.
53. Mohanty, S.; Nayak, S.K. *Polym. Compos.* **2007,** 28, 153.
54. Lange, B. J.; Wyser, Y. *Packag. Technol. Sci.***2003,** 16, 149.
55. Zehetmeyer, G.; Scheibel, J. M.; Soares, R. M. D.; Weibel, D. E.; Oviedo, M. A. S.; Oliveira, R. V. B. *Polym. Bull*. **2013,** 70, 2181.
56. Vladimirov, V.; Betchev, C.; Vassiliou, A.; Papageorgiou, G.; Bikiaris, D. *Compos. Sci. Technol*. **2006,** 66, 2935.
57. Pannirselvam, M.; Genovese, A.; Jollands, M.C.; Bhattacharya, S.N.; Shanks, R.A. *Express. Polym. Lett.* **2008,** 2(6), 429.
58. Sadasivuni, K. K.; Saiter, A.; Gautier, N.; Thomas, S.; Grohens, Y. *Colloid and Polymer Science*. **2013**, *291* (7), 1729.
59. Harres, A.; Mikhov, M.; Skumryev, V.; Andrade, A. M. H.; Schmidt, J. E.; Geshev, J. *J. Magn. Magn. Mater*. **2016,** 402, 76.
60. Geshev, J. *J. Magn. Magn. Mater*. **2008,** 320, 600.
61. Geshev, J. *J. Appl. Phys. Lett.* 2008, 93, 176101.
62. Geshev, J.; Pereira, L. G.; Skumryev, V. *Phys. Rev. Lett.* **2008,** 100, 039701.
63. Masheva, V.: Geshev, J.; Mikhov, M. *J. Magn. Magn. Mater*. **1994,** 137(3), 350.
64. Harres, A.; Geshev, J. *J. Phys. Condens, Matter*. **2012,** 24, 326004.

Annex 6

You are being blind carbon copied ("bcc:'d") on an e-mail "To" "Griselda Barrera Galland" griselda.barrera@ufrgs.br

Dear Prof. Galland,

Your submission entitled "Electrically conductive polypropylene/rGO-CNT-Fe magnetic nanocomposites with improved mechanical, thermal and barrier properties" has been received by journal Macromolecular Materials and Engineering. The manuscript number for your submission is mame.201800128.

To view your submission, please login to https://mme-journal.editorialmanager.com/ by entering your username (********) and password and selecting the "Author Login" option.

This message has been sent to all named co-authors listed in the submission process to serve as notification of submission.

Thank you for submitting your work to the journal.

Kind regards,

Editorial Office

Macromolecular Materials and Engineering

E-mail: macromol@wiley-vch.de

Phone: +49 6201-606-581

http://www.mme-journal.de

Electrically conductive polypropylene/rGO-CNT-Fe magnetic nanocomposites with improved mechanical, thermal and barrier properties

Muhammad Nisar[1], Maria da Graça Sebag Bernd[2], Luiz C.P. da Silva Filho[2], Julian Geshev[3], Nara R. de Souza Basso[4], Griselda Barrera Galland*[1]

[1]Instituto de Química, Universidade Federal do Rio Grande do Sul, Av. Bento Gonçalves 9500, 91501-970 Porto Alegre, RS, Brazil

[2]Laboratório de Ensaios e Modelos Estruturais, Escola de Engenharia Civil, Universidade Federal do Rio Grande do Sul, Av. Bento Gonçalves 9500, 91501-970 Porto Alegre, RS, Brazil

[3]Instituto de Física, Universidade Federal do Rio Grande do Sul, Av. Bento Gonçalves 9500, 91501-970 Porto Alegre, RS, Brazil

[4]Faculdade de Química, Pontifícia Universidade Católica do Rio Grande do Sul, Av. Ipiranga 6681, 90619-900 Porto Alegre, RS, Brazil

Abstract

The magnetic and conducting properties of polypropylene/reduce graphene oxide-carbon nanotubes contains iron (PP/rGO-CNT-Fe) nanocomposites prepared by melt mixing were studied. Carbon nanotubes containing iron (CNT-Fe) were synthesized by the pyrolysis of sawdust from the furniture industry, and reduced graphene oxide (rGO) was produced from graphite flakes. The combination of these two nanostructured materials was used to produce magnetic and conducting properties in a diamagnetic and insulating polypropylene (PP) matrix, with the addition of a small amount of filler. A constant and minute amount of CNT-Fe was sufficient to introduce magnetic characteristics in the PP matrix. A variable amount of rGO was used and the percolation threshold was achieved with the use of only 2.1 wt.% of rGO. All samples reached magnetic saturation at ~4.2 kOe, with an identical

coercivity of 150 Oe and normalized remnant magnetization of 0.14. Scanning and transmission electron microscopies evidence homogenous dispersion of the filler. Thermogravimetric and differential scanning calorimetry analyses show enhancements in the maximum degradation, melting and crystallization temperatures, as well as in the crystallinity percentage. The nanocomposites show better mechanical and barrier properties compared to the neat polymer. The novelty of the work is the production of a low-cost thermoplastic with both magnetic and conducting properties at room temperature.

Key words: Carbon nanotubes, Magnetic Properties, Electrical conductivity, Polypropylene nanocomposites.

*Corresponding author: griselda.barrera@ufrgs.br

1. INTRODUCTION

Nanotechnology has rapidly developed in recent years. Significant research has been focused on the development of polymer nanocomposites with new properties because of their potential applications.[1,2] The increasing attention on nanoparticle (NP) materials is because of their physical properties that are significantly altered from the corresponding bulk materials.[3] Polymer nanocomposites with advanced thermal stability, flame retardancy, mechanical properties, electrical conductivity, magnetic properties and/or chemical resistance, depending on the type of filler used, have increasing scientific significance.[4-6] There is an incredible enrichment in the properties of polymer nanocomposites with the incorporation of a minute amount of filler, for instance, carbon nanotubes (CNTs), exfoliated nanosilicate layers and graphite nanoplatelets. However, a well-built interfacial adhesion within the polymer matrix and a nanosized filler with uniform dispersion of the filler in the polymer matrix are necessary for the efficient performance of these fillers.[7]

CNTs were first reported by Iijima in 1991.[8] In 1994, Ajayan *et al*.[9] reported the first polymeric material using CNTs as a nanofiller. The outstanding combination of the mechanical, electrical and thermal properties, high flexibility and low mass density of the CNTs make them exceptional candidates to replace the usual nanofillers in a variety of fields of study, such as chemistry, physics, materials science and engineering.[10-12] The average Young's modulus of isolated CNTs attains 18 TPa.[13] CNTs consisting of single graphite sheets are referred to as single-walled carbon nanotubes, whereas those with multiple graphite sheets are called multiwalled carbon nanotubes.[14] In the last two decades, the reinforcing performance of CNTs in polymer matrices has also attracted significant interest.[15] Two key aspects must be taken into consideration while using CNTs as fillers to transfer the exceptional properties of the CNTs to the polymer, i.e., the homogenous dispersion of the CNTs and the presence of a degree of interaction between the polymer chains and CNTs.[16] The various techniques used to produce CNTs comprise electric arc discharge, laser ablation and chemical vapor deposition (CVD).[17] The use of CVD techniques is considered the most suitable method for large-scale CNT production.[18] More recently, Filho *et al*.[19,20] developed a low-cost CVD method for the production of CNTs using pyrolysis of waste wood sawdust as a carbon source. The importance of the process has an environmental demand because it also produces hydrogen. Wood sawdust was mixed with a reducing agent (commercial zinc), calcite (bed material) and a catalyst (ferrocene or Fe/Mo/MgO) arranged in a column reactor and then heated to 750 ºC for 3 h without blowing air. The presence of iron in the CNTs makes them suitable for magnetic applications.

The discovery of graphene, a monolayer of sp^2-hybridized carbon atoms, has attracted attention to a new area of research in polymer composites due to its tremendous thermal, mechanical and electrical properties.[21] Brazil has large reserves of graphite and is the third largest producer of graphite, preceded by China and India.[22] Graphene is known to be stronger than steel and a better conductor

of electricity at room temperature than any other material. These incomparable properties promote the industrial applications of graphene enormously.[23] In many technological fields, such as electronics, energy storage and conversion, capacitors and composites materials, graphene has been introduced as an interesting material.[24,25] These properties make graphene an excellent material to improve the properties of neat polymers.[26] However, a major challenge to overcome is obtaining ample quality graphene at reasonable expenditure. The common methods used to produce graphene include CVD, CO reduction and the exfoliation of graphite. The latter method is considered as a suitable technique for the production of large quantities of graphene with affordable costs and is the one used to produce nanocomposites.[22]

Polypropylene (PP) is commercially a very important polyolefin due to its low cost, inertness towards acids, alkalis and solvents, high stiffness and good tensile strength. PP is used in the packaging, textile and automotive industries. However, it is imperative to enhance the properties of PP for advance applications.[27] The mechanical properties of PP can be improved by the incorporation of various fibers and fillers. Recently, in order to improve the electrical conductivity, thermal conductivity and barrier properties, PP/graphene and PP/CNT nanocomposites have been reported.[28-30] Various methods are used to improve the filler polymer interaction solution mixing,[31] *insitu* polymerization[32] and melt blending.[33-36] However, there are limitations of solution mixing in the case of polypropylene and polyethylene, since these polymers are soluble in the solvent above 120 °C, such as xylene and trichlorobenzene, which cause serious health risks.[7] *Insitu* polymerization is not suitable for large-scale production. Melt mixing is one of the most used techniques due to its simplicity, high yield and fast production, easy operation and the fact that it does not need a hazardous solvent that could cause health problems.[37]

The potential application of multifunctional magnetic polymer composites has attracted the interest of both industrial and academic researchers. These materials can be used in various fields, such as microwave absorbers, biomedicine, magnetic recording materials, information technology, energy storage devices, magnetic resonance imaging, magnetic sensors, catalysis, drug delivery, telecommunications and environmental remediation.[33,38-40] Magnetic polymer nanocomposites can be obtained by the introduction of a range of magnetic elements, such as iron, nickel and cobalt, in a diamagnetic polymer matrix using different polymerization techniques.[41]Although iron is one of the conventionally used magnetic materials,[42] the easy oxidation of iron NPs is a hot topic of discussion when using NPs as fillers in polymer matrices. NPs have a tendency to agglomerate in order to decrease the energy related with their high surface areas. The chemical stabilization of the magnetic constituent is achieved by coating with silica or carbon to avoid aggregation.[43] The encapsulation of iron NPs in CNTs synthesized by the CVD method, where ferrocene is used as a catalyst and precursor of synthesis, is considered a suitable strategy.[44-46] In recent works, we obtained polyethylene-CNT-Fe, polyethylene/rGO-CNT-Fe and PP-CNT-Fe nanocomposites with good magnetic properties at room temperature using CNT-Fe synthesized by CVD form ferrocene and *in situ* polymerization for the production of nanocomposites.[47-49]

In the present work, we aimed to produce a low-cost PP/rGO-CNT-Fe dual stimuli-responsive material under electrical and magnetic fields at room temperature, using rGO to introduce a conductive network in the isolated PP matrix via an eco-friendly process developed by Filho *et al*.[19,20] that produces CNT-Fe from a low-cost source, such as wood sawdust from furniture industry waste. PP/rGO-CNT-Fe nanocomposites were fabricated using the melt mixing technique and commercial PP. These multifunctional materials can be used in different industrial applications, including sensors in medicine, electronic devices, low-temperature heaters, energy storage devices,

solar cells, magnetic recording materials, magnetic sensors and microwave absorbers, as well as in the aerospace and automotive industries.[50-53]

2. EXPERIMENTAL

Commercially available PP was used as the polymer matrix, iPP (PP2621) with a melt flow rate of 26 g/10 min (2.16 kg/230 °C) (Norm ASTM D-1238/95), Mw= 195 kg/mol, Mn= 71 kg/mol, PDI= 2.72 and a melting point of 160 °C provided by Petroquim S.A. (Hualpén, Chile). Irganox 1010 was used as an antioxidant agent during the composite preparation.

2.1 CNT synthesis

Sawdust from the furniture industry was gathered to be utilized as a raw material for the synthesis of CNTs using a reported method.[19] Commercially available zinc served a reducing agent. Ferrocene (Fe $(C_2H_5)_2$) was used as a catalyst of synthesis. The method of synthesis is elaborated in detail in Refs.19 and 20.

2.2 Graphene oxide synthesis and thermal reduction

A modified Staudenmaier method was used to synthesize graphene oxide from flakes.[54,55] The Graphite oxide (GO) was heated up to 600°C for 3 s in an oven to obtain rGO, under a normal atmosphere in a closed quartz ampoule. The amount of oxygen calculated by elemental analysis was 27%. The complete characterization of the rGO can be found in Ref. 55.

2.3 Filler composition

Three filler compositions, $GCFe_1$ (2.0 wt.%),$GCFe_2$ (2.6 wt.%) and $GCFe_3$ (3.1 wt.%), were used. These fillers are composed of a mixture of a constant amount of CNT-Fe (1.0 wt.%) and a variable amount of rGO of 1.0, 1.6 and 2.1 wt.%, respectively.

2.4 Melt compounding

For the preparation of the composites, a melt mixer, Bra bender Plasti-Corder (Diusburg, Germany), operating at 190 °C at a speed of 110 rpm was used. Calculated amounts of iPP and rGO-CNT-Fe and a small amount (~0.005 g) of Irganox1010 as an antioxidant were used per mixing, with the total accumulated amount being~30 g. The amount of filler varied from 0 to 3.1 wt.%. The iPP was first mixed with the antioxidant, and subsequently half the amount of the polymer (~13 g) was added to the mixer operating at 110 rpm. After the following 2 min, the filler was added to the melted polymer for 3 min. In the last step, the rest of the polymer pellets was added and the speed of the mixer was kept constant at 110 rpm for 10 min. The total mixing time was ~15 min.

2.5 Characterization

The morphology of the nanoparticles (CNT-Fe) and rGO were investigated using transmission electron microscopy (TEM) (JEOL (JEM-2010)) operating at 200 kV and scanning electron microscopy (SEM)(JEOL JSM 6500F). The nanocomposites (iPP/rGO-CNT-Fe) were also analyzed using TEM (JEOL 1011) operating at 120 kV. Ultrathin films (~50 nm thick) cut under cryogenic conditions with a Leica Ultracut UCT microtome at -70 °C placed on a grid were used to prepare the samples. SEM (Phillips XL30)operating at 20 kV was used to examine the nanocomposites. Samples were deposited on an aluminum stub and coated with gold.

An EZ9MicroSense vibrating sample magnetometer was used at room temperature with a magnetic field (H) cycled between−20and +20 kOe to investigate the magnetic properties of the CNT nanocomposites.

A megohmmeter (Megger BM11) operating at the highest voltage of 1200 V was used to measure the electric resistivity. A standard two-point method was used with this set-up. For each electrical value presented in this contribution, at least four samples were prepared and four measurements

were carried out for each one. In general, differences of around one order of magnitude were detected in the non-percolated samples with low conductivity values (~10^{-9} S/cm). For percolated samples, the experimental error for the conductivities was less than 50%. The samples prepared for this test were 40 mm × 15 mm with a thickness of 1 mm.

The thermal properties were measured using differential scanning calorimetry (DSC), with a Perkin–Elmer differential calorimeter (model DSC Q20). The temperature was incremented from 0 to 180 °C at 10 °C/min. The second scan was used to determine the melting temperature T_m, and the percent crystallinities were calculated from the enthalpy of fusion data obtained from the DSC curves (207J/g was used for PP 100% crystalline).[56,57] A thermogravimetric analysis (TGA) performed with a SDT Q600 thermal analyzer Q20 (TA Instruments, New Castle, USA) was used to study the thermal stability of the nanocomposites with respect to the neat polymer. The samples were scanned in the range of 0 to 800 °C at a scanning rate of 20 °C/min.

Oxygen permeability was measured using L100-5000 permeability equipment manufactured in the United Kingdom connected to a vacuum pump and a cooling and heating bath to control the temperature. The tolerance in percentage to equilibrium was 2, and the oxygen pressure was maintained at 5 bar. Three measurements were obtained for each sample, and the results were the average of these three measurements.

The water contact angle test was carried out using the sessile drop method, where a drop of 2 µL of deionized water at room temperature was steadily deposited on the surface of the neat PP matrix and its nanocomposites, using a microsyringe. The images were captured using “Drop Shape Analysis system” equipment, Kruss, DSA. Each measurement was repeated at least five times at different positions. A digital video camera was used to capture the images that were analyzed by Surftens 3.0 software for contact angle measurements.

An HP model D-500 dynamometer according to ASTMD638-10 at ~25 °C was used to measure the mechanical properties. Five samples were tested for each wt.% of nanocomposite, and the results were the average value of these five measurements (typical deviation of ca.5%). The bone-shaped sample shave an overall length of 120 mm with a distance between the two grips of 80 mm, a width of 11.5 mm and a thickness of 1mm at a cross head. A rate of 50 mm/min was tested.

3. RESULTS AND DISCUSSION

3.1 Thermal analysis

The variation in the stability of the polymers with the incorporation of the rGO-CNT-Fe was determined using DSC and TGA. Table 1 gives the results of a number of the nanocomposites with the filler ranging from 0 to 3.1 wt.%. The amount of filler in wt.% was determined from the amount added to the mixture and the polymer yield. It can be seen from Table 1 that the initial (T_{onset}) and maximum (T_{max}) degradation temperatures gradually shift to higher temperatures as the filler concentration increases from 0 to 3.1 wt.%, and increases of 31 and 18°C were observed in T_{onset} and T_{max}, respectively. There is an exceptional increase in the thermal stability with the incorporation of a very small amount of filler, 3.1 wt.%, and the maximum weight loss temperature of the nanocomposites surpasses the degradation temperature of the neat polymer by ~18 °C. The enhancement in the thermal stability of the polymer is mostly attributed to the formation and stabilization effect of the filler-bonded macroradicals and filler barrier effect.[58]

Table 1: Thermal properties of PP/rGO-CNT-Fe nanocomposites

Samples	Filler[a] (%)	T_c (^{0}C)	T_m (^{0}C)	X_c (%)	T_{onset} (^{0}C)	T_{max} (^{0}C)
PP	0	112	158	59	427	470
PP/GCFe$_1$	2.0	122	162	60	455	475
PP/GCFe$_2$	2.6	122	162	65	453	486
PP/GCFe$_3$	3.1	123	162	63	458	488

[a]Filler = GCFe=rGO+CNT-Fe

Table 1 shows the DSC results of the neat PP and its nanocomposites. It can be seen that, with the introduction of the filler, increases of 4 and 11°C are observed in the melting and crystallization temperatures, respectively. Similarly, the percentage (%) crystallinity also shows an increase of 6% compared to neat PP, demonstrating that the filler acts as a nucleating agent.

3.2 Morphology of nanocomposites

Figure 1 gives the scanning electron micrographs of the fractured surface of pristine PP and its nanocomposites with different wt.% of rGO-CNT-Fe. The samples were first cooled in liquid nitrogen and then broken without deformation. The rGO-CNT-Fe seems to be well distributed in the PP matrix, where no agglomerates were observed. When the concentration of the filler is increased, a more layered structure of the polymer matrix appears, which shows a strong interaction between the filler and the polymer matrix.

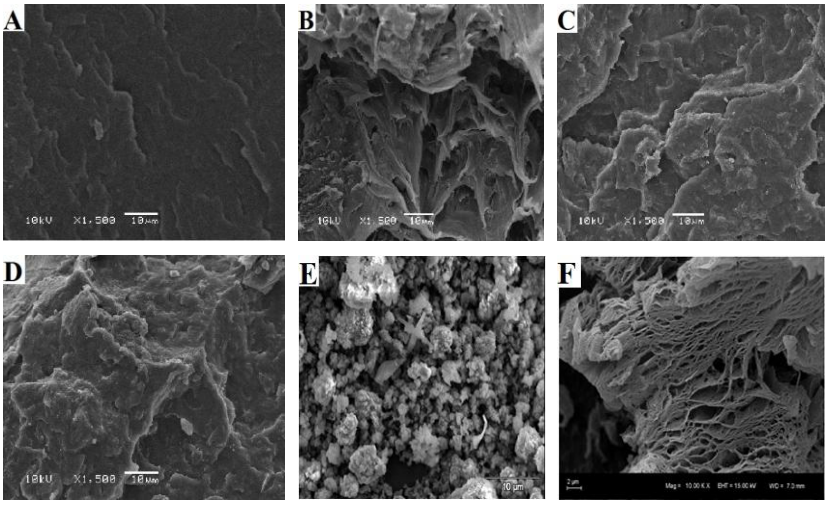

Figure 1. SEM images: (a) neat PP, (b), (c) and (d) 2, 2.6 and 3.1wt.% of PP/rGO-CNT-Fe nanocomposites, respectively, (e) CNT-Fe and (f) rGO.

The TEM morphological evaluation of the nanocomposites was carried out to see the morphology and dispersion of the filler in the polymer matrix. Figure 2 shows TEM images of the neat CNT-Fe (Figure 2(a)) and rGO (Figure 2(b)), and the PP/rGO-CNT-Fe nanocomposites with 2 wt.% filler (Figures 2(c-e)) and 3.1 wt.% (Figures (f-h)), respectively. It is clear from the micrographs that the filler is uniformly distributed in the polymer matrix. The polymer matrix seems to be wrapped around the filler and no aggregation was observed. In Figures 2(e) and (h), an isolated CNT was observed.

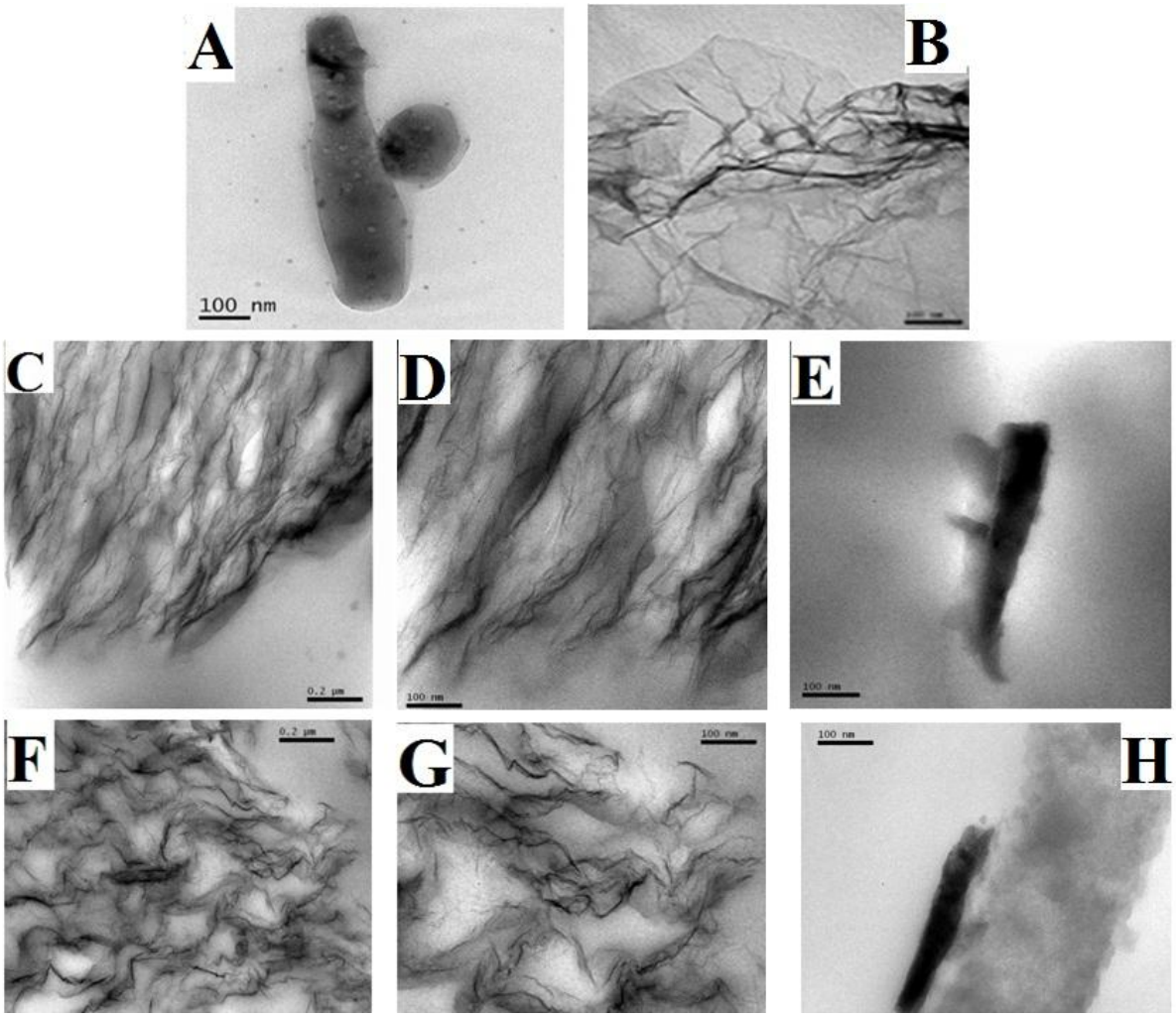

Figure 2. TEM images: (c),(d) and (e) 2 wt.% PP/rGO-CNT-Fe nanocomposites, (f),(g) and (h) 3.1 wt.% PP/rGO-CNT-Fe nanocomposites, (a) CNT-Fe and (b) rGO.

3.3 Mechanical properties

Normally, the mechanical properties of the polymer are changed with introduction of the filler, which depends on the degree of dispersion of the filler and its aspect ratio, given that the TEM and SEM studies show a uniform distribution of the filler in the PP matrix. Figure 3(a) demonstrates the effect of the filler on the Young's modulus and elongation at break. It is clear from the results that, with the incorporation of only 2.6% filler, an increase of ~13% (183 MPa) are observed, which

reaches a higher value of ~22% (314 MPa) with the incorporation of 3.1% filler. This enhancement in the modulus is attributed to the uniform dispersion of the filler in the polymer matrix and an effective load transfer from the filler to the matrix due to strong interfacial adhesion.[7] The results show the improvement of the material's rigidity as a result of the filler loading.[59]A similar enhancement in the Young's modulus was shown by Song *et al.*[7] and Hunang *et al.*[60] for PP/graphene nanocomposites.

The results of the elongation at the break point measurement are presented in Figure 3(b). It can be seen that, with the increase of the filler from 2.6% to 3.1%, decreases of 37% and 50% in the elongation at break occur, respectively, as compared to neat PP. A similar decreasing tendency in the elongation at break for graphene/PP nanocomposites has been reported by other researchers.[61,

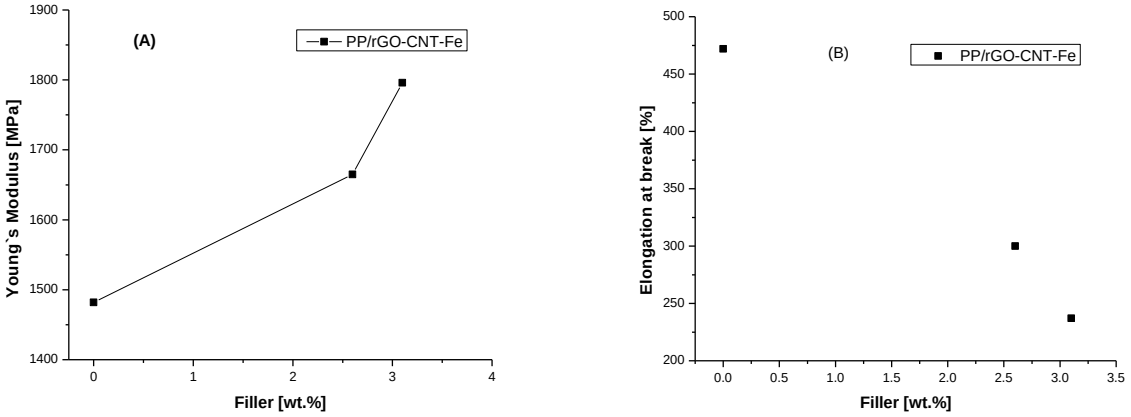

Figure 3.Modulus (a) and elongation at break (b) of the neat PP and PP/rGO-CNT-Fe nanocomposites.

3.4 Electrical conductivity

One of the main objectives of this work is to transform the PP insulating material to a semiconductor to broaden the industrial applications of the materials. Forming a conductive network of the filler and transforming the insulating material to a semiconductor are achieved only when the amount of conductive

filler is above the electrical percolation threshold.[63] Table 2 and Figure 4 show the conductivity of the neat PP and PP/rGO-CNT-Fe nanocomposites. Table 2 also shows the electrical conductivity results of the polyethylene/graphite nanocomposites from previous works. It can be seen that the PP shows an insulating nature as the amount of the filler increases to 2.6 wt.% and the PP/rGO-CNT-Fe nanocomposites still remain insulating. A significant drop in the electrical resistivity is observed as the filler amount increases to 3.1 wt.%. This indicates that the electrical percolation threshold falls between 2.6 and 3.1 wt.%, and the cross linking network structure of naturally conductive rGO has been formed, which is the main source of conductivity in this study. Li *et al.*[64] reported the electrical percolation between 8 and 12 wt.% for PP/graphene nanoplatelet nanocomposites. The amount we incorporated is almost three times lower than theirs. This improved conductivity is attributed to the good exfoliation of rGO.[65]

Table 2: Contact angle, conductivity and oxygen permeability of PP/rGO-CNT-Fe nanocomposites

Samples	rGO(wt %)	CNT-Fe (wt %)	[b]WCA (°)	Conductivity(S cm^{-1})	Oxygen permeabilit 0%[c]RH(mL/m^2 ×24h
PP	0	0	107.3±0.2	5.6×10^{-11}	52.0
PP/$GCFe_1$[a]	1.0	1.0	107.4±0.3	8.3×10^{-11}	36.3
PP/$GCFe_2$[a]	1.6	1.0	111.5±0.2	7.5×10^{-11}	29.0
PP/$GCFe_3$[a]	2.1	1.0	109.4±0.1	2.3×10^{-8}	27.3
PE/GCFe[d]	2.4	0.46	---	4.99×10^{-6}	--
PErGO[f]	2.2	--	---	8.5×10^{-8}	--
PEGNS[f]	15.3	--	---	1.6×10^{-7}	--

[a]Filler = GCFe=rGO+CNT-Fe, [b]Water Contact angle, [c]Relative humidity, [d]Data from Ref.48, [f]Data from Ref.22.

In our recent work, using the same graphene obtaining polyethylene/rGO-CNT-Fe nanocomposites by *in situ* polymerization, we obtained a conductivity of 4.99×10^{-6} Scm^{-1} using 2.4% of the graphene, which is very similar to the present results.[48] Previous studies [22] show that rGO is more exfoliated than GNS and has fewer graphene layers per sheet, using GNS to obtained polyethylene nanocomposites by *in situ* polymerization gave conductivity only when a higher amount of filler 15.3 wt.% is used. The differences in the type of graphite used have a remarkable influence on the conductivity of the composite materials obtained.

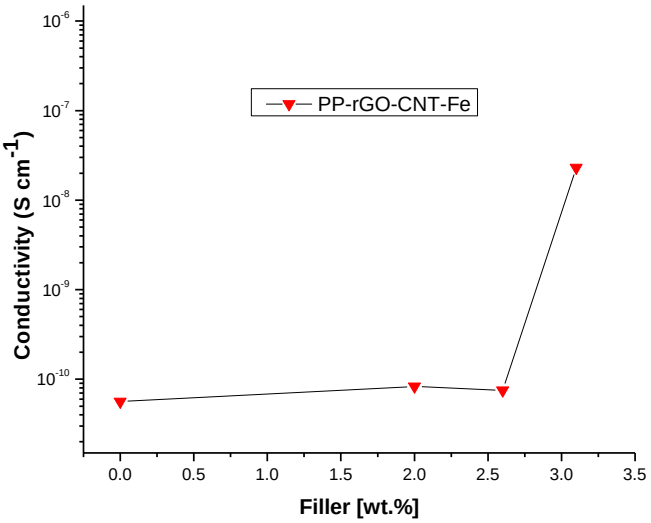

Figure 4.Electrical conductivity of neat PP and PP/rGO-CNT-Fe nanocomposites.

3.5 Oxygen barrier properties

The permeability of polymers to gases and liquids has been an area of growing scientific interest for many years, as it is an important property on the basis of which a material can be evaluated for a range of industrial applications. Gas barrier materials have potential for applications in the field of packaging materials, electronic and medical applications.[66] PP is broadly used as a packaging material. To improve the barrier properties of plastic materials, two common techniques are used, i.e., surface coating or the introduction of nanoparticles to form nanocomposites.[67] Table 2 and Figure 5 demonstrate the effect of the filler percentage on the permeability to oxygen at 23 °C for neat PP films and their nanocomposites with a thickness of ~0.25 mm. It can be seen that with the addition of the filler, the permeability reduces steadily up to 30% with the addition of only 2 wt.% filler and reduces to a higher value, ~50%, with the incorporation of 3 wt.% filler. Isotatic PP contains both crystalline and amorphous regions, the gas permeability in the crystalline region is considered negligible, and the permeation of the gas takes place only in the amorphous region, as

supported by our DSC results, the percentage crystallinity increases with the incorporation of the filler.[68] From previous studies, the rGO and CNTs act as nucleating agents for the PE and PP matrix.[22,48,58,] The nanocomposites are considered to be a multiphase system in which the existence of different phases, crystalline, inorganic and amorphous, can cause complex phenomena on the procedure of gas permeation. The presence of the filler rGO-CNT-Fe introduces a more limited path for the gas molecules to pass through the polymer. The reduction in the penetrability is clear from the experimental results, due to the existence of the more tortuous path, apart from the crystalline region which is comparatively less permeable as the gas molecules have to pass through the filler, which are considered impermeable.[68]

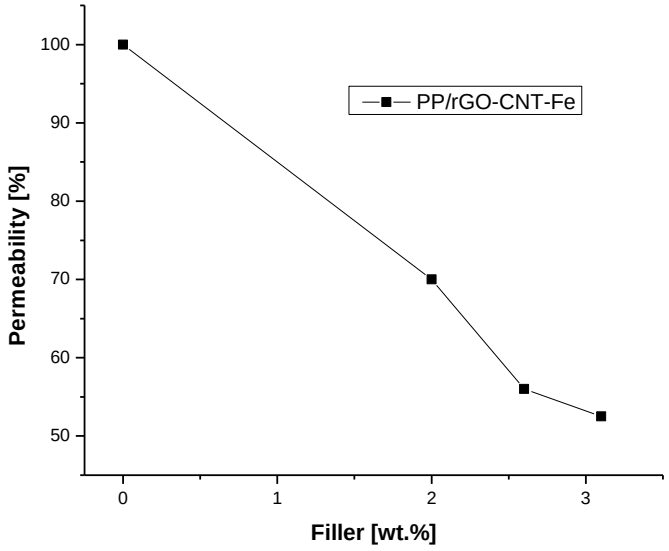

Figure 5.Effect of filler (wt.%) on the permeability of the nanocomposites towards oxygen.

3.6 Contact angle study

For advanced application of the composite materials, knowledge of the affinity toward water is an important parameter. To be considered superhydrophobic, the surface has to exhibit high water

contact angles (WCAs) (>150°).[69] Table 2 shows the results of WCA where it can be seen that, with the addition of the filler, a slight increase in the angle is observed, demonstrating an improvement in the hydrophobic nature of the material.

3.7 Magnetic properties

The normalized (to their respective saturation values) magnetization hysteresis loops of the PP/rGO-CNT-Fe nanocomposites and that of the powder (filler), traced at room temperature, are shown in Figure 6. A diamagnetic correction was applied on each measured curve. We also assured that the magnitude of the maximum magnetic field used was sufficiently high to avoid minor-loop effects.[70-73] As can be seen, all loops are practically identical, with a normalized remnant magnetization of 0.14 and coercivity equal to 150 (±2) Oe. All curves are effectively saturated above ~4.2 (±0.1) kOe. One may conclude that, differently from the other properties, the magnetic ones do not change from those of the starting magnetic material as it is used as filler and is introduced into the polymer matrix.

At sufficiently high temperatures, the magnetic moments of very small particles are thermally agitated so they can rotate to their equilibrium directions. Such particles are called super paramagnetic (SPM). Here, we consider that our samples contain two magnetic phases: (i) non-interacting SPM particles and (ii) stable (interacting small and/or larger ferromagnetic) grains, and we performed numerical simulations that allowed us to estimate the average size (D) of the SPM particles by fitting the experimental hysteresis loops using the method described elsewere.[74,75] The solid line in Figure 6 is calculated assuming a system of randomly-oriented single-domain uniaxial-anisotropy particles with a Gaussian distribution of the SPM particle size with $D = 3.8$ nm and standard deviation equal to 1.8 nm.

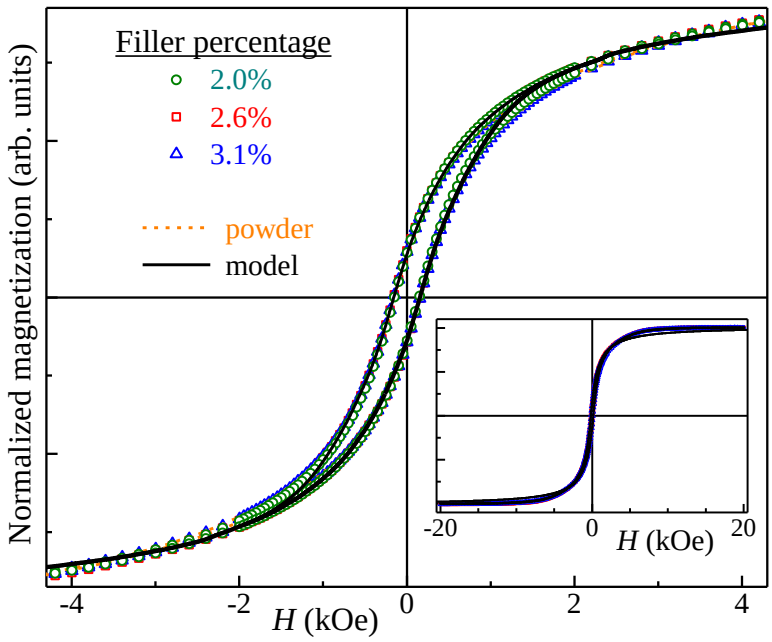

Figure 6. Low-field magnetization hysteresis loops traced at room temperature for the PP/rGO-CNT-Fe nanocomposites with different filler contents together with that traced on the powder. The solid line is a model one obtained assuming that the system consists of both ferromagnetic and super paramagnetic single-domain particles. The inset presents the whole-field-range loops.

4. CONCLUSIONS

Low-cost nanocomposites made from PP/rGO and CNT-Fe produced from wood sawdust from the furniture industry was obtained. The morphological characterization reveals a uniform dispersion of the filler. The synthesized materials showed improvement in thermal stability and higher crystallization temperatures than PP. Nanocomposites with only 3.1 wt.% filler present a reduction of oxygen permeability of 50% and an enhancement of 22% (314 MPa) in the Young's modulus. The obtained CNTs have magnetic properties due to the use of a catalyst containing iron. The room

temperature magnetization hysteresis showed that the nanocomposites consist of both ferromagnetic and super paramagnetic parts with a very low percentage of filler. The value of the room temperature coercivity shown by the nanocomposites is a rather remarkable result given that most research in this area has reported materials that are magnetic only at very low temperatures. The conductivity results from the presence of rGO that forms conducting network in the polymer matrix.

Conflicts of interest

There are no conflicts of interest to declare.

Acknowledgments

The authors are grateful to the TWAS-CNPq for the fellowship to Muhammad Nisar (grant number 3240274293) and to CNPq for grant 302902/2013-9. We thank Professor Raúl Quijada from the University of Chile for the support. We also thank CME and LRNANO from UFRGS for the microscopy analysis. The magnetic characterization was performed in collaboration with the Laboratory of Magnetism at IF-UFRGS.

REFERENCES

1. A. Funck, W. Kaminsky, *Compos. Sci. Technol*. **2007**, 67, 906.
2. R. Mulhaupt, T. Engelhardt, N. Schall, *Kunststoffe* **2001**, 91, 178.
3. N.A.D. Burke, H.D.H. Stover, F.P. Dawson, *Chem. Mater.* **2002,** 14, 4752.
4. J. Jancar, J.F. Douglas, F.W. Starr, S.K. Kumar, P. Cassagnau, A.J. Lesser, S.S. Sternstein, M. Buehler, *Polymer* **2010,** 51 , 3321.
5. I.Y. Jeon, J.B. Baek, *Materials* **2010**, 3 , 3654.
6. Q. He, T. Yuan, J. Zhu, Z.Luo, V. Haldolaarachchige, L.Sun, A. Khasanov, Y.Li, D.P. Young, S.We, Z.Guo, *Polymer* **2012**, 53, 3642.
7. P. Song, Z. Cao, Y. Cai, L. Zhao, Z. Fang, S. Fu, *Polymer* **2011**, 52, 4001.
8. S. Iijima, *Nature* **1991**, 354, 56.
9. P.M. Ajayan, O. Stephan, C. Colliex, D. Trauth, *Science* **1994**, 265, 1212.
10. C.A. Cooper, R.J. Young, M. Halasll, *Compos. Part A.* **2001**, 32, 401.
11. G. Gao, T. Cagin, W.A. Goddard III, *Nanotechnology* **1998,** 9 , 184.
12. M. Moniruzzaman, K.I. Winey, *Macromolecules* **2006,** 39, 5194.
13. M.M.J. Treacy, T.W. Ebbesen, J.M. Gibson, *Nature* **1996,** 381, 678.
14. K.R. Reddy, B.C. Sin,C.H.Yoo,D.Sohn, Y. Lee, *J. Colloid Interface Sci.* **2009**, 340, 160.
15. A.K.T. Lau, D. Hui, *Compos. Part B* **2002**, 33, 263.
16. J. F. Vaga, J.M. Salazar, M. Trujillo, M.L.Arnal, A.J. Muller, S. Bredeau. Ph. Dubois, *Macromolecules* **2009**, 42, 4719.
17. P. Ramesh, T. Okazaki, T. Sugai, J. Kimura,N.Kishi, K.Sato,Y.Ozeki, H.Shinohara, *Chem. Phys. Lett.* **2006**, 418, 408.

18. N.M. Mubarak, E.C. Abdullah,N.S.Jayakumar, J.N. Sahu, *J. Ind. Eng. Chem.* **2014**, 20, 1186.
19. G.S. Bernd,S.R.Braganca, N. Heck,C.P.Luiz, D.S.Filho, *J. Mater. Res. Technol*. (2017)https://doi.org/10.1016/j.jmrt.2016.11.003.
20. S.Filho, C.P. Luiz,N.C.Heck, M.G.S. Bernd,Patente No. BR 10, 2012,022053-9 A2 [http://hdl.handle.net/10183/107424].
21. J.R.Potts, D.R.Dreyar, C.W.Bielawski, R.S. Rouff, *Polymer* **2011,** 52, 5.
22. G. Pavoski, T.Maraschin, M.A. Milani, D.S.Azambuja,R.Quijada,C.M.Moura, N.R.S.Basso, G.B.Galland, *Polymer* **2015,** 81, 79.
23. A. K. Geim, *Science* **2009**, 324, 1530.
24. A.K. Geim, K.S.Novoselov, *Nat. Mater.* **2007**, 6, 183.
25. D.A.Dikin,S.Stankovich,E.J.Zimney,R.D.Piner,G.H.B. Dommett, G. Evmenenko, S.T. Nguyen, R.S. Ruoff, *Nature* **2007**, 448 , 457.
26. K.Wakabayashi, C. Pierre,D.A.Dikin,R.S.Rouff,T.Ramanathan, L.C. Brinson, J.M. Torkelson, *Macromolecules* **2008**, 41, 1905..
27. J. An, G. Jeon, *Fiber. Polym.* **2012,** 13, 507.
28. G.W.Lee, S. Jagannathan, H.G. Chae, M.L.Mimus, S. Kumar, *Polymer* **2008**, 49, 1831.
29. K. Kalaitzidou, H.Fukushima,L.T.Drzal, *Carbon* **2007,** 45, 1446.
30. Y.J. Huang, Y. W. Qin, Y. Zhou, H. Niu, Z.Z. Yu, Y.J. Dong, *Chem. Mater.* **2010**, 22, 4096,
31. S. Curran, A.P. Davey, J. Coleman, A. Dalton, B. McCarthy, S. Maier, *Synth. Met.* **1999**, 103, 2559.
32. A. Funck, W. Kaminsky, *Compos. Sci. Technol.* **2007**, 67, 906.

33. J. Riquelme, C.A. Garzon, C.P. Bergmann, J. Geshev, R. Quijada, *Eur. Polym. J.* **2016**, 75, 200.

34. P. Potschke, A.R. Bhattacharyy, A. Janke, *Carbon* **2004,** 42, 965.

35. W.E. Dondero, R.E. Gorga, *J. Polym. Sci. Polym. Phys.* **2006,** 44, 864.

36. T. Yasin, M. Nisar, M. Shafiq, Y. Nho, R. Ahmad, *Polym.Compos.* **2013**, 34, 408.

37. S.P. Bao, S.C. Tjong, *Mater. Sci. Eng. A.* **2008**, 485, 506.

38. J.M.D. Coey, *J. Magn. Magn. Mater.* **1999**, 196, 1.

39. R.D. Shull, L.H. Bennett, *Nanostruct. Mater.* **1992**, 1 , 83.

40. J. Zhu, S. Wei, M. Chen, H. Gu, S.B. Rapole, S. Pallavkar, T.C. Ho, J. Hopper,Z. Guo, *Adv. Powder. Technol.* **2013**, 24, 459.

41. G. Schinteie, V.Kuncser, P. Palade,R.Alexandrescu, I. Morjan, G.J.Filoti, *Alloy. Compd.* **2013**, 564, 27.

42. S. Wei, Q. Wang, J. Zhu, L. Sun, H. Lin, Z. Guo, *Nanoscale* **2011**, 3, 4474.

43. K. Susheel, K. Sarita, K. Amit, H. Yuvaraj, K. Bandan, K. Rajesh, *Colloid. Polym. Sci.* **2014**, 292, 2025.

44. R. Bhatia, V. Prasad, *Solid State Commun.* **2010**,150 , 311..

45. A.G. Osorio, C.P. Bergmann, *Appl. Surf. Sci.* **2013**, 264,794.

46. A.G.Osorio, L.G.Pereira, J.B.M. Da Cunha, C.P. Bergmann, *Mater. Res. Bull.* **2013**, 48, 4168.

47. M. Nisar, C. P. Bergmman, J. Geshev, R. Quijada, G.B. Galland, *Polymer* **2016**, 97, 131.

48. M. Nisar, C. P. Bergmman, J. Geshev, R. Quijada, T. Maeaschin, N.R.S. Basso, E.G. Barrera, G.B. Galland, *J. Appl. Polym. Sci*. **2017**, 134, 45382.

49. M. Nisar, C.P. Bergmman, J. Geshev, R. Quijada, G. B. Galland, *Polymer* **2017,** 118, 68.

50. P. Kim, N.M. Doss, J.P.Tillotson, P.J. Hotchkiss, M.J. Pan, S. R. Marder, J. Li, J. P. Calame, J.W. Perry, *ACS Nano* **2009**, 3, 2581.
51. Q. Dai, D. Berman, K.Virwani, J.Frommer, P.O.Jubert, M. Lam, T. Topuria, W. Imaino, A. Nelso, *Nano Lett.* **2010,** 10 , 3216..
52. T. Shimad, K. Ookubo, N. Komuro, T. Shimizu, N.Uehara, *Langmuir* **2007**, 23,11225.
53. Z. Guo, S.E. lee, H. Kim, S. Park, H.T. Hahn, A. B. Karki, D.P.Young, *Acta Mater.* 2009, 57, 267.
54. L. Staudenmaier, *Chem. Ges.* **1898**, 31, 1481.
55. G. Pavoski, T.Maraschin, F.C. Fim,N.M.Balzaretti, G.B.Galland, C.S.Moura, N.R.S. Basso, *Mater. Res*. **2017**, 20, 53.
56. M.K. Seo, S.J. Park, *Matter. Eng.* **2004**, 289, 368.
57. T.G. Gopakumar, D.J.Y.S. Pagé, *Polym.Eng. Sci*. **2004,** 44, 1162.
58. A.A. Koval'chuk, A.N.Shchegolikhin, V.G.Shevehenko, P.M.Nedorezovz, A.N.Klyamkina, A.M. Aladyshev, *Macromolecules* **2008,** 41, 3149.
59. H. Zou, S. Wu, J. Shen, *Chem. Rev.* **2008,** 108, 3893.
60. C.L. Huang, C.W.Lou, C.F. Liu, C.H. Huang, X.M. Song, J.H. Lin, *Appl. Sci.* **2015**, 5, 1196.
61. B.Yuan,C.Bao, L. Song, N. Hong , K.M. Liew, Y. Hu, *Chem. Eng. J.* **2014,** 237, 411,
62. M.E. Achaby, F.E. Arrakhiz, S.B. Vaudreuil, A.K. Qaiss, M. Bousmina, O.F.Fehri, *Polym. Composit.* **2012**, 33, 733.
63. K.Wongtimnoi, B. Guiffard, A.B. de Moortele, L. Seveyrat, C. Gauthiev, J.Y. Cavaille, *Compos. Sci. Technol.* **2010**, 71, 885.
64. Y.Li, J.Zhu. S.Wei, J. Ryu, L. Sun, Z. Guo, *Macromol. Chem. Phys*. **2011**, 121, 1951.

65. J. H. Park, A. Choudhury, B.L. Farmer, T.D. Dang, S.Y. Park, *Polymer* **2012**, 53, 3937.

66. A. Hiltner, R.Y.F. Liu, Y.S. Hu, E. Baer, *J. Polym. Sci: Part B: Polym. Phys*, **2005**, 43, 1047.

67. G. Zehetmeyer, J.M. Scheibel, R. M. D. Soares, D.E. Weibel, M.A.S. Oviedo, R.V.B. Oliveira, *Polym. Bull.* **2013**, 70, 2181.

68. V. Vladimirov, C. Betchev, A. Vassiliou, G. Papageorgiou, D. Bikiaris, *Compos. Sci. Technol.* **2006**, 66, 2935..

69. G.R.Chagas, D.E.Weibel, *Polym. Bull.* **2017**, 74, 1965..

70. J. Geshev, *J. Magn. Magn.Mater.* **2008,** 320, 600.

71. J. Geshev, *Appl. Phys. Lett.* **2008**, 93, 176101.

72. J. Geshev, L.G. Pereira, V. Skumryev, *Phys. Rev. Lett.* **2008**, 100 , 039701.

73. A. Harres, M. Mikhov, V. Skumryev, A.M.H. de Andrade, J.E. Schmidt, J. Geshev, *Magn. Magn.Mater.* **2016**, 402, 76.

74. A.D. Viegas, J. Geshev, L.S. Dorneles, J.E. Schmidt, M. Knobel, *J. Appl. Phys.* **1997,** 82, 3047.

75. V. Masheva, M. Grigorova, N. Valkov, H. J. Blythe, T. Midlarz, V. Blaskov, J. Geshev, M. Mikhov, *J. Magn. Magn.Mater.* **1999**, 196, 128.